

University of Southampton Research Repository ePrints Soton

Copyright © and Moral Rights for this thesis are retained by the author and/or other copyright owners. A copy can be downloaded for personal non-commercial research or study, without prior permission or charge. This thesis cannot be reproduced or quoted extensively from without first obtaining permission in writing from the copyright holder/s. The content must not be changed in any way or sold commercially in any format or medium without the formal permission of the copyright holders.

When referring to this work, full bibliographic details including the author, title, awarding institution and date of the thesis must be given e.g.

AUTHOR (year of submission) "Full thesis title", University of Southampton, name of the University School or Department, PhD Thesis, pagination

University of Southampton
Faculty of Natural and Environmental Sciences

DEVELOPMENT OF BIOCOMPATIBLE POLYMERS FOR
OCULAR APPLICATIONS

By

ANDREW JOHN TREHARNE

Thesis for the degree of Doctor of Philosophy
August 2012

UNIVERSITY OF SOUTHAMPTON

ABSTRACT

FACULTY OF NATURAL AND ENVIRONMENTAL SCIENCES

CHEMISTRY

DOCTOR OF PHILOSOPHY

DEVELOPMENT OF BIOCOMPATIBLE POLYMERS FOR OCULAR
APPLICATIONS

By Andrew John Treharne

Age-related macular degeneration (AMD) is the largest cause of blindness for those over 65 in the developed world. There is currently no treatment for the retinal cellular loss associated with the disease. One potential therapy is to implant retinal stem cells into the eye using a biodegradable polymer scaffold. Blends of the biodegradable polymers, poly(L-lactic acid) (PLLA) and poly(D,L-lactic-co-glycolic acid) (PLGA) have been formulated into microspheres. The influence of changing processing parameters on the size and morphology of the microspheres has been studied. A human retinal pigment epithelial (APRE-19) cell line was shown to adhere, survive and proliferate on the surface of the microspheres *in vitro*. Assays have demonstrated that the nature of the blend influenced cell behaviour.

Transplantation of retinal pigment epithelial (RPE) cells on a supportive matrix has also been investigated as a therapy for AMD. In view of AMD related pathology of the native RPE support, Bruch's membrane (BM), transplanted RPE cells require a scaffold to reside on. Copolymers based on methyl methacrylate (MMA) and poly(ethylene glycol) methacrylate (PEGM) have been synthesised and chemically modified at the PEG terminus. These polymers were subsequently manufactured into a fibrous scaffold using an electrospinning technique and investigated as an artificial BM. RPE cells were shown to attach and proliferate successfully on the surface of the fibrous scaffold *in vitro*. Cell adhesion was significantly enhanced on scaffolds with the PEG chain terminus modification. Significantly less apoptotic cell death was also observed on these surfaces. The diffusion properties of these artificial membranes have also been investigated. In addition, the novel gelation of the produced copolymers under certain conditions has been studied.

Table of Contents

ABSTRACT	iii
Table of figures	x
Table of schemes	xv
Table of tables	xvi
Declaration of authorship	xix
Acknowledgements	xxi
Abbreviations	xxiii
1 Introduction	1
1.1 Introduction.....	1
1.2 Age-related macular degeneration	1
1.3 Wet AMD.....	3
1.4 Dry AMD or geographic atrophy	4
1.4.1 Drusen	5
1.4.2 Inflammatory effects	5
1.4.3 Oxidative stress	6
1.4.4 Bruch’s membrane	6
1.4.5 Advanced glycation end products	9
1.5 Tissue engineering.....	10
1.5.1 Stem cells and their potential in regenerative medicine ..	10
1.5.2 Regenerating the retina without use of a scaffold.....	12
1.6 Use of scaffolds in tissue engineering.....	15
1.6.1 The extracellular matrix – nature’s scaffold.....	15
1.6.2 Use of natural materials for tissue engineering	17
1.6.3 Use of synthetic scaffolds for tissue engineering.....	18

1.7	Control of cells on surfaces	23
1.8	Aims of research.....	30
2	Developing biodegradable microspheres as a cell carrier	31
2.1	Introduction.....	31
2.2	Microspheres	32
2.2.1	Manufacture.....	32
2.2.2	Using microspheres for controlled release	34
2.2.3	Use of microspheres for cell delivery	36
2.3	Optimising the production of PLLA/PLGA microspheres for use as an ocular cell delivery system.....	40
2.3.1	Introduction	40
2.3.2	Preparation of microspheres using different concentrations of polymer solution	40
2.3.3	Preparation of microspheres using different concentrations of stabiliser solution.....	41
2.3.4	Experiments to introduce porosity into PLGA microspheres.....	45
2.3.5	Preparation of a range of microspheres using blends of PLGA and PLLA	47
2.3.6	RPE cell seeding on a range of PLLA/PLGA microspheres	50
3	Towards an artificial Bruch's membrane	61
3.1	Introduction.....	61
3.2	Key properties of an artificial Bruch's membrane	61
3.3	Electrospinning	64
3.3.1	Introduction	64
3.3.2	Mechanism and parameters for fibre production.....	65
3.3.3	Using electrospun matrices to mimic the extracellular matrix (ECM).....	71
3.3.4	Biomedical applications of electrospun matrices	72
3.3.5	Advances in electrospun matrices for use in retinal tissue engineering	73
3.4	Initial steps in developing a methacrylate copolymer	74

3.5	Creating a poly(methyl methacrylate-co-poly(ethylene glycol) methacrylate) fibrous matrix.....	75
3.5.1	Initial polymer synthesis.....	75
3.5.2	Testing the basic biocompatibility of 75:25 P(MMA-co-PEGM) polymers (Polymers 3.5 and 3.14) with RPE cells	86
3.5.3	Development of a P(MMA-co-PEGM) copolymer containing a higher PEG content	93
3.5.4	Testing the biocompatibility of 60:40 P(MMA-co-PEGM) polymers (Polymers 3.6 and 3.15) with RPE cells.....	98
3.5.5	Investigating the effect of hydrophilicity, PEG chain length and end group on RPE cell adhesion.....	106
3.5.6	Investigating the diffusion characteristics of fibrous polymer networks	118
3.6	Investigation of gelation characteristics observed in P(MMA-co-PEGM) succinimidyl carbonate copolymers	123
4	Discussion and conclusions	129
4.1	Development of biodegradable microspheres as an ocular cell delivery system	129
4.1.1	Discussion of progress achieved through results presented in this thesis	129
4.1.2	Future prospects	132
4.2	Development of an artificial Bruch's membrane	134
4.2.1	Discussion of progress achieved through results presented in this thesis	134
4.2.2	Future prospects	140
5	Experimental	141
5.1	Microsphere synthesis.....	143
5.1.1	Preparation of PLLA/PLGA microspheres using a constant polymer solution concentration.....	143
5.1.2	Preparation of PLGA microspheres with a varying polymer solution concentration	144
5.1.3	Preparation of PLGA microspheres with varying stabiliser (PVA) concentration	145

5.1.4	Preparation of PLGA microspheres with varying polymer solution and stabiliser (PVA) concentration.....	145
5.1.5	Preparation of PLGA microspheres with the introduction of an effervescent salt.....	146
5.2	Synthesis of methacrylate-based copolymers	147
5.2.1	Synthesis of P(MMA-co-HEMA) copolymers – Polymers 3.1, 3.2 and 3.4.....	147
5.2.2	Preparation of 60:40 P(MMA-co-HEMA) – Polymer 3.3 ...	148
5.2.3	Preparation of P(MMA-co-PEGM) – Polymers 3.5, 3.6, 3.7 and 3.17.....	149
5.2.4	Preparation of a carboxylated P(MMA-co-PEGM) copolymer – Polymers 3.8, 3.9 and 3.10	151
5.2.5	Preparation of an <i>N</i> -hydroxysuccinimide activated ester of P(MMA-co-PEGM) – Polymers 3.11, 3.12 and 3.13	153
5.2.6	Preparation of a succinimidyl carbonate of P(MMA-co-PEGM) – Polymers 3.14, 3.15, 3.16 and 3.18	155
5.2.7	Spin coating and contact angle.....	156
5.3	Electrospinning of polymers.....	157
5.3.1	Assessment of fibre diameter and surface porosity	158
5.4	Investigation of gelation characteristics observed in P(MMA-co-PEGM) succinimidyl carbonate copolymers	159
5.4.1	Investigation into the gelation of Polymer 3.15	159
5.4.2	Investigation into the gelation of Polymer 3.16	159
5.4.3	Investigation of the use of 4-dimethylaminopyridine (DMAP) as a base for synthesis of Polymer 3.15.....	159
5.4.4	Investigation of the influence of disuccinimidyl carbonate on gelation of Polymer 3.7	159
5.4.5	Investigation of gel formation using Polymer 3.15	160
5.4.6	Investigation into the influence of capping with acetyl groups on gelation of Polymer 3.6	160
5.5	Investigation of diffusion across an artificial Bruch’s membrane	161
5.6	Investigation of the response of RPE cells to microsphere surfaces	162

5.6.1	Cell line maintenance	162
5.6.2	Preparation of microspheres for cell seeding.....	162
5.6.3	Dissociation of cells from culture flask.....	162
5.6.4	Trypan blue exclusion assay	163
5.6.5	Cell seeding	163
5.6.6	Fixing and immunocytochemistry of microspheres	164
5.6.7	Lactate Dehydrogenase (LDH) assay	164
5.6.8	Terminal deoxynucleotidyl transferase dUTP nick end labelling (TUNEL) assay	165
5.6.9	3-(4,5-Dimethylthiazol-2-yl)-2,5-diphenyltetrazolium bromide (MTT) assay.....	166
5.6.10	Scanning electron microscopy (SEM)	167
5.7	Investigation of the response of RPE cells to fibrous methacrylate-based polymer surfaces	168
5.7.1	Preparation of electrospun polymer scaffolds for cell seeding	168
5.7.2	Peptide and protein attachment to electrospun scaffold surfaces.....	168
5.7.3	Cell seeding	168
5.7.4	Quantification of cell area.....	169
5.7.5	TUNEL assay.....	169
5.7.6	MTT assay.....	170
5.7.7	LDH assay	170
5.7.8	Scanning electron microscopy (SEM)	170
5.7.9	Statistical analysis	170
6	Appendices	173
6.1	Appendix A – Publications	173
6.2	Appendix B – List of polymer numbers and structures for Chapter 3.....	201
6.3	Appendix C – Data tables from cell-based assays	207
7	References	219

Table of figures

Figure 1.1 - A cross-section of the human eye showing key components including the macula area of the retina.	2
Figure 1.2 - Images showing the impact of AMD on vision.	2
Figure 1.3 - A simplified cross-section of the human macula showing key structures.	3
Figure 1.4 - A retinal photograph showing soft drusen accumulation.	5
Figure 1.5 - Transmission electron micrograph showing the five anatomical layers of BM.	7
Figure 1.6 - Diagram to show the differentiation pathways of mesenchymal stem cells.	12
Figure 1.7 - Cartoon showing the implantation of a sheet of RPE and choroid.	13
Figure 1.8 - The chemical structure of the Arginine-Glycine-Aspartic acid (RGD) peptide.	16
Figure 1.9 - Cartoon showing the distribution of proteins in the extracellular matrix.	17
Figure 1.10 - Cartoon showing the effects of integrin ligands.	26
Figure 2.1 - Chemical structures of poly(L-lactic acid) (PLLA) and poly(DL-lactic-co-glycolic acid) (PLGA).	32
Figure 2.2 - An illustration of a simple emulsion-based microsphere preparation technique.	33
Figure 2.3 - Cartoon showing the use of microspheres for cell delivery.	37
Figure 2.4 - Scanning electron micrographs showing A) 0.05, B) 0.10 and C) 0.15g/ml PLGA microspheres.	41
Figure 2.5 - Scanning electron micrographs showing 0.1g/ml microspheres produced using A) 0.5%, B) 1% and C) 2% PVA concentration.	42

Figure 2.6 - Scanning electron micrographs showing 0.05 (A) and 0.01 g/ml (B) PLGA microspheres in a 0.1% stabiliser solution concentration.	43
Figure 2.7 - Scanning electron micrographs showing 0.05 (A) and 0.01 g/ml (B) PLGA microspheres in a 0.25% stabiliser solution concentration.	44
Figure 2.8 - Scanning electron micrographs showing 0.01 (A) and 0.05 g/ml (B) PLGA microspheres produced using a 2% stabiliser solution concentration.	45
Figure 2.9 - Scanning electron micrographs showing microspheres produced using a gas foaming technique.	46
Figure 2.10 - Scanning electron micrograph showing microspheres produced using a 50:50 PLLA:PLGA polymer solution.	47
Figure 2.11 - Scanning electron micrographs comparing microspheres produced using a 10:90 (A) and 90:10 (B) PLLA:PLGA blend.	49
Figure 2.12 - Scanning electron micrograph showing microspheres produced using a 0.05g/ml PLLA solution.	49
Figure 2.13 - Comparison of the influence of polymer blend on microsphere size distribution.	50
Figure 2.14 - Immunocytochemical characterisation of ARPE-19 cells cultured for 1 week on laminin-coated microspheres.	52
Figure 2.15 - Scanning electron micrographs of ARPE-19 seeded PLGA microspheres showing a cobblestone morphology (A) and apical microvilli (B).	53
Figure 2.16 - Bar chart representing LDH release from ARPE-19 cells cultured on coated and uncoated microspheres.	54
Figure 2.17 - Bar chart showing percentage ARPE-19 cell death on coated and uncoated microsphere blends by TUNEL assay.	56
Figure 2.18 - Bar chart showing ARPE-19 cell viability by MTT assay on coated and uncoated microsphere blends.	58
Figure 3.1 - Scanning electron microscope images showing the fibrous morphology of a porcine Bruch's membrane.	64

Figure 3.2 - Diagram showing the equipment required for the electrospinning process.....	65
Figure 3.3 - Image of an electrospinning jet showing bending instabilities.	66
Figure 3.4 - Scanning electron microscope image showing 'beaded' polymer fibres produced by electrospinning.	67
Figure 3.5 - Scanning electron microscope (A) and transmission electron microscope (B) images of an electrospun fibre of a polymer latex.	70
Figure 3.6 - NMR spectrum of P(MMA-co-PEGM).	78
Figure 3.7 - Scanning electron micrograph showing 75:25 P(MMA-co-PEGM) electrospun fibres (Polymer 3.5).	80
Figure 3.8 - NMR spectrum of P(MMA-co-PEGM) following reaction with succinic anhydride.	82
Figure 3.9 - NMR spectrum of P(MMA-co-PEGM) with succinimidyl ester functionality.	83
Figure 3.10 - NMR spectrum of P(MMA-co-PEGM) with succinimidyl carbonate functionality.	84
Figure 3.11 - Scanning micrograph of fibres electrospun from a solution of 0.5g/ml succinimidyl carbonate functionalised 75:25 P(MMA-co-PEGM) (Polymer 3.14) in 2-butanone.	86
Figure 3.12 - Bar graph showing absorbance at 492nm of LDH assay samples from polymer scaffolds with different combinations of peptides or protein.....	89
Figure 3.13 - Bar graph showing absorbance at 492nm of MTT assay samples of polymer 3.14 alone and in combination with cell adhesive peptides and proteins.....	90
Figure 3.14 - Light microscope image of a cell seeded polymer scaffold (A) and the same image under ultraviolet light following labelling of cell nuclei with DAPI (B).	91
Figure 3.15 - Scanning electron micrograph showing cells seeded onto a 75:25 P(MMA-co-PEGM) succinimidyl carbonate (Polymer 3.14) fibre surface.....	92

Figure 3.16 – Scanning electron micrograph showing 60:40 P(MMA-co-PEGM) succinimidyl carbonate (Polymer 3.15) electrospun into fibres.	94
Figure 3.17 – Scanning electron micrograph of electrospun fibres of 60:40 P(MMA-co-PEGM) succinimidyl carbonate (Polymer 3.15) at a flow rate of 9.5ml/hr (A) and 1.5ml/hr (B).	95
Figure 3.18 – Images taken from a water contact goniometer of a water droplet on polymer coated glass surfaces.	96
Figure 3.19 – Fluorescence microscope images showing fibre samples of Polymer 3.6 (B) and 3.15 (A) following immersion in a solution of K(Flu)RGD in PBS. Scale bar: 52µm.	97
Figure 3.20 – Chemical structures of the three peptide sequences used for cell adhesion assays.	99
Figure 3.21 – Bar graph illustrating absorbance in LDH assay averaged over time for samples of fibrous scaffolds.	102
Figure 3.22 – Bar graph showing absorbance in the MTT assay used as an indirect measure of cytotoxicity.	103
Figure 3.23 – Graph showing cell apoptosis (as a percentage of total cells) by TUNEL assay.	104
Figure 3.24 – Graph showing cell attachment (as a percentage of total fibre area) on various fibre samples.	105
Figure 3.25 – Scanning electron micrographs of fibres from polymer 3.15.	106
Figure 3.26 – Scanning electron micrograph of electrospun fibres of 60:40 P(MMA-co-PEGM) succinimidyl ester (Polymer 3.12) at a solution concentration of 0.55g/ml (A) and 0.65g/ml (B).	113
Figure 3.27 – Scanning electron micrographs showing fibres of a 40:60 P(MMA-co-PEGM) succinimidyl carbonate (Polymer 3.16).	113
Figure 3.28 – Histogram showing the results of an LDH assay assessing cell survival on different copolymer scaffolds. For data see Appendix C.	114
Figure 3.29 – Bar graph showing results of MTT assay averaged over all time points for different fibrous scaffolds.	115

Figure 3.30 - Bar graph depicting apoptotic cell death expressed as percentage of total cell number, assessed by TUNEL assay.	116
Figure 3.31 - Bar graph depicting percentage ARPE-19 cell area, assessed by nuclear labelling.....	117
Figure 3.32 - Diagram to show apparatus for diffusion experiments.	119
Figure 3.33 - Line graph showing the change in absorbance over time of a FITC-dextran solution on one side of a diffusion chamber and of a PBS solution on the other side of the chamber.....	120
Figure 3.34 - Line graph showing the change in absorbance over time of a FITC-dextran solution on one side of a diffusion chamber and of a PBS solution on the other side of the chamber.....	121
Figure 3.35 - Line graph showing the change in absorbance over time of a FITC-dextran solution on one side of a diffusion chamber and of a PBS solution on the other side of the chamber.....	122
Figure 3.36 - Inversion test of P(MMA-co-PEGM) gel formed by reaction with triethylamine and disuccinimidyl carbonate (DSC)....	124
Figure 3.37 - Crystal formation on the surface of a P(MMA-co-PEGM) gel.	125
Figure 3.38 - ¹ H NMR spectrum showing both succinimidyl (δ 2.79ppm) and acetic (δ 2.17ppm) carbonate groups present in a P(MMA-co-PEGM) polymer.	127
Figure 5.1 - Structure of P(MMA-co-PEGM) acetic ester.	160
Figure 5.2 - Diagram to show apparatus for diffusion experiments.	161

Table of schemes

Scheme 3.1 - Scheme to show the synthetic route to P(MMA-co-HEMA).	75
Scheme 3.2 - Scheme to show the synthetic route for creation of a succinimidyl ester on a PEG chain followed by peptide coupling.	77
Scheme 3.3 - Scheme showing the reaction of P(MMA-co-PEGM) with disuccinimidyl carbonate to give a succinimidyl carbonate substituted product.	83
Scheme 3.4 - Scheme showing the reaction of P(MMA-co-PEGM) with discuccinimidyl carbonate.....	108
Scheme 3.5 - Reaction scheme to show the proposed crosslinked polymer product.....	126

Table of tables

Table 2.1 – Table showing the range of microspheres sizes produced at different polymer and stabiliser concentrations.....	45
Table 2.2 – The diameters and size distributions of the produced range of microspheres.....	48
Table 2.3 – Overall comparison of LDH absorbance from coated and uncoated microsphere blends and controls.	55
Table 2.4 – The overall comparison of apoptotic cell death on coated and uncoated microsphere blends and controls.	57
Table 2.5 – The overall comparison of cytotoxicity from coated and uncoated microsphere blends and controls.	59
Table 3.1 – Table detailing the effect of changing different electrospinning parameters on fibre morphology.	69
Table 3.2 – Table showing the average fibre diameter of fibres electrospun from a solution of 75:25 P(MMA-co-PEGM) in 2-butanone.	81
Table 3.3 – Summary of monomer feed ratios and data from polymers 3.5 and 3.14.	85
Table 3.4 – Summary of polymer samples tested with RPE cells.	88
Table 3.5 – Summary of monomer feed ratios, comonomer ratios and GPC data for Polymers 3.6 and 3.15.....	93
Table 3.6 – Table showing average diameters of electrospun fibres of 60:40 P(MMA-co-PEGM) succinimidyl carbonate (Polymer 3.15) at different concentrations.	96
Table 3.7 – Table showing average contact angles for different polymers. sem: standard error of the mean.....	96
Table 3.8 – Summary of polymer samples tested with RPE cells.	100
Table 3.9 – Table showing average diameters of electrospun fibres of 40:60 P(MMA-co-PEGM) succinimidyl carbonate copolymer (Polymer 3.16) at different concentrations.....	107

Table 3.10 - Table showing the structures of copolymers produced and the concentration of electrospinning solution used to create fibres for biocompatibility testing with RPE cells.....	110
Table 3.11 - Table showing mean fibre diameter, scaffold porosity and contact angle for different copolymers.	112
Table 5.1 - Polymer concentrations and blend ratios used.....	144
Table 5.2 - Monomer feed ratios for P(MMA-co-HEMA) polymerisation reactions.	147
Table 5.3 - Summary of monomer feed ratios for P(MMA-co-PEGM) polymers and the estimated actual ratio based on NMR spectroscopy data.	150
Table 5.4 - Summary of data from P(MMA-co-PEGM) polymers produced.....	150
Table 5.5 - Summary of data from polymers with succinimidyl carbonate functionality.	156
Table 5.6 - Data from contact angle experiments on various polymers.....	156
Table 5.7 - Electrospinning parameters used for different polymers.	158
Table 6.1 - Data from LDH assay on experiments using Polymers 3.5 and 3.14.	209
Table 6.2 - Data from MTT assay on experiments using Polymers 3.5 and 3.14.	209
Table 6.3 - LDH assay data from experiments involving polymers 3.6 and 3.15.	210
Table 6.4 - MTT assay data for experiments involving polymers 3.6 and 3.15.	211
Table 6.5 - TUNEL assay data for experiments involving polymers 3.6 and 3.15.	212
Table 6.6 - Cell attachment data for experiments involving polymers 3.6 and 3.15.....	213
Table 6.7 - LDH absorbance data from experiments involving polymers 3.16, 3.6, 3.15, 3.12, 3.17 and 3.18.....	214

Table 6.8 - MTT assay data from experiments involving polymers 3.6, 3.17, 3.3, 3.15, 3.16, 3.18 and 3.12.....	215
Table 6.9 - TUNEL data from experiments involving polymers 3.6, 3.17, 3.3, 3.15, 3.16, 3.18 and 3.12.....	216
Table 6.10 - Cell attachment data from experiments involving polymers 3.6, 3.17, 3.3, 3.15, 3.16, 3.18 and 3.12.....	217

Declaration of authorship

I, Andrew John Treharne, declare that the thesis entitled “Development of biocompatible polymers for ocular applications” and the work presented in the thesis are both my own, and have been generated by me as the result of my own original research.

I confirm that:

- this work was done wholly or mainly while in candidature for a research degree at this University;
- where any part of this thesis has previously been submitted for a degree or any other qualification at this University or any other institution, this has been clearly stated;
- where I have consulted the published work of others, this is always clearly attributed;
- where I have quoted from the work of others, the source is always given. With the exception of such quotations, this thesis is entirely my own work;
- I have acknowledged all main sources of help;
- where the thesis is based on work done by myself jointly with others, I have made clear exactly what was done by others and what I have contributed myself;

Parts of this work have been published in the following publications:

- Thomson, H.A., Treharne, A.J., Backholer, L.S., Cuda, F., Gossel, M.C., Lotery, A.J., Biodegradable poly(α -hydroxy ester) blended microspheres as suitable carriers for retinal pigment epithelium cell transplantation, *J.Biomed.Mater.Res., Part A*, **2010**, *95*, 1233-1243.

- Treharne, A.J., Gossel, M.C., Lotery, A.J., Thomson, H.A., The chemistry of retinal transplantation: the influence of polymer scaffold properties on retinal cell adhesion and control, *Br.J.Ophthalmol.*, **2011**, *95*, 768-773.
- Treharne, A.J., Thomson, H.A., Gossel, M.C., Lotery, A.J., Developing methacrylate-based copolymers as an artificial Bruch's membrane substitute, *J.Biomed.Mater.Res., Part A*, **2012**, *100*, 2358-2364.

In addition this work has been presented at 3 conferences.

Signed:

Date: August 2012

Acknowledgements

I owe a great debt of gratitude to all those who have helped and supported me through my time as a PhD student. I have received excellent academic support from my supervisors Dr Martin Grossel and Prof Andrew Lotery and also my advisor Prof Phil Gale. The Grossel research group members past and present (Alan, Andrew, Jon, Francesco, Richard, Nick, Dominic, Adam and Darren) have also provided a constant source of advice, entertainment, glassware and trips to the pub. In addition, I would like to thank all members of the Lotery research group for all their guidance and support. Having such supportive research groups around me has made my PhD a much more enjoyable experience. Dr Heather Thomson deserves a special mention for her biological expertise, patience and proof reading abilities. This project would not have been possible without her advice and support. I'm also grateful to my project students (Lucy and Claire) who managed to keep me entertained whilst also achieving some impressive results.

I would particularly like to acknowledge contributions by the following people to work reported in this thesis:

Dr Heather Thomson – Assistance with cell-based experiments and assays. Also for processing of cell-based assay results.

Miss Jennifer Scott – For conducting and processing results from later diffusion studies.

Miss Lucy Backholer – For her contribution to experimental work in microsphere synthesis.

Mr Rob Hanson – For performing gel permeation chromatography and differential scanning calorimetry analysis.

Any project in the physical sciences relies on the support of technical services for its successful completion. I am therefore most grateful to Dr Neil Wells and Joan Street (NMR service), Dr Anton Page (Biomedical Imaging Unit) and Rob Hanson (GPC service at the University of Sheffield). I would also like to thank the staff of the Chemistry stores (Karl, Graham, Tony, Clive and Keith) for their helpful and friendly service.

This research would not have been possible without financial support of Foresight RP and the Gift of Sight charities. I am most grateful for all who donated so generously to these organisations to fund the research contained in this thesis.

I've been extremely lucky to have been supported through my PhD by a strong group of friends and family whose kind words have often kept me motivated when the going was rough. My final thanks must go to Jess. I cannot thank her enough for her tireless support of me through the highs and lows of the PhD, endless patience and amazing culinary abilities.

Abbreviations

~	Approximately
2D	Two dimensional
3D	Three dimensional
AGE	Advanced glycation end products
AIBN	2,2'-Azobisisobutyronitrile
AMD	Age-related macular degeneration
ARPE-19	An immortalised human retina pigment epithelium cell line
ATCC	American tissue culture collection
BM	Bruch's membrane
CNV	Choroidal neovascularisation
Da	Daltons
DAPI	4',6-diamidino-2-phenylindole
DCC	Dicyclohexylcarbodiimide
DCM	Dichloromethane
DI	Deionised
DMAP	4-dimethylaminopyridine
DMEM	Dulbecco's modified eagle medium
DMF	Dimethylformamide
DNA	Deoxyribonucleic acid
DSC	Disuccinimidyl carbonate

ECM	Extracellular matrix
EDC	Ethyl(dimethylaminopropyl) carbodiimide
EDTA	Ethylenediaminetetraacetic acid
FBS	Fetal bovine serum
FITC	Fluorescein isothiocyanate
GPC	Gel permeation chromatography
GRGDSP	The peptide sequence Glycine-Arginine-Glycine-Aspartic acid-Serine-Proline
GRGESP	The peptide sequence Glycine-Arginine-Glycine-Glutamic acid-Serine-Proline
HEMA	2-hydroxyethyl methacrylate
ICL	Inner collagenous layer
IR	Infrared (spectroscopy)
K(Flu)RGD	The peptide sequence Lysine(Fluorescein tagged)-Arginine-Glycine-Aspartic acid
LDH	Lactate dehydrogenase
MMA	Methyl methacrylate
MSC	Mesenchymal stem cell
MTT	3-(4,5-dimethylthiazol-2-yl)-2,5-diphenyltetrazolium bromide
NAD⁺	Nicotinamide adenine dinucleotide
NHS	<i>N</i> -hydroxysuccinimide
NMR	Nuclear magnetic resonance (spectroscopy)
OCL	Outer collagenous layer

PBS	Phosphate buffered saline
PBS-T	Phosphate buffered saline with 0.1% Triton-X100
PCNA	Proliferating cell nuclear antigen
pDNA	Plasmid deoxyribonucleic acid
PDT	Photodynamic therapy
PEG	Poly(ethylene glycol)
PEGM	Poly(ethylene glycol) methacrylate
PFA	Paraformaldehyde
PGA	Poly(glycolic acid)
PHBV8	Poly(hydroxybutyrate-co-hydroxyvalerate)
PHSRN	The peptide sequence Proline-Histidine-Serine-Arginine-Asparagine
PI	Propidium iodide
PLA	Poly(lactic acid)
PLGA	Poly(lactic-co-glycolic acid)
PLLA	Poly(L-lactic acid)
PMMA	Poly(methyl methacrylate)
PVA	Poly(vinyl alcohol)
RGD	The peptide sequence Arginine-Glycine-Aspartic acid
RP	Retinitis pigmentosa
RPC	Retinal progenitor cell
RPE	Retinal pigment epithelium

RPE65	Retinal pigment epithelium-specific 65kDa protein
SC	Succinimidyl carbonate
SE	Succinimidyl ester
SEM	Scanning electron microscopy
sem	Standard error of the mean
TE	Tissue engineering
THF	Tetrahydrofuran
TUNEL	Terminal deoxynucleotidyl transferase dUTP nick end labelling
UK	United Kingdom
UV	Ultraviolet
VEGF	Vascular endothelial growth factor
YIGSR	The peptide sequence Tyrosine-Isoleucine-Glycine-Serine-Arginine

1 Introduction

1.1 Introduction

Sight is one of our most treasured senses. As a consequence, loss of sight can have a profound effect on quality of life. Degenerative retinal diseases such as Age-Related Macular Degeneration (AMD) and Retinitis Pigmentosa (RP) are the leading cause of irreversible blindness in the developed world¹. Despite differences in their pathogenesis, both diseases culminate in death of cells in the photoreceptor layer of the retina leading to blindness. Disruption of the retinal pigment epithelium (RPE) is another common feature of these diseases. There are currently no clinical therapies to reverse this loss of cells. Regenerative medicine offers the potential for a cell-based therapy. This PhD thesis explores the complex nature of creating such a therapy and reviews current attempts to make treatment of these diseases a reality. It will describe experiments to better understand the nature of cell-surface interactions with a view to creating a system to deliver cells to the eye.

1.2 Age-related macular degeneration

It is estimated that 1.5 million people in the United Kingdom (UK) have the early signs of AMD². The cost of care for those affected in the UK is estimated at £1.6 billion per year². Due to increasing longevity of life, the number of sufferers is set to increase. Despite the large prevalence of this disease, its pathogenesis and mechanisms of action have only recently started to be understood. The disease affects the macula, the area of the human retina responsible for central vision (Figure 1.1). The macula contains a high percentage of “cone” photoreceptors which are the cells that provide colour vision and fine detail.

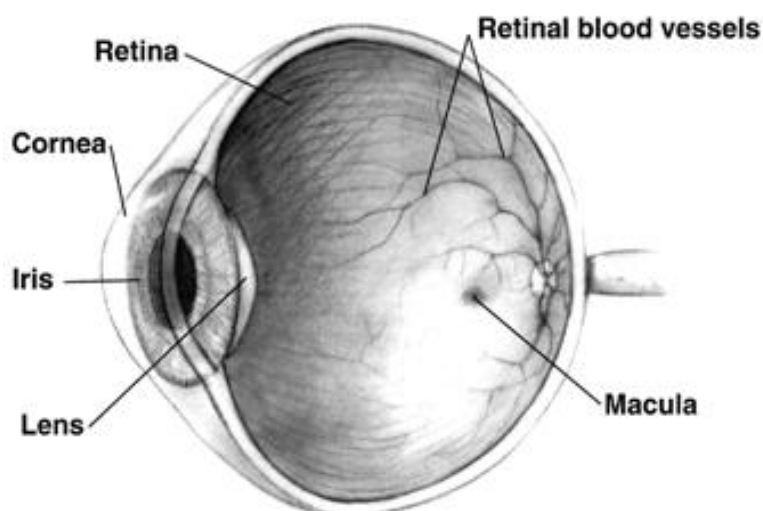


Figure 1.1 - A cross-section of the human eye showing key components including the macula area of the retina. The macula is the area of the retina used for central vision and fine detail. Image courtesy of Wikimedia Commons.

There are two forms of AMD, wet (exudative) and dry (atrophic). The majority of patients (over 90%) have the dry form of the disease (see Section 1.4 below) and for over half of patients with this form it is bilateral. There is currently no treatment for this form of the disease and sufferers undergo a progressive loss of central vision (Figure 1.2). For those with the wet form of the disease, some treatments to halt the loss of vision are available (See Section 1.3 below).

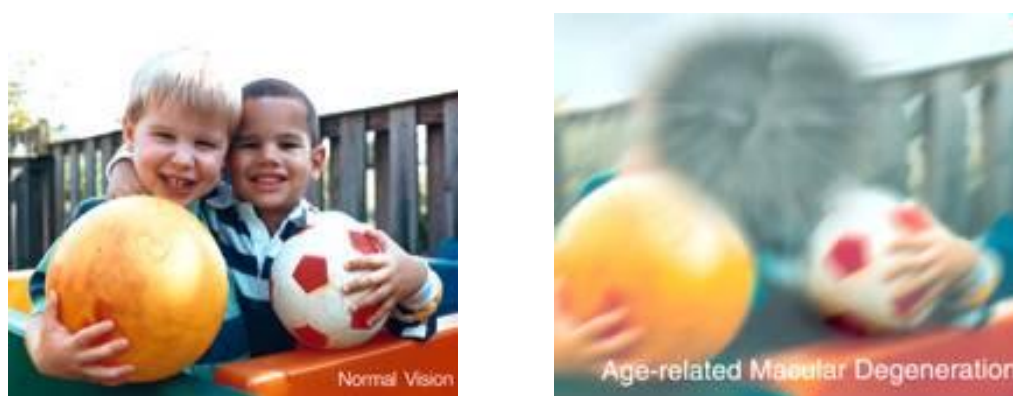


Figure 1.2 - Images showing the impact of AMD on vision. As the disease progresses, there is an increasing loss of central vision. Image courtesy of NIH National Eye Institute.

It is possible for one form of the disease to progress to the other form³. AMD can also be classified as early (little loss of vision) or late (severe loss of vision). In the macula, there are several layers of structure with different functions. Patients with AMD have a dysfunction in one or more of these structures. A simple cross section of the macula is show in Figure 1.3.

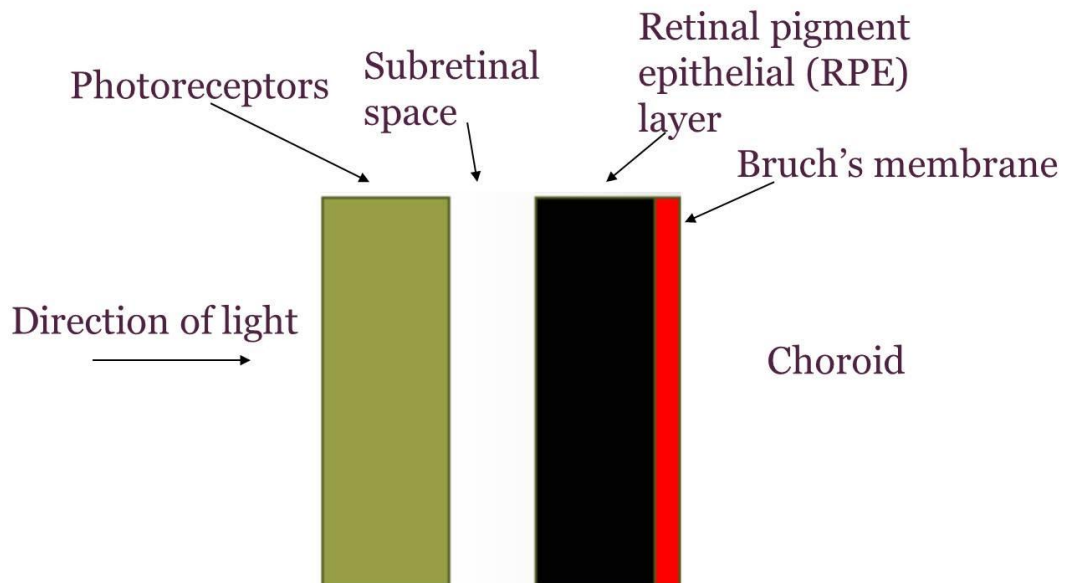


Figure 1.3 - A simplified cross-section of the human macula showing key structures. Bruch's membrane is supportive matrix of the retinal pigment epithelium which in turn supports the function of the photoreceptors. The choroid is one of structures that supplies blood to the retina.

1.3 Wet AMD

The hallmark of wet AMD is the development of new blood vessels growing from the choroid. This process is known as choroidal neovascularisation (CNV). CNV is a result of increased secretion of vascular endothelial growth factor (VEGF) from RPE cells. The reasons for this increase are unclear however hypoxia and inflammation have both been implicated⁴. These new vessels grow through Bruch's membrane (BM) and lie underneath the RPE or grow through the RPE into the subretinal space. Leakage of blood and fluid into and under the retina can also occur. The new blood vessels disrupt the

architecture of the retina leading to RPE detachment and subsequent loss of photoreceptor cells.

A number of therapies have been developed to stabilise CNV⁴. A laser can be used to close or eliminate the leaking blood vessels that are causing the damage. These therapies are thermal laser photocoagulation and transpupillary thermotherapy. An alternative is to use photodynamic therapy (PDT) which utilises a photosensitiser activated by a low energy laser. This results in the production of oxygen free radicals which damage the endothelial cells stabilising the new blood vessels and preventing leakage. The drawbacks to these approaches are that they can cause retinal damage and only stabilise the CNV rather than preventing new vessels from growing. To address this, treatments to block angiogenesis in CNV have been developed. These include anti-VEGF antibodies such as bevacizumab (Avastin)⁵ and ranibizumab (Lucentis)⁶. By blocking the action of VEGF, these agents can arrest the growth of new blood vessels and stabilise the vision of the patient.

1.4 Dry AMD or geographic atrophy

The earliest changes associated with dry AMD are the appearance of basal lamina deposits. These deposits later form drusen which are the clinical hallmark of AMD. Drusen, from the German word for geodes (cavities in rock lined by crystals), appear as yellowy white dots on the retina. As the disease progresses the drusen disappear to leave an area of RPE atrophy. Photoreceptor and choroidal atrophy are also observed. This results in a progressive loss of vision for the patient. The processes that cause these deposits to form and atrophy in the retina are unclear. However, it is likely to be a combination of factors which culminate in the RPE becoming compromised. These factors are discussed below.

1.4.1 Drusen

The deposits between Bruch's membrane (BM) and the RPE known as drusen (Figure 1.4) are generally classified as being either hard (1-63 μ m in diameter) or soft (63-125 μ m in diameter)⁷. They are known to contain many different types of protein, lipid and carbohydrate. Cellular components, of RPE origin, are also found. Despite increasing evidence for the role of the RPE in drusen biogenesis⁷, it is unclear whether drusen formation contributes to or is a consequence of RPE dysfunction.



Figure 1.4 - A retinal photograph showing soft drusen accumulation. The formation of drusen is one of the hallmarks of AMD. Image courtesy of Wikimedia Commons.

1.4.2 Inflammatory effects

More recently, inflammatory events have been linked to the synthesis of drusen⁸. It has been proposed that cellular debris from RPE cells may act as an inflammatory stimulus and a site for drusen formation⁹. In addition, amyloid β which is the pro-inflammatory component of Alzheimer's disease plaques has been found to be present in drusen¹⁰. Discoveries such as this suggest common pathogenic pathways in AMD and other neurodegenerative conditions. Several components which are found to be present in drusen are part of the

complement cascade of the innate immune system. Genetic studies have been able to establish a link between genes for complement proteins and AMD^{11,12}. This provides even stronger evidence that local inflammation plays a key role in the etiology of AMD.

1.4.3 Oxidative stress

The cells of the retina have a high oxygen tension and are exposed to light resulting in an increased vulnerability to protein oxidation¹³. Oxidative modifications to proteins such as crosslinking have been shown to be associated with drusen proteins and are more abundant in AMD than in normal BM¹⁴. This implicates oxidative damage as being a possible cause for drusen formation. The maculas of patients with AMD have been shown to have statistically higher levels of iron¹⁵. Amyloid β plaques found in drusen, which were discussed earlier, have a high affinity for iron. This is a possible explanation of the increased iron concentration in AMD patients. The presence of iron can increase oxidative stress by its ability to form free radicals by the Fenton reaction¹⁵.

1.4.4 Bruch's membrane

BM, named after the German anatomist Karl Bruch, is the support structure for the RPE. It is composed of five layers and lies between the RPE and the choroidal capillaries. Its strategic position results in it being both an anchorage point for the RPE and a diffusion barrier, transporting macromolecules and water between the choroid and the RPE. Of the 5 layers of BM (Figure 1.5), the one closest to the RPE is known as the RPE basal lamina and serves as the attachment point for RPE cells. This attachment is mediated by the interaction between extracellular matrix proteins in Bruch's membrane and cell membrane bound integrin receptors (See Section 1.6.1 for further details). Beneath this there is the inner collagenous layer. This layer seems to be of particular importance in the pathogenesis of AMD as drusen and other deposits accumulate here in preference to other layers of BM¹⁶. Below the inner collagenous layer there lies a layer of elastin

and then the outer collagenous layer. The final layer is the basal lamina of the choriocapillaris serving to connect BM to the choroid. The mechanism for the formation and maintenance of BM is not fully understood. However, it is likely to be secreted from both the RPE and choroidal sides¹⁷. Disruptions to normal functioning of BM can lead to cells in the retina becoming compromised. This has been found to occur in patients with advanced degenerative retinal disorders¹⁸. As RPE cells are anchorage dependant, the integrity of BM is vital to prevent cell death resulting from lack of attachment (anoikis)¹⁹.

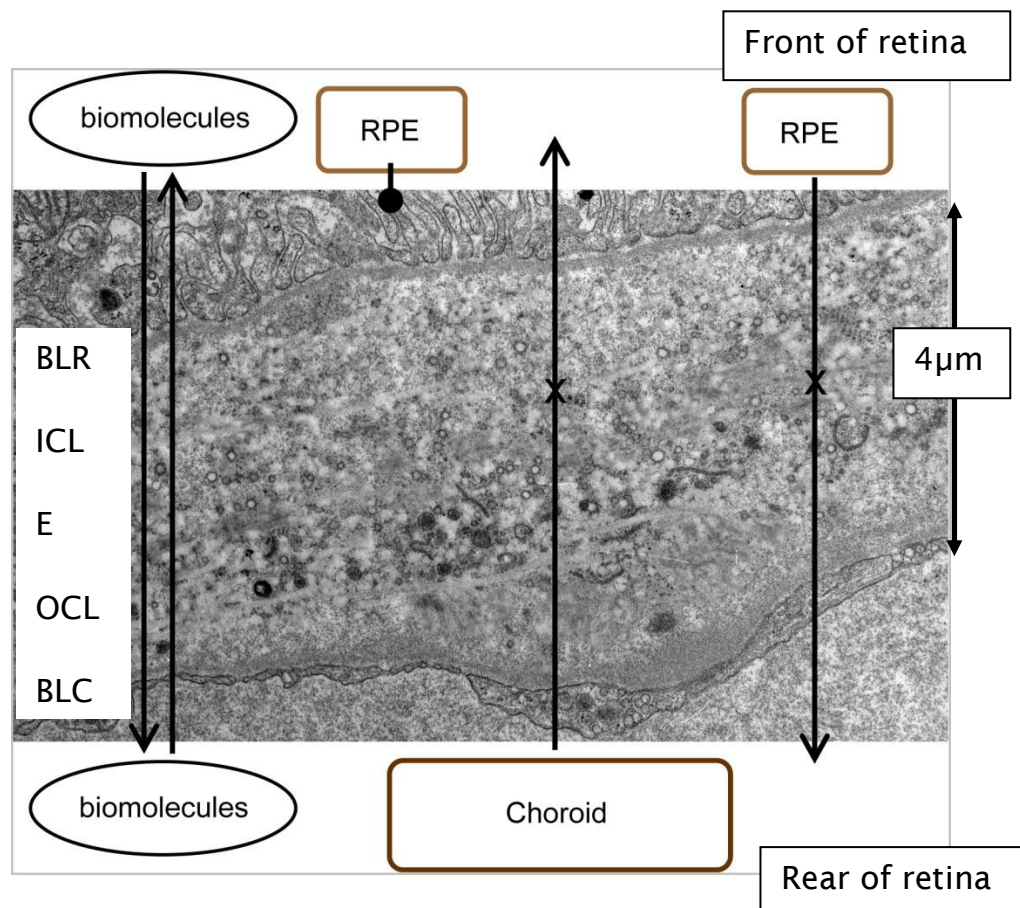


Figure 1.5 – Transmission electron micrograph showing the five anatomical layers of BM. The membrane is permeable to molecular transport but prevents migration of RPE and choroidal cells. BLR: Basal lamina of the RPE, ICL: Inner collagenous layer, E: Elastin layer, OCL: Outer collagenous layer, BLC: Basal lamina of the choriocapillaris. Reprinted from Booij *et al.*, *Prog.Retin.Eye Res.*, 2010, 29, 1-18, Copyright (2009) with permission from Elsevier.

Regardless of disease state, a reduction in macromolecular diffusion across BM with age is observed²⁰. There are a number of reasons for this change in characteristics. It is known that over the course of a lifetime, BM gradually increases in thickness²¹. This creates an increased path length for diffusion leading to a decreased diffusion rate. Also, an increase in collagen crosslinking could reduce the space between fibres in BM resulting in reduced diffusion²². This crosslinking could also explain the reduction in the elasticity of BM with age which has been found to occur independently of AMD²³.

However, the largest factor affecting macromolecular diffusion is likely to be the accumulation of cellular waste products in BM. It is known that there is an accumulation of lipids in the aging BM¹⁷. These lipids have been shown to be of RPE origin and be peroxidised¹³. This again points towards the role of oxidative stress in AMD-related pathology. Lipids are also known to be a component of drusen. It is proposed that lipids inhibit the transport of hydrophilic components across BM. It is not only the diffusion of macromolecules that is affected by the aging BM but also the transport of water (hydrolytic conductivity). The inner collagenous layer of BM has been shown to be the site of major resistance to water transport²⁴. Both remodelling of the structure of BM and the accumulation of lipids have been put forward as reasons for this reduction in water transport²⁵. Any remodelling of the membrane would be controlled by serine proteases and matrix metalloproteinases. Studies of these enzymes could therefore lead to information about how to reverse this process. There is some evidence to show that activation of matrix metalloproteinases from cultured RPE can increase water transport in BM²⁶.

Besides changes in the transport functions of BM, there is evidence to show that adhesion of RPE cells is impaired on aged BM²⁷. As mentioned previously, if RPE cells are not attached to a substrate, they will undergo apoptosis. The amount of apoptotic cells in the

macula is found to increase significantly with age²⁸. In a normal RPE-BM complex, RPE cells attach via integrin receptors on their surface binding to extracellular matrix (ECM) proteins such as laminin and fibronectin which present integrin ligands. Tezel and coworkers have shown that the morphology and fate of RPE cells can alter significantly dependant on the layer within BM to which they are attached^{29,30}. Further to this, it has been shown that debriding and coating of BM with ECM proteins can increase RPE cell survival^{31,32}.

1.4.5 Advanced glycation end products

Advanced glycation end products (AGEs) are compounds which form from reactions between sugars and proteins or lipids. They increasingly accumulate on ECM proteins in BM with age³³. Higher concentrations of AGEs have been found to occur in areas where there are drusen and basal deposits compared with normal areas of BM³⁴. Furthermore, artificial introduction of AGEs to the RPE-choroid complex in a mouse model has been shown to promote RPE aging, inflammation and age-related changes to BM³⁵. AGEs have been shown to induce the activation of AGE receptors in RPE cells contributing to AMD progression³⁶. This creates a strong case for the implication of AGEs and their receptors in the pathogenesis of AMD and other age-related conditions.

1.5 Tissue engineering

Tissue engineering (TE) offers a potential therapy to patients with degenerative retinal diseases. TE “applies the principles of biology and engineering to the development of functional substitutes for damaged tissue”³⁷. It is a multidisciplinary field requiring the skills of chemists, biologists, clinicians and engineers in attempting to mimic nature’s ability to regenerate damaged tissues. In this section, recent advances in the area of TE and how these developments have started to be applied to the treatment of retinal and other disorders will be reviewed.

There are several key strategies involved in using cellular constructs generated by TE for the purpose of regenerative medicine. The first is to implant cells with no support. This involves implanting stem cells or more mature cells into the body with the hope of regenerating lost or damaged tissues. The second involves implanting a synthetic support to encourage tissues to regenerate themselves. The third strategy combines cells with a biodegradable or non-degradable scaffold to support growth and maintenance of regenerated tissues.

1.5.1 Stem cells and their potential in regenerative medicine

The ability of some animals to replace lost or damaged parts of their body has been a constant source of fascination. The newt, for example, can regenerate the whole of its retina following removal³⁸. This has led to some investigating whether the underlying cellular mechanisms involved in this regeneration could be applied to humans³⁹. Central to this strategy is the idea of utilising stem cells as a tool for regeneration. Stem cells are cells which have the capacity for prolonged self-renewal and can become one of many types of cell⁴⁰. They can be broadly divided into two types, embryonic and adult. Embryonic stem cells can be obtained from early-stage embryos whereas adult stem cells (also known as progenitor cells) are found in various tissues of the body. Embryonic stem cells are defined as being pluripotent. This means that given the correct

conditions, these cells have the potential to differentiate into any cell type in the human body⁴¹. In contrast, most adult stem cells are multipotent (or lineage restricted) which means that these cells can only differentiate into cell types within the tissue from which the cells were obtained. More recently, a third category, induced pluripotent stem cells have been gaining interest^{42,43}. These are adult human cells that have been ‘reprogrammed’ to induce pluripotency resulting in a cell that has the same abilities as an embryonic stem cell. This method of obtaining pluripotent cells has the potential to overcome problems with obtaining embryonic cells. However, the ability of both embryonic stem cells and induced pluripotent stem cells to readily form tumours together with potential rejection issues provides a significant obstacle to their safe use in regenerative medicine⁴⁴.

One of the most commonly used class of adult stem cells are mesenchymal stem cells (MSCs). These cells, which can be harvested from bone marrow, can be grown in culture and differentiated into many different types of cell (Figure 1.6). These include bone, muscle, ligament and cartilage⁴⁵. As a consequence, suspensions of MSCs have been utilised in investigating regeneration of the heart⁴⁶. They have also started to be used in several other areas of regenerative medicine such as for bone defects and non-healed skin wounds with some promising results from early clinical trials⁴⁷. In addition to transplantation, several studies have investigated the use of an “*in vivo* bioreactor” for generation of new bone^{48,49}. The idea of these bioreactors is that they are implanted into an area rich in MSCs that can then grow into the reactor to form new tissue. This tissue can then be harvested and moved to the site where it is needed.

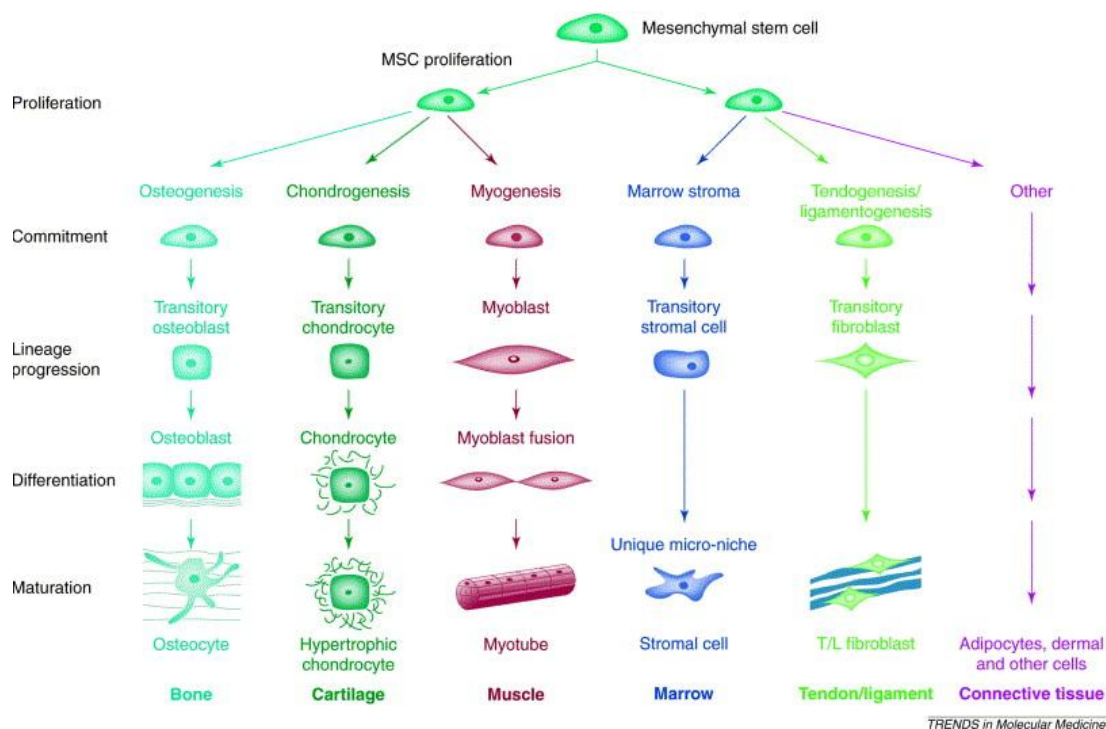


Figure 1.6 – Diagram to show the differentiation pathways of mesenchymal stem cells. The wide variety of tissues that can be derived from these cells has led to extensive investigation of their use for regenerative medicine. Reprinted from Caplan *et al.*, *Trends Mol.Med.*, 2001, 7, 259-264, Copyright (2001) with permission from Elsevier.

1.5.2 Regenerating the retina without use of a scaffold

In the area of retinal regeneration, efforts have focused on generating or harvesting RPE cells for use in RPE transplantation therapy. It is thought that transplantation of RPE under the retina has the potential to support the recovery of photoreceptors and provide a treatment for degenerative retinal diseases¹³. Embryonic stem cells can be differentiated to become RPE precursors. These precursors were observed to form RPE monolayers *in vivo*⁵⁰ providing a potential source of RPE cells. Work in the area of induced pluripotent stem cells has shown that RPE cells can be derived and form highly differentiated RPE monolayers⁵¹. Using this method of RPE production could overcome problems of immune rejection associated with embryonic stem cells as the cells could be derived from the patient's own cells. However, the problem of tumour formation when using these cells still remains⁴⁴. Binder *et al.*⁵² have investigated whether

transplantation of patches of autologous RPE from one site to another could prevent photoreceptor death (Figure 1.7). It was found that such transplantation in a rabbit model decreased photoreceptor loss. Sheets of human foetal retina and RPE have also been transplanted into rat eyes⁵³. However, transplantation of RPE cell suspensions and RPE-choroid sheets in patients with AMD has so far had only limited success⁵⁴. A study of macula translocation in 64 wet AMD patients showed this technique to be more successful. Significant improvements in visual function reported from patients in this trial⁵⁵. However, the complex nature of the surgery involved in this type of therapy could limit its application. In addition, it does not address the underlying neovascularisation.

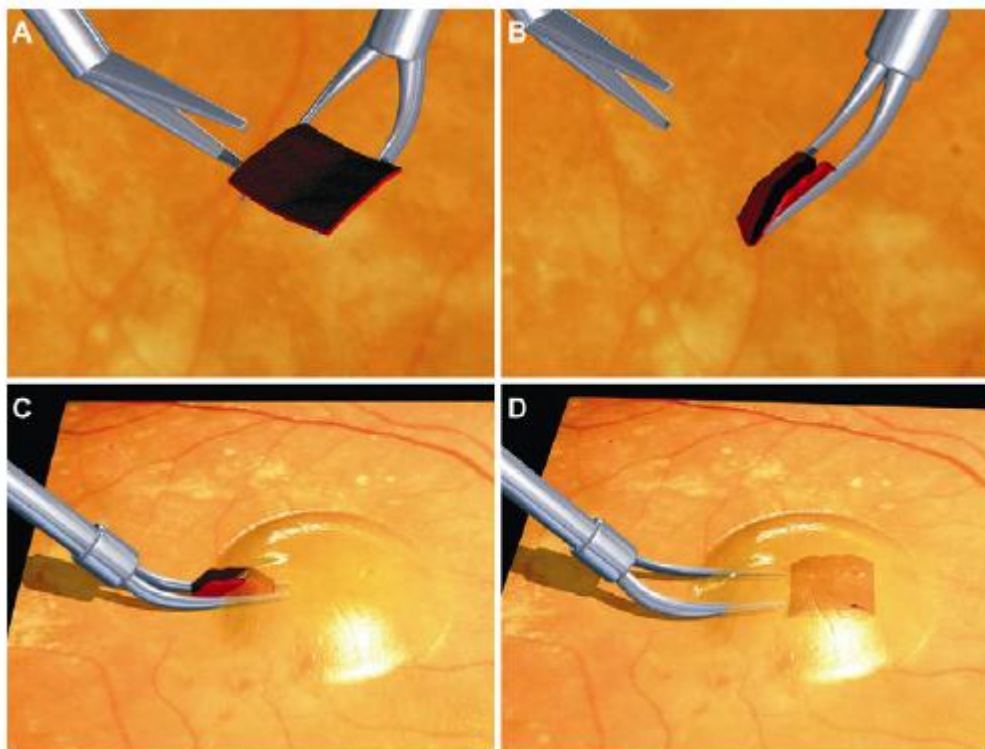


Figure 1.7 - Cartoon showing the implantation of a sheet of RPE and choroid. The sheet is first placed on subretinal forceps (A) before being folded (B). It is then implanted into the subretinal space (C) before being unfolded and positioned (D). Reprinted from Binder *et al.*, *Prog.Retin.Eye Res.*, 2007, 26, 516-554, Copyright (2007) with permission from Elsevier.

In addition to RPE transplantation, the area of photoreceptor replacement has been investigated. It has been shown that retinal cells taken from early post natal mice have the potential to form rod photoreceptors when transplanted into an adult mouse⁵⁶. This study found that the cells needed to be harvested at the peak of photoreceptor genesis in order to achieve good integration into the retina. Further, adult stem cells in the form of retinal progenitor cells (RPCs) have been isolated and found to give rise to different types of retinal cell⁵⁷. Experiments using such cells in mouse models have shown promising results⁵⁸. However, it has been noted that problems such as lack of organisation and poor cell survival can reduce the efficacy of using a cell suspension alone⁵⁹. It has also been shown that modifications to BM would be necessary to support cell transplantation^{32,60}. Such difficulties have led many researchers to use a scaffold-based approach to delivering cells to a target area.

1.6 Use of scaffolds in tissue engineering

1.6.1 The extracellular matrix – nature's scaffold

The use of a cellular scaffold for applications in TE is a further attempt by researchers to mimic nature. In the body, cells are supported by their own natural scaffolding, the extracellular matrix (ECM). In some tissues such as bone and cartilage, the ECM is the main constituent of the tissue. The ECM is not only a structural support but has a vital role in cell signalling⁶¹. The mechanical stiffness of the ECM can influence cell fate. For example, growth of MSCs on softer ECM induced neuronal growth whilst more rigid matrices induced bone growth⁶².

The ECM also signals to cells biochemically via interactions with integrin receptors on the cell surface⁶³. The interaction between ECM proteins and integrin receptors forms the basis of cell adhesion. Integrins are heterodimeric transmembrane proteins. They interact with specific amino acid sequences in ECM proteins such as the Arginine-Glycine-Aspartic acid (RGD) sequence⁶⁴ (Figure 1.8). Crystallographic studies have shown that the guanidinium group of arginine forms a salt bridge to aspartic acid residues in the receptor⁶⁵. The carboxylate group of aspartic acid in the ligand coordinates to a divalent metal ion whilst the carbonyl oxygen forms hydrogen bonds with other amino acids in the receptor. The glycine residue participates via hydrophobic interactions with carbonyl oxygens. The interaction is very specific for certain amino acid sequences such as RGD. Changing the aspartic acid (D) to glutamic acid (E) leads to a ligand that is 2000 times less active towards the receptor⁶⁶. The interaction between the ligand and the integrin causes conformation changes within the receptor protein leading to the clustering of integrins into focal adhesions⁶⁷. Focal adhesions are complexes of proteins and growth factors that join ECM proteins to actin filaments in the cell cytosol. In epithelial cells, the binding of a substrate to the integrin receptor can also lead to the formation of

hemidesmosomes⁶⁸. These complexes join keratin filaments in the cell cytosol to the ECM.

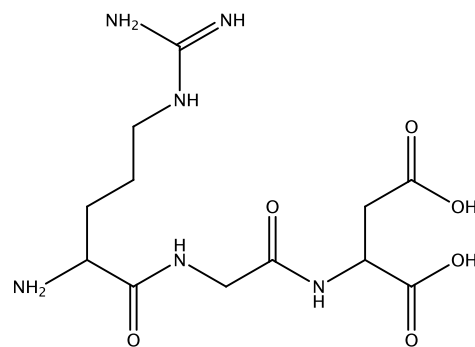


Figure 1.8 – The chemical structure of the Arginine-Glycine-Aspartic acid (RGD) peptide.

The ECM is composed of various structural proteins (Figure 1.9) with the most abundant being collagen. Collagen is known to self-assemble into fibrils which can crosslink into collagen fibres⁶⁹. These fibres provide strength to tissues such as bone and skin. The second most abundant protein in the ECM is fibronectin⁷⁰. This fibrillar protein is rich in the Arginine-Glycine-Aspartic acid (RGD) peptide sequence, an important mediator for cell attachment via integrin receptors. Elastin is another major component of the ECM⁷¹. It is formed by covalent crosslinking of its soluble precursor tropoelastin. As its name suggests, elastin is a mechanically elastic part of the ECM. In addition to these three, laminin, fibrin, hyaluronan and glycosaminoglycans also contribute to different properties of the ECM including wound healing, water retention and cell migration⁷².

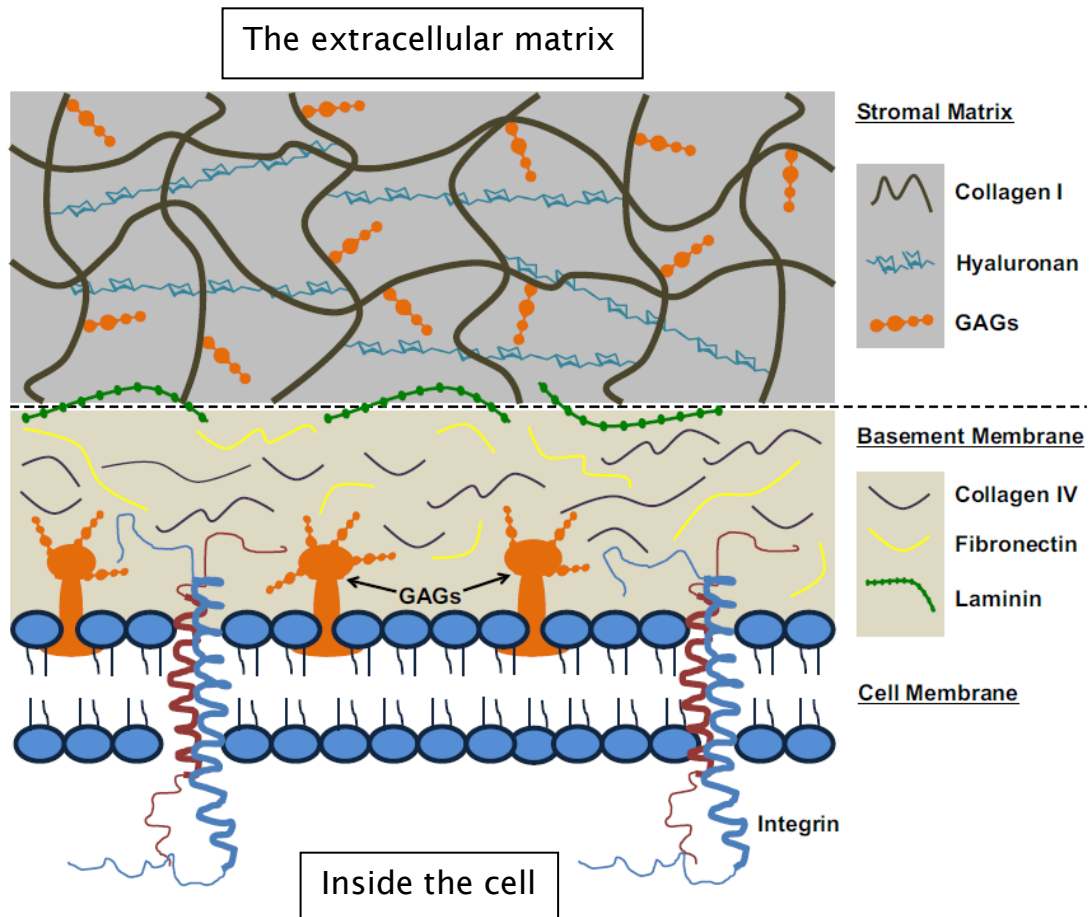


Figure 1.9 - Cartoon showing the distribution of proteins in the extracellular matrix. Reprinted from Kuraitis *et al.*, *Biomaterials*, 2012, 33, 428-443, Copyright (2012) with permission from Elsevier. GAGs: Glycosaminolycans

1.6.2 Use of natural materials for tissue engineering

The natural ability of the ECM to act as a cellular support has led to investigation of the potential for its protein components to be used as a scaffold for TE and regenerative medicine⁷². The ECM is often harvested from cell lines. For example, the ECM of a mouse sarcoma cell line is used for the commercial product Matrigel®. This product is used in various TE applications. In the area of regenerative medicine, a decellularised rat heart has been successfully seeded with neonatal heart cells and shown some level of function⁷³. ECM proteins have also been investigated for regeneration of skin⁷⁴ and muscle⁷⁵. Furthermore, examples of ECM being commercialised and used in the clinic are being seen for regeneration and repair of skin, bone, cartilage and blood vessels⁷⁶. These ECMs include decellularised skin

and demineralised bone. However, the ECM is not the only natural material that has been used for TE. Many researchers have sought to utilise silk as a biomaterial for a variety of TE applications⁷⁷. The problem with using any tissues based on animal components is the possibility of transmitted infection and immunogenicity. In an attempt to overcome this, some researchers have started to develop biomaterials based on synthetic peptides^{78,79}.

In the area of ocular TE, natural materials are being used to aid regeneration of the cornea and the retina. For example, silk has been investigated as a biomaterial for TE in the cornea⁸⁰. In addition, ECM materials such as collagen have been used to mimic the ECM environment of the cornea^{81,82}. Collagen films have also been trialled as a BM replacement to support RPE cell growth⁸³. It was found that these films were comparable in thickness to native BM and that there was sufficient nutrient flow through the membrane to support RPE survival. The permeability of human lens cap has also been shown to be comparable to that of BM giving the potential for another RPE substrate⁸⁴. Hydrogels based on natural polymers have also been investigated as a delivery vehicle for RPCs⁸⁵. These delivery mechanisms were found to more evenly distribute cells within the subretinal space compared to an injection of cells as a suspension. There are, however, a number of significant drawbacks with these natural materials including the potential for immune rejection and a lack of control over the binding of cells to the scaffold surface. In addition, the variability of natural tissues and a lack of availability present additional concerns.

1.6.3 Use of synthetic scaffolds for tissue engineering

Given the drawbacks associated with the use of naturally derived scaffolds, researchers have been synthesising scaffolds from various polymeric materials. A successful synthetic scaffold will employ different techniques to emulate the properties of the ECM. There are many factors to consider in designing such a scaffold centring on the

interaction between the scaffold and its cellular surroundings. Materials intended for use in biological systems are commonly termed biomaterials. The use of biomaterials in medicine has its roots in ophthalmology. Sir Harold Ridley, a British ophthalmologist, observed that some Spitfire pilots returning from World War 2 had shards of plastic imbedded in their eyes⁸⁶. The plastic was found to be poly(methyl methacrylate) (PMMA) and had originated from the cockpit canopy. He found that eye had healed and that the presence of the plastic seemed to be tolerated by the body. This observation led to his development of the intraocular lens made from PMMA for the treatment of patients with cataracts. Since then, the development of polymers for medical purposes has yielded many different materials for use in TE.

In the search for a biocompatible scaffolding polymer, much research has focused around biodegradable polyesters particularly poly(lactide) (PLA) and poly(glycolide) (PGA)-based materials⁸⁷. These biomaterials already have regulatory approval for human clinical use following their use as medical sutures. PLA, PGA and their co-polymers are easily hydrolysed *in vivo* to give lactic and glycolic acid that can be metabolised by the body. These polymers also have the advantage that their degradation and morphology can be tuned dependant on their intended application. PGA is known for its mechanical properties, exhibiting a high stiffness due to its high degree of crystallinity. It degrades over the course of several months. PLA can be made as several different polymers, as lactide is optically active. The naturally occurring isomer, L-lactide, can be made into poly(L-lactide) (PLLA). This polymer degrades slower than PGA due to its increased hydrophobicity. The higher molecular weight forms of this polymer can take several years to fully degrade *in vivo*. The racemic form of PLA, poly(DL-lactide), has a lower strength due to its amorphous nature and a faster degradation time than PLLA and is therefore preferred for some applications. A range of co-polymers

based on PGA and PLA have been developed. The degradation rates of these poly(lactide-co-glycolide)s (PLGA)s can be tuned based on the ratio of different monomer units present. Their cell adhesive properties have made them good candidates for TE applications. PLA, PGA and their co-polymers have been made into many different types of structure for use as a cellular scaffolding material⁸⁸. Examples of their medical application as a cellular scaffold include bone⁸⁹, cartilage⁹⁰ and skin⁹¹. Several other biodegradable polymers have been investigated for their properties as a cellular scaffold such as poly(urethane)s, these have been reviewed in depth elsewhere⁹².

Various non-degradable materials have also been studied for use in biomedical applications. Poly(glycerol sebacate) has been used to create an elastomeric patch for delivery of stem cells to the heart⁹³. Furthermore, poly(2-hydroxyethyl methacrylate) has been tested as artificial skin⁹⁴. It is a useful biopolymer due to its ability to form hydrogels. Poly(2-hydroxyethyl methacrylate) and its co-polymers have also been used for regeneration of nerve conduits⁹⁵.

In the area of retinal regeneration, both degradable and non-degradable polymers have been investigated for their use in cell delivery. Young and co-workers have investigated use of porous scaffolds based on biodegradable polyesters for the delivery of retinal progenitor cells (RPCs)⁹⁶. The authors used a variety of techniques such as phase inversion and solid-liquid phase separation to produce an organised porous film based on PLLA and PLGA. It was found that the films produced by solid-liquid phase separation were appropriate for TE applications. Furthermore, when RPCs were seeded onto these polymer scaffolds, markers for photoreceptor specific differentiation were found to be upregulated. When injected into a mouse model the RPCs on the biodegradable films were found to survive significantly better than cells injected alone⁵⁹. Building on this work, Thomson *et al.*⁹⁷ were able to demonstrate that membranes produced using a solid-liquid phase separation technique from different blends of PLGA

and PLLA could give different surface morphologies. These differences were found to affect adhesion and survival of a human immortalised RPE cell line (ARPE-19). Beyond giving rise to morphological differences, blending the two polymers produces a material with more flexible mechanical properties. Poly(caprolactone) is a polyester that degrades slower than PLLA and PLGA due to its increased hydrophobicity. Nanowires based on this polymer have been manufactured using a spin-cast/solvent evaporation technique⁹⁸. It was found that mouse RPCs could adhere and proliferate on this scaffold. More recently, much attention has focused on scaffolds produced using an electrospinning technique. This technique and its applications will be reviewed later in Chapter 3.

Aside from traditional polyesters, poly(glycerol-sebacate) has been researched as a tool for retinal cell delivery⁹⁹. This polymer has shown superior elasticity compared to other scaffolds making it more suitable for transplantation. Mouse RPCs were found to adhere to scaffolds of this polymer and survive when transplanted into a host retina¹⁰⁰. Poly(hydroxybutyrate)s have received some attention as a potential biomaterial due to their degradation products being a natural component of human blood. This reduces the chance of toxic effects from this polymer. Copolymerising with hydroxyvaleric acid reduces the overall crystallinity of the resulting polymer making it more easily processed. Poly(hydroxybutyrate-co-hydroxyvalerate) (PHBV8) films have been trialled as a vehicle for RPE transplantation¹⁰¹. Films of PHBV8 were found to support the attachment and proliferation of an RPE cell line. It was found that changing the properties of the surface by treatment with an oxygen plasma could change the way that cells interacted with the surface. There has been a large focus on the treatment of biomaterials to control cell-surface interactions. This will be reviewed in more depth in Section 1.7.

Besides biodegradable polymers, non-degradable or biostable polymers have also been considered for retinal repair. Films of

poly(methyl methacrylate) (PMMA) either smooth or with micromachined holes have been tested for the ability to transplant RPCs to the sub-retinal space¹⁰². No adverse response was observed when these scaffolds were transplanted into mouse eyes. Cell adhesion and integration into the host retina appeared to be improved when a porous substrate was used. This again demonstrates the importance of the interaction between cells and the surface in the design of implantable materials. Commercial poly(urethane)s¹⁰³ and poly(dimethylsiloxane)s¹⁰⁴ have also been assessed for compatibility with retinal cell types. They were found to produce monolayers of RPE cells on the surface. However, an air or oxygen plasma treatment was needed in some cases to modify the surface in order for the cells to attach.

1.7 Control of cells on surfaces

In designing materials for regenerative medicine, one of the key considerations is how the material will interact with its biological surroundings. The surface-cell interaction is of particular importance in all areas of TE including the retina¹⁰⁵. Much research has focused on discovering the factors that influence this interaction. The response of cells to a surface is largely mediated by integrin receptors on the cell surface. In a natural tissue, the receptors interact with structural proteins in the ECM such as collagen, laminin and fibronectin. When a biomaterial is inserted into the body, the reaction of surrounding tissues is determined by the interaction between the material and proteins which adsorb onto the material. If proteins adsorb in a non-specific way, then an inflammatory reaction can result as the immune system recognises a foreign body. The control of this interaction between the material and adsorbed proteins is therefore of key importance and is determined by the properties of the surface. There are several strategies involved in mediating this adsorption. One strategy is to prevent protein binding through introduction of hydrophilic groups. However, a surface which is either too hydrophilic or hydrophobic may also resist cell adhesion¹⁰⁶. Therefore, in modifying a surface, the correct hydrophilic/hydrophobic balance must be sought. If an increase in hydrophilicity is required the surface can be modified with polarised chemical groups such as alcohols, amines and carboxyls. It has been shown that these different chemical groups can affect neural stem cell adhesion and differentiation¹⁰⁷. A change in surface chemistry can also be achieved through plasma treatment. Nelea *et al.* were able to show that modification of nylon and poly(propylene) with an ammonia plasma could inhibit production of type X collagen in MSCs¹⁰⁸. This was found to differentiate the cells in the appropriate way for particular types of TE. Carbon dioxide plasma treatments have been shown to improve cell attachment on PLLA surfaces¹⁰⁹. PLGA has been plasma modified with both titanium oxide¹¹⁰ and

amine¹¹¹ plasma for TE uses. In the area of retinal TE, air plasmas were used to treat poly(urethane)¹⁰³ and poly(dimethylsiloxane)¹⁰⁴ resulting in increased adhesion of RPE cells. In addition, treatment of PHBV8 with an oxygen plasma was again found to increase adhesion of an RPE cell line¹⁰¹.

Another strategy in controlling the material-cell interaction is to adsorb or chemically bind ECM proteins such as laminin, fibronectin and collagen to the surface. For example, using plasma and chemical methods to attach the ECM protein laminin to the surface of PLGA was found to increase adhesion of Schwann cells for potential use in nerve TE¹¹². In another study, attachment of collagen to PLGA surfaces was found to increase chondrocyte cell adhesion for potential use in regenerating articular cartilage¹¹³. Coating with laminin has been heavily used in retinal TE to promote the attachment of retinal progenitors^{59,98,100,102}. However, problems can be encountered with using whole proteins such as high cost and obtaining pure proteins. In addition, if proteins bind in an incorrect conformation, cell adhesion may be impeded due to inaccessibility of binding sites.

To overcome the problems associated with whole proteins, researchers have turned their attention to synthetic alternatives. In 1984, Pierschbacher and Ruoslahti discovered that the simple peptide sequence Arginine-Glycine-Aspartic acid (RGD) in fibronectin (and subsequently found in other ECM proteins) was one of the essential recognition sequences for cell adhesion¹¹⁴. It was later found that this was due to interactions between this peptide sequence and integrin receptors. Integrins are heterodimeric proteins having an α and β subunit both containing binding sites for the RGD sequence as discussed previously in Section 1.6.1. Besides RGD, other peptides sequences have been found to bind to integrin receptors thereby promoting cell adhesion⁶⁴. These sequences can be specific to certain ECM proteins and show specificity for certain types of integrin receptor. There is some evidence to show that these other

sequences, such as Tyrosine-Isoleucine-Glycine-Serine-Arginine (YIGSR) found in laminin and Proline-Histidine-Serine-Arginine-Asparagine (PHSRN) found in fibronectin, can act synergistically with the RGD sequence¹¹⁵. Use of longer peptides with amino acids flanking the RGD sequence were found to be more active than RGD alone¹¹⁶.

The introduction of these peptides, which can be produced synthetically, into *in vitro* tissue culture would inhibit cell adhesion by blocking integrin receptors. Therefore, researchers have been developing techniques to chemically couple these peptides to surfaces¹¹⁷ (Figure 1.10). One potential route is to react the peptide with an acid-functionalised surface using a peptide coupling reagent such as dicyclohexylcarbodiimide (DCC) or 1-ethyl-3-(3-dimethylaminopropyl)-carbodiimide (EDC). However, this approach is undesirable as further purification is required which could lead to hydrolysis of the peptide. This problem can be overcome by converting the acid to an *N*-hydroxysuccinimidyl (NHS) activated ester. This allows the peptide coupling to be carried out in phosphate-buffered saline (PBS) immediately prior to cell seeding.

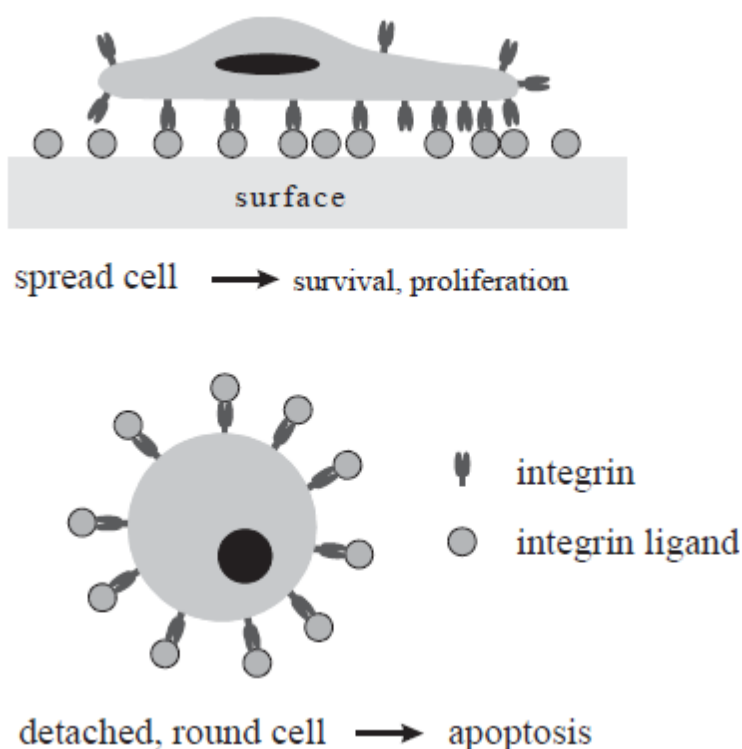


Figure 1.10 – Cartoon showing the effects of integrin ligands. When attached to a surface, integrin ligands such as the RGD peptide sequence encourage cell adhesion and survival. However, if not immobilised, these ligands can act as integrin antagonists and contribute to cell death. Reprinted from Hersel *et al.*, *Biomaterials*, 2003, 24, 4385-4415, Copyright (2003) with permission from Elsevier.

The attachment of a cell adhesion peptide to the surface of an intended biomaterial must be done in a controlled manner to achieve the appropriate cellular effect. In a protein, the cell adhesive peptide sequence will be presented as an exposed peptide sequence¹¹⁴. Therefore, in an artificial system, it has been shown that separating the peptide from the surface by use of a spacer can increase cell adhesion^{118,119}. Surface distribution of these peptides has also been shown to be important. There is some evidence to suggest that the clustering of cell adhesive peptides can improve cell adhesion¹²⁰. In this study, poly(ethylene glycol) (PEG) was used as a spacer between the bulk polymer and the peptides. Using PEG in this way has been shown to create a surface which resists undesired non-specific protein

adsorption¹²¹. Peptides were then attached to the ends of the PEG chains to elicit the desired cellular adhesion. This strategy has also been employed in other TE studies^{122,123}. Other alkyl-based spacers have also been used¹²⁴. The results of several studies have indicated that a distance between the bulk polymer and the integrin ligand of greater than 3.5nm is needed for effective integrin binding^{118,124}.

A greater understanding of the mechanism of interactions between specific peptide sequences and cells, has led to the development of stimuli responsive biomaterials¹²⁵. Materials that can respond thermally, enzymatically, optically and electrochemically to switch between a non-cell adhesive and cell adhesive states have been designed. Furthermore, non-peptide synthetic analogues of the RGD sequence have been synthesised¹²⁶. It was shown that when coupled to a poly(ethylene terephthalate) surface via an triethylene glycol spacer, these peptidomimetics could significantly increase cell adhesion. Additionally, some groups have designed hydrogels containing RGD peptides that can be patterned by light to guide cellular growth in three dimensions^{127,128}.

The deepening knowledge of biomaterial-cell interactions has been translated into improving cellular scaffolds for TE^{129,130}. For example, the presentation of ECM mimicking peptides on a gold surface has been shown to control the differentiation of neural progenitor cells for nerve TE¹³¹. Modification of a poly(urethane urea) polymer with PEG and the cell adhesive peptide YIGSR was found to enhance endothelial cell adhesion whilst resisting platelet adhesion¹³². Achieving this balance is essential in the development of synthetic vascular grafts. Modification of PLGA and PLLA surfaces with RGD peptides has been used to control the growth of osteoblasts creating an enhanced surface for growth of bone graft¹³³. In the area of ocular TE, poly(methyl methacrylate) (PMMA) surfaces were grafted with PEG before cell adhesive peptides were attached to the ends of the PEG chains¹³⁴. It was shown that the presence of PEG resulted in the

material resisting human corneal stromal cell adhesion but when the peptide was introduced, cell adhesion could be restored. This allowed micropatterning of the cells on the PMMA surface. This material has potential applications for generating artificial corneas.

Whilst a major contributing factor, it is not only surface chemistry which controls the behaviour of cells. The morphology of the surface also has an important role. In human tissues, the morphology of the underlying basement membrane has been shown to provide appropriate cues for the cells growing on it^{135,136}. Recent studies demonstrate that cells grow preferentially on rough surfaces rather than smooth^{97,137,138}. It has also been shown that the texture and morphology of electrospun polymer fibres can affect the shape and proliferation of MSCs¹³⁹. There are several possible explanations as to why increases in surface roughness should increase cell adhesion and proliferation^{137,140}. One area to consider is that a rough surface may be able to bind cell adhesion proteins (either in the cell media or secreted by the cell) in different conformations compared to a smooth surface. This may generate more favourable interactions between these proteins adhered to the surface and the cells¹⁴⁰. In addition, a rough surface will generate a higher surface free energy than a smooth one due to increased surface area. When a cell attaches to a surface, binding will be driven by the reduction in free energy of the system. Binding will be favoured when the reduction in surface free energy is greater than the increase in free energy caused by the formation of cell adhesion complexes. This reduction in free energy will be greater on a rough surface than a smooth one¹³⁷. Consideration of appropriate, tissue specific morphology is therefore another essential factor to be considered when designing substrates for cellular growth and TE^{141,142}. The mechanical properties of the scaffold are also an important factor in controlling cellular growth. The stiffness^{143,144} and elasticity^{62,145} of substrates have been shown to

influence differentiation of stem cells and control over cellular function.

1.8 Aims of research

For the majority of patients suffering with AMD, there is currently no treatment. AMD causes the death of photoreceptor and RPE cells which has been linked to a compromised BM. This PhD thesis investigates the interactions between polymeric substrates and RPE cells towards development of a cell-based therapy for degenerative retinal diseases. One aim was to develop a biodegradable scaffold suitable for the delivery of cells to the subretinal space. A successful delivery system could be used to replace cells in the retina lost through disease. The other aim was to create a material that could be used as an artificial BM. This could be utilised as a replacement for the compromised native BM and to aid RPE transplantation. In order to be successful, these materials must readily adhere to and be compatible with RPE cells as well as presenting minimal cytotoxicity. Subsequent chapters will describe the preparation and testing with RPE cells of both biodegradable microspheres and a fibrous methacrylate-based substrate in pursuit of these aims.

2 Developing biodegradable microspheres as a cell carrier

2.1 Introduction

As discussed in Chapter 1, one of the key problems associated with degenerative retinal disorders is loss of retinal pigment epithelial (RPE) and photoreceptor cells. If appropriate stem cells could be successfully delivered to the retina and encouraged to integrate and form functional connections, this could provide a potential therapy. However, injection of stem cell suspension could lead to problems such as immune response, disorganisation of the cells and cell death. Studies by Young and co-workers^{59,96} have demonstrated that by delivering retinal progenitor cells (RPC's) to the retina on a biodegradable scaffold, it is possible to overcome these problems. RPC's are the adult stem cells of the retina and have the potential to differentiate into any retinal cell type⁵⁹. In addition, there is evidence that the presence of a scaffold could encourage RPC's to differentiate into retinal cell types¹⁴⁶. An ideal scaffold for cell-based therapy should be easily injectable, suitable for the adherence of retinal cell types and non-toxic.

The biodegradable cell scaffolds used by Young and co-workers were porous films based on poly(L-lactic acid) (PLLA) and poly(DL-lactic-co-glycolic acid) (PLGA) (Figure 2.1). These type of poly(ester)s have been approved for clinical use as they degrade into water soluble, non-toxic products¹⁴⁷. They are also easily processed and have been used previously for TE applications such as regeneration of bone⁸⁹ and cartilage¹⁴⁸. The degradation rates and mechanical properties of these polymers are determined by the degree of crystallinity. Their properties can therefore be tuned by altering properties such as molecular weight and ratio of lactic to glycolic units¹⁴⁹. This chapter

describes the manufacture of microspheres based on biodegradable poly(ester)s and their development as a retinal cell carrier.

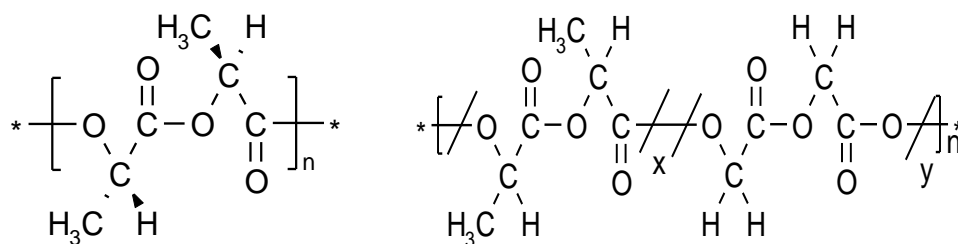


Figure 2.1 - Chemical structures of poly(L-lactic acid) (PLLA) and poly(DL-lactic-co-glycolic acid) (PLGA).

2.2 Microspheres

2.2.1 Manufacture

Most microspheres manufactured for use in a biological setting use either synthetic or naturally occurring polymers¹⁵⁰. Although there are many techniques for producing spheres in the micro- and nano- size range, the most commonly used is an emulsion-based solvent evaporation/extraction system¹⁵⁰. The basic principle of this technique relies on solvent removal from polymer-containing droplets in a non-solvent. Using this method, the chosen polymer is first dissolved in a volatile organic solvent. This solution is then added to agitated water, often containing a stabiliser such as poly(vinyl alcohol) (PVA) (Figure 2.2). As the solvent evaporates, solid microparticles are formed. It is important for this process that the polymer solvent has a lower boiling point than water and is water-miscible. These microparticles can then be harvested using either centrifugation or filtration. It is also common to use a 'double emulsion' variation on this technique whereby an initial emulsion (often water in oil) is added to a large volume of non-solvent to produce microspheres. This technique is often employed to incorporate water soluble compounds into microspheres. It can also be used to create porous microspheres by incorporation of a carbonate in the initial water in oil emulsion¹⁵¹.

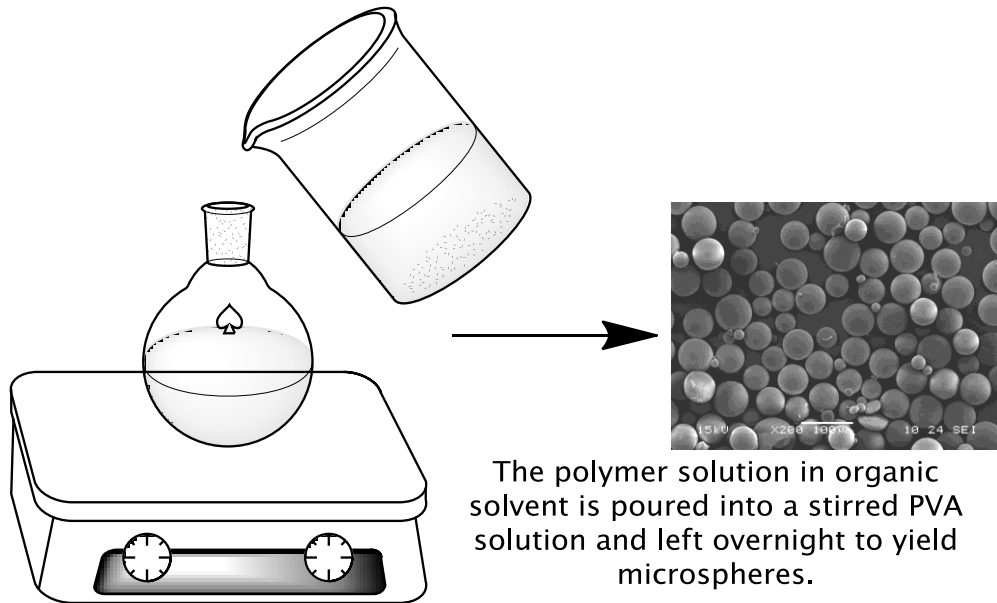


Figure 2.2 - An illustration of a simple emulsion-based microsphere preparation technique.

Using these emulsion-based techniques, several factors can affect the resulting microspheres. Increasing the concentration of the stabiliser has been shown to lead to a decrease in the average diameter of the microspheres¹⁵². However, an increase in polymer solution concentration has been shown to lead to an increase in the average diameter of microspheres^{153,154}. This is because solutions of higher concentration are more viscous and therefore require larger shear forces to generate smaller droplets. In addition, Berkland *et al.*¹⁵⁵ demonstrated that utilisation of acoustic excitation at the needle tip can result in microspheres of a uniform size. Stirring velocity is another factor that can affect droplet formation. It has been shown that increased stirring velocity can decrease the average size of microspheres¹⁵². However, results from Gabler *et al.* suggest that stirring velocity was relatively insignificant when compared with the influence of polymer solution concentration¹⁵³. A drawback of this emulsion-based technique is that any water-soluble components incorporated into the polymer solution could leach out during solvent evaporation in the final step.

An alternative to using a simple emulsion-based approach is to use phase separation to produce microspheres¹⁴⁹. Using this method, the polymer is dissolved in an organic solvent and any water-soluble components are dissolved in water and added to this solution to create a water-in-oil emulsion. The gradual addition of an organic non-solvent results in phase separation creating droplets of polymer which encapsulate the water soluble components. These droplets are transferred to another non-solvent to harden the microspheres. The drawback of this method is that the microspheres can aggregate due to a lack of emulsion stabiliser. However, as this method does not require a solvent that is both water miscible and also has a higher boiling point than water, the solvent system can be more flexible. Spray drying¹⁵⁶, salting out¹⁵⁷ and spinning disk atomisation¹⁵⁸ of polymer solutions have also been used as a technique for microsphere production. The development of microsphere technology is currently increasing in complexity with ion and temperature responsive microspheres being developed¹⁵⁹.

2.2.2 Using microspheres for controlled release

Biodegradable microspheres have been studied intensively for their ability to slowly release various agents *in vivo*. Problems such as patient compliance or having to frequently administer a drug can be overcome using a microsphere-based slow release delivery system. Many of these devices are based on PLLA, PLGA or poly(caprolactone) although some use naturally occurring polymers such as chitosan¹⁶⁰. Many researchers have investigated microsphere systems for drug delivery. Degradation can occur in different ways dependant on the polymer. PLGA is a bulk eroding polymer. Water can penetrate throughout a PLGA microsphere allowing degradation throughout the sphere to occur¹⁶¹. When a drug is loaded into a microsphere and the release is studied, there is often an initial 'burst' effect as drug at or near the surface is released. The remaining drug is then slowly released as the microsphere degrades. This is contrasted with

surface eroding polymers such as poly(anhydride)s in which degradation happens at the surface¹⁶². As well as its chemical composition, the structure of the polymer can also impact on microsphere degradation. For example, crystalline PLLA will degrade much more slowly than amorphous PLGA. However, increasing the proportion of the L-lactide monomer in PLGA will increase degradation time. The same effect is not observed in the case of the racemic D,L-lactide¹⁶¹.

Microsphere size also has an impact on drug release, as smaller microspheres have an increased surface area to volume ratio. This increases the rate of drug release from the sphere. Several types of microsphere based on PLGA combined with various drugs are now commercially available to treat diseases such as prostate cancer¹⁶³. In addition, the benefits of using microspheres to provide site-specific treatment such as that for brain tumours have been investigated¹⁶⁴. Such advances have led some to begin investigating the potential of microspheres for the delivery of drugs intraocularly^{165,166}.

Another major area of interest in microspheres has been in the delivery of proteins¹⁶⁷. This is difficult using standard oral and pulmonary methods as they have short half-lives *in vivo*. Use of a biodegradable microsphere system provides some protection for the protein as well as ensuring slow release. There are many examples in the literature of proteins being incorporated into microspheres which have been reviewed by Sinha *et al.*¹⁶⁷. A few illustrative examples are considered here. Insulin is used by millions of people across the world in the treatment of diabetes. Regular injections are required to maintain an appropriate level within the body. A slow release system could prevent some of these injections. Insulin has been incorporated into PEG/PLGA and PEG/PLLA microspheres to produce successful slow release delivery systems. These systems were able to show high insulin stability and uniform release over 28 days¹⁶⁸. Another protein integrated into PLGA microspheres has been β -

lactoglobulin¹⁶⁹. This protein is responsible for causing milk intolerances in newborn babies. Using a microsphere-based delivery system to introduce the protein orally to newborns can stimulate an anti- β -lactoglobulin response leading to milk tolerance. Microspheres of biodegradable poly(ester)s have also been investigated as vaccine delivery systems for diseases such as tetanus¹⁷⁰ and diphtheria¹⁷¹.

Microspheres are now being developed for use in the rapidly advancing area of gene therapy. This type of therapy is becoming an important tool in the development of new treatments¹⁷². The therapy involves delivering DNA, which encodes for a functional protein, to cells to replace a mutated gene. The proteins produced by the cells then treat the particular condition of the patient. One of the most efficient ways of delivering plasmid DNA (pDNA) is by use of a viral vector. However, safety concerns regarding these delivery vehicles remain a problem¹⁷³. Delivery of the pDNA with no protection results in rapid fragmentation and decomposition of the plasmid. Therefore a slow release delivery mechanism is required. The encapsulation of various pDNAs in biodegradable microspheres has been reported¹⁷³. Despite the challenges of incorporating hydrophilic DNA into the hydrophobic poly(ester)s and maintaining pDNA integrity in the microsphere production process, microsphere delivery of pDNA has been shown to be superior to using bacteria¹⁷⁴.

2.2.3 Use of microspheres for cell delivery

Following their successful employment as a delivery system in other areas, researchers have begun to use biodegradable microspheres for delivery of cells to specific sites¹⁷⁵. The presence of the microspheres can provide both anchorage and structural support for cells to grow. As the cells begin to form new structures, the microspheres can biodegrade so as not to hinder full regeneration. An approach commonly used to achieve this involves allowing cells to attach to microspheres *in vitro* for subsequent injection¹⁷⁵ (Figure 2.3). Alternatively, three dimensional aggregation of microspheres can be

used to create a scaffold on which cells can be grown. This strategy has been successfully employed in the development of matrices for bone repair¹⁷⁶. An advantage of using a biodegradable system is that agents can be incorporated to be released slowly to encourage cell growth or, in the case of stem cells, direct cell fate. Newman *et al.*¹⁷⁷ showed that incorporation of retinoic acid into PLGA microspheres could induce embryonic stem cells to differentiate into neurons. Tatard *et al.*¹⁷⁸ tested various agents including cell adhesive peptides coated onto PLGA microspheres in response to a culture of nerve stem cells. It was found that coating of the microspheres could improve cell proliferation and differentiation.

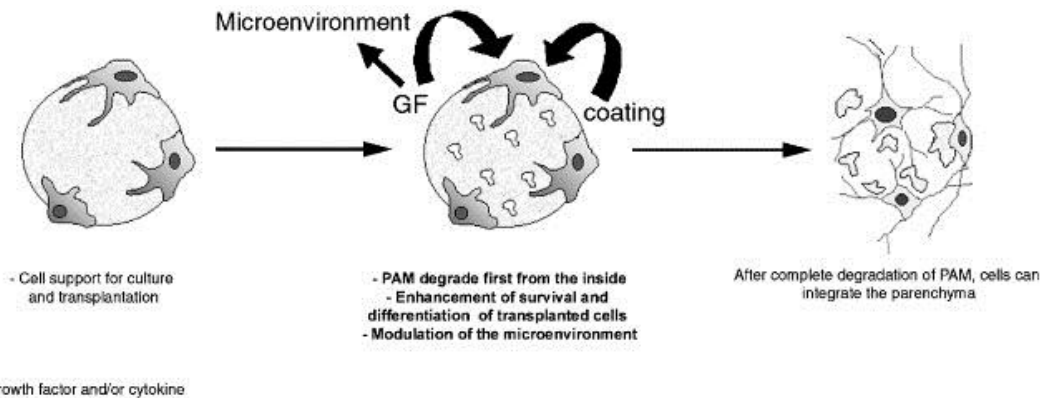


Figure 2.3 – Cartoon showing the use of microspheres for cell delivery. Cells are cultured on biodegradable microspheres and then implanted. Coatings on the microsphere help cells to adhere and grow. Following implantation, the microsphere degrades to leave new tissue. PAM; pharmacologically active microcarrier. Reprinted from Tatard *et al.*, *Biomaterials*, 2005, 26, 3727-3737, Copyright (2004) with permission from Elsevier.

As with other areas of tissue engineering, the surface morphology and chemistry of microspheres can influence cellular behaviour. In developing systems for articular cartilage tissue engineering, Thissen *et al.*¹⁴⁸ manufactured microparticles of different shapes and with different surface chemistries. It was found that spherical particles gave increased proliferation of chondrocytes compared with other types of particle. In addition, the attachment of an amine-terminated dendrimer to the microsphere surface gave a significant improvement

in the proliferation rate. These modifications were not found to affect cell phenotype. Other studies have investigated the effect of different types of PLGA microsphere on chondrocytes for cartilage tissue engineering¹⁵³. The potential for PLGA microcarriers to be efficient at treatment of cellular loss in stroke patients was demonstrated by Bible *et al.*¹⁷⁵. Neural stem cells were grown on the surface of microspheres *in vitro*. These were then delivered via a needle into stroke-induced brain cavities in rats. The cells were found to integrate successfully with the host tissue. However, there has been no demonstration of functional recovery thus far. In an alternative approach, Chan *et al.*¹⁷⁹ demonstrated a production method for self-assembled collagen microspheres incorporating mesenchymal stem cells. The injectable constructs were found to maintain cell viability *in vivo*.

Following the success of early development of the use of microspheres for other cell-based applications, their potential use in retinal tissue engineering has been investigated. Commercially available microcarriers such as Superbeads have been used to culture RPE cells¹⁸⁰. It was found that culturing the cells on microspheres instead of using conventional (2D) techniques yielded greater cell numbers. A limited amount of donor RPE tissue necessitates a high yielding culture system if the cells are to be used for transplantation¹⁸¹. Aside from transplantation, the injection of PLGA microspheres containing glial cell-derived neurotrophic factor was found to slow the degeneration of photoreceptors in a mouse model¹⁸². More recently, a system combining PLGA microspheres with matrix metalloproteinase 2 has been designed¹⁸³. This proteinase has been shown previously to enhance cellular integration between implanted retinal cells and host tissue¹⁸⁴. Cotransplantation of these microspheres with RPCs in a mouse model was found to provide some regeneration of retinal layers. Away from designing therapies, microspheres derived from polystyrene have been used in combination with RPE cells to induce choroidal neovascularisation

Chapter 2 Developing biodegradable microspheres as a cell carrier

(CNV) in a mouse model¹⁸⁵. This model will be used to develop a better understanding of the CNV process. In addition to being investigated as a treatment for retinal conditions, RPE implantation on microspheres is also being studied as a potential treatment for Parkinson's disease¹⁸⁶. Implantation of RPE cells in the brain on gelatin microcarriers has been shown to improve motor function in patients with Parkinson's disease.

2.3 Optimising the production of PLLA/PLGA microspheres for use as an ocular cell delivery system

2.3.1 Introduction

Following previous work investigating the optimisation of RPE cell growth on porous polymer films⁹⁷, the behaviour of these cells on biodegradable microspheres was investigated. The microsphere synthesis work in this chapter was done collaboratively with project student Lucy Backholer. The effect of microsphere surface morphology on interactions with RPE cells has not previously been investigated. Microspheres were prepared from PLLA, PLGA or a blend of both to assess the interaction of RPE cells with the microsphere surface. A simple emulsion-based technique was employed to produce the microspheres. The technique involved pouring a solution of polymer in an organic solvent into a rapidly stirred solution of stabiliser (poly(vinyl alcohol) (PVA)). This generated droplets of polymer solution in the stabiliser phase which became microspheres following solvent evaporation. Variation of different production parameters and their effect on the resultant microspheres was studied.

2.3.2 Preparation of microspheres using different concentrations of polymer solution

PLGA microspheres were prepared using different concentrations of solution to investigate the effect of concentration on microsphere size. The microspheres produced from a 0.05g/ml polymer solution were smooth, defined spheres varying from $\sim 3\mu\text{m}$ to $\sim 125\mu\text{m}$ in diameter (Figure 2.4). The microspheres produced from a 0.1g/ml polymer solution had a larger average diameter with microsphere sizes ranging from $\sim 10\mu\text{m}$ to $\sim 300\mu\text{m}$. Those produced from a 0.15g/ml solution showed a further increase in size with the majority of spheres over $200\mu\text{m}$. These results conform with those in the

literature showing an increase in sphere diameter as polymer solution concentration increases¹⁵³. The increased viscosity of the polymer solution droplet at higher concentrations can resist shear forces that cause droplets to break up resulting in formation of larger microspheres.

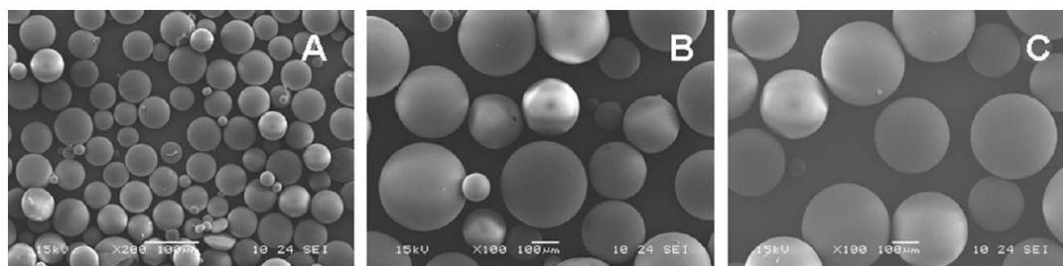


Figure 2.4 – Scanning electron micrographs showing A) 0.05, B) 0.10 and C) 0.15g/ml PLGA microspheres. Scale bar 100µm, original magnification x100.

2.3.3 Preparation of microspheres using different concentrations of stabiliser solution

For the experiments in Section 2.3.2 above, a stabiliser concentration of 2% was used. The stabiliser concentration was adjusted to assess the impact of this change on microsphere morphology and size. Scanning electron microscopy (SEM) analysis of the resultant microspheres showed that the 0.10g/ml PLGA microspheres produced using a 1% PVA solution were larger than those produced using 2% PVA (Section 2.3.2). Microspheres up to 400µm in diameter were observed, with an average size of ~300µm (Figure 2.5B). No microspheres below 70µm were observed using this preparation (Table 2.1). These microspheres were larger on average than those produced using a 0.5% PVA solution (Figure 2.5A). It has been reported that increasing PVA concentration stabilised smaller droplets thereby decreasing the average microsphere diameter¹⁸⁷. In addition, this study found that a PVA concentration of at least 2% was required for the formation of smooth microspheres. However, the experiments described in the literature used a much less concentrated solution of PLGA to prepare the microspheres than the

experiments described here. Increasing the PVA concentration will increase the viscosity of the aqueous phase leading to a decrease in mixing efficiency. It is possible that this resulted in the formation of larger polymer droplets. This effect would be more profound at higher polymer concentrations due to the increased shear forces required to produce smaller droplets. An increase in microsphere size with increasing PVA concentration has been observed previously when using a high concentration of polymer solution to produce microspheres for delivery of insulin¹⁵⁷. In the present study, microspheres produced using a 2% PVA concentration were found to vary considerably in size ranging from 5 μ m to 150 μ m (Table 2.1). The surface of these spheres was found to be smooth as with the 1% PVA solution microspheres. However there were many clusters of smaller microspheres amongst the larger ones using this stabiliser concentration. It is possible that smaller polymer droplets are being stabilised at this concentration of stabiliser resulting in some smaller microspheres. Overall the results seem to show that increasing the stabiliser solution concentration increases both the average size of the microspheres and also the size distribution.

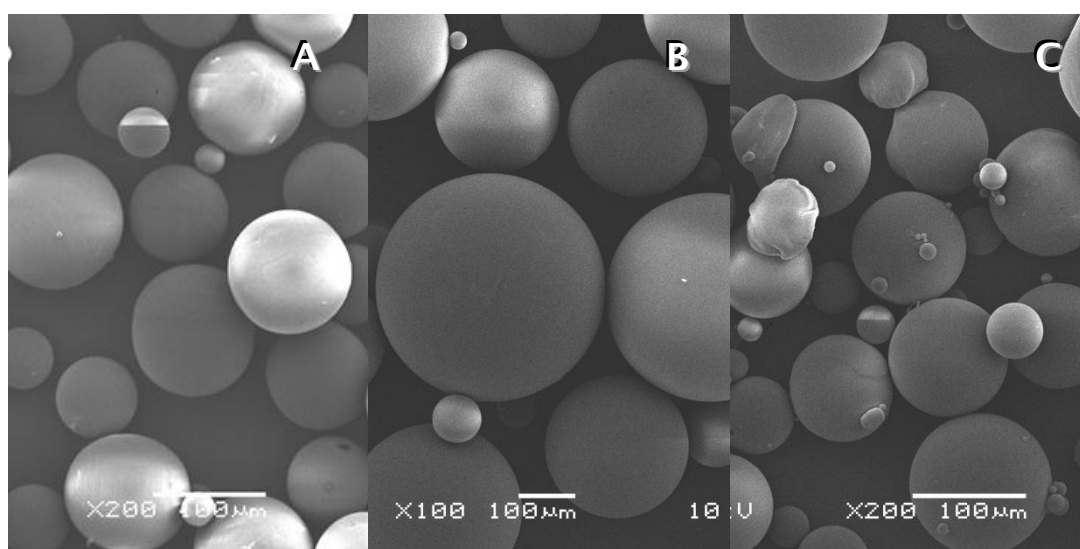


Figure 2.5 - Scanning electron micrographs showing 0.1g/ml microspheres produced using A) 0.5%, B) 1% and C) 2% PVA concentration. Original magnification x200(A and C) and x100(B), scale bar 100 μ m.

To more fully investigate the effect of changing the PVA solution concentration on the size of the microspheres, 0.05g/ml and 0.01g/ml polymer solutions were produced into microspheres using 0.1, 0.25 and 2% PVA concentrations (Table 2.1). Figure 2.6 shows that 0.05g/ml PLGA microspheres in a 0.1% PVA solution gave microspheres under 100 μ m. The 0.01g/ml PLGA microspheres in a 0.1% PVA solution were much smaller in comparison to the higher concentration with an average size of \sim 30 μ m.

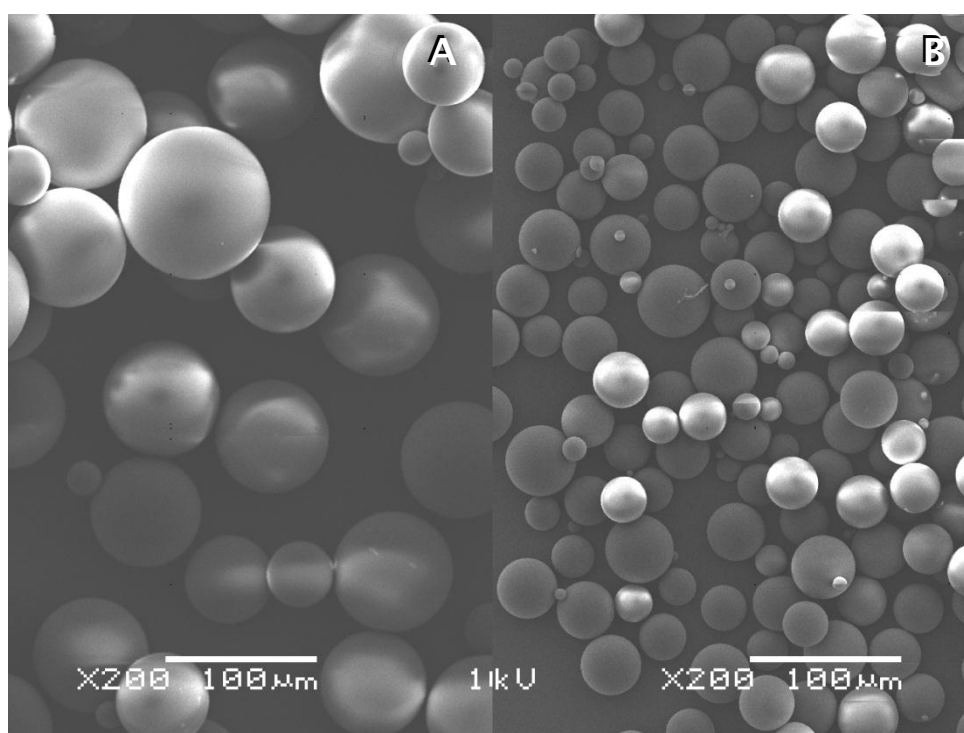


Figure 2.6 - Scanning electron micrographs showing 0.05 (A) and 0.01 g/ml (B) PLGA microspheres in a 0.1% stabiliser solution concentration. Original magnification x200, scale bar 100 μ m.

Microspheres prepared using a 0.05g/ml PLGA solution and a 0.25% PVA solution (Figure 2.7) showed a varied size range with the biggest microspheres just over 100 μ m and the majority just below 100 μ m. The 0.01g/ml PLGA microspheres in a 0.25% PVA solution were much smaller when compared with the 0.05g/ml sample obtained at the same PVA concentration (Table 2.1). All the microspheres were under 50 μ m with an average of \sim 30 μ m. These results showed that changes in PVA concentration were relatively insignificant compared with

changes to polymer solution concentration in accordance with the literature data¹⁵³.

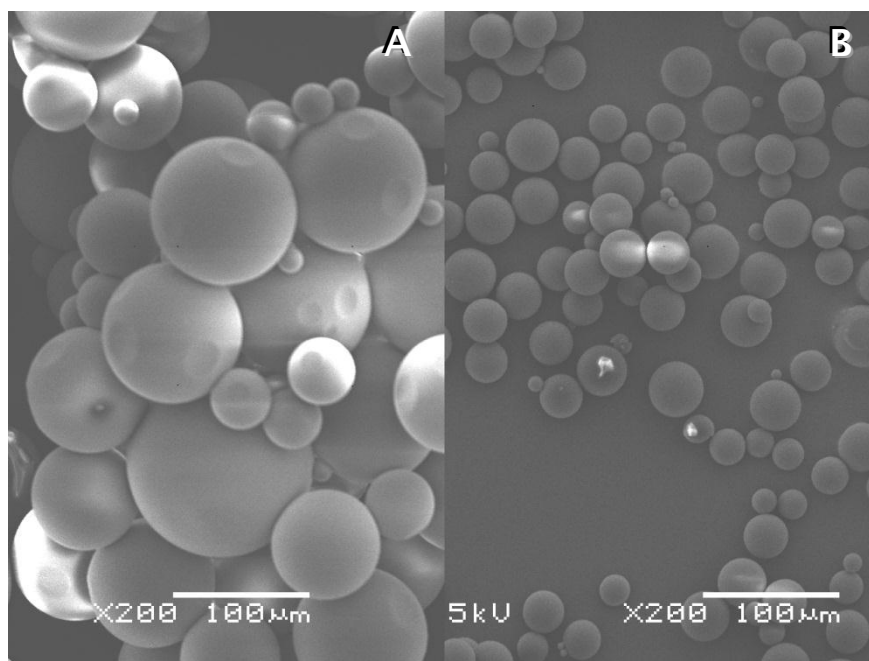


Figure 2.7 – Scanning electron micrographs showing 0.05 (A) and 0.01 g/ml (B) PLGA microspheres in a 0.25% stabiliser solution concentration. Original magnification x200, scale bar 100 μ m.

The 0.05g/ml PLGA microspheres prepared with a 2% PVA solution had a size distribution ranging from \sim 15 μ m to \sim 150 μ m with the majority of the microspheres being formed at either end of this range. This again suggests stabilisation of smaller polymer droplets at this PVA concentration. The 0.01g/ml microspheres with the same concentration of PVA had a size range from \sim 2 μ m to 50 μ m. Overall, increasing either the polymer concentration or the stabiliser concentration resulted in microspheres having a larger average diameter (Table 2.1). However, polymer concentration appeared to be the dominating factor in determining the average size of the microspheres produced. Comparing these results with those in the literature suggests that the effect of the stabiliser concentration can differ dependant on polymer solution concentration¹⁸⁷.

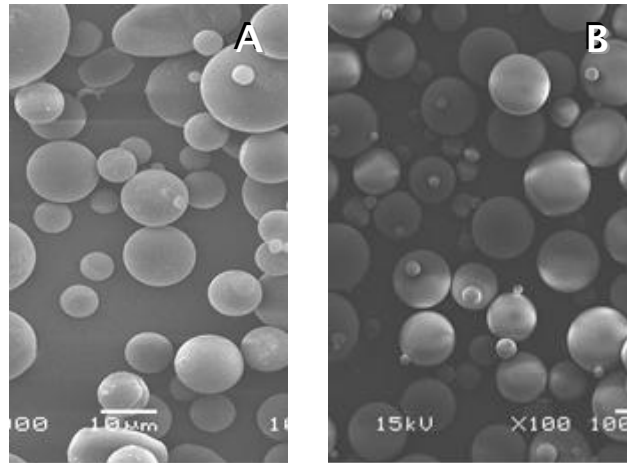


Figure 2.8 - Scanning electron micrographs showing 0.01 (A) and 0.05 g/ml (B) PLGA microspheres produced using a 2% stabiliser solution concentration. Original magnification x1000 (A) and x100 (B).

Polymer concentration (g/ml)	Stabiliser	Range of microsphere sizes
0.01	0.1%	1-50μm
0.05	0.1%	3-100μm
0.01	0.25%	1-50μm
0.05	0.25%	5-100μm
0.1	0.5%	7-100μm
0.1	1%	70-400μm
0.01	2%	2-50μm
0.05	2%	3-125μm
0.1	2%	10-300μm
0.15	2%	All >200μm

Table 2.1 - Table showing the range of microspheres sizes produced at different polymer and stabiliser concentrations.

2.3.4 Experiments to introduce porosity into PLGA microspheres

A previous study into RPE cell fate on biodegradable poly(ester) surfaces established that surface morphology influenced cell behaviour⁹⁷. Therefore, it was desirable to investigate the effects of microspheres with various surface morphologies on RPE cell behaviour. A gas-forming method has been developed to generate

porous microspheres¹⁵¹. This technique uses the incorporation of an effervescent salt (ammonium bicarbonate) to generate carbon dioxide during the solvent evaporation process. The evolution of this gas gives the resultant microspheres a porous structure. In an attempt to generate porous microspheres using this technique, sodium, potassium and ammonium hydrogen carbonate (1% w/v solution) were incorporated into the synthesis of microspheres (Chapter 5). The resultant microspheres were investigated by SEM (Figure 2.9). The porosity reported by Kim *et al.*¹⁵¹ was not observed in these microsphere preparations. Apart from occasional pores observed in some deformed spheres, the smooth surface morphology of previous PLGA microsphere preparations was shown. These microspheres were therefore not pursued as an RPE scaffold.

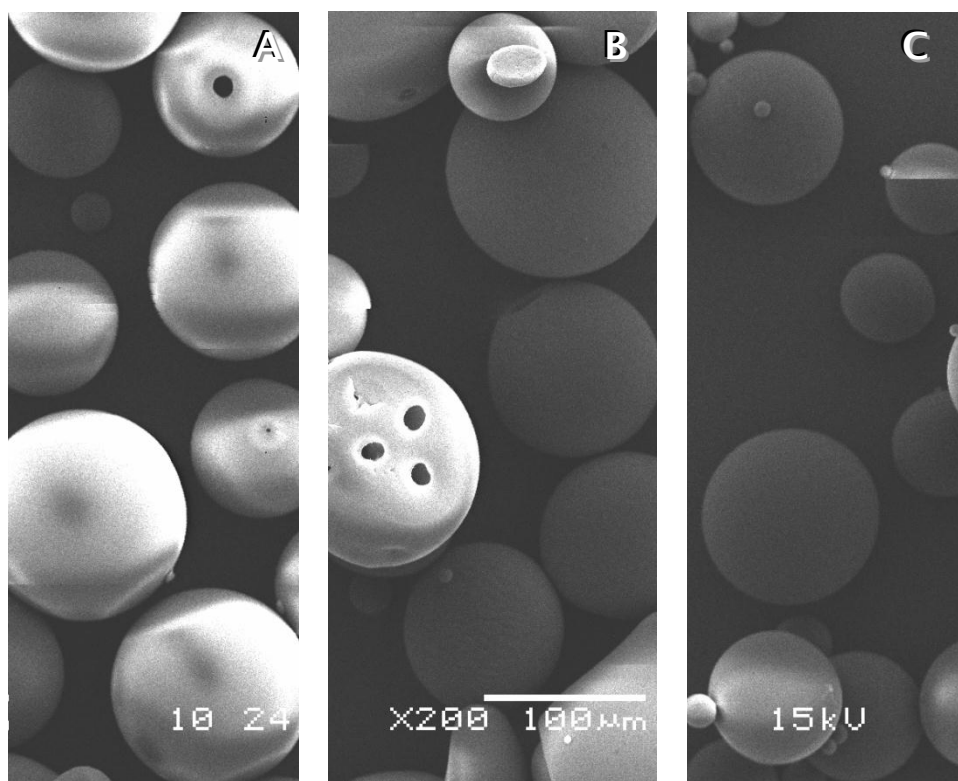


Figure 2.9 – Scanning electron micrographs showing microspheres produced using a gas foaming technique. An aqueous solution containing 1% w/v sodium (A), potassium (B) and ammonium (C) hydrogen carbonate was added to the polymer solution prior to the solvent evaporation process. Original magnification x200.

2.3.5 Preparation of a range of microspheres using blends of PLGA and PLLA

A range of PLLA/PLGA blends were used to produce microspheres. The effect of altering the quantities of PLLA and PLGA in the blend and subsequent attachment of an RPE cell line was then investigated. The ratios chosen had been used previously for the production of biodegradable porous films (10:90, 25:75, 50:50, 75:25 and 90:10)⁹⁷. A standard procedure was followed using a polymer concentration of 0.05g/ml, a 0.5% PVA solution as the stabiliser and dichloromethane as the polymer solvent (Chapter 5). The 50:50 PLLA:PLGA blend was produced first (Figure 2.10) and showed a rougher surface morphology when compared with the microspheres produced using PLGA alone. This initial result suggested that the addition of PLLA was causing the spheres to appear less smooth. The accuracy of the blending ratios was confirmed using inverse-gated ¹³C NMR as with previous studies using blended PLLA and PLGA⁹⁷.

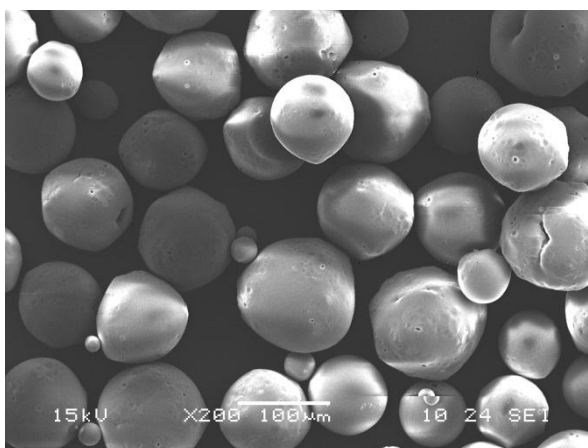


Figure 2.10 – Scanning electron micrograph showing microspheres produced using a 50:50 PLLA:PLGA polymer solution. Original magnification x200, scale bar 100µm.

Having investigated the 50:50 blend, a range of blends was prepared using a polymer concentration of 0.05g/ml. The microspheres produced are summarised in Table 2.2. It can be seen that microspheres produced from PLLA gave both the largest mean diameter and size distribution. In contrast, the 25:75 blend gave the

lowest mean diameter and the smallest size distribution. Table 2.2 shows that the introduction of PLLA initially causes a decrease in mean diameter. This is due to the interaction of the two polymers of containing different molecular weight distributions. Based on studies using polyoxyethylene, the hydrodynamic radius of PLGA chains would be 6.6-12nm whereas that of PLLA chains would be 12-23.4nm¹⁸⁸. The interaction between the PLGA chains (smaller hydrodynamic radius) and the PLLA chains (larger hydrodynamic radius) disrupts entanglements between the polymer chains. This leads to a less viscous solution producing smaller polymer solution droplets resulting in smaller microspheres. As the PLLA quantity in the blend is increased, the higher proportion of longer chains can overcome this effect resulting in larger microspheres. This effect of molecular weight distributions on polymer solution dynamics has been previously observed for methacrylate-based systems¹⁸⁹.

Polymer Blend	Minimum Diameter (µm)	Maximum Diameter (µm)	Mean Diameter (µm)	^a S.D.
PLLA	32.74	120.4	72.07	19.94
PLLA 90:10 PLGA	25.21	89.18	58.25	9.71
PLLA 75:25 PLGA	30.32	70.07	49.18	7.54
PLLA 50:50 PLGA	12.67	75.89	44.81	11.66
PLLA 25:75 PLGA	6.17	41.92	24.20	8.79
PLLA 10:90 PLGA	4.10	60.08	31.02	8.68
PLGA	26.86	71.72	52.86	8.16

Table 2.2 - The diameters and size distributions of the produced range of microspheres. ^aS.D. Standard deviation.

SEM studies on these new blends confirmed the initial observation that inclusion of PLLA resulted in a more distorted surface morphology. As the PLLA ratio was increased, the resulting microspheres had a less smooth appearance and a rougher surface morphology. This is exemplified by comparing the 10:90 and 90:10 (PLLA:PLGA) blends (Figure 2.11).

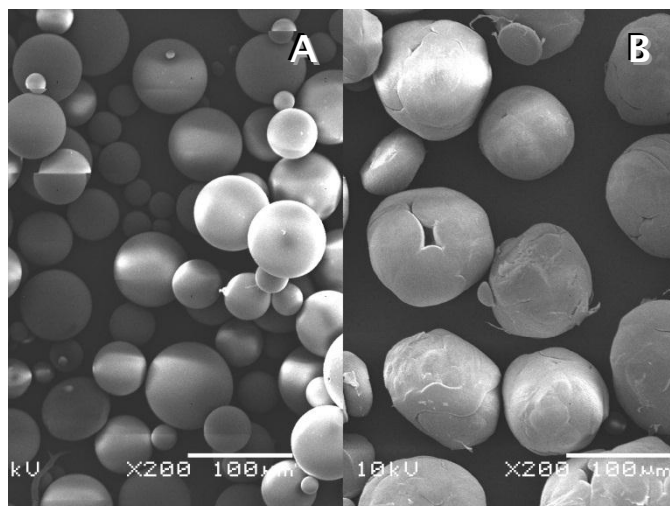


Figure 2.11 - Scanning electron micrographs comparing microspheres produced using a 10:90 (A) and 90:10 (B) PLLA:PLGA blend. Original magnification x200, scale bar 100µm.

Microspheres from PLLA alone were also prepared using a polymer in a solvent concentration of 0.05g/ml. The microspheres displayed a rough surface morphology (Figure 2.12). SEM micrographs of the spheres show they were larger than previous preparations with a mean diameter of 72µm. The size of the microspheres was also more widely spread around the average value (Figure 2.13).

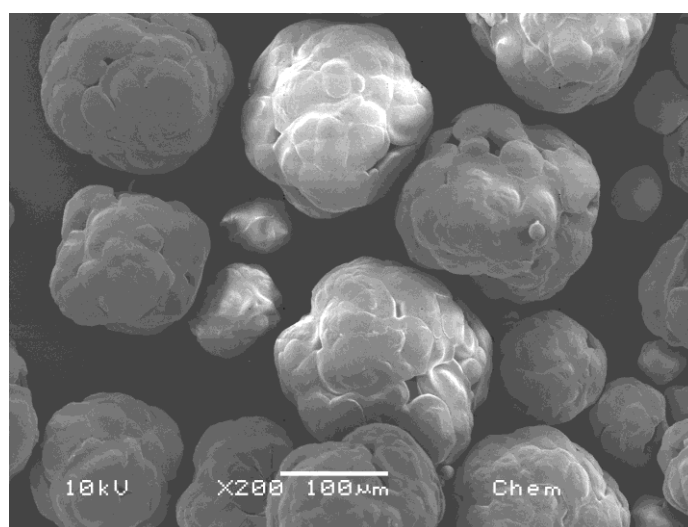


Figure 2.12 - Scanning electron micrograph showing microspheres produced using a 0.05g/ml PLLA solution. Original magnification x200, scale bar 100µm.

Across all the blends it was noted that an increased level of PLLA within a polymer blend increased the average diameter of

microspheres once there was more than 50% PLLA by weight (Figure 2.13). This was attributed to PLLA having a higher inherent viscosity than PLGA. This increased viscosity resulted in higher shear forces being required to produce both smaller and smoother droplets of polymer to become microspheres upon solvent evaporation. As all of the microspheres were prepared using the same stirring velocity, this explained why the solutions containing increased quantities of PLLA formed rougher and larger microspheres.

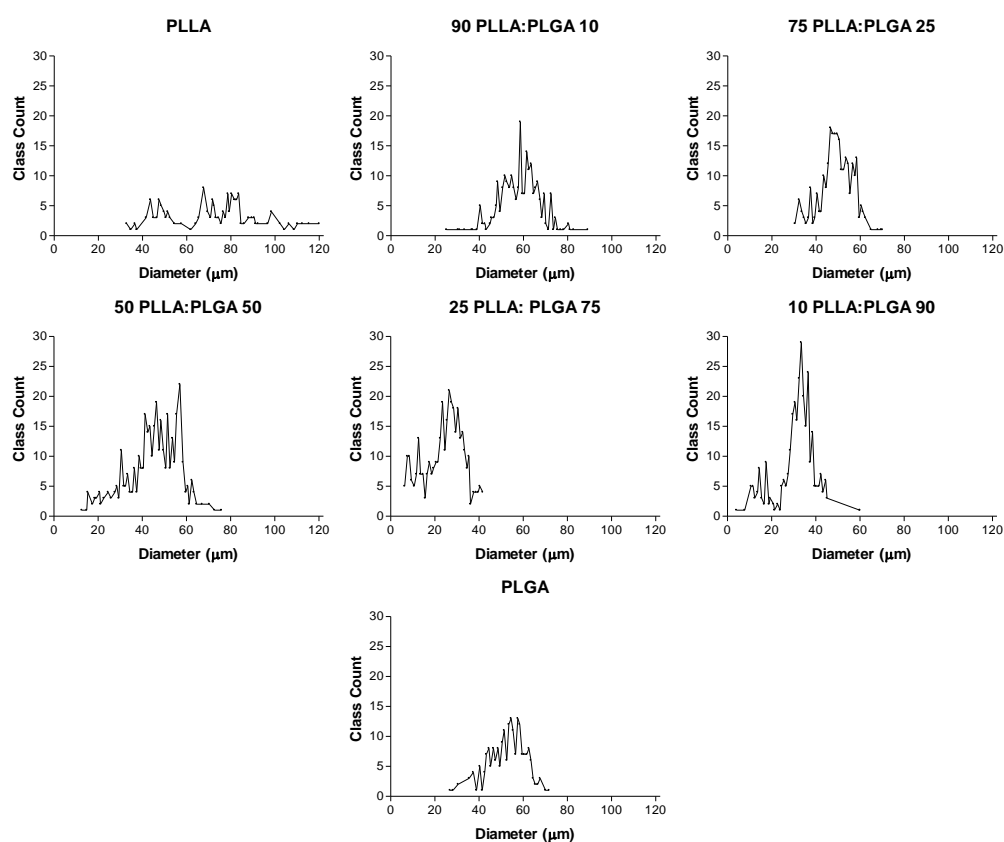


Figure 2.13 – Comparison of the influence of polymer blend on microsphere size distribution.

2.3.6 RPE cell seeding on a range of PLLA/PLGA microspheres

In order to assess the response of retinal cell types to the microspheres, immortalised human RPE cells were seeded onto prepared microspheres. The cellular work described in this section was done collaboratively with Dr Heather Thomson. The 5 blends of microspheres were used as well as preparations using PLGA alone and PLLA alone. For each blend, two experiments were carried out, one

involving 'blank' microspheres and the other using microspheres with a coating of laminin. Laminin is an extracellular matrix protein which has been used previously to increase retinal cell attachment to a substrate⁵⁹. Samples of unseeded microspheres with no cells were set up as a control experiment. Cells from an immortalised human RPE cell line (ARPE-19) were seeded onto the microspheres and cultured for a period of 2 weeks. Seeded and unseeded microspheres were incubated and maintained in the same culture environment. When growing cells in culture it is important to check that cells are proliferating and retaining phenotype. RPE cells have previously been observed to transdifferentiate into fibroblasts whilst in cell culture¹⁹⁰. Immunocytochemical staining followed by fluorescence imaging was used to confirm that cells were proliferating and retaining phenotypic characteristics in culture. In order to confirm retention of phenotype, a primary antibody specific to RPE cells (RPE65) was applied followed by a fluorescently tagged (green) secondary antibody (Figure 2.14B). The fluorescently tagged antibody binds to the primary antibody causing all cells with RPE phenotype to fluoresce green. Cell nuclei were counterstained with DAPI (4',6-diamino-2-phenylindole) which intercalates into DNA and causes all cells to fluoresce blue under UV light (Figure 2.14A, D and G). By overlaying the image from the RPE65 marker with that of the DAPI stain (Figure 2.13C) the number of cells of the RPE phenotype can be determined. The same process was used with another antibody, PCNA (Proliferating Cell Nuclear Antigen), to confirm that cells were proliferating (Figure 2.14E). An experiment in which no primary antibody was applied was used as a control (Figure 2.13H). The results of these assays showed the cells to be proliferating and retaining phenotype.

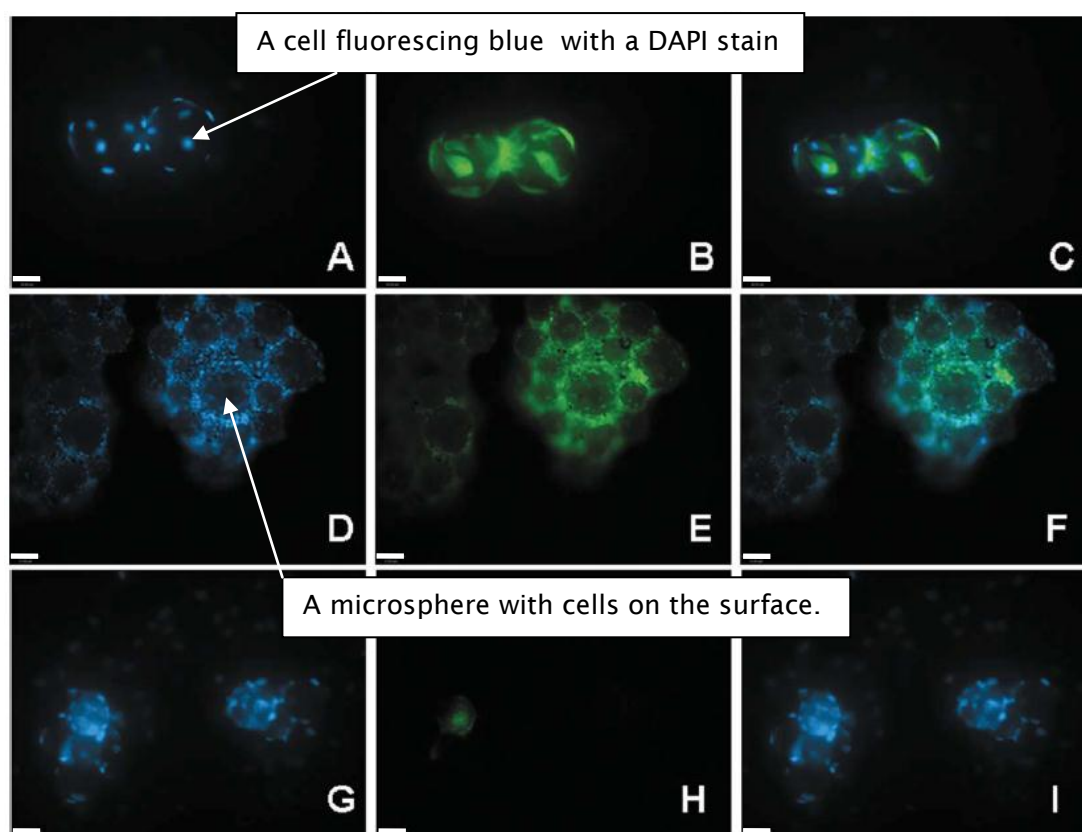


Figure 2.14 - Immunocytochemical characterisation of ARPE-19 cells cultured for 1 week on laminin-coated microspheres using antibodies directed against: (B) the retinal pigment epithelium marker-retinal pigment epithelium-specific protein-65 kDa (RPE 65) and (E) the cell cycle marker—proliferating cell nuclear antigen (PCNA). Control in the absence of primary antibodies (H). Cell nuclei are labelled in blue with 4',6-diamidino-2-phenylindole (DAPI) (A, D, G). Merged images (C, F, I). Images A-C, G-I 75:25 PLLA: PLGA and images D-F 25:75 PLLA:PLGA. Scale bar: 26 μ m.

To further investigate the presence of cells on the microsphere surface, the cell-seeded microspheres were fixed and dehydrated for SEM analysis. Micrographs showed that the cells on the surface presented a hexagonal morphology and appeared to be adopting a monolayer conformation (Figure 2.15A). As RPE are polarised cells with an apical and basal pole, it is important to ascertain that the cells are correctly polarised. Apical microvilli (hair-like projections from the cell surface) were observed to be protruding from the cell indicative of correct cell polarisation (Figure 2.15B).

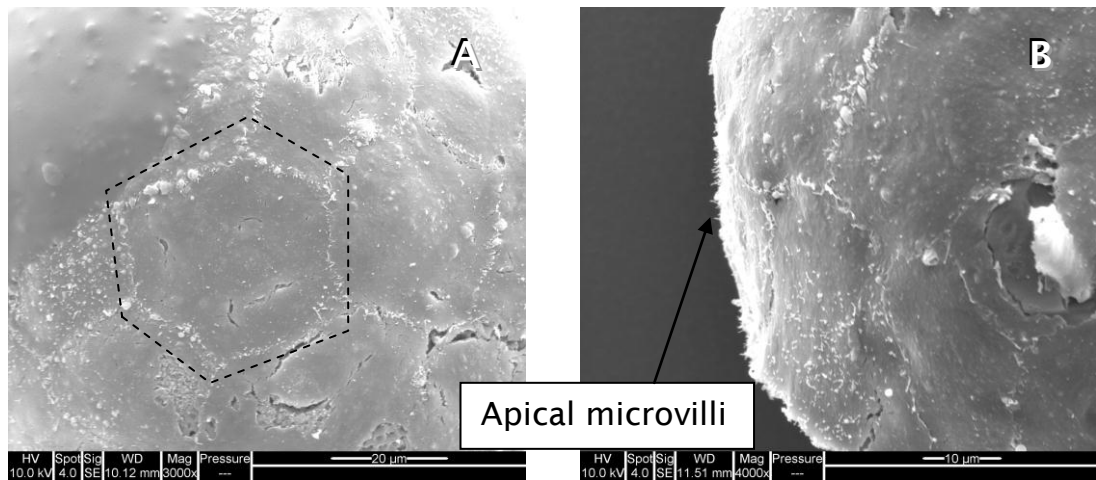
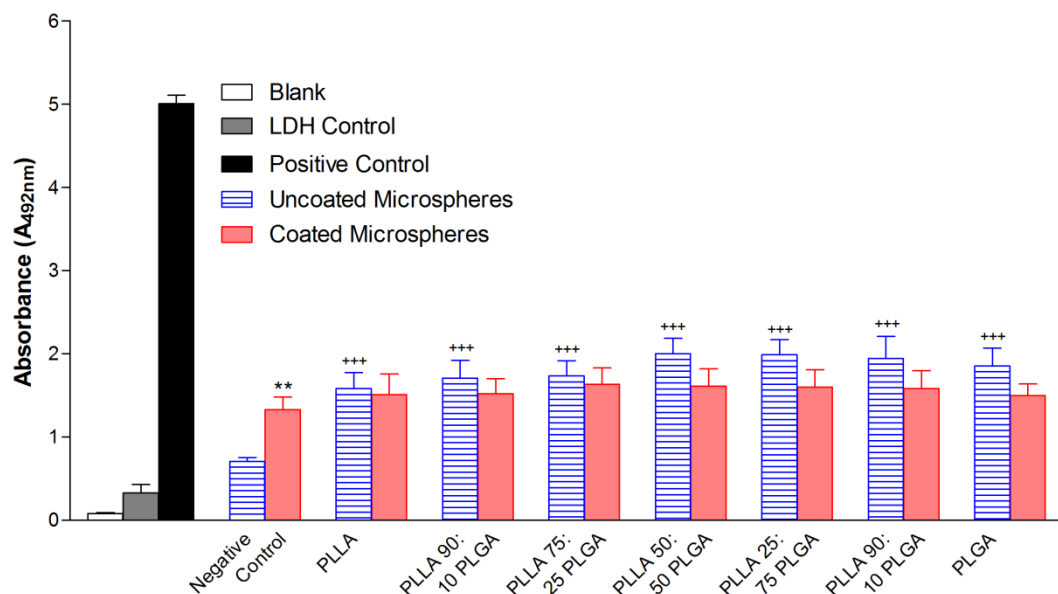


Figure 2.15 - Scanning electron micrographs of ARPE-19 seeded PLGA microspheres showing a cobblestone morphology (A) and apical microvilli (B). The dashed line in (A) shows the outline of a cell on the surface of a microsphere. Original magnification x3000 (A) and x4000 (B), scale bar 20 μ m (A) and 10 μ m (B).

Once it had been established that cells had successfully attached to the microspheres, and that cells were proliferative and had retained appropriate phenotype, it was important to quantify the influence that each polymer blend had on cell viability. Three different assays were used to assess this. Lactate dehydrogenase (LDH) is normally present in the cytosol of cells and is only released when cells die. Thus, quantification of LDH content in tissue culture medium is an indirect measure of cell viability. This can be measured using a colorimetric assay where more absorbance is indicative of more cell death. Samples of media were taken from all blends every two days over the two week culture period. Figure 2.16 below shows the mean LDH assay result over the two week period for all the blends, PLLA alone and PLGA alone.



Microsphere Blend

Values are expressed as mean \pm SEM (n=7). ** p < 0.01 compared to uncoated respective polymer blend. +++ p < 0.001 compared to matched negative control. All values significantly different compared to positive control p < 0.001.

Figure 2.16 – Bar chart representing LDH release from ARPE-19 cells cultured on coated and uncoated microspheres from each blend, PLLA alone and PLGA alone.

Results from the LDH assay show a statistically significant ($p=0.0154$) increase in LDH release from cells cultured on uncoated microspheres compared to their coated counterparts (Table 2.3). This implies that the presence of a laminin coating on some microsphere samples gave significantly less cell death. It has been shown that RPE cells are anchorage-dependant and that a lack of cell attachment can result in cell death¹⁹. Therefore, the laminin coating could be resulting in increased cell adhesion and therefore increased survival. The LDH control was obtained from LDH activity from the tissue culture medium alone. The positive control was a medium sample taken from cells incubated in the presence of 0.2% Triton which disrupts the cell membrane and produces maximal LDH release. This was shown to give a significantly higher absorbance than any other sample (Figure 2.16). The negative control was from cells cultured on tissue culture plastic in the absence of microspheres. There were minimal

differences in absorbance noted between all the coated microspheres and the coated negative control. However, on the uncoated samples, all samples produced significantly more LDH release than the negative control. This could be a result of some RPE cells not attaching to the microsphere surface and therefore undergoing apoptosis. The lowest absorbance of any uncoated microspheres was from those produced using PLLA, suggesting increased attachment on these microspheres.

LDH ASSAY	Value (Absorbance)	sem	No. of Replicates	Statistics
Blank	0.10	0.03	21	
LDH Control	0.33	0.10	21	
Positive Control	5.01	0.10	21	
TCP Control (uncoated)	0.71	0.05	21	
TCP Control (coated)	1.33	0.15	21	p= 0.0003 *
Polymer Blends (uncoated)	1.83	0.08	21	p< 0.0001 *
Polymer Blends (coated)	1.57	0.07	21	p= 0.0154 **

Table 2.3 – Overall comparison of LDH absorbance from coated and uncoated microsphere blends and controls. A higher value indicates more cell death. *p<0.05 compared to cells cultured on uncoated tissue culture plastic (TCP). **p<0.01 compared to cells cultured on uncoated microspheres. sem: standard error of mean.

The terminal deoxynucleotidyl transferase dUTP nick end labelling (TUNEL) assay is used to detect DNA fragmentation in damaged or dying cells. Deoxynucleotidyl transferase attaches to fragmented DNA which, in turn, catalyses the addition of modified bases (dUTPs) which are labelled with a fluorescent marker. Comparing those cells labelled with TUNEL against the total cell number gives a quantitative analysis of apoptosis. Results from the TUNEL assay concurred with those from the LDH assay by showing that there was more cell death on uncoated microspheres compared to laminin-coated microspheres

(Figure 2.17). However, this effect was not statistically significant. In addition, the 75:25 and 25:75 blends showed least cell death by this assay.

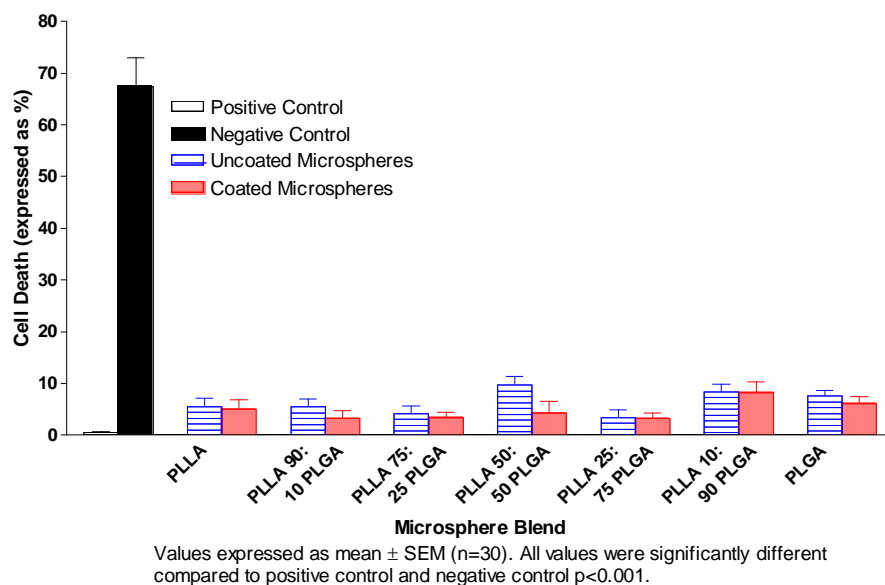


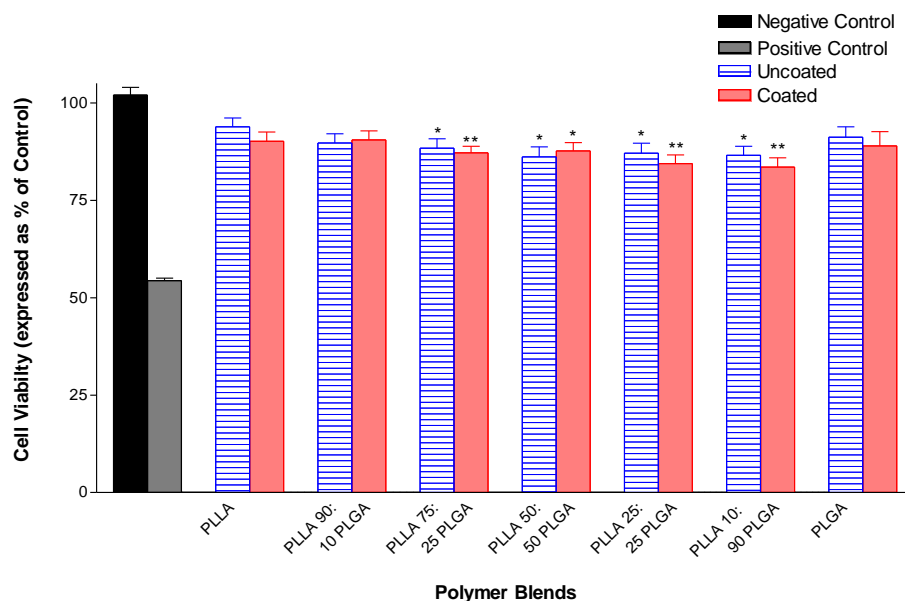
Figure 2.17 – Bar chart showing percentage ARPE-19 cell death on coated and uncoated microsphere blends by TUNEL assay.

The negative control represents cells incubated with 0.2% Triton, to induce apoptosis, as with the LDH assay. This negative control gave a mean cell death of 67% compared to 10% or less on all other samples (Table 2.4). The positive control was taken from cells cultured on tissue culture plastic in the absence of microspheres. Minimal (less than 1%) cell death was observed with this control. Whilst a higher percentage of cell death was observed when microspheres were used compared to tissue culture plastic, use of a laminin coating was observed to reduce cell death in most cases. This increased cell death could be due to some cells not attaching to the microspheres causing apoptosis. Further optimisation of microsphere formulation to increase cell adhesion may result in a lower level of cell death.

TUNEL ASSAY				
	Value (%)	sem	No. of Replicates	Statistics
Negative Control	0.53	0.20	24	
Positive Control	67.32	5.69	24	
TCP Control (uncoated)	2.01	0.29	24	ns
TCP Control (uncoated)	1.92	0.45	24	ns
Polymer Blends (uncoated)	7.52	1.19	24	*p< 0.05
Polymer Blends (coated)	6.31	0.99	24	ns

Table 2.4 - The overall comparison of apoptotic cell death on coated and uncoated microsphere blends and controls. ns: no significant difference compared to cells cultured on tissue culture plastic (TCP) or uncoated polymer blend. *p<0.05 compared to cells cultured on uncoated TCP. sem: standard error of mean.

The MTT (3-(4,5-Dimethylthiazole-2-yl)-2,5-diphenyltetrazolium bromide) assay is based on the reduction of MTT solution to formazan (giving a purple colour) in the presence of reductase enzymes present in live cells. This can be used to indirectly test for any cytotoxic compounds being released by the microspheres. Culture media samples taken from microsphere cultures were applied to fresh cultures of RPE cells on tissue culture plastic. The MTT assay is then performed on these cultures to assess if any compounds in the media are causing cell death. A graph showing cell viability as a percentage of the control is shown below (Figure 2.18).



Values represent mean \pm (n= 36). *p< 0.05, ** p< 0.01 compared to positive control. All values significantly different to negative control p< 0.001.

Figure 2.18 – Bar chart showing ARPE-19 cell viability by MTT assay on coated and uncoated microsphere blends.

The positive control represents cells which have been cultured in the presence of 0.2% Triton solution. Cell viability was reduced to less than 55% using this control (Table 2.5). The negative control represents cells cultured in normal culture medium producing 100% cell viability. Results from the MTT assay showed significantly ($p<0.01$) improved cell viability compared to the positive control on all blends. Although there was a small reduction in cell viability on microsphere samples, cell viability remained between 88% and 93% for all samples. The drop in cell viability compared to the negative control did not reach statistical significance.

MTT ASSAY				
	Value (%)	sem	No. of Replicates	Statistics
Negative Control	102	2.00	32	
Positive Control	54.39	0.62	32	
TCP Control (uncoated)	96.39	2.12	24	ns
TCP Control (coated)	92.20	2.59	24	ns
Polymer Blends (uncoated)	88.98	0.94	24	ns
Polymer Blends (coated)	87.49	0.93	24	ns

Table 2.5 - The overall comparison of cytotoxicity from coated and uncoated microsphere blends and controls. All values were not significantly (ns) different when compared to cells cultured on tissue culture plastic (TCP) or respective polymer blend.

Overall, these results show that RPE cells can successfully adhere to and survive on the surface of PLLA:PLGA microspheres. Electron microscopy was used to visualise the cells on the microsphere surface and show that they were adopting an appropriate morphology in a monolayer and displaying some apical microvilli indicative of correct polarisation of the cells. Furthermore, the cells were found to retain appropriate phenotype and there was no evidence of toxic products being released from the microspheres. Coating the microspheres with the ECM protein laminin was shown to decrease cell death. In addition, the TUNEL assay results suggest that microspheres with rougher surfaces led to better cell survival. Whilst it has been observed in the literature that cells grow preferentially on a rougher surface¹³⁷, this behaviour has not previously been observed using microspheres. Investigation of the interaction between RPE cells and microspheres enables the development of the system further towards a stem cell delivery system for the eye¹³⁸.

3 Towards an artificial Bruch's membrane

3.1 Introduction

Chapter 1 introduced degenerative retinal diseases and reviewed the therapeutic strategies currently in development aimed at treating these diseases. The key biological problems associated with these conditions are degeneration of the photoreceptor and retinal pigment epithelial (RPE) cells and a dysfunction of Bruch's membrane (BM). Although there have been some investigations aimed towards generation of an artificial BM for use in a cell-based therapy¹³, few have focused on methacrylate-based polymers known for their biocompatibility with ocular tissues¹⁰². No therapy currently exists to treat the cellular atrophy associated with diseases such as macular degeneration. Development of an artificial BM would move research closer to clinical therapy. In addition, an artificial BM would be useful in generating an *in vitro* retinal model. This model could be used to better understand retinal physiology and for drug development. In this chapter, progress towards an artificial BM using a methacrylate-based copolymer system will be discussed. A fibrous membrane produced by the technique of electrospinning has been investigated for its ability to mimic the native BM. The development of this electrospun polymer substrate to increase its compatibility with RPE cells and achieve control over the cell-substrate interaction will be a key feature of the discussion.

3.2 Key properties of an artificial Bruch's membrane

As was discussed in Chapter 1, there are many factors that control the interaction between cellular layers and their extracellular environments. In the development of an artificial membrane, these factors must be optimised to produce a material which will interact

favourably with host tissue and encourage regeneration. One important property to consider is the mechanical strength of the replacement membrane. The artificial membrane should attempt to closely match the elasticity and strength of the native membrane. Whilst pure poly(methyl methacrylate) is brittle, its copolymers have been shown to be more pliable and therefore more compliant with biological systems¹⁹¹. As any material implanted into the body will have to interact with a highly hydrated environment, it is also important that they have a degree of hydrophilicity. Poly(ethylene glycol) (PEG) is often included in biomaterials to increase hydrophilicity. PEG alone is water soluble if not crosslinked. Therefore, it is often incorporated into other polymer systems. In designing a suitable copolymer for an artificial membrane, it was decided to focus on copolymers of methyl methacrylate (MMA) with 2-hydroxyethyl methacrylate (HEMA) and poly(ethylene glycol) methacrylate (PEGM). These hydrophilic comonomers help to improve the compatibility of the resulting copolymer with a water rich environment.

Possibly the most important factor in designing a replacement BM is the interaction between the material and RPE cells. Native BM supports a monolayer of RPE cells. It has been shown that RPE cells do not adhere well to aged/diseased BM²⁹. This could be as a result of AMD-related pathology and therefore creates a good case for utilising a synthetic BM in the treatment of degenerative retinal disorders. RPE cells are anchorage dependant, they must attach to a substrate to avoid anoikis (apoptosis caused by cells detaching from the surface)¹⁹. Control over surface chemistry plays an important role in ensuring good cell-surface interactions. Various surface modifications have been used in the literature to control cell behaviour¹⁰⁵. These include coating with extracellular matrix (ECM) proteins⁵⁹, plasma treatment¹⁰³ and attaching ligands for cell surface integrin receptors¹¹⁷. In addition to binding cells in an appropriate

manner, any implanted material should resist non-specific protein adsorption which can lead to a lack of control over cell binding¹²⁰. The inclusion of PEG in biomaterials is effective at resisting this adsorption due to its hydrophilic nature¹⁹². Oxygen atoms in the PEG chain form hydrogen bonds with water molecules. The water molecules become trapped between PEG chains creating a hydration shell and making the adsorption of proteins energetically unfavourable. Steric repulsion has also been reported to contribute to the protein repellent properties of PEG¹⁹³.

RPE cells are polarised (having a basal and apical pole) and should display apical microvilli on the surface which is not attached to a substrate¹⁹⁴. An ideal replacement for BM would facilitate the formation of a correctly polarised RPE monolayer. In addition, any material to be implanted into the body should be tested to ensure that it does not release cytotoxic compounds. Any such effects would prevent clinical application of the device.

Aside from matching the native membrane in mechanical and surface chemistry properties, any artificial cell substrate should also mimic its topology. It has been shown that the morphology of a substrate can influence cell-material interactions^{105,137}. Investigations into the morphology of BM have revealed a fibrous structure of collagen and elastin (Figure 3.1). This type of structure is also important as it allows diffusion of macromolecular substrates across the membrane. Lack of diffusion in aged BM has been implicated in RPE and photoreceptor atrophy associated with degenerative retinal diseases²². Any replacement membrane must therefore have diffusion properties which have been tuned to be similar to that of a young/healthy BM. In order to mimic native BM topology and facilitate correct diffusion, an artificial system should ideally be fibrous. Researchers are increasingly turning to the technique of electrospinning to produce robust micro fibrous substrates for use in tissue engineering and regenerative medicine.

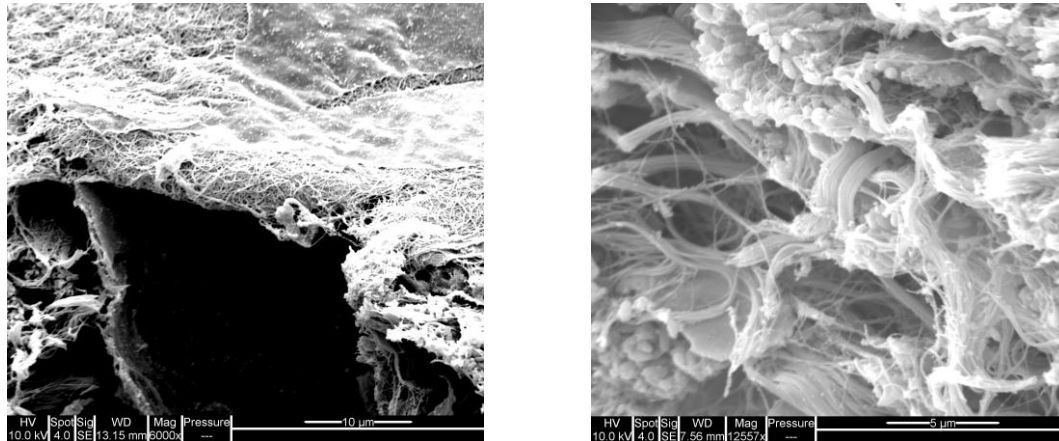


Figure 3.1 – Scanning electron microscope images showing the fibrous morphology of a porcine Bruch's membrane. BM consists of layers of collagen and elastin. BM supports RPE cell function and acts as a diffusion barrier between the RPE and the choroid.

3.3 Electrospinning

3.3.1 Introduction

The process of obtaining polymer fibres on the micro and nano scale by use of an electric field for tissue engineering (TE) dates back over 30 years. However, it is only within the last decade that this field has grown significantly¹⁹⁵. This conceptually simple technique is now known as electrospinning. At the start of the process to create fibres, a polymer melt or solution in an organic solvent is loaded into a syringe and a needle is attached. As the melt or solution is driven through the syringe, a high voltage is applied to the needle. This results in electrostatic repulsion that counteracts surface tension causing the polymer solution or melt to 'spin' into fibres. These fibres can then be collected on a grounded metal sheet (Figure 3.2). In the case of using a solution, the solvent is evaporated as the fibres move through the air before being deposited on the collector. Despite the simplicity of the idea, there are various parameters which need to be optimised in order to produce fibres.

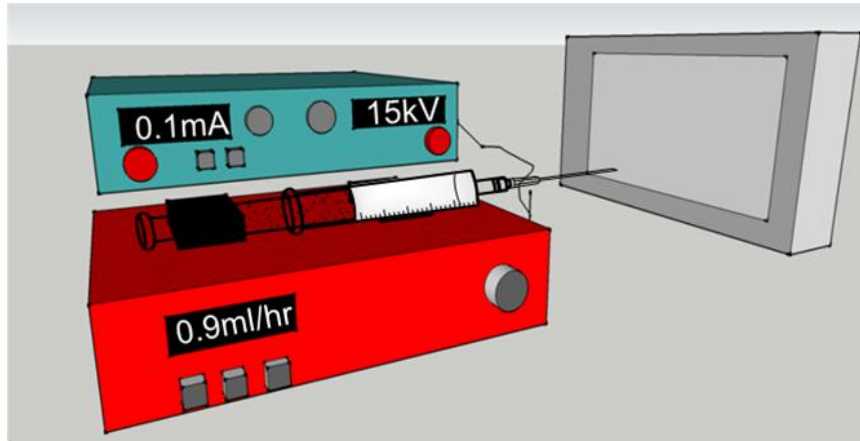


Figure 3.2 – Diagram showing the equipment required for the electrospinning process. A syringe driver (red) extrudes a polymer solution through a needle attached to a high voltage supply (green). Electrostatic repulsion causes the solution to ‘spin’ into fibres which are then collected on a grounded plate.

3.3.2 Mechanism and parameters for fibre production

Fibre formation is a result of interactions between the electric field and the polymer solution. Initially, the polymer drop emanating from the needle is deformed into a cone (the Taylor cone)¹⁹⁶. With increased voltage, surface tension forces are overcome and a jet emerges from the deformed drop. The interaction between the electric field and surface charging on the polymer jet causes a bending instability which results in the formation of fibres^{197,198} (Figure 3.3). These fibres then elongate and solidify before being collected on a grounded sheet. There are several key parameters that need to be optimised for the successful formation of smooth, uniform fibres. These include polymer concentration, viscosity, conductivity, solvent volatility and surface tension.



Figure 3.3 - Image of an electrospinning jet showing bending instabilities. Reprinted from Han *et al.*, *Polymer*, 2007, 48, 6064-6076, Copyright (2007) with permission from Elsevier.

The concentration of the polymer solution is critical to fibre formation. The concentration must be high enough to ensure good entanglement of the polymer chains. If the solution is too dilute then surface tension forces will overcome the chain entanglement and droplets will form as opposed to fibres. This process is known as electro spraying. However, if the concentration is too high then fibres will not form as the electric field will be unable to overcome the surface tension effects and a consistent flow at the needle tip will not be possible¹⁹⁹. Within the range of concentrations where fibre formation occurs, as polymer concentration increases, there is an increase in fibre diameter²⁰⁰. At the lower end of the range, fibres tend to have an uneven diameter and 'beading' is often observed. When 'beading' occurs, caused by instabilities in the electrospinning jet, the result is a non-uniform fibre with varying diameter (Figure 3.4). At the higher end of the fibre-forming window, smooth fibres of regular diameter are observed. Besides adjustments in polymer

concentration, changing the molecular weight or polydispersity of the polymer used will also have an impact on viscosity. An increase in polymer molecular weight will increase fibre diameter due to stronger entanglement between polymer chains. Whilst increased polydispersity will require a more concentrated solution to produce fibres due to the interactions of chains with varying hydrodynamic radii¹⁸⁹.

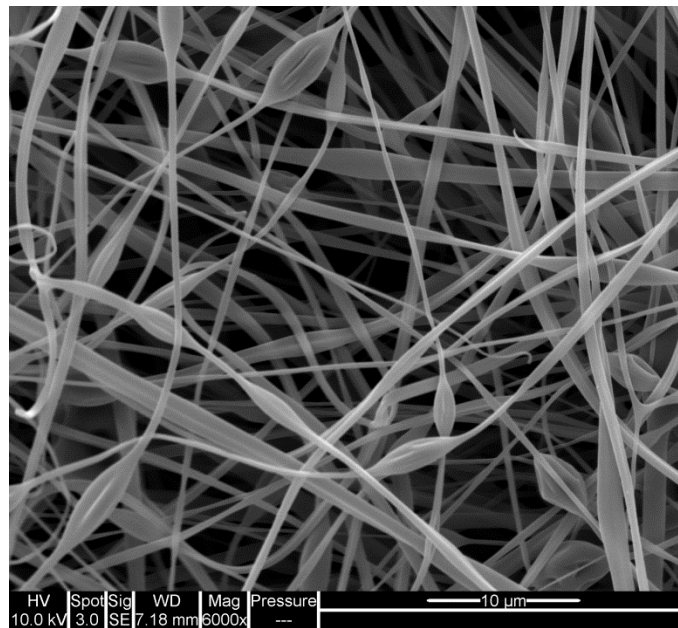


Figure 3.4 – Scanning electron microscope image showing ‘beaded’ polymer fibres produced by electrospinning. This effect can occur when the solution being electrospun is too dilute to give sufficient polymer chain entanglement.

Solvent volatility also has a role in determining the nature of the fibres produced. A solvent that evaporates too readily will result in polymer accumulation at the needle tip blocking the flow of the polymer solution. Occasionally, a mixed system containing solvents with high and low boiling points is used to overcome this problem. However, use of such a system can result in a porous fibre morphology¹⁹⁵. The solvent must also be able to carry an electric charge. A salt or surfactant can be added to achieve this which can also reduce the ‘beading’ effect by distributing charges more evenly across the surface. However, a polymer solution with a higher

conductivity will be influenced more by an electric field. Highly conductive solutions can therefore form very unstable fibrous jets resulting in the production of a wide range of fibre diameters. Furthermore, Jiang *et al.*²⁰¹ were able to demonstrate that the introduction of the protein bovine serum albumin to an electrospinning solution of dextran had a significant impact on the diameter of the fibres produced. Given that there was no difference in solution viscosity, the change was attributed to a difference in charge within the solution resulting from the presence of the protein.

Aside from solution-based properties, the applied voltage has a large impact on the fibres produced. A voltage that is too low could result in poorly formed fibres or a lack of jet formation. An increased voltage can change the nature of the Taylor cone and therefore the resulting jet. Using a poly(ethylene oxide)/water electrospinning system, Deitzel *et al.* were able to show that increasing the voltage beyond a certain level resulted in increased beading²⁰⁰. This is due to a decrease in droplet size at the end of the needle with increased voltage. It is proposed that the increased electrostatic repulsion is repelling the solution faster than it can be delivered resulting in an unstable jet. This leads to the discussion of solution flow rate as another parameter affecting fibre formation. The flow rate has been found to affect fibre size, porosity and shape²⁰². A high flow rate can result in significant beading on the fibres.

Whilst not as significant as other factors mentioned, the distance between the needle tip and collector can also have an impact on fibre size¹⁹⁹. Fibre diameter is found to decrease with increasing distance between the needle and collector. This is most likely due to the fibrous jets having more time to elongate before reaching the collector. There is also evidence of increased beading at shorter needle-collector distances attributed to insufficient drying of the fibre before reaching the collector²⁰². The parameters affecting fibre morphology and their influence are summarised in Table 3.1.

Parameter	Effect on fibre morphology
Applied voltage ↑	Fibre diameter ↓ initially, then ↑
Flow rate ↑	Fibre diameter ↑ (beaded morphologies occur if the flow rate is too high)
Distance between capillary and collector ↑	Fibre diameter ↓ (beaded morphologies occur if the distance between the capillary and collector is too short)
Polymer concentration (viscosity) ↑	Fibre diameter ↑ (within optimal range)
Solution conductivity ↑	Fibre diameter ↓ (broad diameter distribution)
Solvent volatility ↑	Fibres exhibit microtexture (pores on their surfaces, which increase surface area)

Table 3.1 - Table detailing the effect of changing different electrospinning parameters on fibre morphology. Adapted from Table 1 in Sill *et al.*, *Biomaterials*, 2008, 29, 1989-2006, Copyright (2008) with permission from Elsevier.

In addition to smooth, cylindrical fibres it is possible to produce fibres of differing morphologies. For example, flat ribbons can be formed when a polymer skin forms on the surface of a jet²⁰³. Once this skin is formed, the solvent inside can evaporate leaving a hollow tube. The tube then collapses into either a flat ribbon or one with two cylinders one on either side. This process can also occur with beads in the fibres. The beads can collapse as solvent evaporates to give a shrunken bead. Branched fibres can also be produced as fibre elongation and solvent evaporation result in charge instabilities in the polymer jet causing branching. Micro range polymer 'cups' of poly(methyl methacrylate) can also be produced by an electrospinning type process²⁰⁴. Electrospinning can also be used to produce fibres of polystyrene using a polystyrene latex, a small amount of poly(vinyl alcohol) (PVA) and water as a solvent (Figure 3.5). The fibres are templated by the presence of the PVA which is then removed yielding fibres composed of polystyrene particles²⁰⁵.

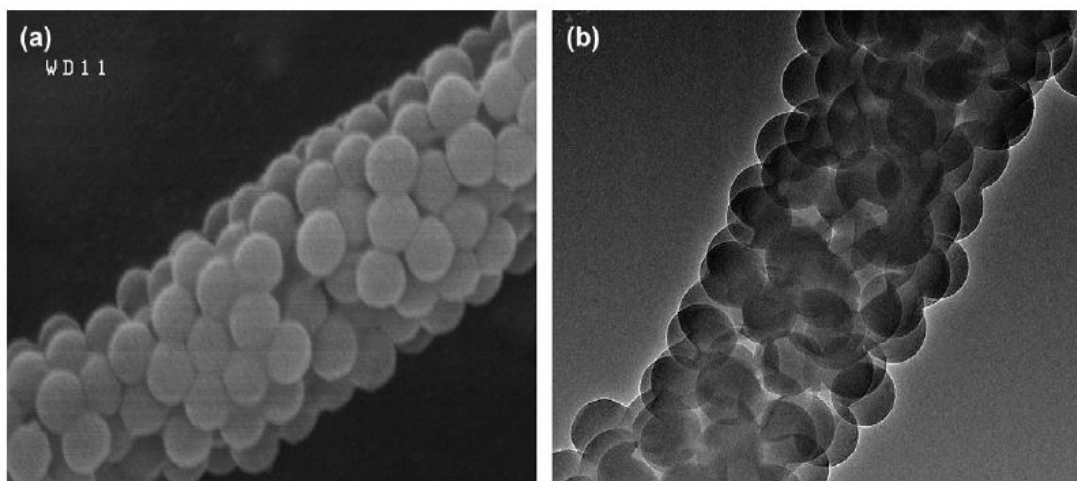


Figure 3.5 - Scanning electron microscope (A) and transmission electron microscope (B) images of an electrospun fibre of a polymer latex. Reprinted from Stoiljkovic *et al.*, *Polymer*, 2007, 48, 3974-3981, Copyright (2007) with permission from Elsevier.

The electrospinning examples described so far have used a flat metal collector. However, more intricate collectors can be used to create different fibrous matrices. Use of a rotating cylinder collector can yield aligned fibres as opposed to a random network²⁰⁶. This is achieved when the rate of deposition can be matched by the rotation speed of the cylinder. As an adaptation of this, using a wheel with a sharp edge as a collector can also be used to produce linearly aligned fibres²⁰⁷. The repulsion between fibres having the same charge combined with the rotation of the wheel causes deposition of fibres with regular spacing between them. Different types of frame materials have also been utilised in producing linearly arranged fibres¹⁹⁶. In addition to changing the collector, the configuration of the needle and syringe can also be adjusted to produce different types of fibre. Two needle and syringe assemblies can be placed side by side to combine two different polymers. Alternatively, a coaxial configuration with one polymer flowing inside another can be used. The coaxial assembly can be used to create core-sheath fibres which can contain drugs or even living cells in the core¹⁹⁵.

3.3.3 Using electrospun matrices to mimic the extracellular matrix (ECM)

The capability to produce micro- and nano- scale fibres has inspired many researchers to design electrospun matrices for biomedical applications²⁰⁸⁻²¹⁰. Such matrices are often designed to mimic the ECM. A natural starting point for such a mimic is to electrospin ECM proteins such as collagen. Matthews *et al.*²⁰⁹ used collagens to create electrospun membranes. Different types and sources of collagen were found to affect the resulting electrospun fibres. In addition, a rotating drum was used to collect fibres. It was found that rotating the drum at the correct speed could result in more linear fibres. Adhesion and proliferation of smooth muscle cells was observed on these membranes. As with other types of polymer, altering the concentration of collagen in a solvent has been found to control the diameter of the fibres produced²¹¹. These collagenous matrices have great potential for vascular and skin TE. Similar studies have focused on the use of the ECM protein elastin to produce electrospun membranes. In its native form, elastin is highly insoluble. Therefore, in order to successfully electrospin this protein, it must either be solubilised or the elastin precursor tropoelastin must be used. Recent studies have shown that tropoelastin has greater elasticity than solubilised elastin²¹². This greatly enhances the potential use of this form for TE applications. The proteins gelatin²¹³ and fibrinogen²¹⁴ have also been electrospun into fibres for TE applications.

One of the drawbacks of using naturally derived polymers is the lack of control over mechanical and other properties⁷⁶. As a result, the blending of ECM proteins with synthetic polymers has been used to combine the cell-adhesive properties of the proteins with the level of control offered by synthetic polymers. For example, collagen has been combined with PLLA to form a MSC scaffold for bone TE²¹⁵. Blends of collagen with poly(caprolactone)²¹⁰ and poly(dioxanone)²¹⁶ have also been successfully electrospun with their use targeted at

vascular TE. Poly(dioxanone) has also been electrospun with elastin as a potential vascular graft²¹⁷. These composites were found to be mechanically similar to native arteries. A layer by layer approach can also be utilised as an alternative to blending. This has been achieved with polyurethanes and collagen²¹⁸. A layered structure more closely resembles the native structure of membranes in the body. Another strategy is to co-electrospin different synthetic and natural polymers. For example, PLGA, elastin and gelatin were co-electrospun to produce a cellular scaffold. These structures were shown to have potential uses for soft TE²¹⁹.

The inclusion of any protein component in a cellular scaffold restricts the level of control available to tissue engineers in designing regenerative systems. If the proteins included adopt an incorrect conformation then cell binding may not occur. Additionally, any injected proteins, especially from non-human sources, need to be carefully purified and often chemically modified before they can be electrospun. This has led to some researchers pursuing a completely synthetic cell support for TE. Electrospinning of biodegradable polymers already used in TE such as PLGA²⁰⁸, PLLA²²⁰ and PCL²²¹ has been achieved. Non-degradable polymers such as poly(methyl methacrylate) have also been electrospun¹⁸⁹.

3.3.4 Biomedical applications of electrospun matrices

As has been discussed, there are many materials which can be electrospun into fibres¹⁹⁶. One of the main applications of these fibres is as a material for regenerating tissues within the human body²²². Many different tissues have been targeted for TE using electrospun scaffolds. Electrospun cellulose acetate has been investigated as a replacement for the urinary bladder matrix²²³. The production technique used for this investigation allowed for the creation of a multi-layered structure using only a single step process. This allowed for accurate replication of the natural ECM. Electrospun fibres have also been put to use in regenerating cells of the nervous

system. Ghasemi-Mobarakeh *et al.*²²⁴ used an electrospun poly(caprolactone)/gelatin scaffold to culture nerve stem cells. These cells were found to elongate parallel to the fibre direction and to successfully proliferate on the fibrous matrix. It was particularly noted that the blending of the poly(caprolactone) with gelatin gave an improved cellular response compared with poly(caprolactone) alone. Electrospun PLLA²²⁰ and PLGA²²⁵ have also been utilised in the search for TE scaffolds for nerve regeneration.

Electrospun fibres are also being used to aid regeneration of structural tissues. Many research groups are focusing on developing electrospun matrices to replace or repair bone tissue. For example, poly(caprolactone) scaffolds seeded with mesenchymal stem cells cultured with osteogenic supplements were found to form bone-like cellular structures²²⁶. In addition, electrospun silk fibroin seeded with preosteoblast cells was found to repair bone defects in a rabbit model²²⁷. Hydroxyapatite naturally strengthens bone in the body and is found amongst collagen in the ECM. PLLA²²⁸ and gelatin²²⁹ have been blended with hydroxyapatite and then electrospun. Studies of these materials with bone cells have shown that the inclusion of hydroxyapatite gave much improved cellular activity compared with PLLA or gelatin alone^{228,229}. This demonstrates that correct cellular control through appropriate chemical cues is essential in engineering a successful ECM mimic. Various other materials have been investigated for bone TE including collagen, chitosan and bioactive glasses²³⁰. Different types of electrospun polymer systems are also being developed for regeneration of cartilage²³¹, skin²³² and muscle²³³.

3.3.5 Advances in electrospun matrices for use in retinal tissue engineering

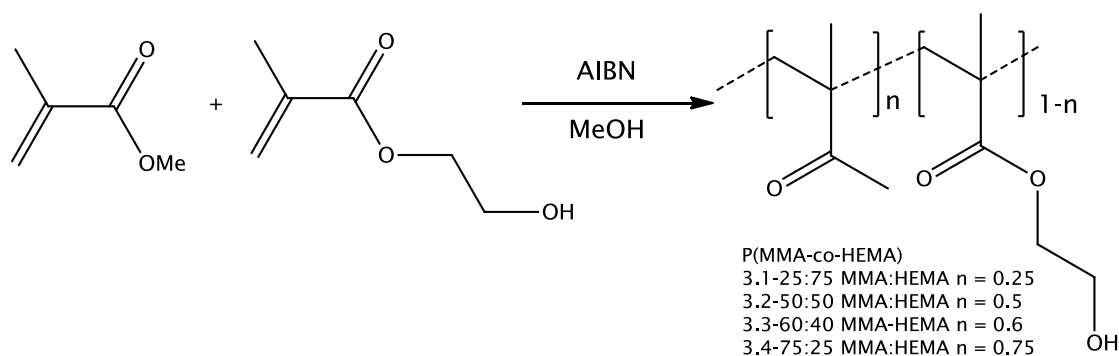
The use of electrospun matrices in an increasingly diverse range of applications in regenerative medicine has led some researchers to experiment with using these matrices for retinal TE. Chen *et al.*²³⁴ produced electrospun fibres of poly(caprolactone) blended with

chitosan-grafted poly(caprolactone). Various blends of the polymers were tested with mouse RPCs. It was found that cells grown on the blended polymer fibres were more encouraged to differentiate into the correct cell type when compared to fibres of poly(caprolactone) alone. This again shows the importance of the polymer chemistry in the control of cell behaviour on a surface. Following the early successes of using poly(glycerol-sebacate) to transplant retinal cells¹⁰⁰, Pritchard *et al.* have designed a more complex system based on a poly(glycerol-sebacate) membrane together with electrospun poly(caprolactone) and laminin^{235,236}. This membrane combined with photoreceptor layers was implanted into a pig model. Despite successful implantation and degradation of the membrane, problems regarding integration between the implanted and host retina were still observed. In an attempt to overcome problems with integration, Tucker *et al.* included matrix metalloproteinase 2 in a PLGA electrospun membrane¹⁸⁴. This proteinase has been shown to block the action of the CD44 glycoprotein and neurocan. These ECM molecules provide a barrier to cellular migration and integration. When the membranes were combined with retinal explants and implanted into mice, improved integration and retinal repopulation was observed. In the rest of this chapter, the development of an electrospun copolymer matrix as an artificial BM will be discussed. The compatibility of this substrate with RPE cells will be a key feature of the discussion.

3.4 Initial steps in developing a methacrylate copolymer

Following the use of methacrylate-based polymers in previous studies with RPE¹³⁴ and RPCs¹⁰², it was decided to initially synthesise copolymers of methyl methacrylate (MMA) and 2-hydroxyethylmethacrylate (HEMA) (Scheme 3.1). Similar copolymers have been used to produce soft contact lenses²³⁷. P(MMA-co-HEMA) with a variety of monomer feed ratios was produced (Chapter 5 – Section 5.2.1). These copolymers were characterised and found to be

in good agreement with those reported in the literature²³⁸. The different copolymers contained differing amounts of the MMA and HEMA monomers. The polymer containing the highest amount of HEMA monomer was found to form an insoluble hydrogel (Polymer 3.1). The other 3 polymers were soluble in various organic solvents. These copolymers were used for initial calibration of electrospinning apparatus.



Scheme 3.1 – Scheme to show the synthetic route to P(MMA-co-HEMA). A pull out table of all polymer numbers and structures can be found in Appendix B.

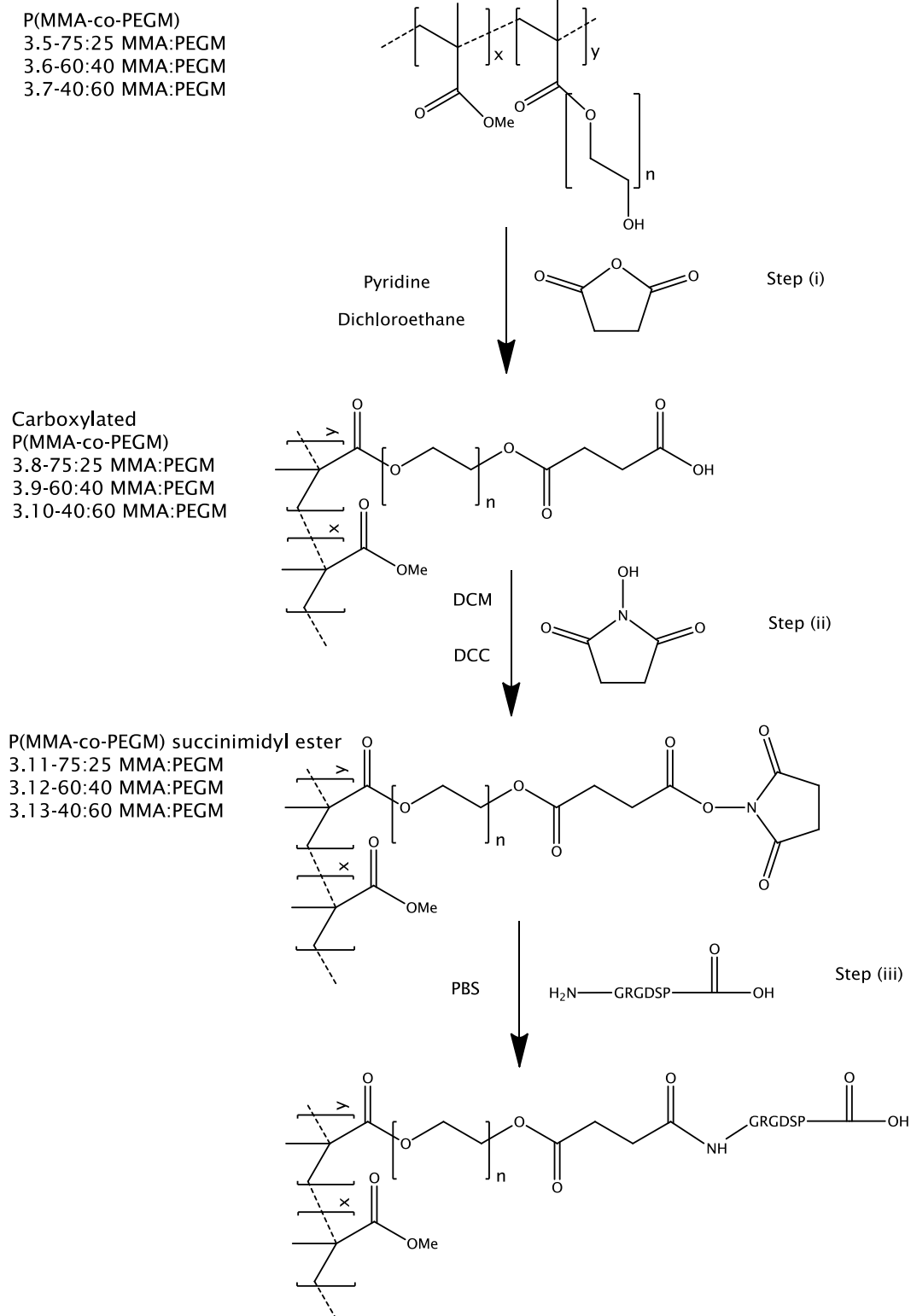
3.5 Creating a poly(methyl methacrylate-co-poly(ethylene glycol) methacrylate) fibrous matrix

3.5.1 Initial polymer synthesis

For trials with retinal cells, a polymer was produced with a poly(ethylene glycol) (PEG) group in place of the HEMA group. PEG is frequently incorporated into copolymer biomaterials to increase hydrophilicity¹⁹² and as a spacer between integrin ligands and the hydrophobic polymer backbone¹²⁰. This system enabled the incorporation of cell adhesive ligands such as peptides and ECM proteins via chemical attachment to the end of the PEG chain. These ligands have been shown to interact with integrin receptors on the cell surface to improve adhesion which would improve the survival of anchorage-dependant RPE cells¹¹⁷. The inclusion of PEG in the system would create a hydrophilic segment of the polymer to resist non-specific protein absorption. The PEG branches from the methacrylate

backbone also act as a spacer arm for the introduction of integrin ligands. This use of a spacer has been shown in the literature to be useful for binding of integrin receptors to a ligand^{118,119}. The integrin ligands used were peptide fragments of ECM proteins such as the Glycine-Arginine-Glycine-Aspartic acid-Serine-Proline (GRGDSP) sequence from fibronectin⁶⁴ and the Tyrosine-Isoleucine-Glycine-Serine-Arginine (YIGSR) sequence from laminin¹¹⁵. In addition, the protein laminin was used to assess if a whole protein could improve cell adhesion to a greater extent than using short chain peptides.

To generate a PEG-containing copolymer, methyl methacrylate (MMA) was copolymerised with poly(ethylene glycol) methacrylate (PEGM) using free radical polymerisation initiated by azobisisobutyronitrile (AIBN) (Chapter 5 - Section 5.2.3). A mechanism to facilitate peptide attachment to the end of the PEG chain was then sought. Peptide coupling can be achieved by reaction of an acidic end group with the amino groups on a peptide using a coupling reagent such as dicyclohexylcarbodiimide (DCC). However, it was desirable for the peptide coupling to be achieved under mild conditions immediately prior to cell seeding to minimise the opportunity of the peptide to hydrolyse. As an alternative, the acid group can be converted to a succinimidyl ester (SE). As the succinimidyl group is a stable leaving group, it can react with a free amine under mild conditions to give the required coupling¹¹⁷. This advantage led to the pursuit of an SE functionality on the PEG chain terminus as shown in Scheme 3.2. The SE groups could act as attachment points for cell adhesive ligands. The intention of the design was that using PEG to limit non-specific protein absorption¹⁹² would enhance the interaction between integrin receptors on the cell surface and peptides at the PEG chain terminus.



Scheme 3.2 - Scheme to show the synthetic route for creation of a succinimidyl ester on a PEG chain followed by peptide coupling. A pull out table of all polymer numbers and structures can be found in Appendix B.

Initially, a P(MMA-co-PEGM) copolymer was produced with a monomer feed ratio of 75:25 (MMA:PEGM) by weight (Polymer 3.5). A PEGM monomer with an average molecular weight of 360Da was used for these experiments. This copolymer was analysed by nuclear magnetic resonance (NMR) (Figure 3.6) and infrared (IR) spectroscopy as well as gel permeation chromatography (GPC). Signal overlap in NMR spectra made absolute determination of comonomer ratios challenging. However, estimating the integral from ^1H NMR of the -OMe group in the MMA comonomer and that of the protons adjacent to the ester group in the PEG chain indicated a ratio of 91:9 (MMA:PEGM) monomer units. NMR studies indicate that this ratio was consistent in all batches. Using data from gel permeation chromatography (GPC) a M_w of 85,228Da and a polydispersity of 2.43 for this copolymer were determined (Table 3.3). As the molecular weight distribution was relatively broad, a higher viscosity electrospinning solution was necessary compared to if a narrower molecular weight distribution polymer were used¹⁸⁹.

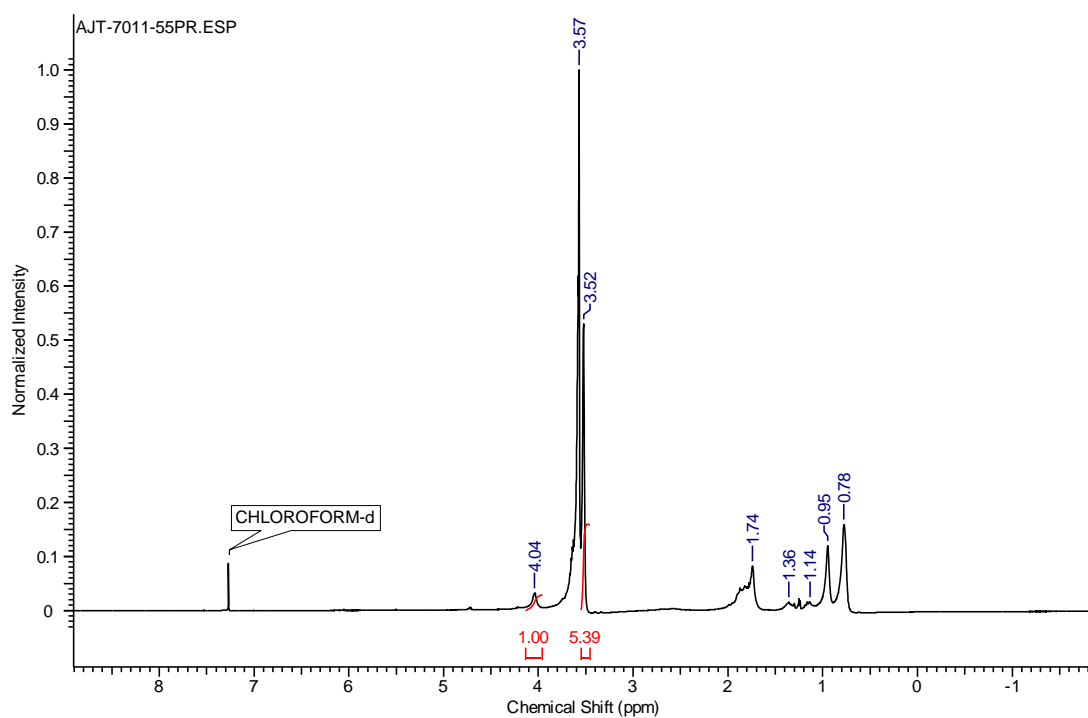


Figure 3.6 – NMR spectrum of P(MMA-co-PEGM).

Following synthesis, trials were conducted using various solvents and polymer concentrations to optimise parameters for electrospinning the polymer into a fibrous matrix. Polymer solutions in chloroform and dichloromethane (DCM) produced some fibres. However, these fibres formed a very sparse network and the rapidly evaporating solvent frequently blocked the needle tip. Using a solvent with a higher boiling point (2-butanone) resulted in the formation of large quantities of the more desirable dense fibrous networks. The optimum concentration for producing large amounts of fibrous material was found to be 0.45g of polymer per 1ml of solvent. Investigation of the fibrous substrate by scanning electron microscopy (SEM) revealed a smooth, ribbon-like morphology. A high degree of homogeneity was observed with most fibres having a diameter of $4\mu\text{m}$ and a thickness of $1\mu\text{m}$ (Figure 3.7). There was some evidence of fibres having broken. This was attributed to the brittle nature of this copolymer due to its high proportion of MMA monomers.

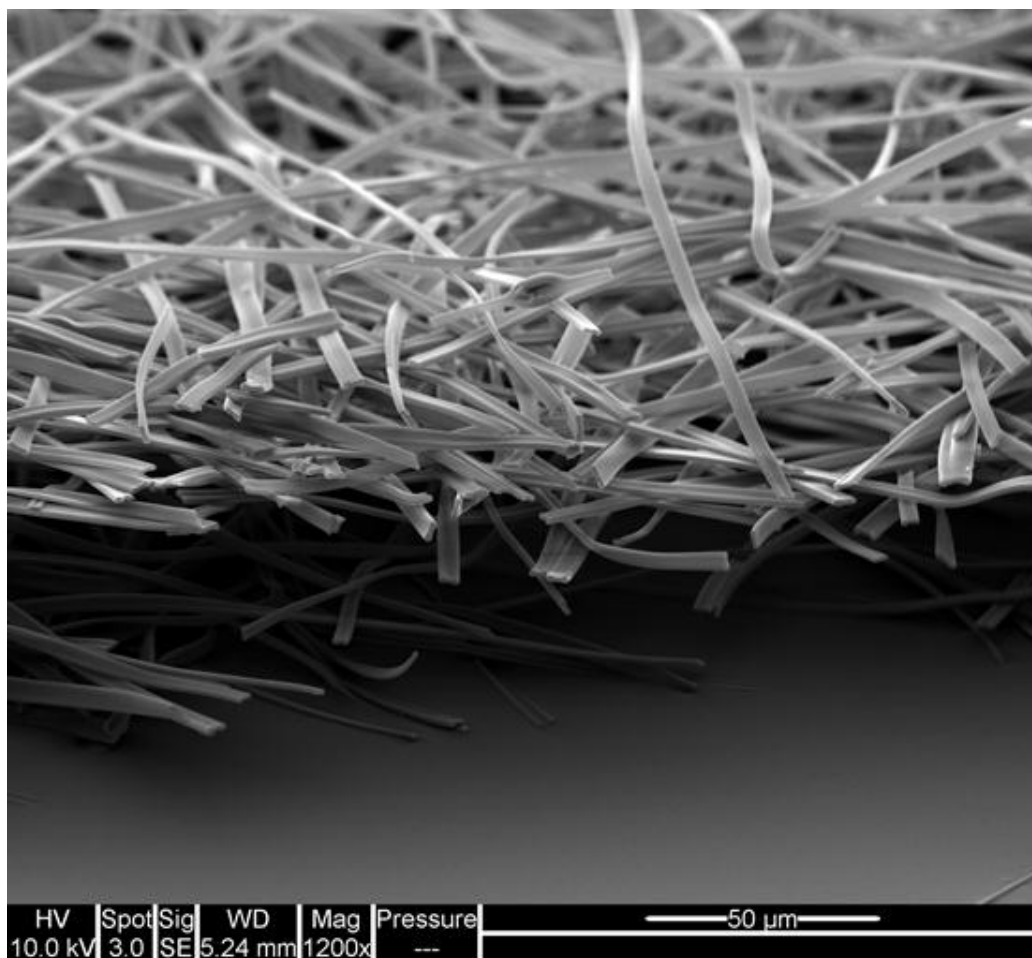


Figure 3.7 - Scanning electron micrograph showing 75:25 P(MMA-co-PEGM) electrospun fibres (Polymer 3.5). Taken at x1200 magnification with the SEM stub at a 60° angle to the electron beam.

One of the factors that can influence fibre diameter is the voltage applied to the needle tip. Literature suggests that with increasing applied voltage, fibre diameter should initially decrease but then increase¹⁹⁵. A solution of polymer 3.5 in 2-butanone was used to investigate the effect of changing this parameter on the resulting fibres. Electrospinning was conducted using the same polymer solution at different applied voltages (Table 3.2). Variables such as flow rate, solution concentration and distance from needle tip to collector were kept constant. The resulting fibrous networks were investigated by SEM to determine fibre diameters. Fibres produced at 20kV and 25kV had a larger diameter on average than those produced at 14kV. It was noted that at these higher voltages, it was

more difficult to collect a dense network of fibres. Both an increase in fibre diameter and a decrease in fibre density have been reported in the literature previously with other polymer systems²⁰⁰. The initial decrease in fibre diameter can be attributed to a change in droplet shape with increased applied voltage. The subsequent increase in fibre diameter has been attributed to an increase in mass flow rate due to increased electrostatic force²³⁹. The decrease in fibre density is most likely the result of increased electrostatic repulsion between fibres at these voltages.

Voltage applied (kV)	Average fibre diameter (μm) (n = 8) \pm sem
14	2.07 \pm 0.18
17	1.93 \pm 0.12
20	2.60 \pm 0.10
25	2.30 \pm 0.19

Table 3.2 - Table showing the average fibre diameter of fibres electrospun from a solution of 75:25 P(MMA-co-PEGM) in 2-butanone. sem: standard error of the mean.

Following successful production of a P(MMA-co-PEGM) copolymer, the synthesis of a succinimidyl ester group on the PEG chain terminus was investigated by adapting the work of Irvine *et al.*¹²⁰. This was achieved by first converting the alcohol terminus on the PEG chain to an acid by ring opening of succinic anhydride followed by carbodiimide coupling with *N*-hydroxysuccinimide (NHS) (Scheme 3.2 Steps (i) and (ii)). In the succinic anhydride step, a new peak at δ 4.25ppm for protons adjacent to the newly created ester group in the ¹H NMR spectrum confirmed the addition (Figure 3.8). A new signal observed at δ 2.65ppm for protons from the ring-opened anhydride further confirmed the structure of the product.

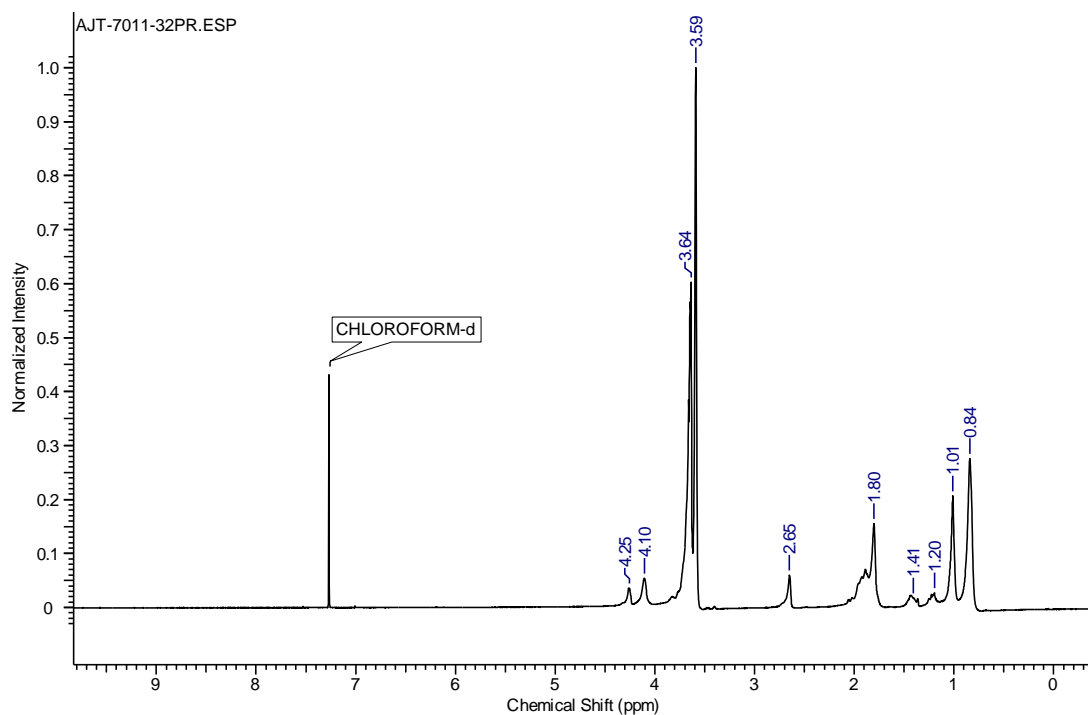


Figure 3.8 – NMR spectrum of P(MMA-co-PEGM) following reaction with succinic anhydride.

Overlapping signals made characterisation of the succinimidyl ester difficult. However, new signals in the ^1H NMR in the δ 2.6-3ppm region indicated successful addition of the new group (Figure 3.9). This data combined with the appearance of a new signal for the cyclic imide carbonyl group in the infrared (IR) spectrum confirmed the formation of the product. It was difficult to obtain pure samples of these polymers in high yield. This was attributed to difficulties in removing *N*-hydroxysuccinimide and succinic anhydride starting materials from the final polymer products by precipitation. To overcome problems using this route, a more efficient method for peptide coupling was sought.

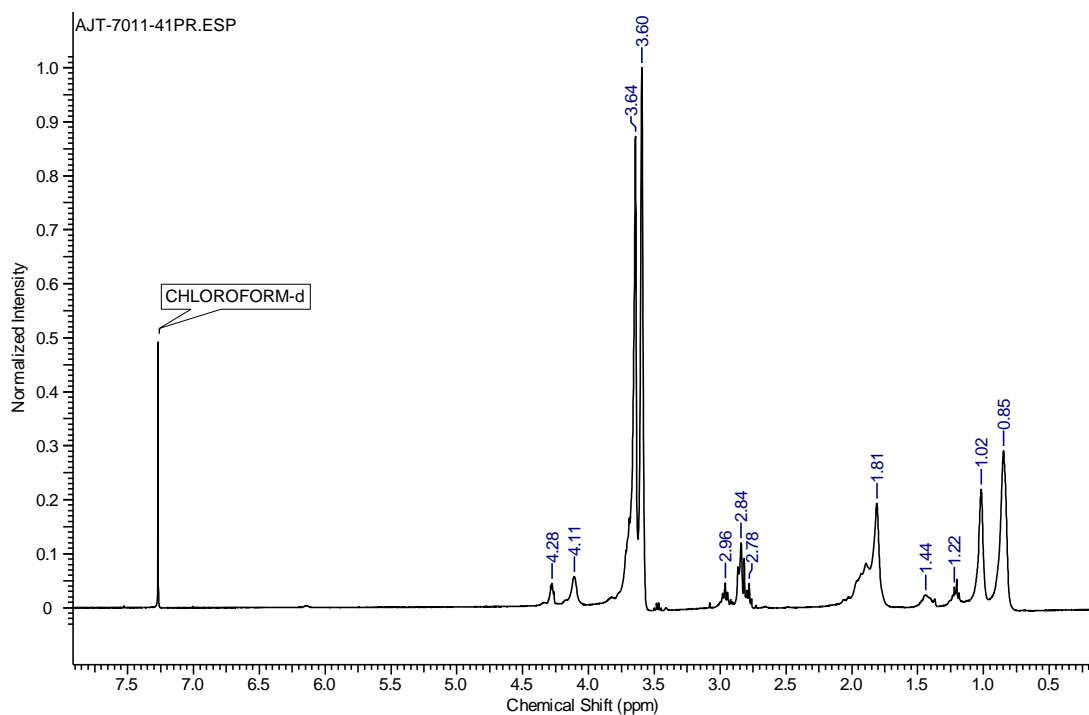
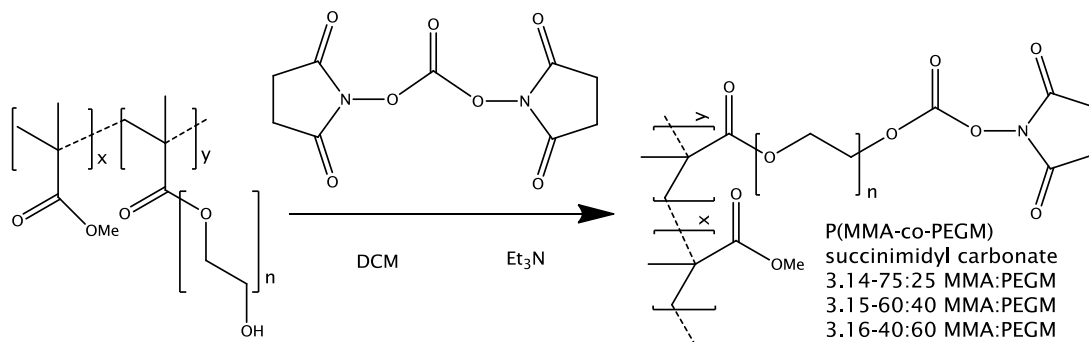


Figure 3.9 – NMR spectrum of P(MMA-co-PEGM) with succinimidyl ester functionality.

By adapting work by Morpurgo *et al.*²⁴⁰, a synthetic route to a succinimidyl carbonate on the PEG chain terminus was devised (Scheme 3.3). This route involved reaction of the deprotonated alcohol on the PEG chain terminus with disuccinimidyl carbonate and had the advantage of using only one step. Polymer 3.5 was reacted in this way to give a succinimidyl carbonate product (Polymer 3.14) (Table 3.3). This product was purified much more readily than the previously produced ester.



Scheme 3.3 – Scheme showing the reaction of P(MMA-co-PEGM) with disuccinimidyl carbonate to give a succinimidyl carbonate substituted product.

Peaks at ca. δ 2.8ppm in the NMR spectrum confirmed addition of protons from a succinimidyl group. (Figure 3.10). This was further confirmed by the appearance of a new carbonyl peak in the IR spectrum indicative of the presence of a cyclic imide. The appearance of a peak at ca. δ 4.5ppm for protons adjacent to the new carbonate linkage was additional evidence of successful functionalisation. By comparing the integrals of the protons adjacent to the ester linkage in the PEG chain (δ 4.1ppm) with protons adjacent the new carbonate group (δ 4.5ppm), an estimation of the proportion of PEG chains containing the new group can be obtained. Initially, when dimethylformamide (DMF) was used as a solvent for this reaction, low conversion rates to the succinimidyl carbonate (less than 60%) were observed. Changing the reaction solvent to dichloromethane (DCM) increased the conversion rates to over 80%. This is due to better solvation of the starting materials.

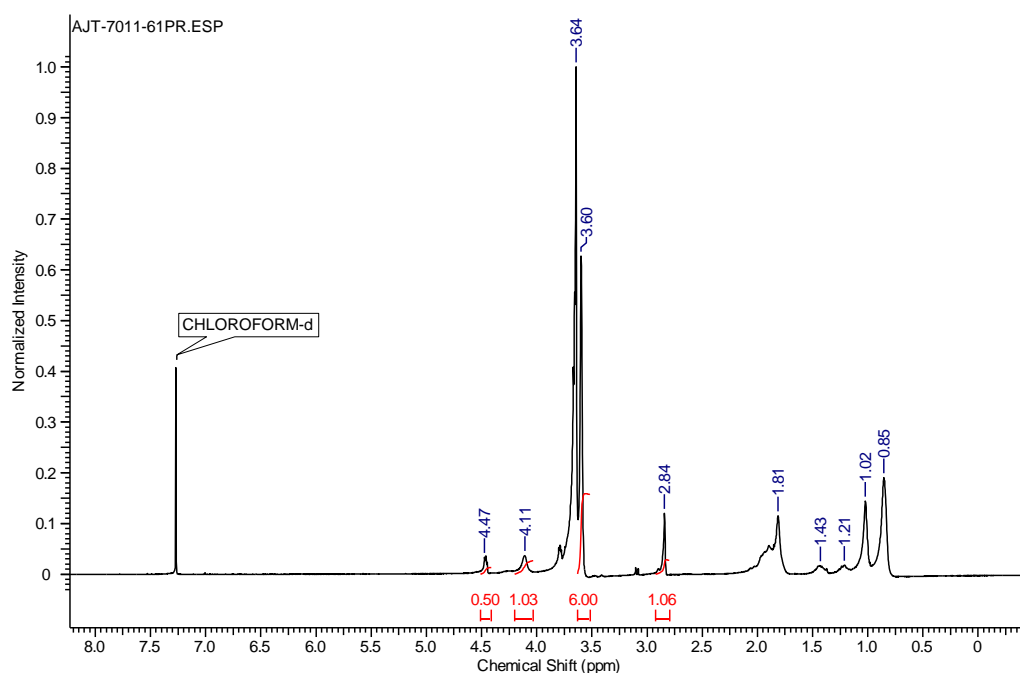


Figure 3.10 – NMR spectrum of P(MMA-co-PEGM) with succinimidyl carbonate functionality. The appearance of peaks at δ 2.8ppm and δ 4.5ppm confirmed successful addition of the succinimidyl carbonate group.

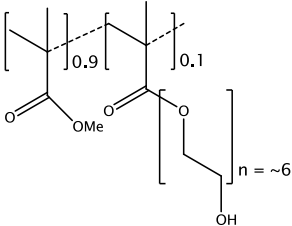
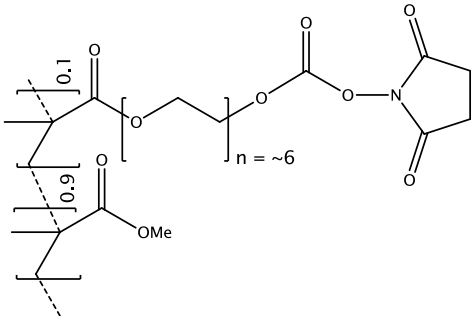
Polymer	3.5	3.14
Parameter		
Structure		
Amount of MMA (g)	8.4	8.4
Amount of PEGM (g)	2.82	2.82
PEGM Average Mw (Da)	360	360
Estimated monomer ratio from NMR	91:9	91:9
Mn	35053	22307
Mw	85228	35327
Polydispersity index	2.43	1.58

Table 3.3 - Summary of monomer feed ratios and data from polymers 3.5 and 3.14.

Following successful synthesis of this succinimidyl carbonate (SC) functionalised polymer (Polymer 3.14), it was necessary to optimise conditions for electrospinning. A range of polymer concentrations (0.4, 0.5 and 0.6g/ml) were used to find the optimum concentration for fibre production. Analysis by SEM showed that increasing polymer solution concentration increased the average fibre diameter in agreement with the literature¹⁹⁵. The 0.5g/ml solution was found to be most effective at creating large amounts of fibrous polymer (Figure 3.11). Following production, the networks of fibre were vacuum dried

to remove any residual 2-butanone. Complete solvent removal was confirmed by ^1H NMR.

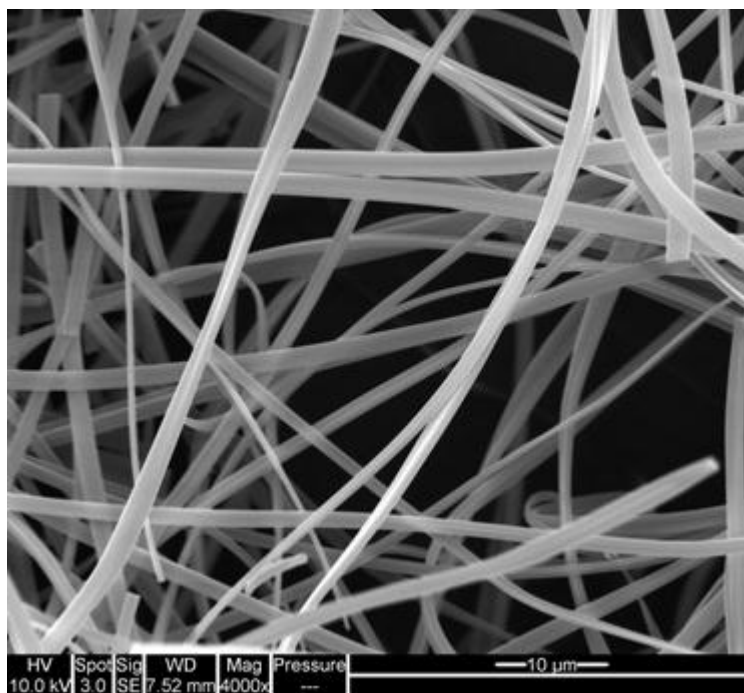


Figure 3.11 - Scanning micrograph of fibres electrospun from a solution of 0.5g/ml succinimidyl carbonate functionalised 75:25 P(MMA-co-PEGM) (Polymer 3.14) in 2-butanone.

3.5.2 Testing the basic biocompatibility of 75:25 P(MMA-co-PEGM) polymers (Polymers 3.5 and 3.14) with RPE cells

To further develop the system, it was necessary to investigate how retinal cells responded to this fibrous polymer substrate. The cellular work in this section was done collaboratively with Dr Heather Thomson. The compatibility of the copolymer fibres with human RPE cells was assessed by seeding an RPE cell line (ARPE-19) onto sections of the fibrous structures and subsequently assessing their attachment and viability. Polymer fibres with and without the succinimidyl carbonate functionality were tested and some samples were modified with peptides or proteins known to increase cell adhesion. The coupling of these ligands to polymer fibres was conducted in phosphate-buffered saline (PBS) (Scheme 3.2 Step (iii)). The cell adhesion peptides used were GRGDSP and YIGSR, both shown in the

literature to be effective cell adhesive ligands^{115,241}. In addition, some samples contained a combination of GRGDSP and YIGSR to assess whether these peptides could act synergistically to improve cell adhesion as has been observed in the literature¹¹⁵. The ECM protein laminin was also added to some samples as it had proved effective for encouraging RPE cell adhesion both in the literature³¹ and in previous microsphere experiments (Chapter 2). The samples used are summarised in Table 3.4. Cell-seeded fibre samples were grown in culture for a period of two weeks before assessment of the attachment, survival and proliferation of cells on the polymer surface. The culture medium was changed and samples of media were taken every two days for use in assays for the duration of the experiment. The main focus of these experiments was to assess the survival of cells on the polymer surface and if a cellular monolayer could be successfully formed.

Polymer number	Structure	Samples tested and conditions
3.5		1) Polymer alone 2) with cells
3.14		1) Polymer alone 2) with cells 3) with YIGSR and GRGDSP peptides 4) with GRGDSP peptide 5) with YIGSR peptide 6) with Laminin 7) Condition 3 + cells 8) Condition 4 + cells 9) Condition 5 + cells 10) Condition 6 + cells

Table 3.4 – Summary of polymer samples tested with RPE cells. Each condition was repeated three times using 0.5g/ml polymer fibres.

Following two weeks in culture, a lactate dehydrogenase (LDH) and a 3-(4,5-dimethylthiazol-2-yl)-2,5-diphenyltetrazolium bromide (MTT) assay were used to assess cell survival and cytotoxicity. Figure 3.12 shows the results of LDH assays on media samples taken from the different substrates averaged over the time course of the experiment. Most samples were shown to not have a cytotoxicity that was significantly greater than standard tissue culture plastic alone. The only samples giving a significantly higher absorbance were those of the SC functionalised polymer (Polymer 3.14) alone with no peptide attached. However, this could be due to there being more cells on these surfaces as a limitation of the LDH assay is that it does not show cell death as a proportion of total cell number. It is therefore possible that the same proportion of cells are dying on all of the different substrates but that those showing a higher absorbance

contained more cells. The LDH assay is therefore only a qualitative assessment of cell death. The positive control for this assay was taken from cells lysed with Triton solution to produce maximum LDH release (For data see Appendix C).

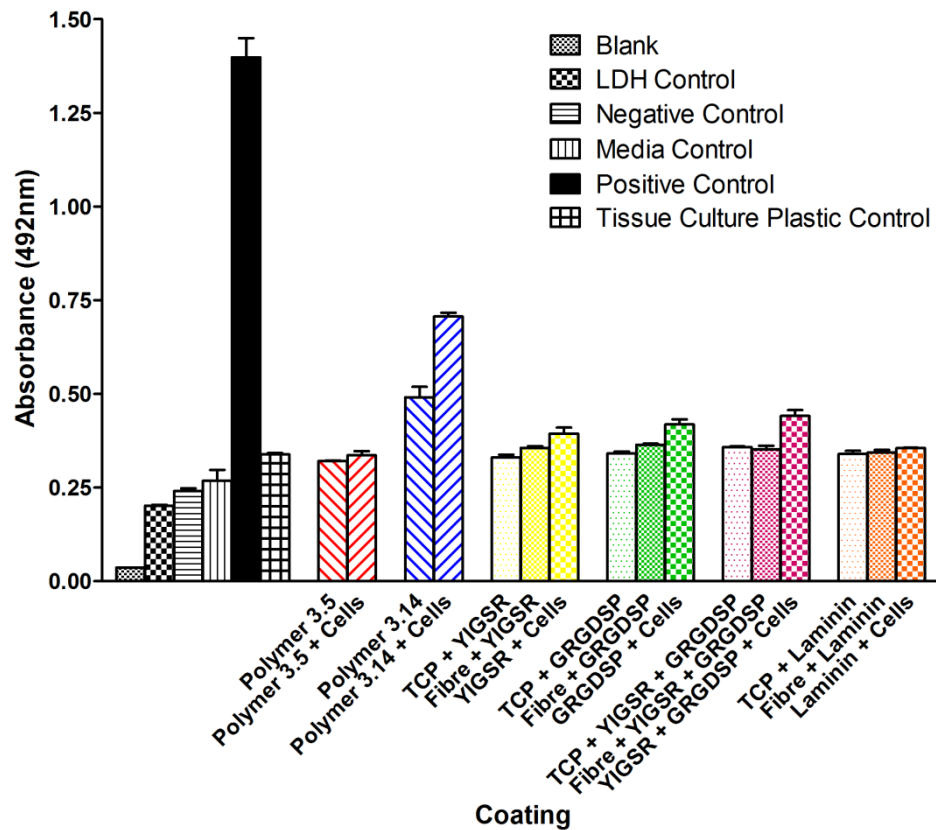


Figure 3.12 – Bar graph showing absorbance at 492nm of LDH assay samples from polymer scaffolds with different combinations of peptides or protein. TCP: Tissue culture plastic. For data see Appendix C

An important characteristic of any material for implantation is that it does not release any cytotoxic compounds. Release of cytotoxic compounds can be investigated by incubation of tissue culture media samples taken from cultures with fibres to fresh ARPE-19 cell cultures. Media samples from these cultures can then be analysed by an MTT assay to investigate cell viability. If any cytotoxic compounds were being released into the culture media by the fibres, cell death would be observed with this assay. Figure 3.13 below shows the results of the MTT assay from this experiment averaged over time.

The positive control in this experiment was from cells lysed with Triton solution. It can be seen that no significant cytotoxicity was observed with any of the fibrous polymer samples as all were significantly different ($p < 0.001$) different from the positive control.

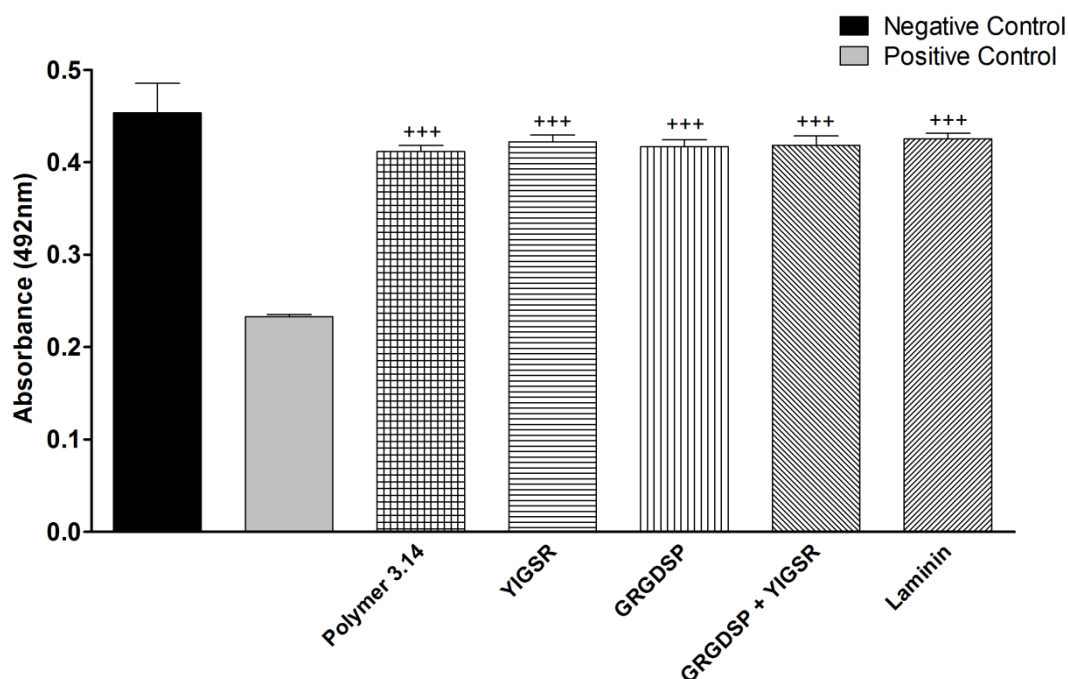


Figure 3.13 - Bar graph showing absorbance at 492nm of MTT assay samples of polymer 3.14 alone and in combination with cell adhesive peptides and proteins. Values represent mean \pm sem ($n = 16$) +++ $p < 0.001$ compared to positive control. For data see Appendix C

To determine if cells had successfully adhered to the surface of the fibrous substrates, immunocytochemical staining and SEM were employed. When 4',6-diamidino-2-phenylindole (DAPI) is applied to a cell culture, it intercalates in the DNA of the cell nuclei causing them to fluoresce blue under ultraviolet light. As can be seen in Figure 3.14, cells attached to and covered the fibrous surface. The creation of a surface on which RPE cells can adhere and proliferate was an important step in the pursuit of creating an artificial BM.

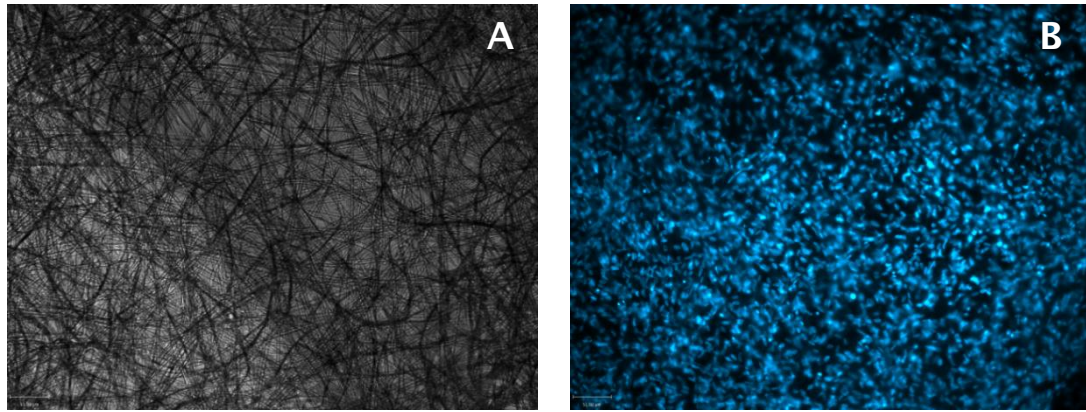


Figure 3.14 - Light microscope image of a cell seeded polymer scaffold (A) and the same image under ultraviolet light following labelling of cell nuclei with DAPI (B). Scale bar 52 μ m.

Further cell seeded samples of fibres were dehydrated in ethanol, fixed using 3% glutaraldehyde with 4% formaldehyde and sputter coated with gold/palladium for SEM analysis. The images showed a layer of cells sitting on the surface of the fibres (A sample image can be seen in Figure 3.15). The cellular layer appears cracked in this image; this was attributed to the dehydration process. Cells on the surface appeared to form a monolayer which is an essential quality for a replacement RPE layer. When cells are grown on tissue culture plastic, trypsinisation is required to move cells from one location to another which disrupts the monolayer. The ability to create an RPE monolayer on a fibrous, moveable substrate is therefore advantageous for tissue engineering as it facilitates transplantation. This type of substrate could also be useful in developing an *in vitro* retinal model as it could provide a basement membrane on which cellular structures could be formed and moved without disruptive trypsinisation.

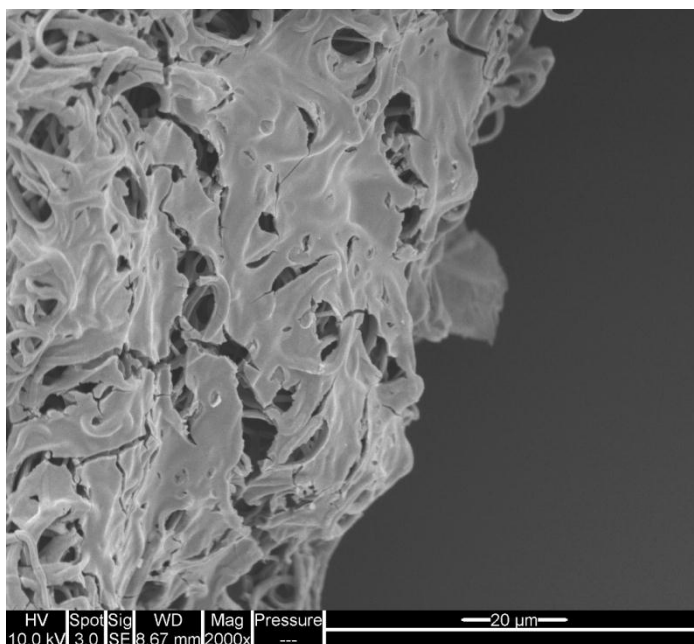


Figure 3.15 – Scanning electron micrograph showing cells seeded onto a 75:25 P(MMA-co-PEGM) succinimidyl carbonate (Polymer 3.14) fibre surface.

This series of initial experiments investigating the behaviour of RPE cells seeded onto synthetic fibrous scaffolds showed that retinal cells could attach to and survive successfully on these substrates. Furthermore, the fibres did not release any cytotoxic compounds and RPE cells appeared to be forming a monolayer across the scaffold surface. No differences in LDH release or cytotoxicity were observed when cell adhesive peptides and proteins were used. However, a limitation of the fibrous substrates was that they were observed to resist being immersed in tissue culture media. This was attributed to the low PEG content in this polymer resulting in the fibres being more hydrophobic than desired. In addition, the low amount of PEG resulted in only a small number of end groups being available for attachment of cell adhesive peptides. This suggested that a polymer with a higher quantity of PEG chains was required. Also, further data were required to complement the LDH and MTT assays to gain an accurate representation of cell attachment and survival on these surfaces.

3.5.3 Development of a P(MMA-co-PEGM) copolymer containing a higher PEG content

To increase the hydrophilicity of fibres, a polymer containing more PEG methacrylate monomer was synthesised. The monomer feed ratio was changed from 75:25 (MMA:PEGM) to 60:40 (MMA:PEGM) by weight. ¹H NMR integrals were again used to estimate the comonomer ratio. This copolymer (Polymer 3.6) was shown to contain approximately 20% PEGM comonomer units. Polymer 3.6 was then converted to the succinimidyl carbonate (Polymer 3.15) using the same method as previously described in Section 3.5.2 (Table 3.5).

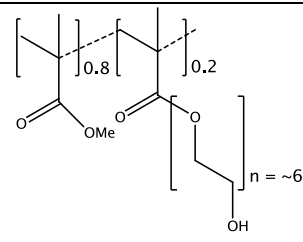
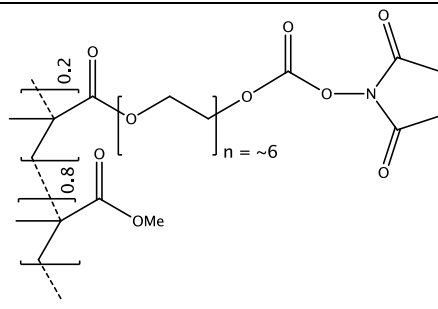
Polymer	3.6	3.15
Parameter		
Structure		
Amount of MMA (g)	6.72	6.72
Amount of PEGM (g)	4.51	4.51
PEGM Average Mw (Da)	360	360
Estimated monomer ratio from NMR	80:20	80:20
Mn	23165	22536
Mw	38789	39943
Polydispersity index	1.67	1.77

Table 3.5 – Summary of monomer feed ratios, comonomer ratios and GPC data for Polymers 3.6 and 3.15.

This polymer was characterised by IR and NMR spectroscopy as well as GPC. Solutions of both the unfunctionalised (Polymer 3.6) and SC functionalised (Polymer 3.15) polymer in 2-butanone were electrospun into fibres (0.55g/ml polymer solution in 2-butanone) and analysed by SEM (Figure 3.16). The resultant fibres were less homogenous than those prepared using the previous copolymer. They were also less ribbon-like than previous preparations and more cylindrical in cross section. These differences are likely to be due to altered solvent evaporation during the electrospinning process resulting from the increased PEG content.

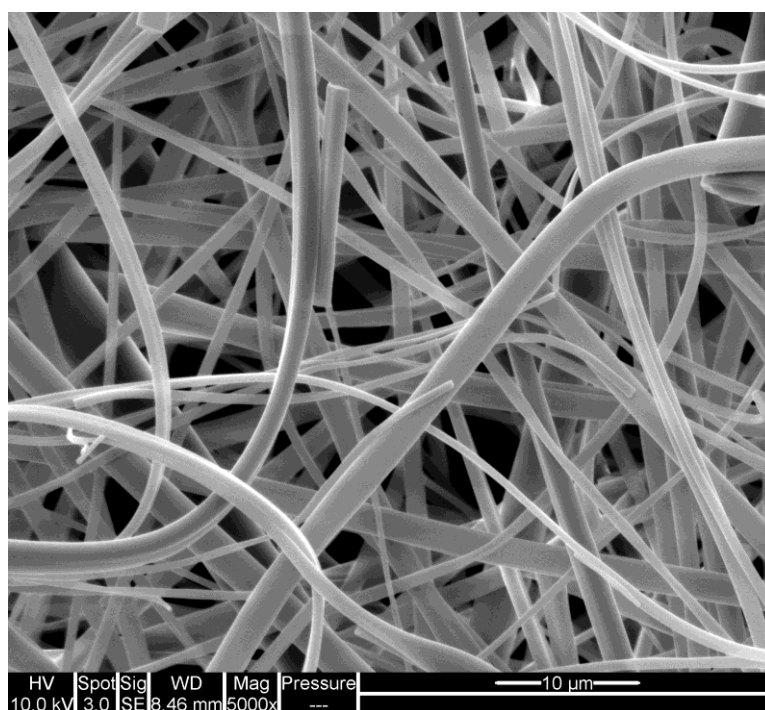


Figure 3.16 – Scanning electron micrograph showing 60:40 P(MMA-co-PEGM) succinimidyl carbonate (Polymer 3.15) electrospun into fibres.

The morphology of electrospun fibres can be affected by various factors such as flow rate, applied voltage, distance from collector and solution viscosity¹⁹⁵. Having investigated the effect of changing applied voltage with previously produced copolymers, the effect of changing solution flow rate was determined. A solution of polymer 3.15 was electrospun at a flow rate of 9.5ml/hr and 1.5ml/hr with all other parameters remaining constant. Figure 3.17 below shows that

lowering the flow rate caused some beading in the fibres and reduced the average fibre diameter (Table 3.6). The increase in beading is due to a decrease in the volume of the droplet on the end of the needle during the electrospinning process²⁰⁰. If there is an insufficient flow of polymer solution to this droplet, instabilities in the electrospinning jet can result. It is these instabilities that lead to beading. A smaller volume of solution in this droplet will also cause the electrostatic force present to be concentrated. This can result in a smaller electrospinning jet leading to fibres with a reduced diameter.

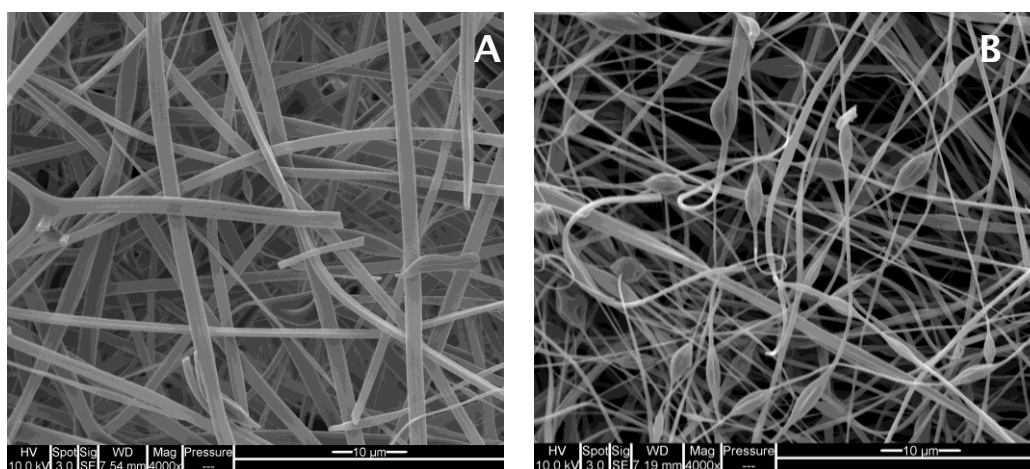


Figure 3.17 - Scanning electron micrograph of electrospun fibres of 60:40 P(MMA-co-PEGM) succinimidyl carbonate (Polymer 3.15) at a flow rate of 9.5ml/hr (A) and 1.5ml/hr (B).

The effect of changing solution concentration was also investigated for this polymer. Solutions of polymer 3.15 were used for this experiment. The results are summarised below (Table 3.6). As would be expected based on the literature¹⁹⁵, there was an increase in average fibre diameter associated with an increase in solution concentration. Polymer solutions are less viscous at lower concentrations enabling smaller diameter fibres to be formed. At higher concentrations, there is more entanglement of the polymer chains. This increases the stability of the polymer jet resulting in larger diameter fibres.

Solution concentration (g/ml)	Average fibre diameter (μm) (n = 15) \pm sem
0.45	1.63 \pm 0.07
0.5	1.80 (9.5ml/hr) \pm 0.11 0.75 (1.5ml/hr) \pm 0.10
0.55	2.54 \pm 0.16

Table 3.6 - Table showing average diameters of electrospun fibres of 60:40 P(MMA-co-PEGM) succinimidyl carbonate (Polymer 3.15) at different concentrations. The effect of changing the solution flow rate is also shown. sem: standard error of the mean.

Contact angle measurements were used to demonstrate the difference in hydrophilicity between polymers 3.5 and 3.6. Both were spin coated onto glass along with a sample of poly(methyl methacrylate) (PMMA) as a control. The contact angle of a water droplet to each of the surfaces was measured using a goniometer. Images from this analysis are shown below (Figure 3.18). The increase in hydrophilicity with increasing PEG content can be clearly seen as the water contact angle decreases (Table 3.7).

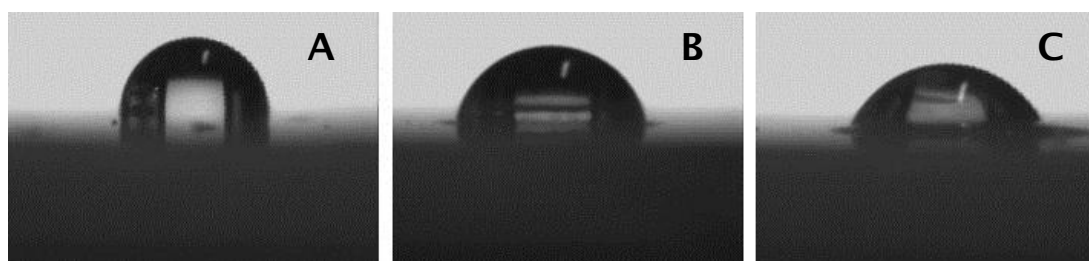


Figure 3.18 - Images taken from a water contact goniometer of a water droplet on polymer coated glass surfaces. The different polymers used were PMMA (A), Polymer 3.5 (B) and Polymer 3.6 (C).

Polymer	Average contact angle ($^{\circ}$) (n = 3) \pm sem
PMMA	101.2 \pm 0.35
3.5	77.1 \pm 0.65
3.6	59.7 \pm 2.88

Table 3.7 - Table showing average contact angles for different polymers. sem: standard error of the mean.

Characterising the presence of small quantities of peptides on the surface of functionalised polymer fibres had proved challenging. To overcome this problem a fluorescein (Flu)-tagged peptide, Lysine(Flu)-Arginine-Glycine-Aspartic acid (K(Flu)RGD), was dissolved in phosphate-buffered saline (PBS) at the same concentration (1mg/ml) used in cell seeding experiments. Samples of SC functionalised (Polymer 3.15) and unfunctionalised (Polymer 3.6) fibres were then immersed in 1ml of this solution overnight before being washed in PBS and dried. The samples were then imaged using a fluorescence microscope (Chapter 5 - Section 5.7.2). The images shown in Figure 3.19 indicate that the tagged peptide had bound successfully to the fibres with the SC functionality (Polymer 3.15) but not to the other fibres (Polymer 3.5).

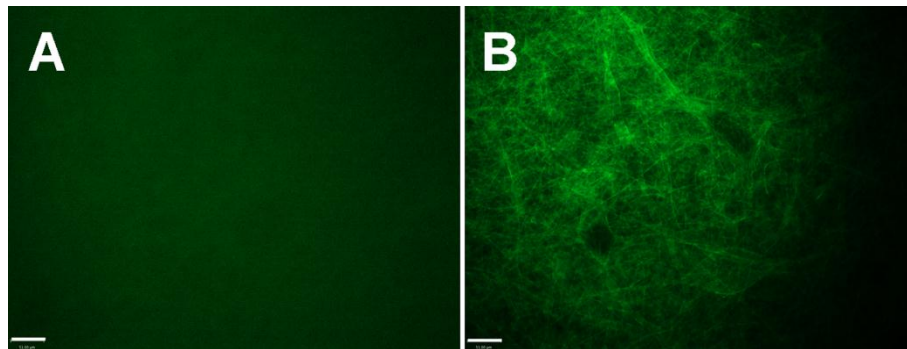


Figure 3.19 - Fluorescence microscope images showing fibre samples of Polymer 3.6 (B) and 3.15 (A) following immersion in a solution of K(Flu)RGD in PBS. Scale bar: 52 μ m.

3.5.4 Testing the biocompatibility of 60:40 P(MMA-co-PEGM) polymers (Polymers 3.6 and 3.15) with RPE cells

As with previous fibrous scaffolds, it was necessary to assess the compatibility of the fibres produced with RPE cells. The peptides GRGDSP and YIGSR (Figure 3.17) along with the protein laminin were combined with the fibrous substrates to assess their impact on cell adhesion. The peptide GRGESP (Figure 3.17) was also included and as this peptide should have reduced abilities to enhance cell adhesion compared with GRGDSP⁶⁴. Despite the difference between these sequences being only one amino acid, the change in the shape of the molecule is sufficient to disrupt the non-covalent interactions that govern molecular binding to the integrin receptor. As the aspartic acid (D) carboxylate group coordinates to a metal ion when binding to an integrin receptor, changing the position of this group in glutamic acid (E) may result in reduced affinity for the receptor. It has been reported that these peptides may adopt a folded conformation when in low surface concentration whereas when they are close together an extended conformation is favoured²⁴².

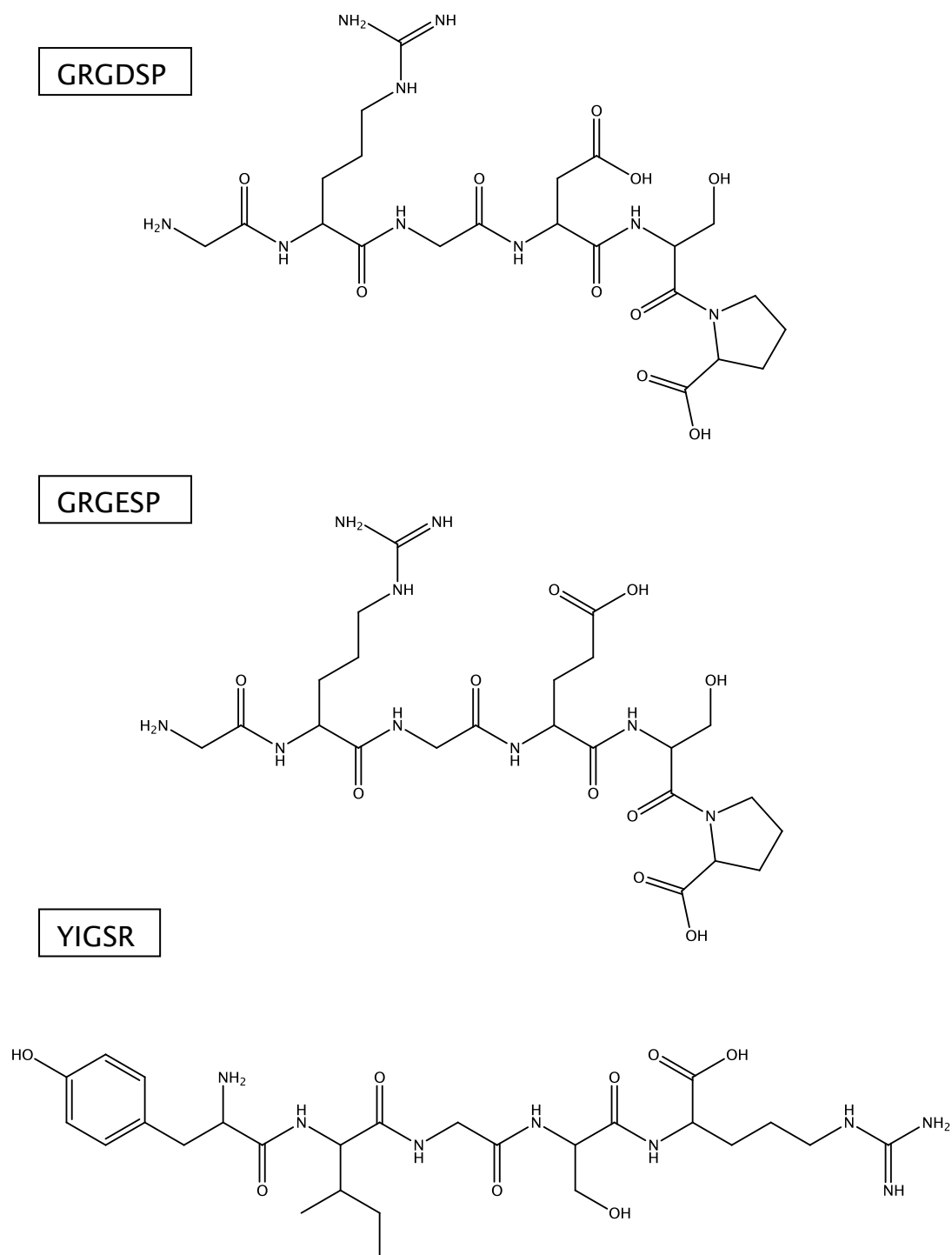


Figure 3.20 – Chemical structures of the three peptide sequences used for cell adhesion assays.

ARPE-19 cells were seeded onto a range of fibrous copolymer samples combined with peptides or proteins (Table 3.8). These more hydrophilic polymer fibres were found to be easier to immerse in tissue culture media than those used in Section 3.5.2. As native BM is

responsible for some conductance of water, this result suggests that this polymer would perform better *in vivo* than the previously produced polymer. In addition to the assays used for the previous experiment, a terminal deoxynucleotidyl transferase dUTP nick end labelling (TUNEL) assay was used to obtain a quantitative measure of cell survival. The cells were stained with propidium iodide (PI), a DNA intercalating agent that causes cell nuclei to fluoresce red under the correct wavelength of light. This was used to quantify the density of cells attached to the fibrous substrates.

Polymer number	Structure	Samples tested and conditions
3.6		1) Polymer alone 2) with cells
3.15		1) Polymer alone 2) with cells 3) with GRGESP peptide 4) with GRGDSP peptide 5) with YIGSR peptide 6) with YIGSR and GRGDSP peptides 7) with Laminin 8) Condition 3 + cells 9) Condition 4 + cells 10) Condition 5 + cells 11) Condition 6 + cells 12) Condition 7 + cells

Table 3.8 – Summary of polymer samples tested with RPE cells. Each condition was performed three times with 0.55g/ml electropun fibres.

Samples of media for LDH and MTT assays were taken every two days during the culture period. Figure 3.21 shows the results of the LDH assay averaged over time for each of the combinations of fibres with

peptides used in this experiment. These results show that cell death on all the scaffolds was significantly ($p < 0.001$) lower than the positive control. There was a trend towards increased LDH release on the fibrous scaffolds compared with cells grown on tissue culture plastic. This could be either a result of increased cell death on the fibres or the same proportion of cells dying but there being a greater number on the fibrous samples due to an increase surface area for cell attachment. In contrast to the previous study, there was no significant difference between LDH release on SC-functionalised fibres compared with those that were unfunctionalised. The greatest LDH release was observed on fibres with a combination of the GRGDSP and YIGSR peptides attached. However, these fibres were found to have the highest level of cell attachment by day 15 (Figure 3.24).

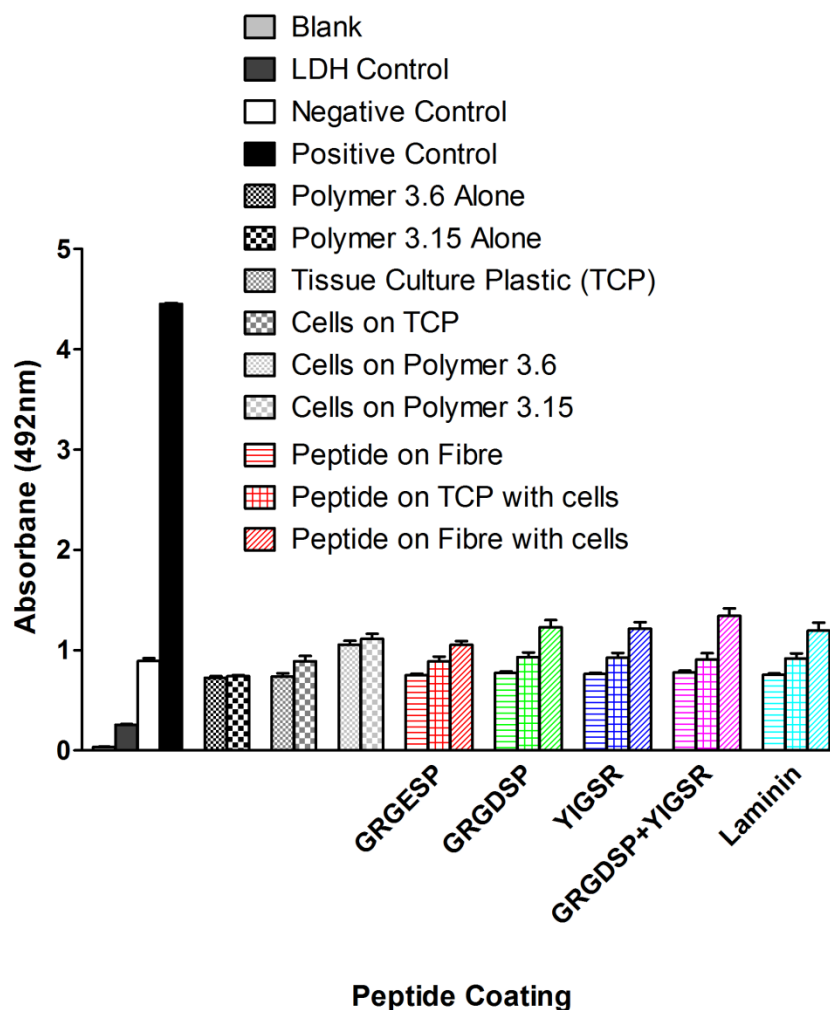


Figure 3.21 - Bar graph illustrating absorbance in LDH assay averaged over time for samples of fibrous scaffolds. All values were significantly different ($p < 0.001$) compared with positive control. TCP: Tissue culture plastic. For data see Appendix C.

As with the previous study (Section 3.5.2), an MTT assay was used to assess the presence of any cytotoxic compounds being released from the fibrous samples. The results of this assay averaged over the time course of the experiment can be seen in Figure 3.22. There was no statistical difference between results obtained from media taken from fibrous samples and the negative control. Cell viability for all the samples was significantly different to the positive control (taken from cells lysed with 0.2% Triton). As with the previous experiments, the results show that no cytotoxic compounds are being released from the fibrous scaffolds.

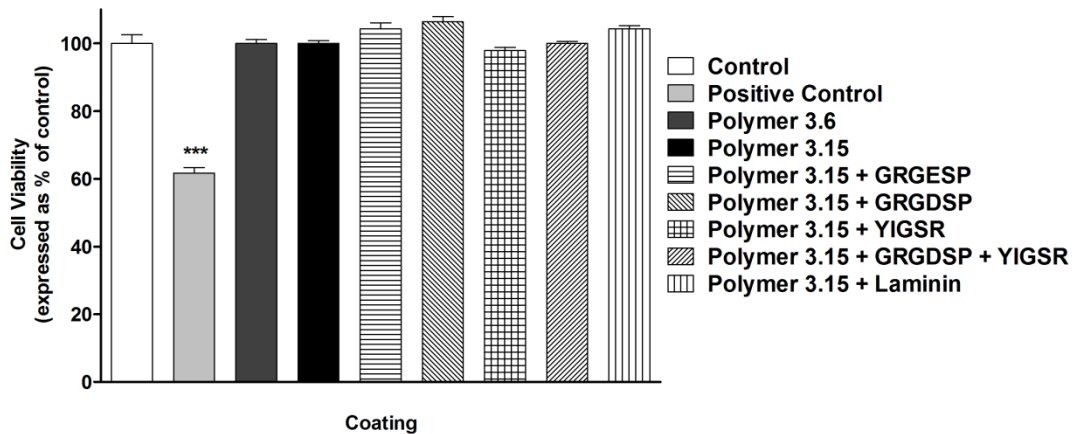


Figure 3.22 - Bar graph showing absorbance in the MTT assay used as an indirect measure of cytotoxicity. Results for each fibre sample are averaged over time. A decrease in absorbance indicates cell death. Values represent mean \pm sem (n = 16) ***p<0.001 compared to all fibrous samples. For data see Appendix C.

The TUNEL assay detects DNA fragmentation resulting from cell apoptosis providing a quantitative assessment of cell survival. 'Nicks' within the DNA are identified by the enzyme terminal deoxynucleotidyl transferase. This enzyme can then incorporate modified nucleotides which can be fluorescently tagged to indicate the presence of an apoptotic cell. Samples of fibres with cells seeded were taken at days 5, 10 and 15 *in vitro* for use in this assay. The assay was performed in triplicate for each type of fibre. It can be seen that on the fibres of polymer 3.6, the percentage cell apoptosis over the total cell area increased significantly from 8% to 20% between day 5 and day 15 of the experiment (Figure 3.23). This is due to a lack of cell attachment on these fibres (Figure 3.24). This trend is reversed for fibres of the SC functionalised polymer (Polymer 3.15) for which cell apoptosis decreases from 8% to 2% between days 5 and 15. The addition of peptides, including the control GRGESP peptide, was observed to generally decrease cell apoptosis over time. In particular, fibres combined with either YIGSR or GRGDSP/YIGSR peptides gave significantly (p<0.01) improved cell viability compared with fibres of polymer 3.6.

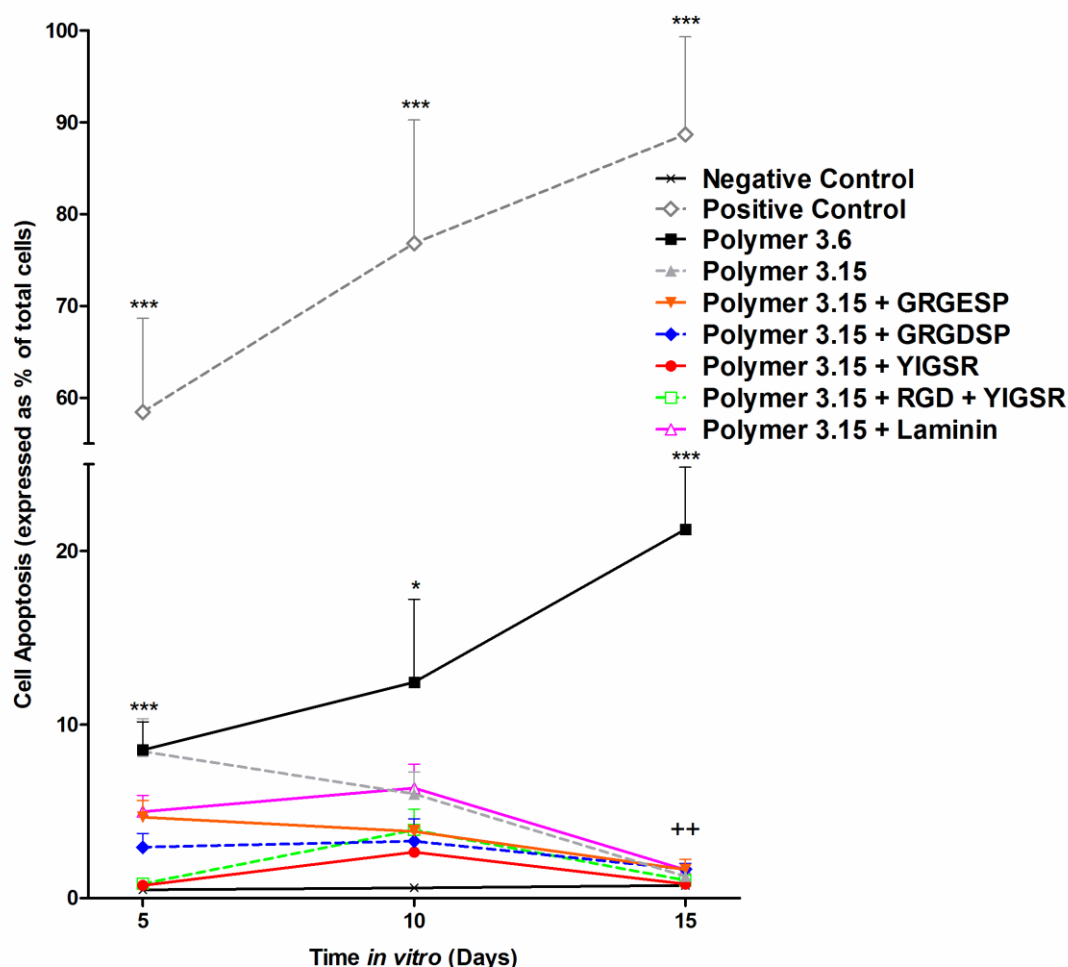


Figure 3.23 – Graph showing cell apoptosis (as a percentage of total cells) by TUNEL assay on various fibre samples at days 5, 10 and 15 *in vitro*. *** $p < 0.001$, * $p < 0.05$ compared to negative control. ** $p < 0.01$ compared to polymer 3.6. For data see Appendix C.

To investigate the influence of cell attachment on RPE cell survival, samples from different time points during the experiment were stained with PI. The results are shown below in Figure 3.24. As might have been expected given the results of the TUNEL assay, cell attachment decreased over 15 days on the fibres produced from polymer not containing the SC functionality (Polymer 3.6). This result concurs with previous experiments by Tezel *et al.*¹⁹ showing cell apoptosis increases when RPE cells are not attached to a surface. At day 15, the highest cell densities were observed on the samples that showed lowest percentage of cell apoptosis. These were fibres with

either YIGSR or a combination of GRGDSP and YIGSR peptides coupled to the surface. This indicates that some synergy between these sequences as reported in the literature¹¹⁵ may be occurring. It has been proposed¹¹⁵ that this synergy results from the ability of the YIGSR peptide combined with RGD to promote focal adhesion sites. These sites provide mechanical strength to attachment points between cells and the ECM²⁴³. The peptide GRGESP produced the lowest cell attachment at day 15 of any of the peptides used.

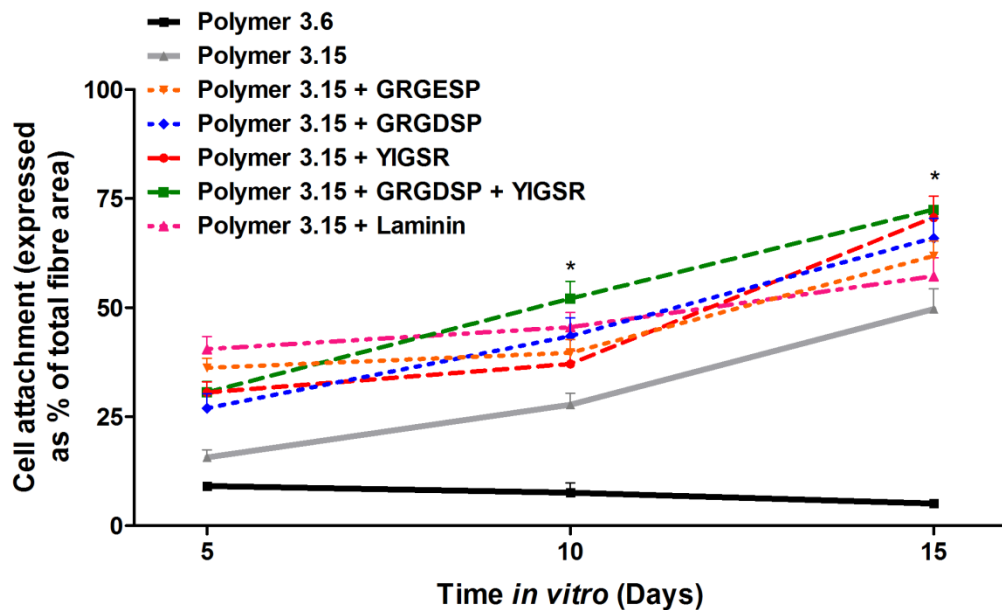


Figure 3.24 - Graph showing cell attachment (as a percentage of total fibre area) on various fibre samples at days 5, 10 and 15 *in vitro*. * $p < 0.01$ compared with polymer 3.6. For data see Appendix C.

As described previously in Section 3.5.2, SEM was used to investigate the morphology and polarisation of cells on the substrate surface. Micrographs (Figure 3.25) show RPE cells forming a monolayer on top of the fibres. The cells also appeared to be adopting a hexagonal morphology and displaying microvilli on the surface. This shows that the cells were adopting typical shape and indicates correct polarisation.

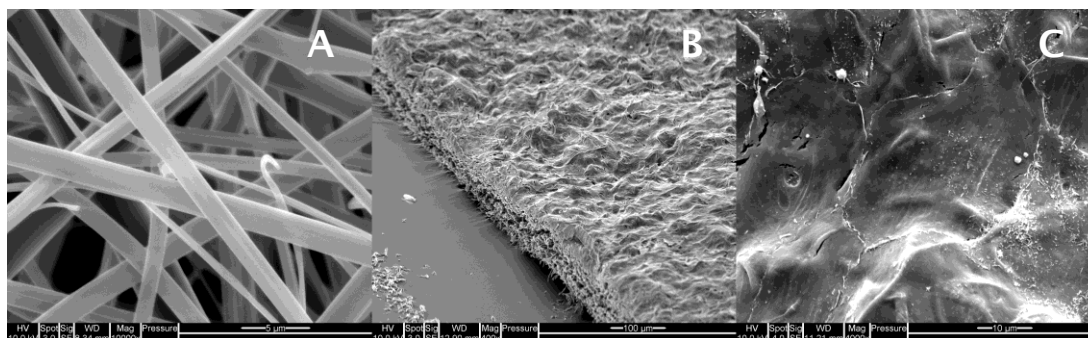


Figure 3.25 – Scanning electron micrographs of fibres from polymer 3.15 without cells (A), a cross section of a fibrous mat (Polymer 3.15) with cells (B) and a view of cell morphology on scaffold surface (C).

The results of this set of experiments showed that successful RPE cell adhesion and growth could be achieved using the SC-functionalised 60:40 P(MMA-co-PEGM) copolymer (Polymer 3.15). Whereas the polymer containing an alcohol-terminated PEG chain (Polymer 3.6) had the reverse effect on cell adhesion and survival. The fibres produced showed improved handling qualities compared to those produced in Section 3.5.1 and quantitative data on cell adhesion and survival was obtained. The use of basic chemistries to control the interactions between cells and surfaces is of great interest in the field of regenerative medicine. Therefore, the discovery that addition of a succinimidyl group could give a significant difference in cell adhesion invited further investigation.

3.5.5 Investigating the effect of hydrophilicity, PEG chain length and end group on RPE cell adhesion

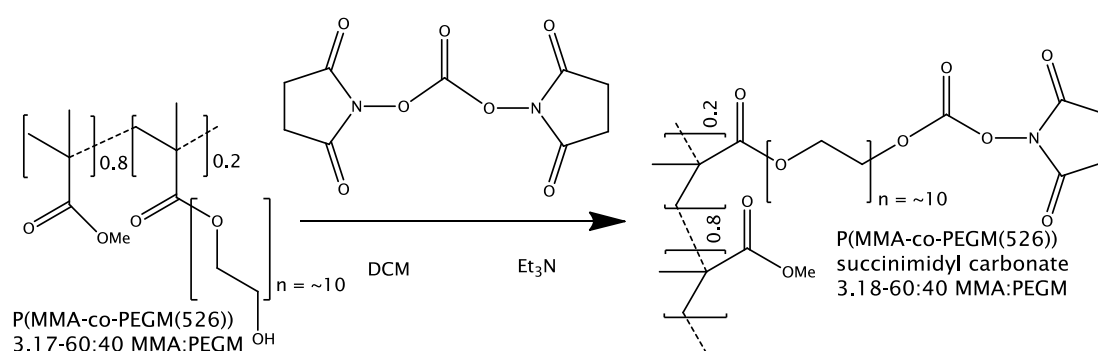
A new set of experiments were designed to more fully investigate the effect of changing aspects of the PEG component of the copolymer system with respect to cell adhesion. These experiments did not include any peptide component and focused solely on the impact of polymer chemistry on cell adhesion. A range of copolymers were synthesised and characterised (Chapter 5 – Section 5.2). These included polymers 3.6 and 3.15 used in the previous study as well as a more hydrophilic version of the P(MMA-co-PEGM) polymer containing 40:60 MMA:PEGM by weight (Polymer 3.7). The polymers

produced are summarised in Table 3.8. As with the copolymers described in Sections 3.5.2 and 3.5.3, it was necessary to estimate ^1H NMR integrals due to signal overlap. These estimated integrals revealed that polymer 3.7 had approximately 40% PEGM comonomer units. As with previous polymers, polymer 3.7 was reacted to generate an SC functionality (Polymer 3.16). Experiments investigating the impact of changing solution concentration on the diameter of fibres produced using polymer 3.15 (Section 3.5.4) concluded that an increase in solution concentration resulted in an increase in average fibre diameter. This experiment was repeated using three concentrations of polymer 3.16 (Table 3.9) and shows that the same trend was observed with this polymer. However, it was noted that a more concentrated solution of polymer 3.16 was required to produce the same diameter fibre achieved by polymer 3.15. GPC results showed that the polydispersity index of polymer 3.16 was greater than that of polymer 3.15 (Chapter 5 – Section 5.2.6). The molecular weight distribution of methacrylate-based polymers has been shown in the literature to influence the electrospinning process¹⁸⁹. It has been proposed that the differences in hydrodynamic volume between shorter and longer chains can result in instabilities in chain entanglement. The result is that a more concentrated solution of the more polydisperse polymer is needed to achieve the same entanglement. The level of entanglement of polymer chains is key to the diameter of the electrospinning jet and therefore the resultant fibres.

Solution concentration (g/ml)	Average fibre diameter (μm) (n = 15) \pm sem
0.55	1.36 \pm 0.10
0.65	2.94 \pm 0.20
0.75	3.78 \pm 0.19

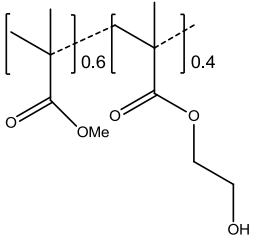
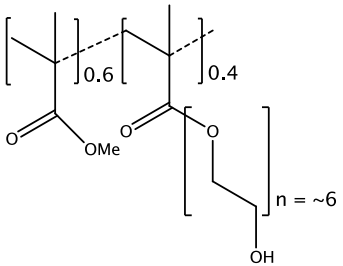
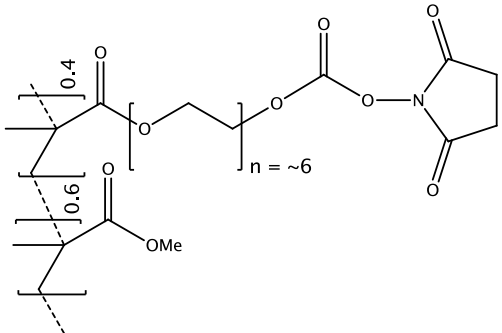
Table 3.9 – Table showing average diameters of electrospun fibres of 40:60 P(MMA-co-PEGM) succinimidyl carbonate copolymer (Polymer 3.16) at different concentrations. sem: standard error of the mean.

In addition to investigating the effect of the SC group, 60:40 and 40:60 P(MMA-co-PEGM) copolymers with succinimidyl ester PEG end groups were also prepared (Polymers 3.12 and 3.13 respectively). However, attempts to produce fibres of polymer 3.13 were unsuccessful. This polymer could therefore not be used in any cell testing. Fibres of polymer 3.12 were successfully produced (Figure 3.26) and used in biocompatibility tests. The influence of the PEG chain was also researched in these experiments. To achieve this, longer and shorter PEG chains than had been used for the experiments in Section 3.5.3 were incorporated. A PEGM monomer with a higher average molecular weight was obtained (Average Mw 526) and copolymerised with MMA to achieve a copolymer (Polymer 3.17) that had longer PEG chains on average (Scheme 3.4). The monomer feed ratio was set to give the same proportion of PEGM units as the 60:40(MMA:PEGM) copolymer. NMR data showed that approximately 22% of the comonomer units were PEGM, comparable to the average 20% given with polymer 3.6 (using PEGM with average molecular weight 360Da). This copolymer was also successfully functionalised with an SC group on the end of the PEG chain (Polymer 3.18). A P(MMA-co-HEMA) copolymer (Polymer 3.3) was synthesised to investigate the effect of a short alcohol-terminated chain on RPE cell culture.



Scheme 3.4 - Scheme showing the reaction of P(MMA-co-PEGM) with disuccinimidyl carbonate.

The resulting copolymers were electrospun from a series of solutions in 2-butanone. The polymers (apart from polymers 3.3 and 3.12) were electrospun from a 0.55g/ml solution. As polymers 3.3 and 3.12 did not give successful fibrous substrates at this concentration, an alternative concentration was used (Table 3.10).

Compound	Structure	Concentration used
60:40 P(MMA-co-HEMA) (Polymer 3.3)		0.45g/ml
40:60 P(MMA-co-PEGM) (Polymer 3.7)		Very hydrophilic. Dissolved in water and therefore could not be used.
40:60 P(MMA-co-PEGM) SC functionalised (Polymer 3.16)		0.55g/ml

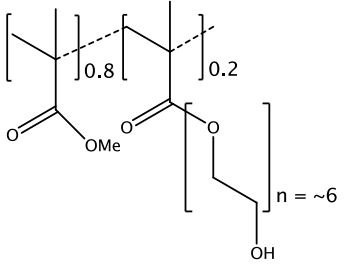
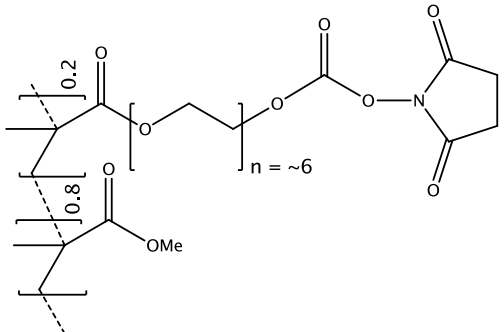
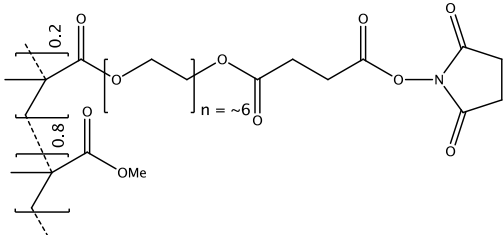
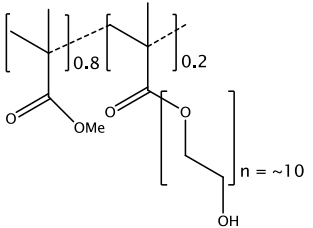
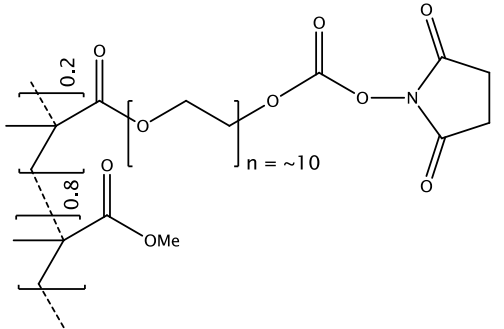
<p>60:40 P(MMA-co-PEGM) (Polymer 3.6)</p>		0.55g/ml
<p>60:40 P(MMA-co-PEGM) SC functionalised (Polymer 3.15)</p>		0.55g/ml
<p>60:40 P(MMA-co-PEGM) succinimidyl ester functionalised (Polymer 3.12)</p>		0.65g/ml
<p>60:40 P(MMA-co- PEGM(526)) (Polymer 3.17)</p>		0.55g/ml
<p>60:40 P(MMA-co- PEGM(526)) SC functionalised (Polymer 3.18)</p>		0.55g/ml

Table 3.10 - Table showing the structures of copolymers produced and the concentration of electrospinning solution used to create fibres for biocompatibility testing with RPE cells. SC: Succinimidyl carbonate

Following electrospinning, the fibrous networks were characterised by SEM to assess fibre morphology and size (Table 3.11). All of the matrices produced had an average fibre diameter of less than 10 μ m. It was found that matrices of smaller fibres gave handling advantages for cell seeding compared with larger diameter fibres. Material handling properties are an important factor when considering the future surgical applications of these matrices. Polymers that did not contain a succinimidyl functionality (Polymers 3.6 and 3.17) had a slightly larger average fibre diameter than that of their functionalised counterparts (Polymer 3.15 and 3.18). This is because the solutions of polymers 3.6 and 3.17 gave a more viscous solution at the same concentration as other polymers. The porosity of the fibres was determined by evaluating areas covered by fibres in relation to the total area of the sample (Chapter 5 - Section 5.3.1). The least porous matrix was produced using polymer 3.15, while the most porous matrix produced was manufactured using polymer 3.12. Scaffold porosity did not appear to correlate with fibre diameter (Table 3.11). Differences observed in scaffold porosity did not reach statistical significance. As with previous copolymers, samples were spin coated onto glass to enable determination of water contact angles to assess the relative hydrophilicity of different copolymers. These data are also summarised in Table 3.11 below. Polymer 3.17 with longer PEG chains (PEG Av MW ~526) was shown to be more hydrophilic than Polymer 3.6 (PEG Av MW ~360) as might be expected. Conversion of the PEG terminus alcohol group into either a SC or an ester resulted in an increase in hydrophobicity. This effect was more pronounced in the copolymers containing longer PEG chains.

Polymer	Fibre diameter (μm) (n = 15)	Scaffold porosity (%) (n = 10)	Contact angle ($^{\circ}$) (n = 3)
3.3	9.82 \pm 0.73 ***	31.88 \pm 3.30	58.6 \pm 0.4
3.6	2.05 \pm 0.27 +	34.82 \pm 2.48	59.7 \pm 2.9
3.12	1.34 \pm 0.20	35.18 \pm 3.13	67.1 \pm 0.8
3.15	1.80 \pm 0.11	22.54 \pm 1.34	67.8 \pm 0.4
3.16	1.36 \pm 0.10	33.17 \pm 1.93	74.6 \pm 0.6
3.17	2.24 \pm 0.22 ++	30.98 \pm 1.89	57.0 \pm 0.7
3.18	1.44 \pm 0.11	29.90 \pm 4.47	77.5 \pm 1.2

Table 3.11 - Table showing mean fibre diameter, scaffold porosity and contact angle for different copolymers. Values expressed as mean \pm sem. Statistical analysis by Student's t-test for fibre diameter and by ANOVA followed by post-hoc comparison for scaffold porosity. Statistical difference * $p < 0.001$ compared to all other fibres tested. Fibres of polymer 3.6 (+ $p < 0.05$) and 3.17 (++ $p < 0.01$) were statistically different compared to fibres of polymers 3.12, 3.16 and 3.18.**

As with previously synthesised copolymers, the effect of changing solution concentration was investigated using polymer 3.12. Figure 3.26 below shows that reducing the solution concentration can cause significant beading in the fibres. In lower viscosity solutions, the entanglement of polymer chains is reduced. This can lower the stability of the electrospinning jet leading to beading.

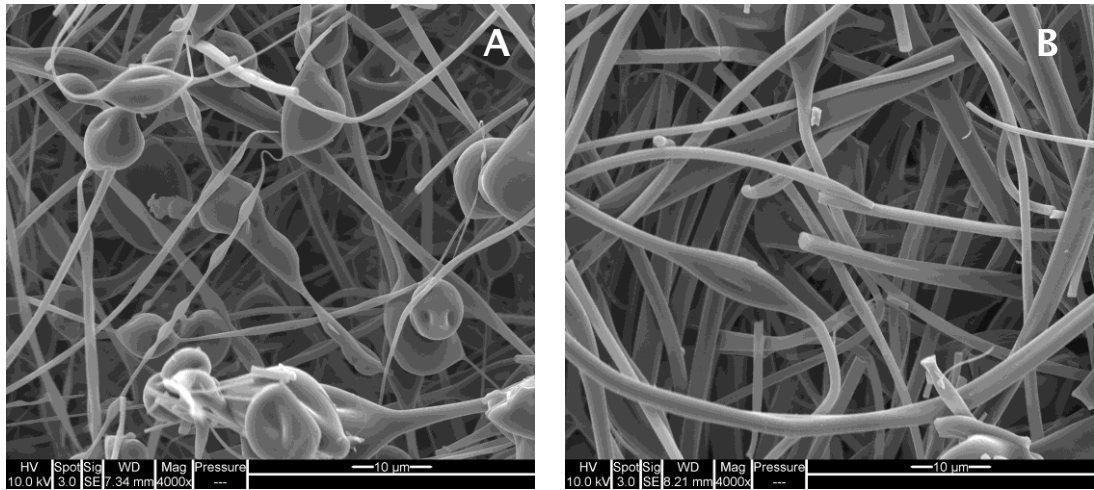


Figure 3.26 - Scanning electron micrograph of electrospun fibres of 60:40 P(MMA-co-PEGM) succinimidyl ester (Polymer 3.12) at a solution concentration of 0.55g/ml (A) and 0.65g/ml (B).

SEM was used to show cells on the surface of the fibrous scaffolds (Figure 3.27). The cells appear to be forming a tight monolayer with typical cobblestone morphology. The junctions between cells are clearly visible and apical microvilli are present. These microvilli indicate correct polarity of the RPE cells which has shown to be important for growth factor secretion¹⁹⁴.

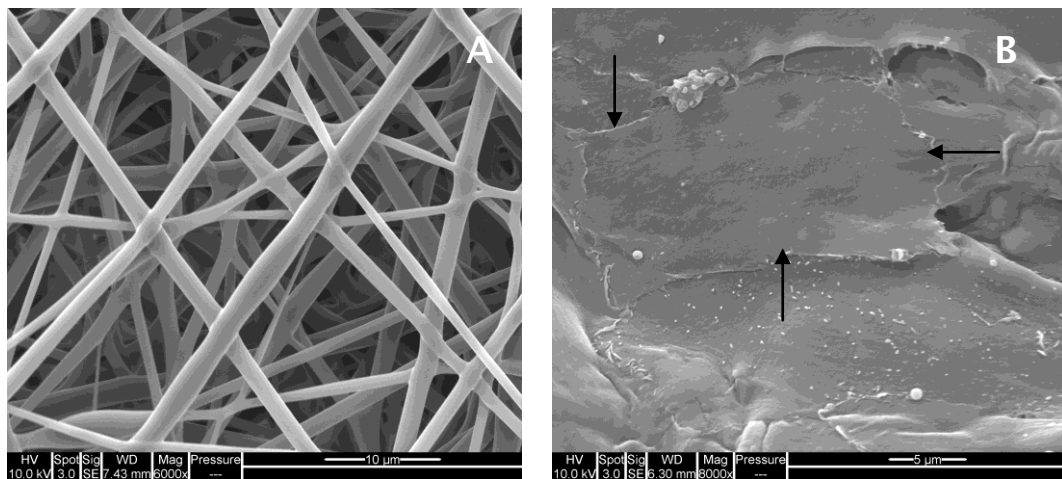


Figure 3.27 - Scanning electron micrographs showing fibres of a 40:60 P(MMA-co-PEGM) succinimidyl carbonate (Polymer 3.16) both without cells (A) and seeded with cells (B). Black arrows on the image indicate the junctions between cells.

An LDH assay was undertaken using the same parameters as for previous experiments. It can be seen from Figure 3.28 that all of the fibrous samples caused less cell death than the positive control at all time points tested by day 15. The positive control gave an absorbance of over 3 whereas no fibrous samples gave a value above 2.5 (Appendix C). The results of this assay indicate that the more hydrophilic copolymers gave reduced cell death. Further to this, the results indicate more LDH release on polymer 3.6 fibres than on their SC functionalised counterparts (Polymer 3.15). This result concurs with previous results showing that the unfunctionalised fibres cause more cell death.

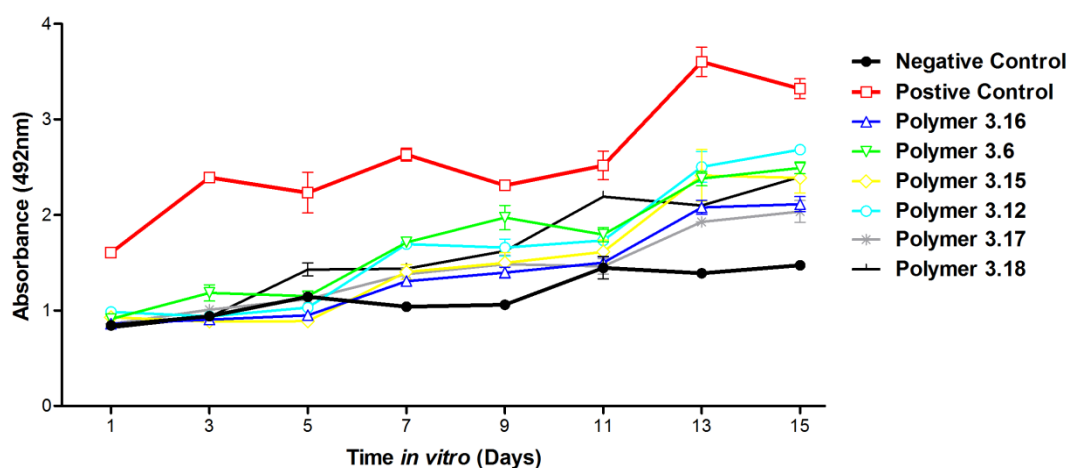


Figure 3.28 - Histogram showing the results of an LDH assay assessing cell survival on different copolymer scaffolds. For data see Appendix C.

Samples of cell culture media taken every two days during the two week culture period from scaffolds incubated without cells were used for an MTT assay. It can be seen from Figure 3.29 that when the results of the assay are averaged over time, all of the fibre samples were statistically different from the positive control. Cell viability was 40% with the positive control which contrasts with over 80% for all fibrous samples indicating the low cytotoxicity of these samples.

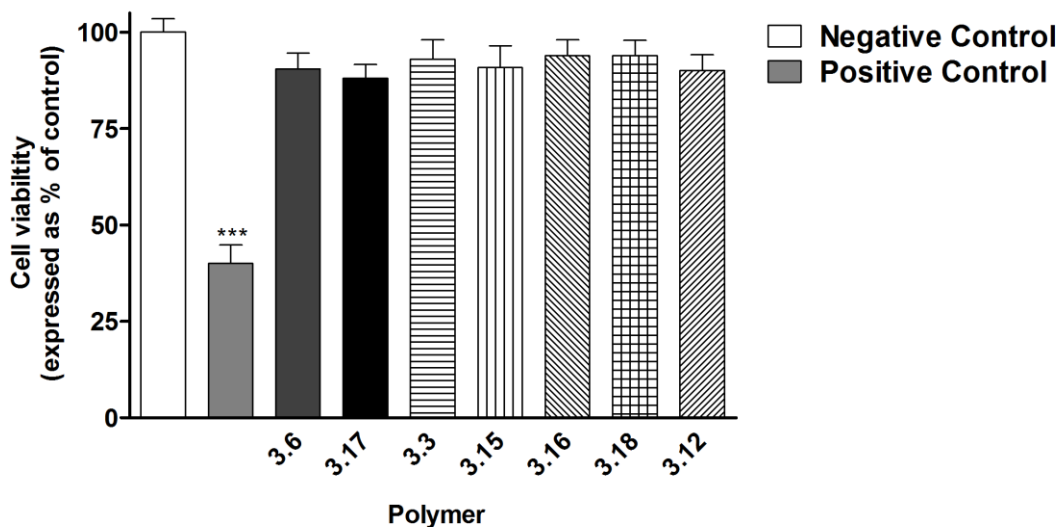


Figure 3.29 – Bar graph showing results of MTT assay averaged over all time points for different fibrous scaffolds. ***Statistical difference ($p < 0.001$) to all fibrous samples. For data see Appendix C.

Further to the LDH and MTT assays, a TUNEL assay was undertaken to determine quantitative cell survival on fibrous polymer surfaces. The results of this assay are summarised in Figure 3.30. It is clear from these results that there was significantly ($p < 0.001$ by day 15) more cell death on fibres produced from copolymers containing hydroxyl-terminated PEG chains (Polymers 3.6 and 3.17) compared with other types of fibre. At day 15, there was over 70% cell death on polymers 3.6 and 3.17 compared to less than 10% for all other samples. Polymers 3.6 and 3.17 had statistically higher cell death in comparison with the negative control. The lowest percentage of cell death on any of the fibrous samples at day 15 was observed on the fibres of polymer 3.16. As this polymer contained the highest percentage of SC groups, this suggests a key role for this group in cell survival. Polymer 3.7 was found to dissolve at room temperature in water and therefore could not be used for cell testing.

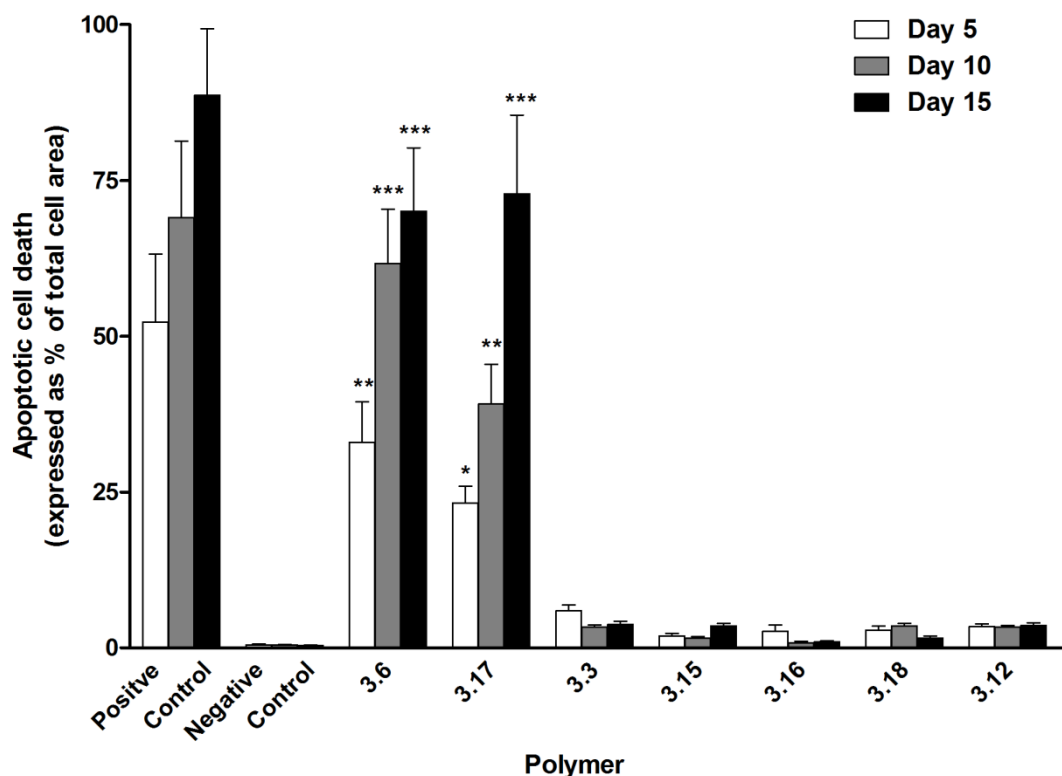


Figure 3.30 – Bar graph depicting apoptotic cell death expressed as percentage of total cell number, assessed by TUNEL assay. Results represent mean \pm sem ($n=9$). Values are grouped according to polymer and by time *in vitro*. Statistical analysis by ANOVA followed by Tukey-Kramer multiple comparison test. Significant difference * $p<0.05$, ** $p<0.01$, *** $p<0.001$ compared to negative control. There was statistically ($p<0.001$ at all time points) less cell death on fibres of polymers 3.3, 3.12, 3.15, 3.16 and 3.18 when compared to positive control and fibres of polymer 3.6. For data see Appendix C.

To quantify the density of cells adhered to the polymer surface; a PI stain was used to label cell nuclei. The results of this cell attachment assay are presented in Figure 3.31. The figure shows the area covered by cells as a percentage of the total fibre area. It can be seen that there is a cell area of below 5% on fibres of polymer 3.6 and 3.17 (those containing alcohol terminated PEG chains). The cell area on these fibres was significantly lower than areas on all other types of fibre suggesting low cell attachment. This explains the high rates of cell apoptosis on these fibres. On the surface of all of the other fibrous scaffolds, cell area is seen to increase over time. The largest

cell areas (65% and above) were observed on fibres of polymers 3.12, 3.15 and 3.16. This indicates that the best fibres for cell adhesion were those containing a shorter PEG chain and a succinimidyl functionality. Of these three polymers, the highest rate of apoptosis was seen with polymer 3.12. SEM images of this fibrous scaffold (Figure 3.26) showed a more beaded structure with less smooth fibres. This could have contributed to increased cellular death on scaffolds of this polymer.

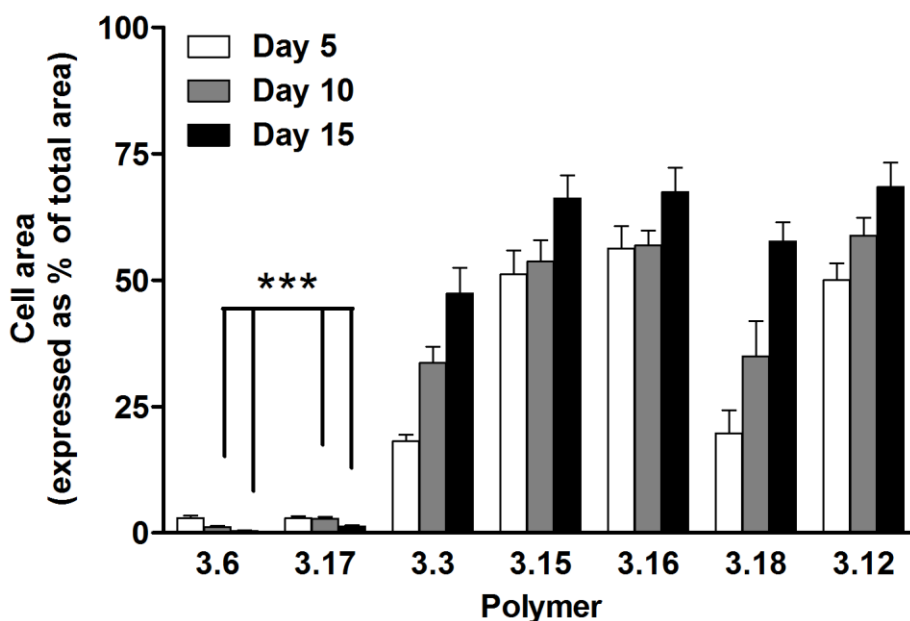


Figure 3.31 – Bar graph depicting percentage ARPE-19 cell area, assessed by nuclear labelling. Results represent mean \pm sem (n= 10). Values are grouped according to polymer and by time *in vitro*. Statistical analysis by ANOVA followed by Tukey-Kramer multiple comparison test. At days 10 and 15 there was a significant difference (***) $p < 0.001$ in percentage cell area on polymers 3.6 and 3.17 compared to polymers 3.3, 3.15, 3.16, 3.18 and 3.12. For data see Appendix C.

3.5.6 Investigating the diffusion characteristics of fibrous polymer networks

As Bruch's membrane (BM) is primarily a diffusion barrier between the cells of the eye and the blood supply in the choroid, it is important to test diffusion across any possible artificial membrane. Experiments were conducted by Hussain *et al.*²² to investigate the diffusion characteristics of human BM and how these characteristics change with age. It was found that diffusion across BM decreases with age. The equipment used for these experiments included a modified Ussing chamber with two reservoirs one on either side of a cassette containing a sample of BM. One reservoir was then filled with a solution of fluorescein isothiocyanate labelled dextran (FITC-dextran) in phosphate-buffered saline (PBS) and the other filled with PBS alone. Samples of the two reservoirs were then taken at regular intervals and the change in fluorescence was measured by a spectrophotometer. A copy of this experimental equipment (Figure 3.32) was kindly donated to us by Dr Ali Hussain (University College, London) who designed the experiment for human BM's.

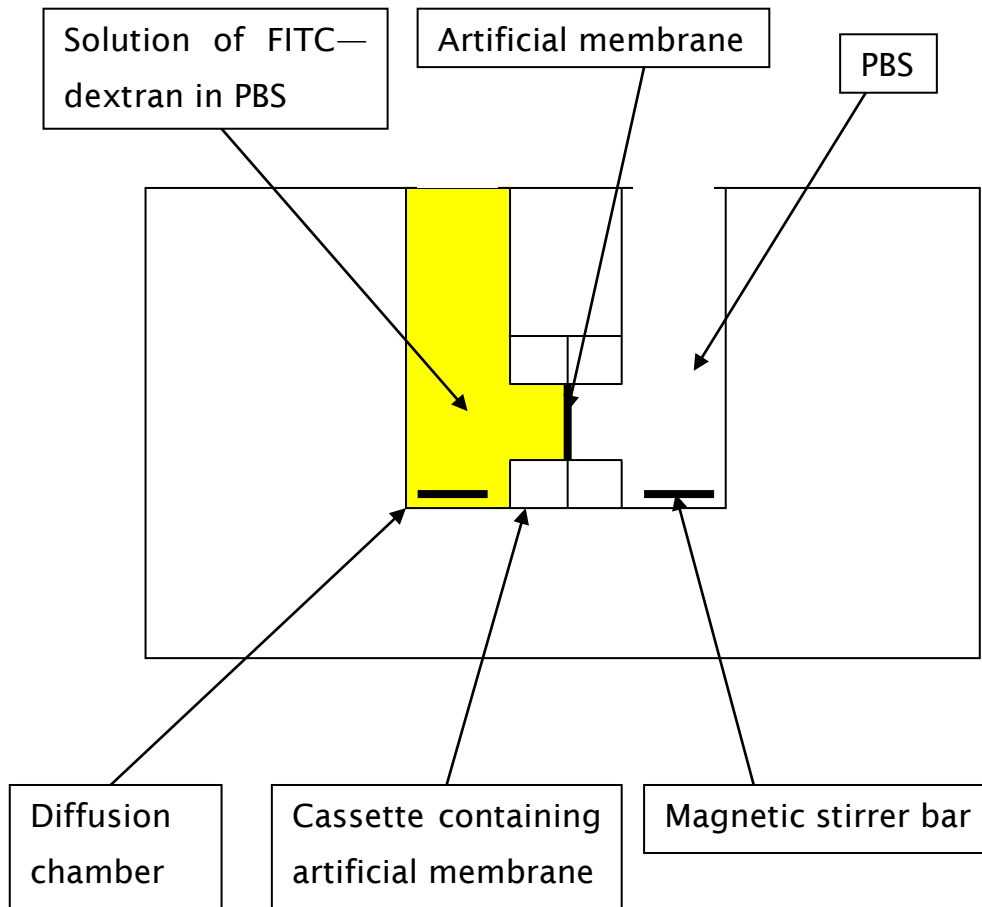


Figure 3.32 - Diagram to show apparatus for diffusion experiments. Diffusion was assessed by the movement of FITC-dextran across the membrane over time.

The effect of varying copolymer components and fibre diameter on diffusion characteristics was investigated. The results of diffusion experiments using copolymers with different ratios of MMA:PEGM (Polymers 3.14 and 3.15) are shown in Figure 3.33 below. These results show that copolymers with a higher content of PEGM give a slower rate of diffusion (0.0367/min compared with 0.07/min). It is postulated that the increased level of hydrophilic PEG in these polymers causes the fibres to swell in an aqueous environment. This swelling could reduce the size of pores between the fibres causing reduced diffusion.

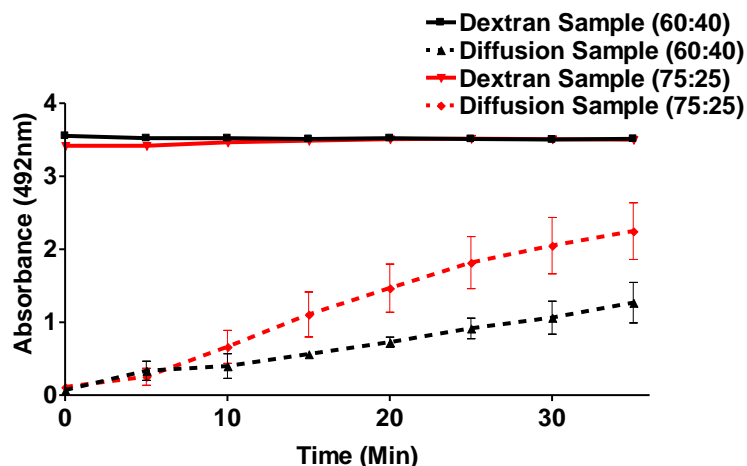


Figure 3.33 – Line graph showing the change in absorbance over time of a FITC-dextran solution on one side of a diffusion chamber and of a PBS solution on the other side of the chamber. Data for both 60:40 P(MMA-co-PEGM) (Polymer 3.15) and 75:25 P(MMA-co-PEGM) (Polymer 3.14) succinimidyl carbonate polymers are shown. Dextran sample: absorbance recorded from dextran containing chamber. Diffusion sample: absorbance recorded from PBS containing chamber.

The nature of the interaction between the polymer fibres and water also appeared to influence the diffusion rate. To study this further, the diffusion across a 'dry' fibrous network was compared with that of one that had been previously immersed in PBS. The membrane that had been immersed in PBS gave less diffusion over 20 minutes compared to the 'dry' membrane (Figure 3.34). This was attributed to the polymer swelling in PBS resulting in smaller pores between fibres for the diffusion of dextran. However, it was noted that after an initial 'lag' phase using pre-wetted fibres a rate of diffusion comparable with dry fibres was observed. This is possibly due to channels within the polymer network being formed to allow more diffusion.

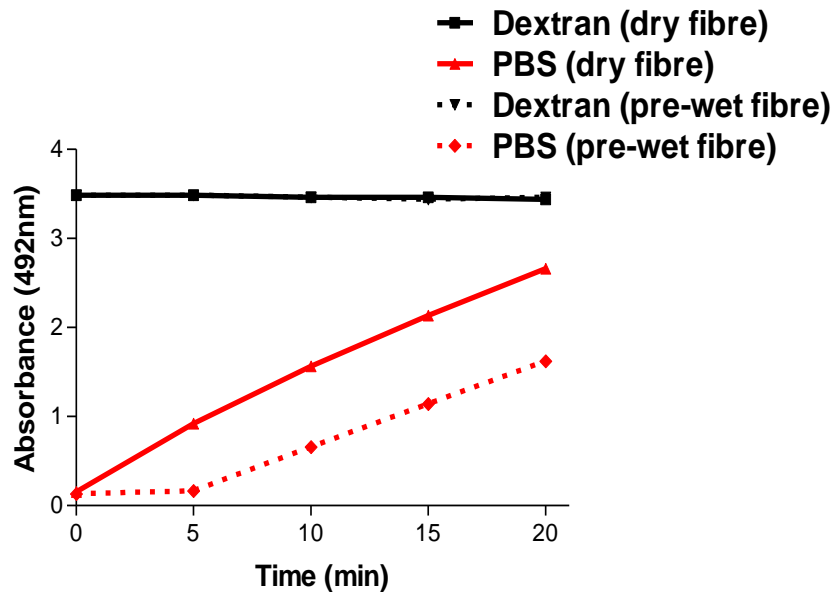


Figure 3.34 - Line graph showing the change in absorbance over time of a FITC-dextran solution on one side of a diffusion chamber and of a PBS solution on the other side of the chamber. Data for both 'dry' and pre-wetted 60:40 P(MMA-co-PEGM) succinimidyl carbonate (Polymer 3.15) are shown. Dextran sample: absorbance recorded from dextran containing chamber. PBS sample: absorbance recorded from PBS containing chamber.

To investigate varying fibre size on diffusion properties, fibres electrospun from two different concentrations of solution were used. Those fibres produced from the 0.45g/ml solution had a smaller diameter. Fibres formed from this solution were expected to give a tighter interwoven network and slower diffusion than those produced using the 0.55g/ml solution. Results show that this was the case with very little diffusion observed over 30 minutes when fibres from the 0.45g/ml solution were used (Figure 3.35).

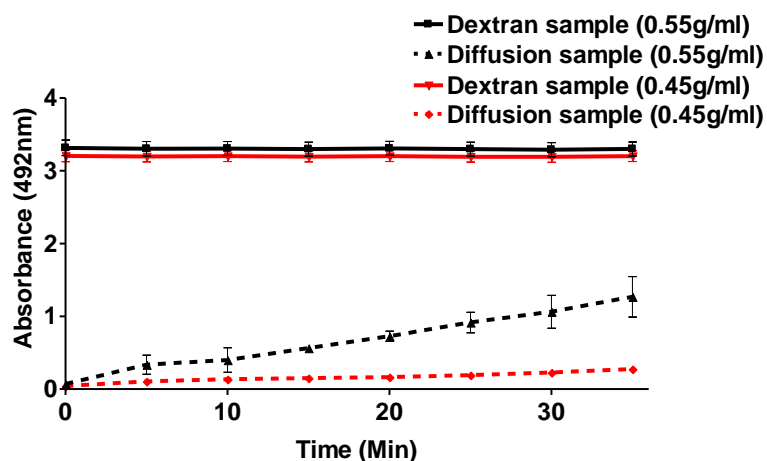


Figure 3.35 - Line graph showing the change in absorbance over time of a FITC-dextran solution on one side of a diffusion chamber and of a PBS solution on the other side of the chamber. Data for both 0.55g/ml and 0.45g/ml 60:40 P(MMA-co-PEGM) succinimidyl carbonate (Polymer 3.15) are shown. Dextran sample: absorbance recorded from dextran containing chamber. Diffusion sample: absorbance recorded from PBS containing chamber.

3.6 Investigation of gelation characteristics observed in P(MMA-co-PEGM) succinimidyl carbonate copolymers

During the initial development of the P(MMA-co-PEGM) succinimidyl carbonate copolymers, a gelation process was observed under certain conditions. The gelation occurred both *in vitro* and if the disuccinimidyl carbonate reaction was left to react for too long (over one week with polymer 3.6 and overnight with polymer 3.7). Instead of dissolving in organic solvents as with those reacted for shorter amounts of time, these compounds now swelled as a gel. Gelation properties of these types of system had not been previously reported in the literature and therefore represented a novel gel synthesis. The mechanism for this gel formation was not immediately apparent.

To further investigate the mechanism of this gel formation, polymer 3.7 was used. As this compound contained more PEG groups and had exhibited a more rapid gelation time, it was proposed gel formation was linked to the functionalisation of PEG groups. When the reaction between polymer 3.7 and disuccinimidyl carbonate (DSC) with triethylamine as base was conducted, initially no gel formation was observed. However, when the reaction mixture was concentrated *in vacuo* a swollen gel was formed within 1 hour. Additionally when the reaction was performed on polymer 3.6 using 4-dimethylaminopyridine (DMAP) as a base instead of triethylamine, gelation was observed within 10 minutes. Literature suggests that DMAP should increase the efficiency of this type of reaction²⁴⁴. Gel formation was confirmed by inversion test (Figure 3.36). These results suggested that gel formation was dependent on the efficiency of the reaction between DSC and the alcohol PEG end group.



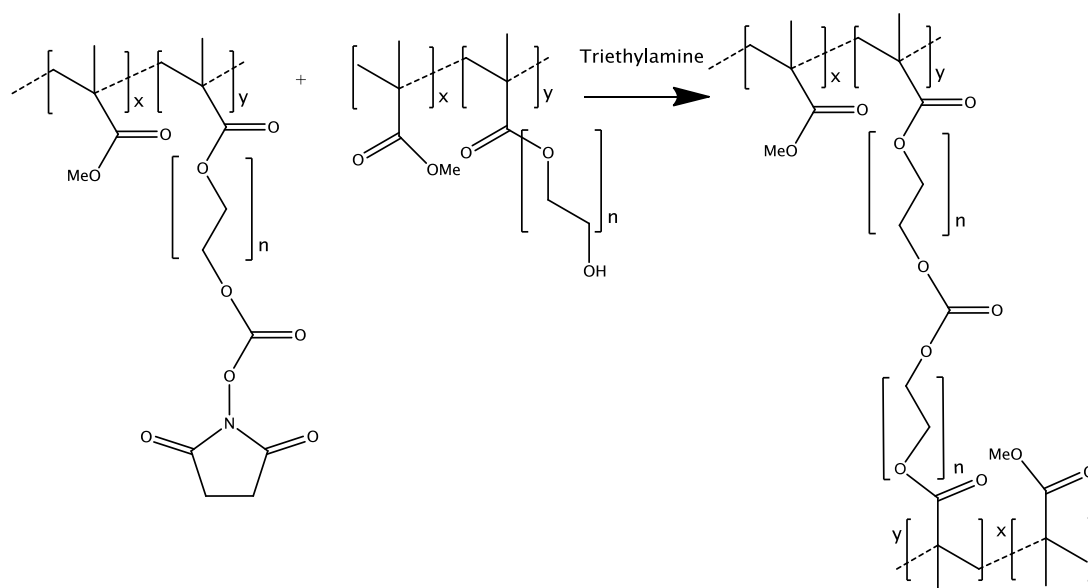
Figure 3.36 – Inversion test of P(MMA-co-PEGM) gel formed by reaction with triethylamine and disuccinimidyl carbonate (DSC).

To ascertain if the gelation could be achieved by simply adding base, a small scale reaction was performed. Triethylamine was added to a small amount of polymer 3.7 in both dichloromethane (DCM) and tetrahydrofuran (THF). The reaction mixture remained a solution and a gel was not formed. Upon addition of the DSC, a gel formed over the course of 1 hour in DCM. A gel was also observed using THF as solvent but this took longer to form (ca. 12 hours). Therefore, the most likely reason for gel formation is the DSC acting as a crosslinking agent between PEG units. In a further experiment, the reaction mixture was washed with hydrochloric acid (2M) following precipitation in diethyl ether prior to gelation. The resulting polymer was stored dry at room temperature for several weeks without forming a gel. NMR studies indicated the successful formation of the succinimidyl carbonate functionality in this compound. When triethylamine was added to this polymer dissolved in DCM, a gel was formed in less than 1 hour suggesting that the polymer was a gel precursor. When left for long periods (ca several weeks), crystals were observed to grow on the surface of the gel due to phase separation (Figure 3.37). Investigations concluded that these were crystals of a triethylamine salt.



Figure 3.37 - Crystal formation on the surface of a P(MMA-co-PEGM) gel. These crystals of triethylamine formed upon leaving the gel in storage for several weeks.

It was hypothesised that if the reaction between the alcohol-terminated PEG chains and disuccinimidyl carbonate had not gone to completion, there would be residual alcohol groups. In the presence of base, these groups could react with succinimidyl carbonate functionalised PEG chains to give a product containing crosslinked PEG chains (Scheme 3.5). Therefore, if these free alcohol groups could be blocked before the crosslinking reaction could occur, a gel would not form.



Scheme 3.5 – Reaction scheme to show the proposed crosslinked polymer product

To investigate this process further, a reaction mixture from the succinimidyl carbonate reaction was mixed with acetic anhydride. The product was not observed to form a gel. ^1H NMR indicated the presence of both succinimidyl carbonate and acetic carbonate groups (Figure 3.38). If left for longer (overnight), acetic ester groups were observed to replace all of the succinimidyl carbonate groups resulting in a compound that did not gelate. As this gelation seemed to be occurring slowly *in vitro*, this would change the mechanical properties of the fibres. More investigation of this gelation phenomenon is necessary to elucidate a full mechanism.

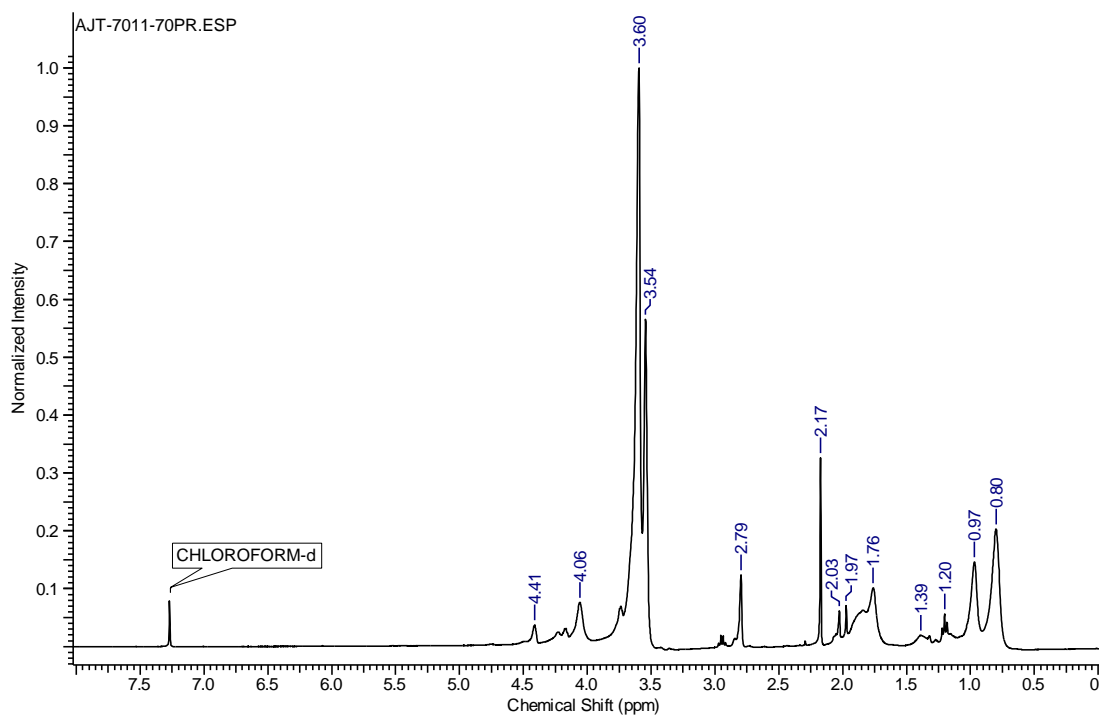


Figure 3.38 - ¹H NMR spectrum showing both succinimidyl (δ 2.79ppm) and acetic (δ 2.17ppm) carbonate groups present in a P(MMA-co-PEGM) polymer.

To conclude, fibrous substrates based on P(MMA-co-PEGM) copolymers have been developed to adhere and support the growth of human RPE cells. It has been found that the hydrophilicity and PEG chain end group of the polymer affect cell adhesion and survival. RPE cells were found to adhere and survive more effectively to those polymer fibres containing a succinimidyl carbonate group than those containing an alcohol group. The cells were found to produce a monolayer and showed apical microvilli indicative of correct polarisation. Furthermore, the reaction to produce SC functionality yielded a gel given a longer reaction time or more effective base. The parameters affecting production of fibres of this type of polymer by the electrospinning process have been investigated. In addition, the diffusion characteristics of membranes produced from these copolymers have been studied. The copolymer matrices can now be optimised towards *in vivo* studies as an artificial BM and as a supportive structure for RPE transplantation.

4 Discussion and conclusions

4.1 Development of biodegradable microspheres as an ocular cell delivery system

4.1.1 Discussion of progress achieved through results presented in this thesis

There is currently no therapy for the cellular loss associated with degenerative retinal disorders such as age-related macular degeneration (AMD) and retinitis pigmentosa (RP). Cell-based therapies such as retinal pigment epithelium (RPE) transplantation and stem cell delivery offer a potential solution^{13,59,245}. Use of a polymer scaffold has been shown to be an effective way of enhancing cell survival *in vivo*⁵⁹. In this work, the development of biodegradable microspheres based on poly(α -hydroxy ester)s has enabled the interactions between retinal cells and spherical substrates to be investigated. For the first time, it has been shown that RPE cells can attach to these substrates and that cell adhesion and survival is dependent on the surface morphology of the microspheres. In addition, it has been shown that the cells are proliferative and have retained appropriate phenotype. These microspheres have the potential to be used as an intraocular cell delivery system.

When poly(DL-lactic-co-glycolic acid) (PLGA) was used for the production of microspheres, increasing polymer solution concentration was found to increase average microsphere diameter. This is in agreement with other published studies^{153,154}. The increased viscosity of the polymer solution at higher concentrations results in a higher shear force being required to produce smaller solution droplets and therefore smaller microspheres. The microspheres also had a smooth surface morphology. When PLGA was blended with poly(L-lactic acid) (PLLA), increasing PLLA content was found to increase the average diameter of the microspheres. This effect is as a

result of the PLLA used having a higher molecular weight than the PLGA. The influence of polymer molecular weight on microsphere size has previously been reported in the literature²⁴⁶. When PLLA and PLGA of the same molecular weight are used, no significant changes in average diameter are observed with changing PLLA/PLGA blend²⁴⁷. Increasing PLLA content in the microspheres was also found to produce a less uniform surface morphology. This has previously been observed in the literature and could be due to increased inherent viscosity of PLLA compared to PLGA²⁴⁶. Increasing the concentration of the aqueous phase containing the stabiliser poly(vinyl alcohol) (PVA) was shown to increase the average size of the microspheres. This has been attributed to the increased amount of PVA in the solution causing a decrease in mixing efficiency. The increased viscosity of the polymer-containing organic phase decreases mixing efficiency and results in larger spheres being produced. However, polymer solution concentration was found to be the dominant effect in determination of microsphere size.

In order to assess biocompatibility, a range of PLLA/PLGA blended microspheres were seeded with a human RPE cell line. The overall trend was shown to be that increasing PLLA content in the polymer blend led to an increase in cell survival. This is attributed to these blends producing rougher surfaced microspheres. It has been reported in the literature that changing the morphology of a surface can have an impact of cell behaviour¹⁰⁵. In addition, it has been shown that cells grow preferentially on rough surfaces due to differences in surface energy¹³⁷. The process of cell adhesion is mediated by cell membrane-bound integrin receptors. The substrates for these receptors have been shown to be specific peptide sequences found in extracellular matrix (ECM) proteins such as laminin and fibronectin⁶⁴. The addition of a laminin coating to microspheres prior to seeding with RPE cells resulted in increased cell adhesion and survival which reached significance when measured by lactate

dehydrogenase (LDH) assay. This is attributed to the laminin interacting with the RPE cell integrin receptors to improve cell adhesion. It has previously been shown that adhesion of RPE cells to a surface is essential for cell survival as interactions between the cells and the ECM regulate cell survival¹⁹. Whilst beneficial for increasing cell adhesion for *in vitro* studies, use of whole proteins such as laminin may be counterproductive in an *in vivo* setting. Problems surrounding purity, high cost and the animal-derived nature of these proteins has the potential to cause difficulties when seeking a cost-effective clinical solution for the treatment of retinal degeneration⁷⁶. Furthermore, use of these foreign proteins may illicit an immune response *in vivo*. As inflammation caused by an innate immune system response has been implicated in exacerbating retinal degeneration¹², any additional immune response would be particularly undesirable. A potential solution could be to use short chain cell adhesion peptides containing sequences such as Arg-Gly-Asp (RGD) which have been shown to mimic the cell adhesion characteristics of whole proteins⁶⁴. These peptides would be less likely to undergo conformational changes that could occur with whole proteins and overcome some of the problems surrounding cost and purity. However, for a cost-effective clinical solution, the utilisation of simple chemical functionality to improve cell adhesion would be desirable⁷⁶.

The experiments performed demonstrate that these PLLA/PLGA microspheres show minimal cytotoxicity towards RPE cells. Increasing PLLA content in PLLA/PLGA blends was shown to increase cell viability by the MTT assay. This effect reached significance with the blends containing 25% and 10% PLLA. In addition, immunocytochemical staining using an antibody specific for RPE cells (RPE65) showed that RPE cells retained appropriate phenotype whilst growing *in vitro* on the microsphere surface. Monitoring of phenotype retention is important as RPE cells have previously been observed to transdifferentiate into fibroblast-like cells following

prolonged periods of culture *in vitro*¹⁹⁰. RPE cells on the microspheres were shown to adopt a typical hexagonal cobblestone morphology when observed by scanning electron microscopy (SEM). Apical microvilli were also shown to be present on the cells indicative of correct cell polarisation. This polarisation is important for several functions of RPE cells including secretion of appropriate growth factors when transplanted¹⁹⁴ and correct integration with photoreceptor cells.

The results of the cell-based experiments have demonstrated the potential of blended PLLA/PLGA microspheres to act as a cell substrate for RPE transplantation. Furthermore, these microspheres could also be used to deliver stem cells to the sub-retinal space for the regeneration of lost photoreceptor and RPE cells. Although several different systems have been trialled for this purpose^{59,98,100,102}, the work in this thesis further investigates the important area of how cells interact with a 3D culture system.

In conclusion, the ability to grow RPE cells on the surface of microspheres has been demonstrated. The impact of blending PLLA and PLGA on the size and morphology of these biodegradable microspheres has been achieved and the impact of these changes on RPE cell growth has been evaluated. Cells were observed to retain their phenotypic and morphological characteristics whilst in culture. The feasibility of using biodegradable microspheres for human RPE cell growth and as a potential delivery system has been demonstrated for the first time.

4.1.2 Future prospects

Future challenges for this work will include refining the system to meet the practical requirements for implantation such as a narrower size distribution. The importance of optimising these parameters for TE-based applications has been recognised in the literature¹⁵³. *In vivo* trials with animal models of AMD could be used to investigate the

efficacy of delivering cells to the retina and probe the integration between implanted cells and the existing tissues. The response of implanted cells to the degradation of the microspheres and subsequent integration between tissues would also need to be investigated¹⁸⁴. In addition to being studied as a therapy, the development of microspheres on which cells can be successfully grown offers the possibility of development of a 3D retinal cell culture system. Biodegradable microspheres are currently being developed as an intraocular drug delivery system¹⁶⁵. Incorporation of growth factors or drugs within the microspheres could be used to observe the effect of slow release of these agents on attached cells. These microspheres could be used to construct 3D tissue *in vitro* to act as models for how *in vivo* systems might behave. Microspheres have already been used in other areas of TE for the creation of *in vitro* models²⁴⁸.

4.2 Development of an artificial Bruch's membrane

4.2.1 Discussion of progress achieved through results presented in this thesis

It has been recognised that the integrity of Bruch's membrane (BM) is vital for survival and function of the RPE³⁰. This integrity is found to be compromised in those with advanced degenerative retinal diseases¹⁶. Whilst progress has been made in transplantation of RPE cells⁵⁴, problems related to their underlying substrate, the Bruch's membrane, have yet to be addressed. Several materials such as PLLA/PLGA⁵⁹ and poly(hydroxybutyrate-co-hydroxyvalerate)¹⁰¹ have been investigated as potential artificial Bruch's membranes. However, a cohesive system for delivery and support of RPE cells *in vivo* has yet to be demonstrated¹³. The potential of methacrylate-based fibrous polymer systems for this application has not previously been investigated. Despite some investigation into the use of plasma treatments¹⁰³ and protein coating⁵⁹, there have been few studies into the response of RPE cells to changing surface chemistry. Understanding this interaction is of fundamental importance in creating an effective artificial Bruch's membrane for the treatment of AMD.

Fibrous substrates derived from methacrylate copolymers have been developed to act as an artificial substitute for Bruch's membrane. For the first time, the influence of surface chemistry using electrospun methacrylate copolymers on the adhesion and survival of RPE cells has been investigated. This research has shown that changes in surface chemistry through addition of a succinimidyl group can have a significant impact on cell adhesion. Experiments have sought to discover the diffusion characteristics of these artificial membranes and how changes in composition can affect diffusion properties. In addition, the polymers synthesised have been observed to undergo a novel gel formation under certain reaction conditions.

In order to mimic the fibrous nature of natural BM, synthesis of a fibrous matrix was sought. Following the use of methacrylate-based polymers in the development of intraocular lenses⁸⁶, a methacrylate comb copolymer was chosen as a target. The copolymer system had a methacrylate backbone with pendant poly(ethylene glycol) (PEG) chains. The incorporation of PEG into a methacrylate-based copolymer has been shown to decrease non-specific protein accumulation¹⁹² which could lead to unwanted reactions *in vivo*. In addition, the increase in hydrophilicity resulting from the inclusion of PEG chains increased the compatibility of the produced membranes with a hydrated environment. A range of copolymers were produced containing different quantities of PEG and different lengths of PEG chain. Relative hydrophilicities were determined using water contact angle measurements. Evaluation by ¹H NMR, whilst not able to give definitive comonomer ratios due to signal overlap, was used to provide an estimate of different groups present within the copolymers. Electrospinning was chosen as the technique to obtain polymer fibres due to its robust ability to generate fibres on the micrometre scale²⁴⁹.

The production of a copolymer with monomer feed ratios of 75% methyl methacrylate (MMA) to 25% poly(ethylene glycol) methacrylate (PEGM) allowed for electrospinning parameters to be refined. Peptides and proteins are frequently coupled to polymers in the literature in order to increase cell adhesion¹¹⁷. To facilitate coupling to P(MMA-co-PEGM), it was necessary to modify the PEG chain end with a more stable leaving group. The succinimidyl group was chosen following its previous use in the literature to facilitate peptide coupling¹¹⁷. A successful reaction to produce a succinimidyl carbonate (SC) group on the PEG chain terminus was developed. Whilst this reaction has previously been used on PEG chains alone²⁴⁴, it has never been shown for these copolymers or been tested for its reaction to cell culture. Reactions to generate a succinimidyl ester

PEG end group were also carried out but were found to be more complex and give a lower yield than producing a SC group. When human RPE cells (ARPE-19) were seeded onto the surface of fibres derived from SC-functionalised P(MMA-co-PEGM), minimal cell death and cytotoxicity were observed when assessed by LDH and MTT assays. However, it was noted that fibres of these polymers resisted immersion in tissue culture medium. This was attributed to the large percentage of MMA groups giving the polymer a hydrophobic nature.

To improve the biocompatibility of the fibrous substrate, a polymer with an increased number of PEG chains was developed and electrospun into fibres. The increased hydrophilicity of this polymer was demonstrated using water contact angle measurements. A fluorescently-tagged peptide was utilised to show that peptide coupling was being achieved on SC-functionalised polymer fibres but not on unfunctionalised surfaces. Investigation by SEM revealed that the substrate had a surface of smooth fibres with an average diameter of 1.9 μ m. In previous studies, the protein laminin has been used to enhance RPE adhesion to substrates^{59,138}. Problems surrounding purity and high cost have encouraged some use of short chain peptides to mimic the cell adhesive action of whole proteins¹¹⁷. To investigate the impact of various cell adhesive agents on ARPE-19 cell behaviour, GRGDSP (a fibronectin derived peptide⁶⁴), YIGSR (a laminin derived peptide¹¹⁵), GRGESP (a nonsense peptide⁶⁶) and the whole protein laminin were coupled to the surface of SC functionalised fibres. ARPE-19 cells were seeded onto the surface of these fibres and the results were compared with those for fibres of polymer without the SC functionality. Increasing the PEG content of the polymer was observed to increase the compatibility of the fibrous substrate with cell culture media. Results from these experiments showed an increase in cell apoptosis over time on fibrous substrates derived from polymers without SC functionality. However, on those surfaces with SC functionality, cell apoptosis decreased over time.

This change in cell behaviour associated with the addition of a SC group has not previously been observed in the literature. Although the addition of cell adhesive peptides was observed to further decrease apoptosis, this effect did not reach significance.

In order to more fully assess the impact of surface chemistry on RPE cell adhesion and survival, a further study was conducted to assess changes in PEG chain length, quantity and end groups. Contact angle studies were again used to probe changes in hydrophobicity. It was found that conversion of the PEG chain end group to either a SC or ester caused an increase in hydrophobicity. The effect was shown to be more pronounced on polymers containing longer PEG chains. Following seeding with RPE cells onto a range of different copolymers, apoptotic cell death was investigated by TUNEL assay. On fibrous substrates derived from PEG-containing copolymers with no SC functionality, there was increasing and significant cell death over 15 days. Substrates derived from methacrylate-based copolymers that contained a HEMA group instead of a PEG group were found to have larger cell areas. Those substrates derived from a PEG-containing polymer which had either SC or succinimidyl ester functionality were found to induce the lowest percentage of apoptotic cell death. The surface which produced one of the highest cell areas and lowest cell death was the SC-functionalised PEG-containing polymer with the largest quantity of PEG chains. This indicates that both the presence of PEG and SC functionality produces a surface that is highly compatible with cells.

In the search for cost effective biomaterials, techniques such as plasma discharge to modify surfaces for increased biocompatibility have been examined¹⁰⁵. The objective of these is to change the surface chemistry of a substrate to increase cellular compatibility. In this context, the discovery that chemical modification of a polymer with an SC group can significantly impact on cell behaviour is an important observation. The mechanism by which this surface

chemistry change impacts on cell behaviour is not immediately apparent. It is possible that the altered surface chemistry is causing a more favourable interaction with the cell surface. It has been shown that a balance between a hydrophilic and hydrophobic surface is necessary for cell adhesion¹⁰⁶. Cell survival was shown to be increased on polymers that were observed to be more hydrophobic by contact angle measurements. The more hydrophobic polymers could be binding components of the cell culture media such as foetal bovine serum thus leading to increased cell binding. However, larger cell areas were observed on more hydrophilic HEMA-containing polymer surfaces than those containing PEG. This suggests an influence on cell behaviour of the alcohol-terminated PEG chains beyond changes in hydrophilicity. It has been shown in the literature that increasing PEG chain length and surface density can decrease protein binding by 'shielding' hydrophobic polymers²⁵⁰. Furthermore, it has been shown that a minimum surface density of PEG is required for protein resistance to occur²⁵¹. This could explain the difference in cell adhesion between HEMA- and PEG-containing polymers with the same backbone.

A further possibility is that changes in the mechanical properties of the polymer are impacting on cell behaviour. Further studies on this polymer system have shown gel forming behaviour. This gel forming process could be occurring *in vitro* causing a change in mechanical properties of the artificial membrane. It has been shown in the literature that the mechanical properties of substrates can impact on cell growth¹⁴⁴. However, the change in cellular behaviour resulting from a change in the mechanical properties of a surface are often more focused around phenotype than adhesion¹⁴⁵. ARPE-19 cells on the surface of fibrous polymers were shown to adopt a hexagonal, cobblestone morphology with apical microvilli. This shows retention of an epithelial cell phenotype with appropriate polarisation which is

of importance for interaction between the RPE and photoreceptor cells as well as growth factor secretion.

The Bruch's membrane is an important macromolecular diffusion membrane between the choroid and the cells of the retina¹³. Problems with diffusion across it have been implicated as a possible cause for the photoreceptor and RPE cell death associated with macular degeneration²². The diffusion characteristics of the produced membranes have been investigated. The experiments utilised the same apparatus used by Hussain *et al.*²² to study native BM. To mimic macromolecular diffusion, fluorescently labelled dextran was used. Results showed that increasing the proportion of PEG within the copolymer decreased the rate of diffusion. This was attributed to the increased hydrophilicity of this polymer. The increase in the quantity of PEG chains appeared to result in fibres of the polymer swelling to create smaller pores for diffusion. To study this effect further, the diffusion across a dry membrane was tested against a pre-wetted membrane. Less diffusion was observed using pre-wetted fibres further implicating a swelling effect caused by the presence of water on diffusion rate. Fibres produced from different concentrations of electrospinning solution were also tested. Those fibres produced from a more dilute solution gave fibres of a smaller diameter and therefore a tighter woven network. This was shown to reduce diffusion across the artificial membrane.

Overall, a methacrylate-PEG copolymer has been developed into a fibrous substrate capable of supporting RPE cell growth. A reaction to change to functionality of the PEG chain terminus was developed and found to induce gelation under certain reaction conditions. This change in functionality was found to significantly improve cell adhesion. Changing polymer concentration was found to influence both fibre diameter and the diffusion properties of the membrane. The PEG chain length, density and end group were found to significantly influence cell adhesion and survival. An increase in PEG

chain density was additionally found to decrease diffusion across the fibrous substrate. Polymers containing PEG chains with a SC terminus were found to support RPE cell growth with minimal cytotoxicity. Furthermore, RPE cells were observed to form a layer with typical cobblestone morphology and apical microvilli, important for correct integration with photoreceptor layers. This ability demonstrates the feasibility of using this system to act as an artificial BM for the treatment of degenerative retinal diseases.

4.2.2 Future prospects

There are several future challenges to the use of this system. These include devising an appropriate system to deliver the membrane under the retina. In addition, practical challenges associated with implantation such as thinning of the existing BM will need to be overcome. The mechanical properties of the fibrous structure will need to be studied in depth to assess how the artificial membrane will interact in an intraocular environment. These properties will need to be further refined to more closely match that of native BM. This could involve production of smaller diameter fibres to give thin and high strength networks. In addition, further *in vitro* studies with organotypic retinas could be used to research the potential of these electrospun membranes as an *in vitro* retinal model. To study the interaction between this artificial membrane and the native tissue with a view to creating a therapy, *in vivo* experiments with animal models will be necessary. The novel gelation observed resulting from reaction between P(MMA-co-PEGM) and disuccinimidyl carbonate invites further investigation to elucidate the mechanism of gelation and characterise these gels further.

5 Experimental

General experimental details

All laboratory solvents were obtained from Fisher Scientific, Loughborough, UK with the exception of 2-butanone which was obtained Rathburn, Walkerburn, UK and were used without further purification unless otherwise stated. All other chemicals were obtained from Sigma-Aldrich, Dorset, UK and were used without further purification unless stated otherwise. All equipment for cell-based techniques was obtained from Sigma-Aldrich, Dorset, UK unless stated otherwise.

All NMR spectra were collected using a Bruker AV300 spectrometer (operating at 300MHz for ^1H and 75MHz for ^{13}C spectra) or a Bruker DPX400 spectrometer (operating at 400MHz for ^1H and 100MHz for ^{13}C spectra) (Bruker, Coventry, UK).

Scanning electron microscopy (SEM) was performed using either a JEOL JSM-5910 (JEOL U.K. Ltd., Herts, UK) or a Quanta 200 (FEI, Eindhoven, Netherlands) scanning electron microscope.

All IR spectra were collected using a Thermo Scientific Nicolet 380 FT-IR (Fisher Scientific, Loughborough, UK).

Gel permeation chromatography (GPC) was performed using a Hewlett Packard 1090 liquid chromatograph with a Hewlett Packard 1037A refractive index detector (Hewlett Packard, Bracknell, UK). Molecular weights were calculated based on poly(methyl methacrylate) standards.

Differential scanning calorimetry (DSC) was performed using Perkin Elmer Pyris 1 with liquid nitrogen cooling using a CCA7 (cooling accessory) (Perkin Elmer, Seer Green, UK). The

instrument was calibrated for temperature with indium and zinc and for heat flow with indium.

Samples stained by immunocytochemistry and samples which underwent a TUNEL assay were imaged using a Leica DM IRB microscope (Leica Microsystems UK Ltd, Milton Keynes, UK) with analysis carried out using Volocity software (Improvision, Coventry, UK).

Absorbances for LDH and MTT assays were measured at 490nm using a FLUOstar Optima microplate reader (BMG Labtech, Offenburg, Germany).

5.1 Microsphere synthesis

5.1.1 Preparation of PLLA/PLGA microspheres using a constant polymer solution concentration

General procedure:

Poly(vinyl alcohol) (PVA) (Xg (Table 5.1), RMM 31,000-50,000) was added to deionised (DI) water (50 ml) and the mixture was rapidly stirred (900 rpm). Separately, poly(L-lactide) (PLLA) (Yg (Table 5.1), Resomer® L 207 S, i.v. 1.5-2.0dl/g, RMM obtained from Boehringer Ingelheim) was added to 5ml of dichloromethane (DCM) in a stoppered round bottom flask and the mixture was stirred until all of the polymer had dissolved. Poly(DL-lactide-co-glycolide) (PLGA) (Zg (Table 5.1), Resomer® RG 755 S, i.v. 0.5-0.7dl/g, lactic to glycolic ratio 75:25 obtained from Boehringer Ingelheim) was then dissolved in the PLLA/DCM solution. Once all PVA had dissolved (2 hrs) the PLLA/PLGA solution was added to the rapidly stirring PVA solution. This mixture was stirred overnight to allow the solvent to evaporate. The resulting microsphere suspension was then transferred to a centrifuge tube (50ml) and centrifuged for 5 min at 2000 rpm. The PVA solution was decanted off and the microspheres were washed three times in deionised water. The microspheres underwent a further washing step overnight in 70% ethanol solution followed by three washes (5 min each) with 0.1M pH 7.4 phosphate buffered saline (PBS). This was carried out to ensure there were no traces of DCM remaining in the preparation. The microspheres were filtered and then dried in a vacuum desiccator. The accuracy of the blends was confirmed by inverse-gated ¹³C NMR as described previously⁹⁷.

Following fabrication, samples of each microsphere blend were mounted on carbon stubs and sputter-coated with gold/palladium prior to imaging using a scanning electron microscope. Micrographs at 4 random areas of each blend were taken.

Concentration	PVA (Xg)	Blend PLLA:PLGA	PLLA (Yg)	PLGA (Zg)
0.05g/ml	0.25	0:100 (PLGA)		0.25
0.05g/ml	0.25	10:90	0.025	0.225
0.05g/ml	0.25	25:75	0.0625	0.1875
0.05g/ml	0.25	50:50	0.125	0.125
0.05g/ml	0.25	75:25	0.1875	0.0625
0.05g/ml	0.25	90:10	0.225	0.025
0.05g/ml	0.25	100:0 (PLLA)	0.25	

Table 5.1 - Polymer concentrations and blend ratios used.

5.1.2 Preparation of PLGA microspheres with a varying polymer solution concentration

PVA (1g, RMM 31,000-50,000) was added to deionised water (50 ml) and the mixture was rapidly stirred (900 rpm). Separately, a solution (0.01g/ml, 0.05g/ml or 0.15g/ml) of PLGA (Resomer® RG 755 S, i.v. 0.5-0.7dl/g, lactic to glycolic ratio 75:25 obtained from Boehringer Ingelheim) in DCM was then prepared. Once all PVA had dissolved (2 hrs) the PLGA solution was then added to the rapidly stirring PVA solution and the mixture was stirred overnight to allow the solvent to evaporate. The resulting microsphere suspension was then transferred to a centrifuge tube (50ml) and centrifuged for 5 min at 2000 rpm. The PVA solution was then decanted off and the microspheres were washed three times in deionised water. The microspheres underwent a further washing step overnight in 70% ethanol solution followed by three 5 minute washes with 0.1M PBS (pH 7.4). This was carried out to ensure there were no traces of DCM remaining in the preparation. The microspheres were filtered followed by drying in a vacuum desiccator.

5.1.3 Preparation of PLGA microspheres with varying stabiliser (PVA) concentration

PVA (0.25g, 0.5g or 1g, RMM 31,000-50,000) was added to deionised water (50 ml) and the mixture was rapidly stirred (900 rpm). Separately, a 5ml solution (0.1g/ml) of PLGA (Resomer® RG 755 S, i.v. 0.5-0.7dl/g, lactic to glycolic ratio 75:25 obtained from Boehringer Ingelheim) in DCM was prepared. Once all PVA had dissolved (2 hrs) the PLGA solution was added to the rapidly stirring PVA solution and the resulting mixture was stirred overnight to allow the solvent to evaporate. The resulting microsphere suspension was then transferred to a centrifuge tube (50ml) and centrifuged for 5 min at 2000 rpm. The PVA solution was decanted off and the microspheres were washed three times in deionised water. The microspheres underwent a further washing step overnight in 70% ethanol solution followed by three 5 minute washes with 0.1M PBS (pH 7.4). This was carried out to ensure that there were no traces of DCM remaining in the preparation. The microspheres were filtered and then dried in a vacuum desiccator.

5.1.4 Preparation of PLGA microspheres with varying polymer solution and stabiliser (PVA) concentration

PVA (0.05g, 0.125g or 1g, RMM 31,000-50,000) was added to deionised water (50 ml) and the mixture was rapidly stirred (900 rpm). Separately, a 5ml solution (0.01g/ml or 0.05g/ml) of PLGA (Resomer® RG 755 S, i.v. 0.5-0.7dl/g, lactic to glycolic ratio 75:25 obtained from Boehringer Ingelheim) in DCM was prepared. Once all PVA had dissolved (2 hrs) the PLGA solution was added to the rapidly stirring PVA solution and the resulting mixture was stirred overnight to allow the solvent to evaporate. The resulting microsphere suspension was transferred to a centrifuge tube (50ml) and centrifuged for 5 min at 2000 rpm. The PVA solution was decanted off and the microspheres were washed three times in deionised water. The microspheres underwent a further washing step overnight in 70%

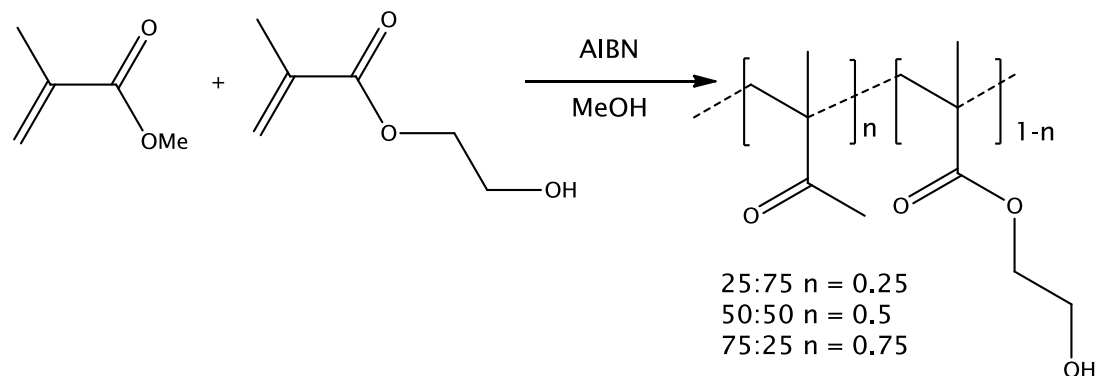
ethanol solution followed by three 5 minute washes with 0.1M PBS (pH 7.4). This was carried out to ensure that there were no traces of DCM remaining in the preparation. The microspheres were then filtered followed by drying in a vacuum desiccator.

5.1.5 Preparation of PLGA microspheres with the introduction of an effervescent salt

PVA (0.1g RMM 31,000-50,000) was added to deionised water (100 ml) and rapidly stirred (900 rpm). Separately, a solution of PLGA (Resomer® RG 755 S, i.v. 0.5-0.7dl/g, lactic to glycolic ratio 75:25 obtained from Boehringer Ingelheim) (0.25g) in DCM (4ml) was prepared. A 1% (w/v) solution of either sodium, potassium or ammonium hydrogen carbonate (1.25ml) was poured into the PLGA solution and rapidly stirred (900rpm) Once all PVA had dissolved (2 hrs) the PLGA/salt solution was added to the rapidly stirring PVA solution and stirred overnight to allow solvent evaporation. The obtained microsphere suspension was transferred to a centrifuge tube (50ml) and centrifuged for 5 min at 2000 rpm. The PVA solution was decanted off and the microspheres washed three times in deionised water. The microspheres underwent a further washing step overnight in 70% ethanol solution followed by three 5 minute washes with 0.1M PBS (pH 7.4). This was carried out to ensure there were no traces of DCM remaining in the preparation. The microspheres were filtered followed by drying in a vacuum desiccator.

5.2 Synthesis of methacrylate-based copolymers

5.2.1 Synthesis of P(MMA-co-HEMA) copolymers - Polymers 3.1, 3.2 and 3.4



Methyl methacrylate (MMA) (X_g , $d:0.936\text{g/ml}$) and 2-hydroxyethyl methacrylate (HEMA) (Y_g , $d:1.073\text{g/ml}$) (Table 5.2) were dissolved in methanol (10ml). Nitrogen was bubbled through the stirred solution for 30 mins. 2,2'-Azobisisobutyronitrile (AIBN) (0.01g, $6.1 \times 10^{-6}\text{mol}$ obtained from Acros Organics) was then added. The reaction mixture was heated under reflux under nitrogen for ca. 24 hrs. The product was then precipitated in diethyl ether (50ml) and redissolved in methanol (50ml) before being reprecipitated in diethyl ether (70ml). The diethyl ether was decanted off to give a white solid product that was subsequently dried *in vacuo*.

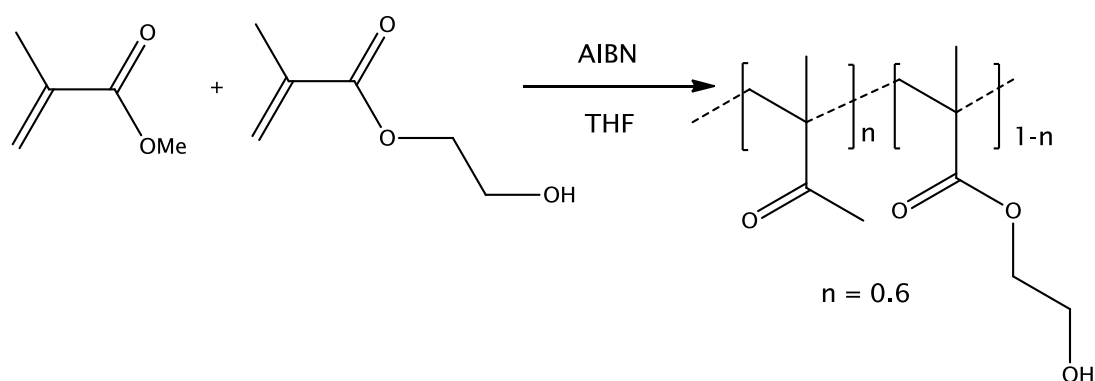
$^1\text{H NMR}$ (300MHz, MeOD) δ_{H} 0.93 (3H, br s, $-\text{CH}_2\text{CCH}_3\text{CH}_2-$), 1.10 (1H, br s, $-\text{CH}_2\text{CCH}_3\text{CH}_2-$), 1.99 (3H, br s, $-\text{CH}_2\text{CCH}_3\text{CH}_2-$) 3.64 (3H, br s, $-\text{OCH}_3$), 3.8 (2H, br s, $\text{OCH}_2\text{CH}_2\text{OH}$), 4.07 (2H, br s, $\text{OCH}_2\text{CH}_2\text{OH}$)

Spectra conformed to that reported previously in the literature²³⁸.

Polymer number	Feed ratio	X (amount of MMA)	Y (amount of HEMA)
3.1	25:75	0.625g	2.44g
3.2	50:50	0.7g	0.91g
3.4	75:25	1.7g	0.72g

Table 5.2 – Monomer feed ratios for P(MMA-co-HEMA) polymerisation reactions.

5.2.2 Preparation of 60:40 P(MMA-co-HEMA) – Polymer 3.3



MMA (0.0677mol, 6.77g, 7.23ml) and HEMA (0.0451mol, 5.87g, 5.47ml) were dissolved in tetrahydrofuran (THF) (150ml). Nitrogen was bubbled through the stirred solution for 30 minutes. AIBN (0.096g, 5.85×10^{-4} mol obtained from Acros Organics) was then added. The reaction mixture was heated under reflux under nitrogen for ca. 24 hrs. The product was then precipitated in diethyl ether (200ml), redissolved in THF (100ml) and then reprecipitated in diethyl ether (150ml). The diethyl ether was decanted off to give a white solid product that was subsequently dried *in vacuo*.

^1H NMR (300MHz, MeOD) δ_{H} 0.93 (3H, br s, $-\text{CH}_2\text{CCH}_3\text{CH}_2-$), 1.10 (1H, br s, $-\text{CH}_2\text{CCH}_3\text{CH}_2-$), 1.99 (3H, br s, $-\text{CH}_2\text{CCH}_3\text{CH}_2-$) 3.64 (3H, br s, $-\text{OCH}_3$), 3.8 (2H, br s, $\text{OCH}_2\text{CH}_2\text{OH}$), 4.07 (2H, br s, $\text{OCH}_2\text{CH}_2\text{OH}$)

Spectra conformed to that reported previously in the literature²³⁸.

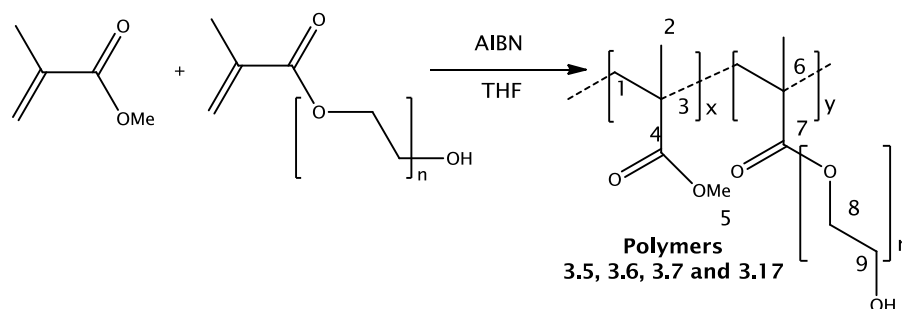
GPC data

Weight average molecular weight (Mw) – 35562

Number average molecular weight (Mn) – 22401

Polydispersity index – 1.59

5.2.3 Preparation of P(MMA-co-PEGM) – Polymers 3.5, 3.6, 3.7 and 3.17



To THF (150ml) was added MMA, poly(ethylene glycol) methacrylate (PEGM) (Average MW 360 or 526) (Feed ratios summarised in Table 5.3) and AIBN (0.096g, 5.85×10^{-4} mol) (Acros Organics). The solution was degassed by bubbling nitrogen for 20 mins before being refluxed for ca. 20 hrs under nitrogen whilst being stirred. The resulting polymer solution was purified by twice precipitating diethyl ether (200ml) yielding a transparent solid before being dried *in vacuo*. Characterisation data summarised in Table 5.4.

FT-IR $\nu_{\max}/\text{cm}^{-1}$ 2991 and 2948 (CH), 1721s (CO)

$^1\text{H NMR}:\delta_{\text{H}}$ (400MHz, CDCl_3) 0.84 and 1.01 (br s, H2), 1.81 (br s, H1), 1.86 (br s, H1), 3.59 (br s, H5), 3.66 (br s, H9), 4.11 (br s, H8)

Due to overlapping signals, it was difficult to obtain accurate integrals from $^1\text{H NMR}$ signals. However, estimated integrals can be used to obtain an estimate of the ratio of MMA to PEGM units by comparing integrals of the -OMe group to that of the ester link to the PEG chain.

$^{13}\text{C}\{^1\text{H}\}$ NMR: δ_{C} (100MHz, CDCl_3) 16.5 and 18.8 (C2), 44.6 (C3), 44.9 (C6), 51.8 (C5), 54.4 (C1), 61.7 (PEG chain), 63.0 (PEG chain), 67.9 (PEG chain), 68.6 (PEG chain), 70.6 (PEG chain), 72.6 (PEG chain) 177.0 (C7), 177.8 (C4)

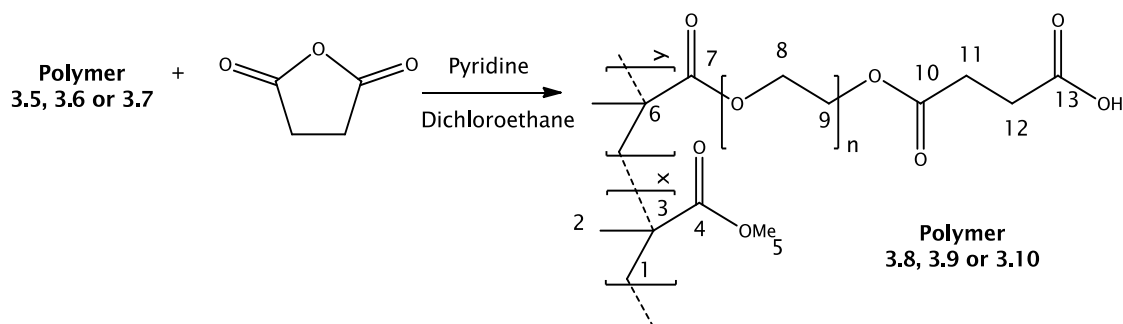
Compound	Amount of MMA/g	Amount of PEGM/g	PEGM Av Mw	Estimated monomer ratio from NMR
3.5	8.4	2.82	360	91:9
3.6	6.72	4.51	360	80:20
3.7	4.51	6.72	360	60:40
3.17	6.72	6.59	526	78:22

Table 5.3 - Summary of monomer feed ratios for P(MMA-co-PEGM) polymers and the estimated actual ratio based on NMR spectroscopy data.

Compound	Number average molecular weight (Mn)	Weight average molecular weight (Mw)	Polydispersity index	Glass transition temperature
3.5	35053	85228	2.43	-
3.6	23165	38789	1.67	57°C
3.7	25001	47789	1.91	Trace did not show evidence of a glass transition
3.17	35760	118752	3.35	21.4°C

Table 5.4 - Summary of data from P(MMA-co-PEGM) polymers produced.

5.2.4 Preparation of a carboxylated P(MMA-co-PEGM) copolymer – Polymers 3.8, 3.9 and 3.10



To a 3-neck round-bottomed flask was added P(MMA-co-PEGM) (Polymer 3.5, 3.6 or 3.7) (8g) and succinic anhydride (0.03mol, 3g). Freshly distilled dichloroethane (100ml) was added and the solution was degassed with nitrogen for 20 mins. Pyridine (2ml) was added dropwise to the stirring solution and the mixture was then refluxed for 2 hrs under nitrogen. The reaction volume was then reduced *in vacuo*. The polymer product was then precipitated in diethyl ether (200ml) before being redissolved in chloroform (30ml) and washed with HCl_(aq) (2M, 30ml). The product was then precipitated in diethyl ether (100ml) and dissolved in THF (30ml) before being reprecipitated in diethyl ether (100ml). The resulting solid was dissolved in chloroform and the solvent was removed *in vacuo*.

FTIR $\nu_{\max}/\text{cm}^{-1}$ 3414br (H-bonded OH) 2993 and 2949 (CH), 1721s (CO)

$^1\text{H NMR}:\delta_{\text{H}}$ (400MHz, CDCl_3) 0.85 and 1.02 (br s, H2), 1.81 (br s, H1), 1.90 (br s, H1), 2.66 (br s, H11 and 12, 4H), 3.60 (br s, H5), 3.65 (br s, H9 in PEG chain), 4.12 (br s, H8, 4H), 4.27 (br s, H9 adjacent to ester, 2H)

Due to overlapping signals, it was difficult to obtain accurate integrals from $^1\text{H NMR}$ signals. However, estimated integrals can be used to obtain an estimate of the percentage of PEG chains that have an acid end group by comparing integral of the protons adjacent to the ester group in the PEG chain to that of the protons in the ring-opened

anhydride group. This indicates that approximately half the PEG chains reacted to give the carboxylated PEG.

$^{13}\text{C}\{^1\text{H}\}$ NMR: δ_{c} (100 MHz, CDCl_3) 16.5 and 18.7 (C2), 44.5 (C3), 44.9 (C6), 45.5 (C11), 51.8 (C5), 52.3 (C1), 54.4 (C1), 61.7 (PEG chain), 63.8 (PEG chain), 68.5 (PEG chain), 69.0 (PEG chain), 70.5 (PEG chain), 72.6 (PEG chain), 177.0 (C7), 177.8 (C4)

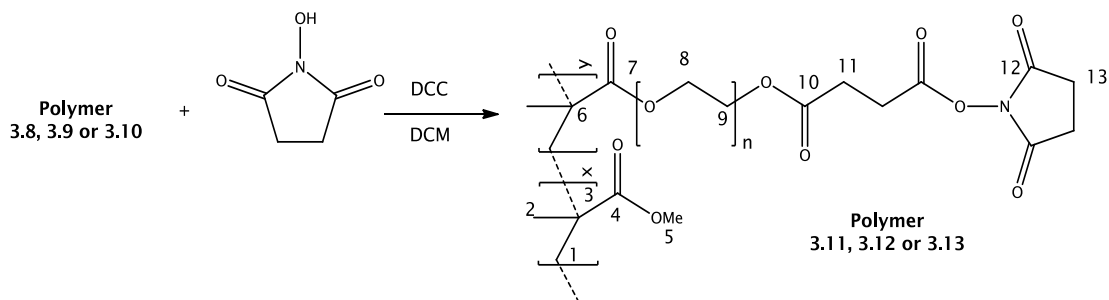
GPC data for Polymer 3.10

Weight average molecular weight (Mw) - 46779

Number average molecular weight (Mn) - 24970

Polydispersity index - 1.87

5.2.5 Preparation of an *N*-hydroxysuccinimide activated ester of P(MMA-co-PEGM) – Polymers 3.11, 3.12 and 3.13



To carboxylated P(MMA-co-PEGM) (Polymer 3.8, 3.9 or 3.10) (5g) and *N*-hydroxysuccinimide (0.01 mol, 1.2g) was added DCM (100ml). Separately, dicyclohexylcarbodiimide (DCC) (0.006 mol, 1.2g obtained from Acros Organics) was dissolved in DCM (50ml). The DCC solution was then added dropwise to the polymer solution. Following complete addition of the DCC solution, the reaction was stirred overnight. The resultant turbid reaction mixture was filtered through cotton wool to remove the dicyclohexylurea. The polymer product was then purified by precipitating twice in diethyl ether (200ml) before being dried *in vacuo*.

FTIR $\nu_{\max}/\text{cm}^{-1}$ 2993 and 2949 (CH), 1784 (CO-N cyclic imide), 1722s (CO)

$^1\text{H NMR}:\delta_{\text{H}}$ (400MHz, CDCl_3) 0.85 and 1.02 (br s, H2), 1.80 (br s, H1), 1.89 (br s, H1) 2.82 (m, H11, 11 and 13), 3.59 (br s, H5), 3.64 (br s C9 in PEG chain), 4.11 (br s, C8), 4.29 (br s, C9 adjacent to ester)

Due to overlapping signals, it was difficult to obtain accurate integrals from $^1\text{H NMR}$ signals.

$^{13}\text{C}\{^1\text{H}\}$ NMR: δ_{C} (100 MHz, CDCl_3) 16.5 and 18.7 (C2), 25.6 (C13) 44.5 (C3), 44.9 (C6), 51.8 (C5), 53.4 (C1), 54.4 (C1), 61.7 (PEG chain), 64.2 (PEG chain), 68.5 (PEG chain), 69.1 (PEG chain), 70.5 (PEG chain), 72.6 (PEG chain), 168.9 (C12), 177.0 (C7), 177.8 (C4)

GPC data for Polymer 3.12

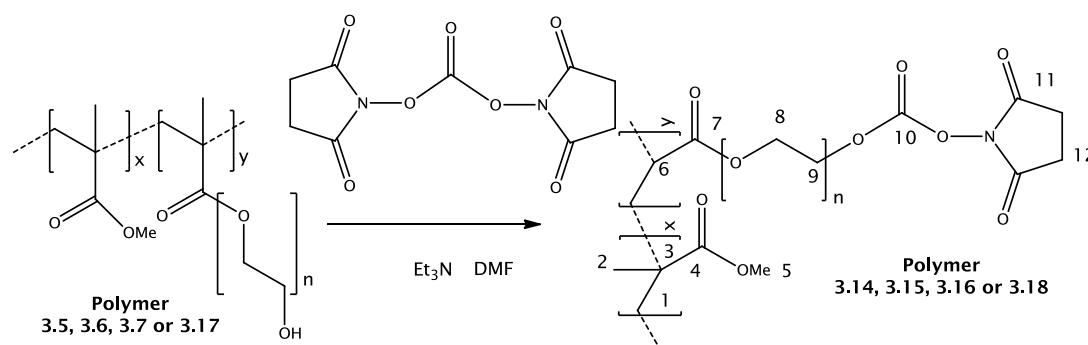
Weight average molecular weight (M_w) - 99613

Number average molecular weight (M_n) - 30217

Polydispersity index - 3.30

Glass transition temperature (T_g) - 40.06°C

5.2.6 Preparation of a succinimidyl carbonate of P(MMA-co-PEGM) – Polymers 3.14, 3.15, 3.16 and 3.18



To P(MMA-co-PEGM) (Polymer 3.5, 3.6, 3.7 or 3.17) (8g) dissolved in DCM (100ml) was added disuccinimidyl carbonate (DSC) (0.0078mol, 2g) and triethylamine (0.014mol, 1.45g, 2ml). This solution was stirred for 2 hrs. The reaction mixture was then washed with $\text{HCl}_{(\text{aq})}$ (2M, 100ml) before being precipitated in diethyl ether (100ml) yielding a white solid. The product was twice dissolved in chloroform (30ml) and precipitated in diethyl ether (50ml). The polymer was then dissolved in chloroform (30ml), the solvent was evaporated and the product was dried *in vacuo*. Characterisation data is summarised in Table 5.5.

FTIR $\nu_{\text{max}}/\text{cm}^{-1}$ 2993 and 2950 (CH), 1790 (CO-N cyclic imide), 1722s (CO)

^1H NMR: δ_{H} (400MHz, CDCl_3) 0.85 and 1.03 (br s, H2), 1.62 (br s, H1), 1.82 (br s, H1), 2.86 (br s, H12), 3.61 (br s, H5), 3.67 (br s, H9 in PEG chain), 4.12 (br s, H8), 4.48 (br s, H9 adjacent to carbonate)

Due to overlapping signals, it was difficult to obtain accurate integrals from ^1H NMR signals. However, estimated integrals can be used to obtain an estimate of the percentage of PEG chains that have a succinimidyl end group by comparing integral of the protons adjacent to the ester group in the PEG chain to that of the protons in the succinimidyl group. This indicates that approximately 80% of the PEG chains reacted to give a succinimidyl group.

$^{13}\text{C}\{^1\text{H}\}$ NMR: δ_{c} (100 MHz, CDCl_3) 16.5 and 18.7 (C2), 25.6 (C12) 44.6 (C3), 44.9 (C6), 51.8 (C5), 54.4 (C1), 68.0 (PEG chain), 68.3 (PEG chain), 70.6 (PEG chain), 177.8 (C7), 178.1 (C4).

Compound	Number average molecular weight (Mn)	Weight average molecular weight (Mw)	Polydispersity index	Glass transition temperature
3.14	22307	35327	1.58	-
3.15	22536	39943	1.77	40°C
3.16	24671	84079	3.40	30°C
3.18	34579	99502	2.88	40°C

Table 5.5 - Summary of data from polymers with succinimidyl carbonate functionality.

5.2.7 Spin coating and contact angle

A polymer solution in DCM (0.5ml, 0.1g/ml) was applied to glass surface and spun at 3000rpm for 1 minute. Contact angles were calculated for a 1 μL water drop using a Kruss DSA100 (Kruss GmbH, Hamburg, Germany) running Drop Shape Analysis (DSA) for windows v1.90.0.14. The data obtained from different polymers is given in Table 5.6.

Polymer	Contact angle (°) (n = 3)	Polymer	Contact angle (°) (n = 3)
PMMA	101.2 \pm 0.4	3.15	67.8 \pm 0.4
3.3	58.6 \pm 0.4	3.16	74.6 \pm 0.6
3.5	77.1 \pm 0.7	3.17	57.0 \pm 0.7
3.6	59.7 \pm 2.9	3.18	77.5 \pm 1.2
3.12	67.1 \pm 0.8		

Table 5.6 - Data from contact angle experiments on various polymers.

5.3 Electrospinning of polymers

General procedure:

A solution of polymer was drawn into a 1ml syringe housed in a syringe pump (World Precision Instruments Inc, Sarasota, USA). A 21 gauge needle (Becton Dickinson Limited, Oxford, UK) was attached to the end of the syringe containing the polymer solution. A stainless steel collector was placed 15cm from the needle tip. The needle was then connected to a high voltage supply (Gamma High Voltage, Ormond Beach, Florida). The syringe pump was set to run and electrospun fibres were collected on the stainless steel plate. The resulting electrospun mats were dried by vacuum desiccation to remove any residual solvent. Parameters used for electrospinning are detailed in Table 5.7. Those highlighted in bold and underlined were the conditions used to produce fibres that were subsequently used in cell biocompatibility tests.

Polymer	Concentration(g/ml)	Applied voltage(kV)	Flow rate(ml/hour)
3.3	<u>0.45</u>	<u>16</u>	<u>9.5</u>
3.5	<u>0.45</u>	14	9.5
		<u>17</u>	<u>9.5</u>
		20	9.5
		25	9.5
3.14	0.4	17	9.5
	<u>0.5</u>	<u>17</u>	<u>9.5</u>
	0.6	17	9.5
3.15	0.45	<u>17</u>	9.5
	0.5		9.5
	<u>0.55</u>		1.5
			<u>9.5</u>
3.6	<u>0.55</u>	<u>17</u>	<u>9.5</u>
3.7	0.55	17	9.5
3.16	<u>0.55</u>	<u>17</u>	<u>9.5</u>
	0.65		
	0.75		
3.17	<u>0.55</u>	<u>17</u>	<u>9.5</u>
3.18	<u>0.55</u>	<u>17</u>	<u>9.5</u>
3.3	<u>0.45</u>	<u>17</u>	<u>9.5</u>
3.12	0.55	<u>17</u>	<u>9.5</u>
	<u>0.65</u>		

Table 5.7 - Electrospinning parameters used for different polymers. Conditions used to produce fibres for biocompatibility tests with RPE cells are shown in bold and underlined.

5.3.1 Assessment of fibre diameter and surface porosity

Fibre diameter and porosity were quantified using SEM images. For assessment of fibre diameter, 15 areas were measured per image. While for surface fibre porosity, fibre area was evaluated in relation to total polymer area (10 images per polymer) using the density slice function on Improvision Volocity software (Improvision, Coventry, UK).

5.4 Investigation of gelation characteristics observed in P(MMA-co-PEGM) succinimidyl carbonate copolymers

5.4.1 Investigation into the gelation of Polymer 3.15

To polymer 3.6 (7g) dissolved in DCM (100ml) was added DSC (0.0078mol, 2g) and triethylamine (0.014mol, 1.45g, 2ml). The reaction was stirred overnight before being stored for one week. An insoluble yellow-coloured gel was formed.

5.4.2 Investigation into the gelation of Polymer 3.16

To polymer 3.7 (8.81g) dissolved in DCM (100ml) was added DSC (0.0078mol, 2g) and triethylamine (0.014mol, 1.45g, 2ml). The reaction mixture was stirred overnight. The solvent volume was reduced to 50ml. An insoluble yellow-coloured gel formed over the course of 2 hrs.

5.4.3 Investigation of the use of 4-dimethylaminopyridine (DMAP) as a base for synthesis of Polymer 3.15

To polymer 3.6 (3g) dissolved in DCM (50ml) was added DSC (0.0039mol, 1g) and 4-dimethylaminopyridine (DMAP) (0.0039mol, 0.48g). The reaction mixture was stirred. An insoluble yellow-coloured gel was observed to form over the course of 10 mins.

5.4.4 Investigation of the influence of disuccinimidyl carbonate on gelation of Polymer 3.7

Polymer 3.7 (0.8g) was dissolved in DCM (1ml). Separately, polymer 3.7 (0.8g) was dissolved in THF (1ml). Triethylamine (0.1ml) was then added to both solutions. These solutions were then both split into two sample vials. To one vial from each solution was added DSC (0.00039mol, 0.1g). In the vials containing DSC, a straw-coloured gel was observed to form within 30 mins (DCM) or overnight (THF). Those vials containing no DSC remained as solutions.

5.4.5 Investigation of gel formation using Polymer 3.15

Polymer 3.15 (0.8g) was dissolved in DCM (1ml). Triethylamine (0.1ml) was added and a straw-coloured gel was observed to form within 30 minutes.

5.4.6 Investigation into the influence of capping with acetyl groups on gelation of Polymer 3.6

A sample of reaction mixture from the synthesis of polymer 3.15 (6ml) was taken. This sample was split equally into 2 vials. To one of the vials was added acetic anhydride (3ml). Within 1 week, the vial containing reaction mixture alone was found to have formed a gel whereas the vial containing acetic anhydride remained as a solution. Characterisation by ^1H NMR suggested that the polymer shown in Figure 5.1 had been formed.

^1H NMR: δ_{H} (400MHz, CDCl_3) 0.84 and 1.01 (br s, H2), 1.81 (br s, H1), 1.86 (br s, H1), 2.06 (br s, H11), 3.59 (br s, H5), 3.66 (br s, H9), 4.09 (br s, H8), 4.21 (br s, H9 adjacent to acetic ester)

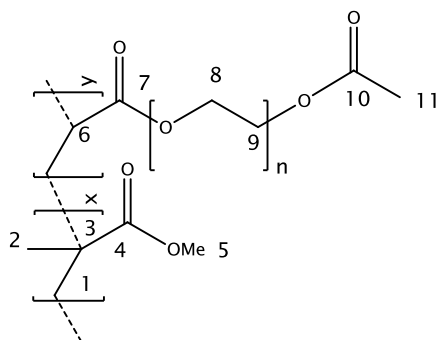


Figure 5.1 – Structure of P(MMA-co-PEGM) acetic ester.

5.5 Investigation of diffusion across an artificial Bruch's membrane

A sample of a fibrous polymer was taken and sealed in a cassette. The cassette was sealed in the test chamber between two liquid reservoirs. One reservoir was then filled with PBS (1.2ml) and the other reservoir with a 0.412mM solution of fluorescein isothiocyanate (FITC)-dextran (Average Mw 40,000) in PBS (1.2ml). Both reservoirs were stirred magnetically (Figure 5.2). At set time points, 100 μ l aliquots were withdrawn from both reservoirs and pipetted onto a 96-well plate (Nunc, Thermo Fisher Scientific, Loughborough, UK). When the experiment was complete, the plate was read in a spectrophotometer (FLUOstar Optima microplate reader (BMG Labtech, Offenburg, Germany)) to give absorbance values.

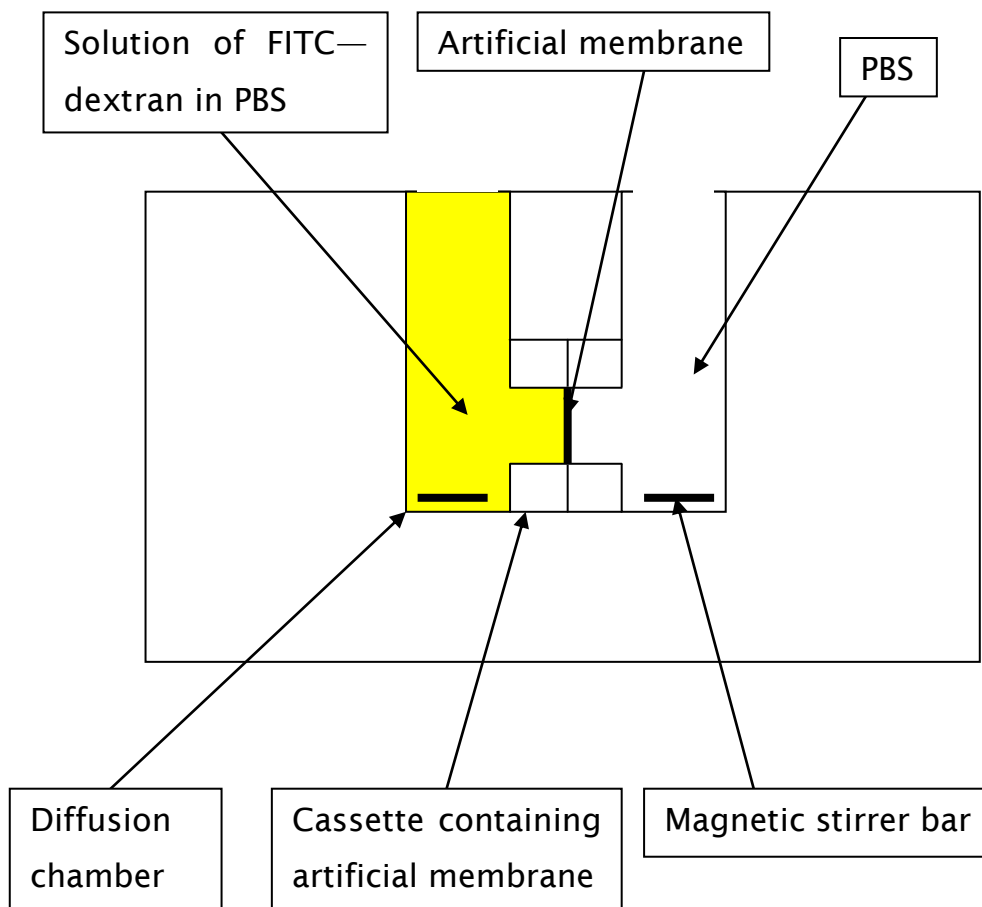


Figure 5.2 - Diagram to show apparatus for diffusion experiments. Diffusion was assessed by the movement of FITC-dextran across the membrane over time.

5.6 Investigation of the response of RPE cells to microsphere surfaces

5.6.1 Cell line maintenance

Biocompatibility was assessed using an RPE cell line (APRE-19) purchased from the American Tissue Culture Collection (Manassas, VA, USA) (ATCC). APRE-19 cells were maintained at 37°C in a humidified atmosphere with 5% CO₂ in culture medium. Culture media comprised of 1:1 (vol/vol) mixture of DMEM:F12 (ATCC) supplemented with 1% antibiotic antimycotic solution (10,000units/ml penicillin G, 10mg/ml streptomycin sulphate, 25µg/ml amphotericin B) (Sigma-Aldrich) and 10% fetal bovine serum (FBS) (ATCC).

5.6.2 Preparation of microspheres for cell seeding

1mg/well of each microsphere blend was weighed out in triplicate. 12 wells in total were used for each blend (laminin coated and uncoated (seeded), laminin coated and uncoated (not seeded)). Microspheres were UV irradiated overnight and then washed in 70% ethanol for 1 hr. Under aseptic conditions, all wells were then washed three times for 5 mins with sterile phosphate buffered saline 0.1M PBS (pH 7.4). Half of the prepared microspheres from each blend were then incubated at 37°C for 60 minutes with laminin solution (Sigma-Aldrich) (0.5ml, 5µg/ml) at 37°C. All wells were then washed three times for 5 mins each with sterile PBS. Tissue culture media (Composition described in Section 5.6.1) (0.3ml) was then added to each well. Cells were then dissociated from the culture flask as described in Section 5.6.3 and counted using a Trypan Blue exclusion assay as described in Section 5.6.4.

5.6.3 Dissociation of cells from culture flask

Tissue culture medium and cell dissociation solution (0.025% (w/v) Trypsin-EDTA) were pre-warmed to 37°C. Medium from the cell culture flask was aspirated and discarded. Cells were then washed with sterile

PBS. Cell dissociation solution (3ml) was then added to the flask and placed in an incubator for 5 mins at 37°C. The flask was removed from the incubator and tapped to release any remaining adherent cells. Warmed culture medium (5ml) was then added to the flask and used to wash any remaining cells from the side of the flask. The cell suspension was then centrifuged at 950rpm for 5 mins. Following centrifugation, the supernatant was discarded and the cell pellet was resuspended in pre-warmed culture medium (10ml). The number of cells in the suspension was then assessed using the Trypan blue exclusion assay described below.

5.6.4 Trypan blue exclusion assay

Trypan blue solution (100µl, 0.25%) was mixed with an equal volume of cell suspension (100µl). The resulting mixture was used to fill both chambers of a haemocytometer. Dead cells were stained blue by the exclusion assay. The number of live cells in four haemocytometer (Fisher Scientific) squares was counted. The number of cells per ml of cell suspension could then be calculated using the following formula.

No. of million cells/ml = no. of cells counted/ no. of squares counted
× 2 / 100

5.6.5 Cell seeding

Cells were seeded at a density of 150,000 cells per well using a cell suspension (200µl). The plates were then agitated (4 hrs) at 1rpm. Culture medium (Composition described in Section 5.6.1) (500µl per well) was then added to each well. Plates were then transferred to a normal incubator and maintained at 37°C in 5% CO₂ in a humidified atmosphere. Half of the prepared microspheres for each blend were not seeded with cells. Culture medium samples (400µl) were taken on day 1, 3, 5, 7, 9, 11 and 13. Culture medium was spun at 950rpm for 5 mins to remove any cells and then frozen at -80°C until required for analysis.

5.6.6 Fixing and immunocytochemistry of microspheres

Samples of seeded microspheres taken on day 1, 5, 9 and 13 were seeded onto 8 well chamber slides (VWR, Leicestershire, UK). Microspheres were allowed to attach for 6-8 hrs. Culture medium was then aspirated from each well. The samples were washed quickly with PBS. Paraformaldehyde (PFA) (4%) was added to each well. Samples were then left at 4°C for 30 mins. Blocking serum (150µl, 5% donkey serum in PBS with 0.1% Triton-X100 (PBS-T)) was added to each well and left for 30 mins at room temperature. The blocking serum was then aspirated and primary antibody (150µl per well, made up in PBS-T with 5% blocking serum) was added and left for 14 hours (overnight) at 4°C. The samples were then washed once in PBS. An Alexa Fluor 488 secondary antibody (Gibco-Invitrogen, 1:1000 dilution in PBS-T with no blocking serum) was then applied and the plate was kept in the dark at room temperature for 1-2 hours. All wells were then washed twice with PBS, 4',6-diamidino-2-phenylindole (DAPI) (5µg ml⁻¹ solution in DI water) was then applied for 6 mins. DAPI was then aspirated and the samples were washed twice in PBS. A negative control with the omission of the primary antibody was included with each plate.

Primary antibodies used:

PCNA: 1:1000 dilution used (Sigma-Aldrich)

RPE65: 1:150 dilution used (Abcam)

5.6.7 Lactate Dehydrogenase (LDH) assay

The assay was performed using a commercially available kit obtained from Roche (Basel, Switzerland). A sample of culture media (Described in Section 5.6.1) (400µl) was taken from each culture well to be tested on day 1, 3, 5, 7, 9, 11 and 13 post seeding. Samples were then centrifuged at 950rpm for 5 mins to remove any remaining cells. The supernatant was then aliquoted into a 96 well plate (100µl per well) in triplicate. Dye solution (11.25ml, iodonitrotetrazolium

chloride and sodium lactate) was then mixed with catalyst solution (250µl, Diaphorase/NAD⁺ mixture) immediately prior to the experiment. This mix was then added to each well (100µl for each well) and incubated at room temperature for 30 mins in the absence of light. Absorbance of the samples at 492nm was then measured using a spectrophotometer.

5.6.8 Terminal deoxynucleotidyl transferase dUTP nick end labelling (TUNEL) assay

The assay was performed using a commercially available kit obtained from Promega (Madison, WI, USA). Samples of seeded microspheres taken on day 1, 5, 9 and 13 were seeded onto 8 well chamber slides. Microspheres were allowed to attach for 6-8 hrs. Cell seeded microspheres were then fixed by immersing slides in 4% PFA for 25 mins at 4°C. Slides were then washed twice by immersion in fresh PBS for 5 mins at room temperature. The PBS wash was repeated. The cells were permeabilised by being immersed in 0.2% TritonX-100 solution in PBS for 5 mins. The slides were rinsed twice by immersion in fresh PBS for 5 mins at room temperature. The samples were then covered with equilibration buffer (100µl) and allowed to equilibrate at room temperature for 5-10 mins. While the cells were equilibrating, a nucleotide mix was thawed on ice and sufficient recombinant terminal deoxynucleotidyl transferase (rTDT) incubation buffer was prepared. Reaction mix (100µl) was then added to each well. The slides were covered with plastic coverslips to ensure even distribution of the reagent. The slides were incubated at 37°C for 60 mins inside a humidified chamber to allow the tailing reaction to occur. The chamber was then covered with aluminium foil to protect it from direct light. 20X Sodium salt solution (SSC) was diluted 1:10 with deionised water and enough of the resulting 2X SSC was added to fill a standard coplin jar (80ml). The coverslips were removed and the reactions were terminated by immersing the slides in 2X SSC for 15 mins at room temperature. The samples were washed three times by

immersing the slides in fresh PBS for 5 mins at room temperature. Samples were then stained with propidium iodide solution 15 mins at room temperature in the dark. The samples were washed three times by immersion in deionised water for 5 minutes at room temperature. Glass coverslips were used to mount the slides. The edges were sealed with clear nail polish. The samples were immediately analysed under a fluorescence microscope using a standard fluorescein filter set to view the green fluorescence of fluorescein at $520 \pm 20\text{nm}$; the red fluorescence of propidium iodide was viewed at $>620\text{nm}$ with analysis carried out using Volocity software (Improvision, Coventry, UK).

5.6.9 3-(4,5-Dimethylthiazol-2-yl)-2,5-diphenyltetrazolium bromide (MTT) assay

The assay was performed using a commercially available kit obtained from Chemicon International/Millipore (Temecula, CA, USA). Samples of culture medium from unseeded microspheres were taken on days 1, 3, 5, 7, 9, 11, 13, 15, 21, 28, 35 and 42 *in vitro*. ARPE-19 cells were passaged as described above. Cells were counted and seeded at 10,000 cells per well in a 96 well plate. Cells were allowed to attach overnight. Culture medium (0.1ml) from unseeded microspheres of each blend (coated and uncoated) was then added to each well. Cells were incubated with test solution at 37°C overnight. At the end of the incubation period, MTT solution (0.01ml) was added to each well. The solution was mixed by tapping gently on the side of the tray and then incubated for 4 hrs at 37°C for cleavage of MTT to occur. The formazan produced in the wells containing live cells appeared as black crystals at the bottom of the wells. Colour development solution (isopropanol with 0.04N HCl) (0.1ml) was added to each well and the contents were mixed thoroughly by repeated pipetting with a multichannel pipettor. Within an hour the absorbance was measured on a plate reader with a test wavelength of 570nm and a reference wavelength of 630nm.

5.6.10 Scanning electron microscopy (SEM)

Cell seeded samples maintained in culture for up to two weeks were fixed in 3% glutaraldehyde with 4% formaldehyde in 0.1M Piperazine-1,4-*bis*-(2-ethanesulfonic acid) buffer (pH 7.2), followed by dehydration through a series of graded ethanol steps to 100% ethanol. Samples were then critical-point dried with CO₂ using a Balzers critical point drier (Bal-Tec, Balzers, Liechtenstein) before being mounted on carbon stubs (Agar Scientific, Stansted, Essex, UK) and sputter-coated with gold/palladium.

5.7 Investigation of the response of RPE cells to fibrous methacrylate-based polymer surfaces

5.7.1 Preparation of electrospun polymer scaffolds for cell seeding

Fibrous samples were cut into 1 cm² sections using a scalpel. Sections were UV irradiated overnight. The sections were then placed into sterile 12 well plates (Fisher Scientific). Under aseptic conditions, all wells were then washed three times for 5 mins with sterile PBS (Sigma Aldrich) 0.1M pH 7.4.

5.7.2 Peptide and protein attachment to electrospun scaffold surfaces

Half of the prepared scaffolds were modified with peptides including GRGESP (nonsense peptide sequence), GRGDSP, YIGSR (1 mg/ml PBS) (All obtained from Peptide Protein Research Ltd, Fareham, UK), Laminin protein (0.5 µg/ml) or a combination of RGD and YIGSR overnight at room temperature, the other half of the prepared copolymer scaffolds remained unmodified. To remove unbound peptide/protein, all scaffolds were rinsed three times in sterile PBS. The plates were then incubated at 37°C overnight.

To visually confirm successful coupling of the peptides to the functionalised copolymer surface, a fluorescein-labelled peptide was used. To sections of both unfunctionalised and functionalised fibrous copolymer scaffolds was added K(Flu)RGD peptide (Peptide Protein Research Ltd) using the same procedure as described above. Samples were imaged using a Leica DM IRB microscope (Leica Microsystems UK Ltd, Milton Keynes, UK).

5.7.3 Cell seeding

Human ARPE-19 cells (ATCC) were maintained at 37°C in a humidified atmosphere with 5% CO₂ in culture medium (using the same composition described in Section 5.6.2). Under aseptic conditions fibrous scaffolds were rinsed 3 times with PBS. All samples were then

flooded with culture medium and allowed to equilibrate for 30 min at 37°C prior to seeding. Cells were then dissociated from the culture flask as described in Section 5.6.3 and counted using the Trypan Blue exclusion assay as described in Section 5.6.4. Cells were seeded at a density of 1.5×10^5 per well. Cell seeding density was established from previous experiments. Culture medium was changed every 48 hrs.

5.7.4 Quantification of cell area

Nuclear labelling was used to confirm and quantify cell area. Samples of seeded electrospun fibres taken on day 5, 10 and 15 post seeding were fixed in 4% PFA for one hour at 4°C. Nuclei were labelled with 5mg/ml propidium iodide (PI) (Gibco-Invitrogen, Paisley, UK). Fibre samples were visualised using a Leica DM IRB microscope (Leica Microsystems UK Ltd). Fibre area and cell area were evaluated using the density slice function on Improvion Volocity software (Improvion, Coventry, UK).

5.7.5 TUNEL assay

Samples of seeded electrospun fibres taken on day 5, 10 and 15 post seeding were fixed in 4% PFA for one hr at 4°C, cryoprotected in 30% sucrose overnight at 4°C before being embedded in optimal cutting temperature media (R. Lamb Ltd., East Sussex, UK) and then cryosectioned at 15µm (OFT 5030, Bright Instrument Company, Cambridge, UK). Evaluation of apoptotic cell death was performed using a commercially available kit (Promega, Madison, WI, USA) in accordance with manufacturers' instructions as described in Section 5.6.8. DNase I treatment was used as a positive control and exclusion of recombinant terminal deoxynucleotidyl transferase (rTDT) from the reaction buffer was used as the negative control. Cell nuclei were visualised using PI. PI positive and TUNEL positive cell areas were evaluated using the density slice function on Improvion Volocity software (Improvion).

5.7.6 MTT assay

Samples of tissue culture medium from unseeded fibre samples were taken on day 1, 3, 5, 7, 9, 11, 13 and 15 in vitro and frozen at -80°C until required for analysis. This tissue culture media was then incubated overnight with APRE-19 cells in 96 well tissue culture plates (Fisher Scientific) seeded at a density of 1×10^4 per well. The MTT assay was performed as per manufacturers' instruction (Chemicon International/ Millipore, Temecula, CA, USA). Absorbance of samples was measured on a FLUOstar Optima microplate reader (BMG Labtech) with a test wavelength of 490nm.

5.7.7 LDH assay

The lactate dehydrogenase (LDH) assay was used as an indicator of cell viability. Assay kits were purchased from Roche (Basel, Switzerland). The procedure previously described in Section 5.6.7 was used. Samples of culture medium (500µl/well) were removed on days 1, 3, 5, 7, 9, 11, 13 and 15 post-seeding. Samples were also taken from unseeded polymers of each blend. Cells cultured on tissue culture plastic, treated with 1% Triton, were used as the positive control. LDH content of cell culture medium and from unseeded polymer medium for each sample was treated as background. LDH activity was measured in a 96-well plate with 3 replicates in each group at an absorbance of 492 nm using a FLUOstar Optima microplate reader (BMG Labtech, Offenburg, Germany).

5.7.8 Scanning electron microscopy (SEM)

SEM was conducted on fibre samples using the same procedure as in Section 5.6.10.

5.7.9 Statistical analysis

All results are expressed as mean \pm standard error of the mean (sem). All data were analysed by either Student's t-test or one way analysis of variance (ANOVA) using GraphPad Prism Software (GraphPad

Software Inc., San Diego, CA, USA). Post-hoc comparisons were made using the Tukey-Kramer Multiple Comparisons Test when the p-value was significant ($p < 0.05$).

6 Appendices

6.1 Appendix A – Publications

Journal publications

- Thomson, H.A., Treharne, A.J., Backholer, L.S., Cuda, F., Grossel, M.C., Lotery, A.J., Biodegradable poly(α -hydroxy ester) blended microspheres as suitable carriers for retinal pigment epithelium cell transplantation, *J.Biomed.Mater.Res., Part A*, **2010**, *95*, 1233-1243.
- Treharne, A.J., Grossel, M.C., Lotery, A.J., Thomson, H.A., The chemistry of retinal transplantation: the influence of polymer scaffold properties on retinal cell adhesion and control, *Br.J.Ophthalmol.*, **2011**, *95*, 768-773.
- Treharne, A.J., Thomson, H.A., Grossel, M.C., Lotery, A.J., Developing methacrylate-based copolymers as an artificial Bruch's membrane substitute, *J.Biomed.Mater.Res., Part A*, **2012**, *100*, 2358-2364.

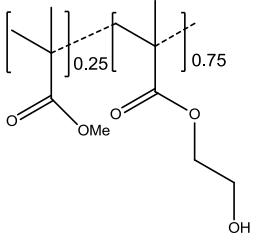
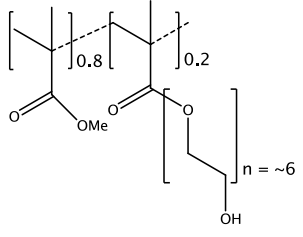
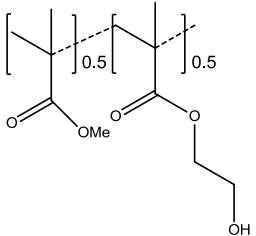
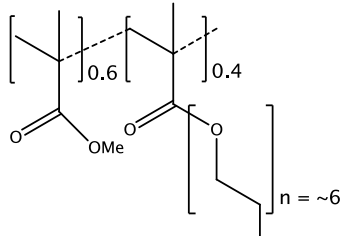
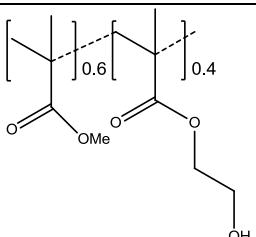
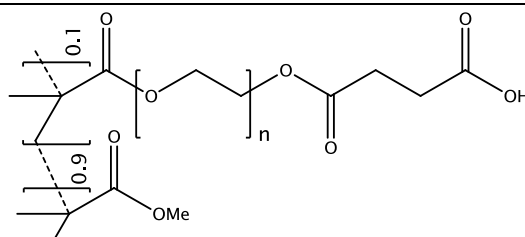
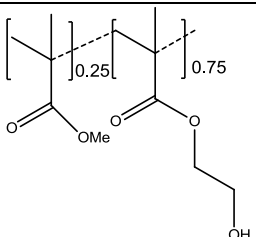
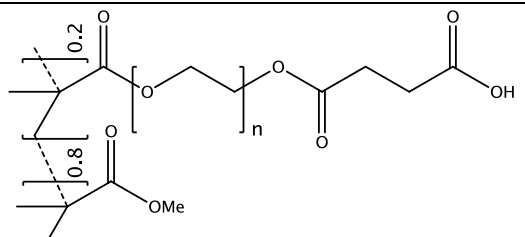
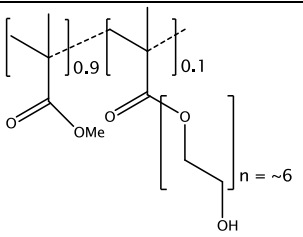
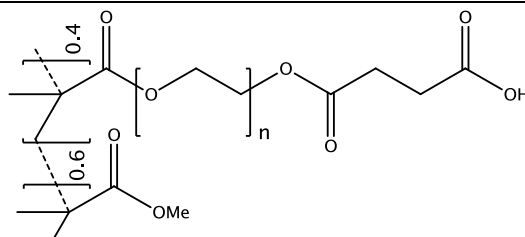
Appendices

Appendices

6.2 Appendix B - List of polymer numbers and structures for Chapter 3

Appendices

Appendices

Polymer number	Structure	Polymer number	Structure
3.1		3.6	
3.2		3.7	
3.3		3.8	
3.4		3.9	
3.5		3.10	

Appendices

Appendices

3.11		3.16	
3.12		3.17	
3.13		3.18	
3.14			
3.15			

Appendices

6.3 Appendix C – Data tables from cell-based assays

Appendices

Data from assays presented in Section 3.5.2

LDH Assay

Sample	Mean absorbance \pm sem
Blank	0.04 \pm 0.0003
LDH Control	0.20 \pm 0.002
Negative Control	0.24 \pm 0.007
Media Control	0.27 \pm 0.029
Positive Control	1.34 \pm 0.050
*TCP Control	0.34 \pm 0.003
Polymer 3.5	0.32 \pm 0.002
Polymer 3.5 + Cells	0.34 \pm 0.012
Polymer 3.14	0.49 \pm 0.028
Polymer 3.14 + Cells	0.71 \pm 0.010
TCP + YIGSR	0.33 \pm 0.008
Polymer 3.14 + YIGSR	0.36 \pm 0.005
Polymer 3.14 + YIGSR + Cells	0.39 \pm 0.016
TCP + GRGDSP	0.34 \pm 0.005
Polymer 3.14 + GRGDSP	0.36 \pm 0.003
Polymer 3.14 + GRGDSP + Cells	0.42 \pm 0.014
TCP + GRGDSP/YIGSR	0.36 \pm 0.002
Polymer 3.14 + GRGDSP/YIGSR	0.35 \pm 0.010
Polymer 3.14 + GRGDSP/YIGSR + Cells	0.44 \pm 0.016

Appendices

Sample	Mean absorbance \pm sem
TCP + Laminin	0.34 \pm 0.008
Polymer 3.14 + Laminin	0.34 \pm 0.007
Polymer 3.14 + Laminin + Cells	0.36 \pm 0.001

Table 6.1 - Data from LDH assay on experiments using Polymers 3.5 and 3.14. sem: standard error of the mean.

MTT Assay

Sample	Mean absorbance \pm sem
Negative Control	0.45 \pm 0.032
Positive Control	0.23 \pm 0.002
Polymer 3.14	0.41 \pm 0.007
Polymer 3.14 + YIGSR	0.42 \pm 0.007
Polymer 3.14 + GRGDSP	0.42 \pm 0.008
Polymer 3.14 + GRGDSP/YIGSR	0.42 \pm 0.010
Polymer 3.14 + Laminin	0.43 \pm 0.006

Table 6.2 - Data from MTT assay on experiments using Polymers 3.5 and 3.14. sem: standard error of the mean.

Appendices

Data from assays presented in Section 3.5.4

LDH Assay

Sample	Mean absorbance \pm sem
Negative Control	0.89 \pm 0.03
Positive Control	4.45 \pm 0.01
TCP alone	0.74 \pm 0.03
TCP with cells	0.89 \pm 0.05
Polymer 3.6	1.06 \pm 0.04
Polymer 3.15	1.11 \pm 0.05
TCP + GRGESP	0.89 \pm 0.05
Polymer 3.15 + GRGESP	1.05 \pm 0.04
GRGDSP coated TCP	0.93 \pm 0.05
Polymer 3.15 + GRGDSP	1.23 \pm 0.07
TCP + YIGSR	0.92 \pm 0.05
Polymer 3.15 + YIGSR	1.22 \pm 0.07
TCP + GRGDSP/YIGSR	0.91 \pm 0.06
Polymer 3.15 + GRGDSP/YIGSR	1.34 \pm 0.08
TCP + Laminin	0.92 \pm 0.05
Polymer 3.15 + Laminin	1.19 \pm 0.08

**Table 6.3 – LDH assay data from experiments involving polymers 3.6 and 3.15.
sem: standard error of the mean.**

Appendices

MTT assay

Sample	Mean absorbance ± sem
Positive Control	0.29 ± 0.02
Negative Control	0.48 ± 0.02
Polymer 3.6	0.47 ± 0.01
Polymer 3.15	0.47 ± 0.01
Polymer 3.15 + GRGESP	0.49 ± 0.02
Polymer 3.15 + GRGDSP	0.50 ± 0.02
Polymer 3.15 + YIGSR	0.46 ± 0.01
Polymer 3.15+ GRGDSP/YIGSR	0.46 ± 0.01
Polymer 3.15 + Laminin	0.49 ± 0.01

Table 6.4 – MTT assay data for experiments involving polymers 3.6 and 3.15. sem: standard error of the mean.

Appendices

TUNEL assay data

Sample	Mean % cell death ± sem Day 5	Mean % cell death ± sem Day 10	Mean % cell death ± sem Day 15
Negative Control	0.49 ± 0.01	0.59 ± 0.02	0.74 ± 0.02
Positive Control	58.45 ± 10.21	76.83 ± 13.43	88.69 ± 10.63
Polymer 3.6	8.54 ± 1.61	12.45 ± 4.78	21.26 ± 3.57
Polymer 3.15	8.45 ± 1.90	6.01 ± 1.27	1.25 ± 0.29
Polymer 3.15 + GRGESP	4.67 ± 0.96	3.84 ± 0.35	1.64 ± 0.60
Polymer 3.15 + GRGDSP	2.94 ± 0.79	3.28 ± 1.27	1.66 ± 0.34
Polymer 3.15 + YIGSR	0.73 ± 0.13	2.66 ± 0.66	0.82 ± 0.25
Polymer 3.15 + GRGRSP + YIGSR	0.83 ± 0.07	3.93 ± 1.18	1.03 ± 0.33
Polymer 3.15 + Laminin	4.99 ± 0.94	6.35 ± 1.37	1.63 ± 0.31

Table 6.5 - TUNEL assay data for experiments involving polymers 3.6 and 3.15.
sem: standard error of the mean.

Appendices

Cell attachment data

Sample	Mean % cell death ± sem Day 5	Mean % cell death ± sem Day 10	Mean % cell death ± sem Day 15
Negative Control	0.49 ± 0.01	0.59 ± 0.02	0.74 ± 0.02
Positive Control	58.45 ± 10.21	76.83 ± 13.43	88.69 ± 10.63
Polymer 3.6	8.54 ± 1.61	12.45 ± 4.78	21.26 ± 3.57
Polymer 3.15	8.45 ± 1.90	6.01 ± 1.27	1.25 ± 0.29
Polymer 3.15 + GRGESP	4.67 ± 0.96	3.84 ± 0.35	1.64 ± 0.60
Polymer 3.15 + GRGDSP	2.94 ± 0.79	3.28 ± 1.27	1.66 ± 0.34
Polymer 3.15 + YIGSR	0.73 ± 0.13	2.66 ± 0.66	0.82 ± 0.25
Polymer 3.15 + GRGRSP + YIGSR	0.83 ± 0.07	3.93 ± 1.18	1.03 ± 0.33
Polymer 3.15 + Laminin	4.99 ± 0.94	6.35 ± 1.37	1.63 ± 0.31

Table 6.6 - Cell attachment data for experiments involving polymers 3.6 and 3.15. sem: standard error of the mean.

Appendices

Data from assays presented in Section 3.5.5

LDH Assay

Time <i>in vitro</i> (days)	1	3	5	7	9	11	13	15
<i>Polymer</i>								
Negative Control	1.61 ± 0.03	2.39 ± 0.05	2.23 ± 0.21	2.63 ± 0.07	2.31 ± 0.05	2.52 ± 0.15	3.60 ± 0.15	3.32 ± 0.10
Positive Control	0.84 ± 0.01	0.94 ± 0.01	1.14 ± 0.03	1.04 ± 0.02	1.06 ± 0.03	1.45 ± 0.12	1.39 ± 0.03	1.47 ± 0.02
Polymer 3.16 + cells	0.86 ± 0.01	0.90 ± 0.02	0.95 ± 0.03	1.30 ± 0.05	1.40 ± 0.06	1.50 ± 0.06	2.08 ± 0.07	2.11 ± 0.08
Polymer 3.6 + cells	0.91 ± 0.03	1.18 ± 0.09	1.15 ± 0.05	1.71 ± 0.04	1.97 ± 0.13	1.79 ± 0.07	2.38 ± 0.08	2.49 ± 0.06
Polymer 3.15 + cells	0.93 ± 0.03	0.88 ± 0.01	0.89 ± 0.02	1.40 ± 0.08	1.50 ± 0.11	1.61 ± 0.12	2.41 ± 0.27	2.39 ± 0.16
Polymer 3.12 + cells	0.99 ± 0.03	0.94 ± 0.02	1.03 ± 0.01	1.70 ± 0.04	1.66 ± 0.09	1.73 ± 0.02	2.50 ± 0.16	2.68 ± 0.04
Polymer 3.17 + cells	0.86 ± 0.02	1.01 ± 0.02	1.12 ± 0.03	1.38 ± 0.06	1.49 ± 0.09	1.46 ± 0.08	1.93 ± 0.04	2.04 ± 0.11
Polymer 3.18 + cells	0.82 ± 0.01	0.93 ± 0.01	1.43 ± 0.07	1.44 ± 0.02	1.62 ± 0.04	2.19 ± 0.02	2.10 ± 0.04	2.40 ± 0.05

Table 6.7 - LDH absorbance data from experiments involving polymers 3.16, 3.6, 3.15, 3.12, 3.17 and 3.18. sem: standard error of the mean.

Appendices

MTT assay

Sample - Final MTT	Cell viability as % of control \pm sem
Negative Control	100 \pm 3.53
Positive Control	40.06 \pm 4.79
Polymer 3.6	90.52 \pm 4.11
Polymer 3.17	88.07 \pm 3.56
Polymer 3.3	92.97 \pm 5.06
Polymer 3.15	90.83 \pm 5.67
Polymer 3.16	93.88 \pm 4.18
Polymer 3.18	93.88 \pm 3.99
Polymer 3.12	90.05 \pm 4.10

Table 6.8 - MTT assay data from experiments involving polymers 3.6, 3.17, 3.3, 3.15, 3.16, 3.18 and 3.12. sem: standard error of the mean.

Appendices

TUNEL assay

Sample	Mean % cell death ± sem Day 5	Mean % cell death ± sem Day 10	Mean % cell death ± sem Day 15
Negative Control	0.49 ± 0.14	0.43 ± 0.10	0.36 ± 0.12
Positive Control	52.31 ± 10.90	69.06 ± 12.25	88.69 ± 10.63
Polymer 3.6	33.00 ± 6.52	61.73 ± 8.66	70.07 ± 10.18
Polymer 3.17	23.26 ± 2.71	39.15 ± 6.38	72.87 ± 12.65
Polymer 3.3	5.93 ± 0.97	3.31 ± 0.35	3.73 ± 0.55
Polymer 3.15	1.93 ± 0.38	1.53 ± 0.30	3.52 ± 0.45
Polymer 3.16	2.66 ± 1.04	0.83 ± 0.20	0.96 ± 0.18
Polymer 3.18	2.85 ± 0.69	3.53 ± 0.41	1.57 ± 0.36
Polymer 3.12	3.42 ± 0.48	3.31 ± 0.32	3.57 ± 0.46

Table 6.9 - TUNEL data from experiments involving polymers 3.6, 3.17, 3.3, 3.15, 3.16, 3.18 and 3.12. sem: standard error of the mean.

Appendices

Cell attachment

Sample	Mean % cell attachment ± sem	Mean % cell attachment ± sem	Mean % cell attachment ± sem
	Day 5	Day 10	Day 15
Polymer 3.6	2.96 ± 0.45	1.11 ± 0.27	0.40 ± 0.09
Polymer 3.17	2.90 ± 0.39	2.80 ± 0.40	1.26 ± 0.25
Polymer 3.3	18.13 ± 1.24	33.60 ± 3.24	47.34 ± 5.05
Polymer 3.15	51.16 ± 4.75	53.70 ± 4.18	66.20 ± 4.52
Polymer 3.16	56.28 ± 4.36	56.86 ± 3.01	67.38 ± 4.89
Polymer 3.18	19.70 ± 4.59	34.97 ± 6.98	57.65 ± 3.76
Polymer 3.12	50.01 ± 3.28	58.80 ± 3.52	68.39 ± 4.85

Table 6.10 – Cell attachment data from experiments involving polymers 3.6, 3.17, 3.3, 3.15, 3.16, 3.18 and 3.12. sem: standard error of the mean.

7 References

1. Pascolini D, Mariotti SP, Pokharel GP, Pararajasegaram R, Etya'ale D, Négre A-D, Resnikoff S. 2002 Global update of available data on visual impairment: a compilation of population-based prevalence studies, *Ophthalmic Epidemiol.* **2004**, *11*, 67-115.
2. Minassian D and Reidy A. Future Sight Loss UK 2: An epidemiological and economic model for sight loss in the decade 2010-2020, *EpiVision and RNIB* **2009**,
3. de Jong PTVM. Age-related macular degeneration, *N.Eng.J.Med.* **2006**, *355*, 1474-1485.
4. Nowak JZ. Age-related macular degeneration (AMD): pathogenesis and therapy, *Pharmacol.Rep.* **2006**, *58*, 353-363.
5. Madhusudhana KC, Hannan SR, Williams CPR, Goverdhan SV, Rennie C, Lotery AJ, Luff AJ, Newsom RSB. Intravitreal bevacizumab (Avastin) for the treatment of choroidal neovascularization in age-related macular degeneration: results from 118 cases, *Br.J.Ophthalmol.* **2007**, *91*, 1716-1717.
6. Mitchell P, Korobelnik JF, Lanzetta P, Holz FG, Prünke C, Schmidt-Erfurth U, Tano Y, Wolf S. Ranibizumab (Lucentis) in neovascular age-related macular degeneration: evidence from clinical trials, *Br.J.Ophthalmol.* **2010**, *94*, 2-13.
7. Hageman GS, Luthert PJ, Victor Chong NH, Johnson LV, Anderson DH, Mullins RF. An integrated hypothesis that considers drusen as biomarkers of immune-mediated processes at the RPE-Bruch's membrane interface in aging and age-related macular degeneration, *Prog.Retin.Eye Res.* **2001**, *20*, 705-732.
8. Penfold PL, Madigan MC, Gillies MC, Provis JM. Immunological and aetiological aspects of macular degeneration, *Prog.Retin.Eye Res.* **2001**, *20*, 385-414.

References

9. Anderson DH, Mullins RF, Hageman GS, Johnson LV. A role for local inflammation in the formation of drusen in the aging eye, *Am.J.Ophthalmol.* **2002**, *134*, 411-431.
10. Anderson DH, Talaga KC, Rivest AJ, Barron E, Hageman GS, Johnson LV. Characterization of β amyloid assemblies in drusen: the deposits associated with aging and age-related macular degeneration, *Exp.Eye Res.* **2004**, *78*, 243-256.
11. Ennis S, Jomary C, Mullins R, Cree A, Chen X, Macleod A, Jones S, Collins A, Stone E, Lotery A. Association between the SERPING1 gene and age-related macular degeneration: a two-stage case-control study, *Lancet* **2008**, *372*, 1828-1834.
12. Gehrs KM, Jackson JR, Brown EN, Allikmets R, Hageman GS. Complement, age-related macular degeneration and a vision of the future, *Arch.Ophthalmol.* **2010**, *128*, 349-358.
13. Binder S, Stanzel BV, Krebs I, Glittenberg C. Transplantation of the RPE in AMD, *Prog.Retin.Eye Res.* **2007**, *26*, 516-554.
14. Crabb JW, Miyagi M, Gu X, Shadrach K, West KA, Sakaguchi H, Kamei M, Hasan A, Yan L, Rayborn ME, Salomon RG, Hollyfield JG. Drusen proteome analysis: an approach to the etiology of age-related macular degeneration, *Proc.Natl.Acad.Sci.U.S.A.* **2002**, *99*, 14682-14687.
15. Hahn P, Milam AH, Dunaief JL. Maculas affected by age-related macular degeneration contain increased chelatable iron in the retinal pigment epithelium and Bruch's membrane, *Arch.Ophthalmol.* **2003**, *121*, 1099-1105.
16. Del Priore LV, Tezel TH, Kaplan HJ. Maculoplasty for age-related macular degeneration: reengineering Bruch's membrane and the human macula, *Prog.Retin.Eye Res.* **2006**, *25*, 539-562.
17. Booij JC, Baas DC, Beisekeeva J, Gorgels TGMF, Bergen AAB. The dynamic nature of Bruch's membrane, *Prog.Retin.Eye Res.* **2010**, *29*, 1-18.

References

18. Ambati J, Ambati BK, Yoo SH, Ianchulev S, Adamis AP. Age-related macular degeneration: Etiology, pathogenesis, and therapeutic strategies, *Surv.Ophthalmol.* **2003**, *48*, 257-293.
19. Tezel TH and Del Priore LV. Reattachment to a substrate prevents apoptosis of human retinal pigment epithelium, *Graefes Arch.Clin.Exp.Ophthalmol.* **1997**, *235*, 41-47.
20. Moore DJ and Clover GM. The effect of age on the macromolecular permeability of human Bruch's membrane, *Invest.Ophthalmol.Vis.Sci.* **2001**, *42*, 2970-2975.
21. Guymer R, Luthert P, Bird A. Changes in Bruch's membrane and related structures with age, *Prog.Retin.Eye Res.* **1999**, *18*, 59-90.
22. Hussain AA, Starita C, Hodgetts A, Marshall J. Macromolecular diffusion characteristics of ageing human Bruch's membrane: Implications for age-related macular degeneration (AMD), *Exp.Eye Res.* **2010**, *90*, 703-710.
23. Ugarte M, Hussain AA, Marshall J. An experimental study of the elastic properties of the human Bruch's membrane-choroid complex: relevance to ageing, *Br.J.Ophthalmol.* **2006**, *90*, 621-626.
24. Starita C, Hussain AA, Patmore A, Marshall J. Localization of the site of major resistance to fluid transport in Bruch's membrane, *Invest.Ophthalmol.Vis.Sci.* **1997**, *38*, 762-767.
25. Starita C, Hussain AA, Pagliarini S, Marshall J. Hydrodynamics of ageing Bruch's membrane: implications for macular disease, *Exp.Eye Res.* **1996**, *62*, 565-572.
26. Ahir A, Guo L, Hussain AA, Marshall J. Expression of metalloproteinases from human retinal pigment epithelial cells and their effects on the hydraulic conductivity of Bruch's membrane, *Invest.Ophthalmol.Vis.Sci.* **2002**, *43*, 458-465.
27. Gullapalli VK, Sugino IK, Van Patten Y, Shah S, Zarbin MA. Impaired RPE survival on aged submacular human Bruch's membrane, *Exp.Eye Res.* **2005**, *80*, 235-248.

References

28. Del Priore LV, Kuo YH, Tezel TH. Age-related changes in human RPE cell density and apoptosis proportion in situ, *Invest.Ophthalmol.Vis.Sci.* **2002**, *43*, 3312-3318.
29. Tezel TH, Kaplan HJ, Del Priore LV. Fate of human retinal pigment epithelial cells seeded onto layers of human Bruch's membrane, *Invest.Ophthalmol.Vis.Sci.* **1999**, *40*, 467-476.
30. Tezel TH and Del Priore LV. Repopulation of different layers of host human Bruch's membrane by retinal pigment epithelial cell grafts, *Invest.Ophthalmol.Vis.Sci.* **1999**, *40*, 767-774.
31. Del Priore LV, Geng L, Tezel TH, Kaplan HJ. Extracellular matrix ligands promote RPE attachment to inner Bruch's membrane, *Curr.Eye Res.* **2002**, *25*, 79-89.
32. Tezel TH, Del Priore LV, Kaplan HJ. Reengineering of aged Bruch's membrane to enhance retinal pigment epithelium repopulation, *Invest.Ophthalmol.Vis.Sci.* **2004**, *45*, 3337-3348.
33. Farboud B, Aotaki-Keen A, Miyata T, Hjelmeland LM, Handa JT. Development of a polyclonal antibody with broad epitope specificity for advanced glycation endproducts and localization of these epitopes in Bruch's membrane of the aging eye, *Mol.Vis.* **1999**, *5*,
34. Yamada Y, Ishibashi K, Ishibashi K, Bhutto IA, Tian J, Luty GA, Handa JT. The expression of advanced glycation endproduct receptors in rpe cells associated with basal deposits in human maculas, *Exp.Eye Res.* **2006**, *82*, 840-848.
35. Tian J, Ishibashi K, Ishibashi K, Reiser K, Grebe R, Biswal S, Gehlbach P, Handa JT. Advanced glycation endproduct-induced aging of the retinal pigment epithelium and choroid: a comprehensive transcriptional response, *Proc.Natl.Acad.Sci.U.S.A.* **2005**, *102*, 11846-11851.
36. Howes KA, Liu Y, Dunaief JL, Milam A, Frederick JM, Marks A, Baehr W. Receptor for advanced glycation end products and age-related macular degeneration, *Invest.Ophthalmol.Vis.Sci.* **2004**, *45*, 3713-3720.

References

37. Langer R and Vacanti J. Tissue Engineering, *Science* **1993**, *260*, 920-926.
38. Araki M. Regeneration of the amphibian retina: Role of tissue interaction and related signaling molecules on RPE transdifferentiation, *Dev.Growth Differ.* **2007**, *49*, 109-120.
39. Tsonis PA and Del Rio-Tsonis K. Lens and retina regeneration: transdifferentiation, stem cells and clinical applications, *Exp.Eye Res.* **2004**, *78*, 161-172.
40. Watt FM and Hogan BL. Out of eden: stem cells and their niches, *Science* **2000**, *287*, 1427-1430.
41. Fuchs E and Segre JA. Stem Cells: A New Lease on Life, *Cell* **2000**, *100*, 143-155.
42. Takahashi K, Tanabe K, Ohnuki M, Narita M, Ichisaka T, Tomoda K, Yamanaka S. Induction of pluripotent stem cells from adult human fibroblasts by defined factors, *Cell* **2007**, *131*, 861-872.
43. Yu J, Vodyanik MA, Smuga-Otto K, Antosiewicz-Bourget J, Frane JL, Tian S, Nie J, Jonsdottir GA, Ruotti V, Stewart R, Slukvin II, Thomson JA. Induced pluripotent stem cell lines derived from human somatic cells, *Science* **2007**, *318*, 1917-1920.
44. Knoepfler PS. Deconstructing stem cell tumorigenicity: A roadmap to safe regenerative medicine, *Stem Cells* **2009**, *27*, 1050-1056.
45. Caplan AI and Bruder SP. Mesenchymal stem cells: Building blocks for molecular medicine in the 21st century, *Trends Mol.Med.* **2001**, *7*, 259-264.
46. Laflamme MA and Murry CE. Regenerating the heart, *Nat.Biotechnol.* **2005**, *23*, 845-856.
47. Kassem M, Kristiansen M, Abdallah BM. Mesenchymal stem cells: Cell biology and potential use in therapy, *Basic Clin.Pharmacol.Toxicol.* **2004**, *95*, 209-214.
48. Holt GE, Halpern JL, Dovan TT, Hamming D, Schwartz HS. Evolution of an in vivo bioreactor, *J.Orthop.Res.* **2005**, *23*, 916-923.

References

49. Stevens MM, Marini RP, Schaefer D, Aronson J, Langer R, Shastri VP. In vivo engineering of organs: The bone bioreactor, *Proc.Natl.Acad.Sci.U.S.A.* **2005**, *102*, 11450-11455.
50. Aoki H, Hara A, Nakagawa S, Motohashi T, Hirano M, Takahashi Y, Kunisada T. Embryonic stem cells that differentiate into RPE cell precursors in vitro develop into RPE cell monolayers in vivo, *Exp.Eye Res.* **2006**, *82*, 265-274.
51. Buchholz DE, Hikita ST, Rowland TJ, Friedrich AM, Hinman CR, Johnson LV, Clegg DO. Derivation of functional retinal pigmented epithelium from induced pluripotent stem cells, *Stem Cells* **2009**, *27*, 2427-2434.
52. Phillips SJ, Sadda SR, Tso MOM, Humayan MS, Juan E, Binder S. Autologous transplantation of retinal pigment epithelium after mechanical debridement of Bruch's membrane, *Curr.Eye Res.* **2003**, *26*, 81-88.
53. Aramant RB and Seiler MJ. Transplanted sheets of human retina and retinal pigment epithelium develop normally in nude rats, *Exp.Eye Res.* **2002**, *75*, 115-125.
54. Falkner-Radler CI, Krebs I, Glittenberg C, Považay B, Drexler W, Graf A, Binder S. Human retinal pigment epithelium (RPE) transplantation: outcome after autologous RPE-choroid sheet and RPE cell-suspension in a randomised clinical study, *Br.J.Ophthalmol.* **2011**, *95*, 370-375.
55. Mruthyunjaya P, Stinnett SS, Toth CA. Change in visual function after macular translocation with 360° retinectomy for neovascular age-related macular degeneration, *Ophthalmology* **2004**, *111*, 1715-1724.
56. MacLaren RE, Pearson RA, MacNeil A, Douglas RH, Salt TE, Akimoto M, Swaroop A, Sowden JC, Ali RR. Retinal repair by transplantation of photoreceptor precursors, *Nature* **2006**, *444*, 203-207.

References

57. Tropepe V, Coles BLK, Chiasson BJ, Horsford DJ, Elia AJ, McInnes RR, van der Kooy D. Retinal stem cells in the adult mammalian eye, *Science* **2000**, *287*, 2032-2036.
58. Klassen HJ, Ng TF, Kurimoto Y, Kirov I, Shatos M, Coffey P, Young MJ. Multipotent retinal progenitors express developmental markers, differentiate into retinal neurons, and preserve light-mediated behavior, *Invest.Ophthalmol.Vis.Sci.* **2004**, *45*, 4167-4173.
59. Tomita M, Lavik E, Klassen H, Zahir T, Langer R, Young MJ. Biodegradable polymer composite grafts promote the survival and differentiation of retinal progenitor cells, *Stem Cells* **2005**, *23*, 1579-1588.
60. Tsukahara I, Ninomiya S, Castellarin A, Yagi F, Sugino IK, Zarbin M. Early attachment of uncultured retinal pigment epithelium from aged donors onto Bruch's membrane explants, *Exp.Eye Res.* **2002**, *74*, 255-266.
61. Barry M. Cell adhesion: The molecular basis of tissue architecture and morphogenesis, *Cell* **1996**, *84*, 345-357.
62. Engler AJ, Sen S, Sweeney HL, Discher DE. Matrix elasticity directs stem cell lineage specification, *Cell* **2006**, *126*, 677-689.
63. Hynes RO. Integrins: Bidirectional, allosteric signaling machines, *Cell* **2002**, *110*, 673-687.
64. Ruoslahti E. RGD and other recognition sequences for integrins, *Annu.Rev.Cell Dev.Biol.* **1996**, *12*, 697-715.
65. Xiong JP, Stehle T, Zhang R, Joachimiak A, Frech M, Goodman SL, Arnaout MA. Crystal structure of the extracellular segment of integrin $\alpha V\beta 3$ in complex with an Arg-Gly-Asp ligand, *Science* **2002**, *296*, 151-155.
66. Hautanen A, Gailit J, Mann DM, Ruoslahti E. Effects of modifications of the RGD sequence and its context on recognition by the fibronectin receptor, *J.Biol.Chem.* **1989**, *264*, 1437-1442.

References

67. Giancotti FG and Ruoslahti E. Integrin signaling, *Science* **1999**, *285*, 1028-1033.
68. Green KJ and Jones JC. Desmosomes and hemidesmosomes: structure and function of molecular components, *FASEB J.* **1996**, *10*, 871-881.
69. Buehler MJ. Nature designs tough collagen: Explaining the nanostructure of collagen fibrils, *Proc.Natl.Acad.Sci.U.S.A.* **2006**, *103*, 12285-12290.
70. Wierzbicka-Patynowski I and Schwarzbauer JE. The ins and outs of fibronectin matrix assembly, *J.Cell Sci.* **2003**, *116*, 3269-3276.
71. Debelle L and Tamburro AM. Elastin: Molecular description and function, *Int.J.Biochem.Cell Biol.* **1999**, *31*, 261-272.
72. Fernandes H, Moroni L, van Blitterswijk C, de Boer J. Extracellular matrix and tissue engineering applications, *J.Mater.Chem.* **2009**, *19*, 5474-5474.
73. Ott HC, Matthiesen TS, Goh SK, Black LD, Kren SM, Netoff TI, Taylor DA. Perfusion-decellularized matrix: Using nature's platform to engineer a bioartificial heart, *Nat.Med.* **2008**, *14*, 213-221.
74. Huang S and Fu X. Naturally derived materials-based cell and drug delivery systems in skin regeneration, *J.Controlled Release* **2010**, *142*, 149-159.
75. Kuraitis D, Giordano C, Ruel M, Musarò A, Suuronen EJ. Exploiting extracellular matrix-stem cell interactions: A review of natural materials for therapeutic muscle regeneration, *Biomaterials* **2012**, *33*, 428-443.
76. Place ES, Evans ND, Stevens MM. Complexity in biomaterials for tissue engineering, *Nat.Mater.* **2009**, *8*, 457-470.
77. Wang Y, Kim HJ, Vunjak-Novakovic G, Kaplan DL. Stem cell-based tissue engineering with silk biomaterials, *Biomaterials* **2006**, *27*, 6064-6082.
78. Holmes TC. Novel peptide-based biomaterial scaffolds for tissue engineering, *Trends Biotechnol.* **2002**, *20*, 16-21.

References

79. Mart RJ, Osborne RD, Stevens MM, Ulijn RV. Peptide-based stimuli-responsive biomaterials, *Soft Matter* **2006**, *2*, 822-835.
80. Lawrence BD, Marchant JK, Pindrus MA, Omenetto FG, Kaplan DL. Silk film biomaterials for cornea tissue engineering, *Biomaterials* **2009**, *30*, 1299-1308.
81. McLaughlin CR, Acosta MC, Luna C, Liu W, Belmonte C, Griffith M, Gallar J. Regeneration of functional nerves within full thickness collagen-phosphorylcholine corneal substitute implants in guinea pigs, *Biomaterials* **2010**, *31*, 2770-2778.
82. Rafat M, Li F, Fagerholm P, Lagali NS, Watsky MA, Munger R, Matsuura T, Griffith M. PEG-stabilized carbodiimide crosslinked collagen-chitosan hydrogels for corneal tissue engineering, *Biomaterials* **2008**, *29*, 3960-3972.
83. Lu JT, Lee CJ, Bent SF, Fishman HA, Sabelman EE. Thin collagen film scaffolds for retinal epithelial cell culture, *Biomaterials* **2007**, *28*, 1486-1494.
84. Lee CJ, Vroom JA, Fishman HA, Bent SF. Determination of human lens capsule permeability and its feasibility as a replacement for Bruch's membrane, *Biomaterials* **2006**, *27*, 1670-1678.
85. Ballios BG, Cooke MJ, van der Kooy D, Shoichet MS. A hydrogel-based stem cell delivery system to treat retinal degenerative diseases, *Biomaterials* **2010**, *31*, 2555-2564.
86. Apple DJ and Sims J. Harold Ridley and the invention of the intraocular lens, *Surv.Ophthalmol.* **1996**, *40*, 279-292.
87. Nair LS and Laurencin CT. Biodegradable polymers as biomaterials, *Prog.Polym.Sci.* **2007**, *32*, 762-798.
88. Hutmacher DW. Scaffold design and fabrication technologies for engineering tissues--state of the art and future perspectives, *J.Biomater.Sci.Polym.Ed.* **2001**, *12*, 107-124.
89. Yu NYC, Schindeler A, Little DG, Ruys AJ. Biodegradable poly(α -hydroxy acid) polymer scaffolds for bone tissue engineering, *J.Biomed.Mater.Res., Part B* **2010**, *93*, 285-295.

References

90. Temenoff JS and Mikos AG. Review: Tissue engineering for regeneration of articular cartilage, *Biomaterials* **2000**, *21*, 431-440.
91. Kumbar SG, Nukavarapu SP, James R, Nair LS, Laurencin CT. Electrospun poly(lactic acid-co-glycolic acid) scaffolds for skin tissue engineering, *Biomaterials* **2008**, *29*, 4100-4107.
92. Ulery BD, Nair LS, Laurencin CT. Biomedical applications of biodegradable polymers, *J.Polym.Sci.B Polym.Phys.* **2011**, *49*, 832-864.
93. Chen Q-Z, Ishii H, Thouas GA, Lyon AR, Wright JS, Blaker JJ, Chrzanowski W, Boccaccini AR, Ali NN, Knowles JC, Harding SE. An elastomeric patch derived from poly(glycerol sebacate) for delivery of embryonic stem cells to the heart, *Biomaterials* **2010**, *31*, 3885-3893.
94. Young CD, Wu JR, Tsou TL. Fabrication and characteristics of polyHEMA artificial skin with improved tensile properties, *J.Membr.Sci.* **1998**, *146*, 83-93.
95. Belkas JS, Munro CA, Shoichet MS, Johnston M, Midha R. Long-term in vivo biomechanical properties and biocompatibility of poly(2-hydroxyethyl methacrylate-co-methyl methacrylate) nerve conduits, *Biomaterials* **2005**, *26*, 1741-1749.
96. Lavik EB, Klassen H, Warfvinge K, Langer R, Young MJ. Fabrication of degradable polymer scaffolds to direct the integration and differentiation of retinal progenitors, *Biomaterials* **2005**, *26*, 3187-3196.
97. Thomson HAJ, Treharne AJ, Walker P, Grossel MC, Lotery AJ. Optimisation of polymer scaffolds for retinal pigment epithelium (RPE) cell transplantation, *Br.J.Ophthalmol.* **2011**, *95*, 563-568.
98. Redenti S, Tao S, Yang J, Gu P, Klassen H, Saigal S, Desai T, Young MJ. Retinal tissue engineering using mouse retinal progenitor cells and a novel biodegradable, thin-film poly(ϵ -caprolactone) nanowire scaffold, *J.Ocul.Biol.Dis.Infor.* **2008**, *1*, 19-29.

References

99. Neeley WL, Redenti S, Klassen H, Tao S, Desai T, Young MJ, Langer R. A microfabricated scaffold for retinal progenitor cell grafting, *Biomaterials* **2008**, *29*, 418-426.
100. Redenti S, Neeley WL, Rompani S, Saigal S, Yang J, Klassen H, Langer R, Young MJ. Engineering retinal progenitor cell and scrollable poly(glycerol-sebacate) composites for expansion and subretinal transplantation, *Biomaterials* **2009**, *30*, 3405-3414.
101. Tezcaner A. Retinal pigment epithelium cell culture on surface modified poly(hydroxybutyrate-co-hydroxyvalerate) thin films, *Biomaterials* **2003**, *24*, 4573-4583.
102. Tao S, Young C, Redenti S, Zhang Y, Klassen H, Desai T, Young MJ. Survival, migration and differentiation of retinal progenitor cells transplanted on micro-machined poly(methyl methacrylate) scaffolds to the subretinal space, *Lab Chip* **2007**, *7*, 695-701.
103. Williams R, Krishna Y, Dixon S, Haridas A, Grierson I, Sheridan C. Polyurethanes as potential substrates for sub-retinal retinal pigment epithelial cell transplantation, *J.Mater.Sci.Mater.Med.* **2005**, *16*, 1087-1092.
104. Krishna Y, Sheridan CM, Kent DL, Grierson I, Williams RL. Polydimethylsiloxane as a substrate for retinal pigment epithelial cell growth, *J.Biomed.Mater.Res., Part A* **2007**, *80A*, 669-678.
105. Treharne AJ, Grossel MC, Lotery AJ, Thomson HA. The chemistry of retinal transplantation: the influence of polymer scaffold properties on retinal cell adhesion and control, *Br.J.Ophthalmol.* **2011**, *95*, 768-773.
106. Ma Z, Mao Z, Gao C. Surface modification and property analysis of biomedical polymers used for tissue engineering, *Colloids Surf.B.Biointerfaces* **2007**, *60*, 137-157.
107. Ren YJ, Zhang H, Huang H, Wang XM, Zhou ZY, Cui FZ, An YH. In vitro behavior of neural stem cells in response to different chemical functional groups, *Biomaterials* **2009**, *30*, 1036-1044.
108. Nelea V, Luo L, Demers CN, Antoniou J, Petit A, Lerouge S, Wertheimer R, Mwale F. Selective inhibition of type X collagen

References

- expression in human mesenchymal stem cell differentiation on polymer substrates surface-modified by glow discharge plasma, *J.Biomed.Mater.Res., Part A* **2005**, *75*, 216-223.
- 109.Khorasani MT, Mirzadeh H, Irani S. Comparison of fibroblast and nerve cells response on plasma treated poly (L-lactide) surface, *J.Appl.Polym.Sci.* **2009**, *112*, 3429-3435.
- 110.Ryu GH, Yang WS, Roh HW, Lee IS, Kim JK, Lee GH, Lee DH, Park BJ, Lee MS, Park JC. Plasma surface modification of poly (-lactic-co-glycolic acid) (65/35) film for tissue engineering, *Surf.Coat.Technol.* **2005**, *193*, 60-64.
- 111.Djordjevic I, Britcher LG, Kumar S. Morphological and surface compositional changes in poly(lactide-co-glycolide) tissue engineering scaffolds upon radio frequency glow discharge plasma treatment, *Appl.Surf.Sci.* **2008**, *254*, 1929-1935.
- 112.Huang YC, Huang CC, Huang YY, Chen KS. Surface modification and characterization of chitosan or PLGA membrane with laminin by chemical and oxygen plasma treatment for neural regeneration, *J.Biomed.Mater.Res., Part A* **2007**, *82*, 842-851.
- 113.Chen G, Okamura A, Sugiyama K, Wozniak MJ, Kawazoe N, Sato S, Tateishi T. Surface modification of porous scaffolds with nanothick collagen layer by centrifugation and freeze-drying, *J.Biomed.Mater.Res., Part B* **2009**, *90*, 864-872.
- 114.Pierschbacher MD and Ruoslahti E. Cell attachment activity of fibronectin can be duplicated by small synthetic fragments of the molecule, *Nature* **1984**, *309*, 30-33.
- 115.Fittkau MH, Zilla P, Bezuidenhout D, Lutolf MP, Human P, Hubbell JA, Davies N. The selective modulation of endothelial cell mobility on RGD peptide containing surfaces by YIGSR peptides, *Biomaterials* **2005**, *26*, 167-174.
- 116.Pierschbacher MD and Ruoslahti E. Influence of stereochemistry of the sequence Arg-Gly-Asp-Xaa on binding specificity in cell adhesion, *J.Biol.Chem.* **1987**, *262*, 17294-17298.

References

117. Hersel U, Dahmen C, Kessler H. RGD modified polymers: biomaterials for stimulated cell adhesion and beyond, *Biomaterials* **2003**, *24*, 4385-4415.
118. Beer JH, Springer KT, Coller BS. Immobilized Arg-Gly-Asp (RGD) peptides of varying lengths as structural probes of the platelet glycoprotein IIb/IIIa receptor, *Blood* **1992**, *79*, 117-128.
119. Kantlehner M, Schaffner P, Finsinger D, Meyer J, Jonczyk A, Diefenbach B, Nies B, Hölzemann G, Goodman SL, Kessler H. Surface coating with cyclic RGD peptides stimulates osteoblast adhesion and proliferation as well as bone formation, *ChemBioChem* **2000**, *1*, 107-114.
120. Irvine DJ, Mayes AM, Griffith LG. Nanoscale clustering of RGD peptides at surfaces using comb polymers. 1. Synthesis and characterization of comb thin films, *Biomacromolecules* **2001**, *2*, 85-94.
121. Tugulu S and Klok HA. Stability and nonfouling properties of poly(poly(ethylene glycol) methacrylate) brushes under cell culture conditions, *Biomacromolecules* **2008**, *9*, 906-912.
122. Shin H, Jo S, Mikos AG. Modulation of marrow stromal osteoblast adhesion on biomimetic oligo[poly(ethylene glycol) fumarate] hydrogels modified with Arg-Gly-Asp peptides and a poly(ethylene glycol) spacer, *J.Biomed.Mater.Res.* **2002**, *61*, 169-179.
123. Hern DL and Hubbell JA. Incorporation of adhesion peptides into nonadhesive hydrogels useful for tissue resurfacing, *J.Biomed.Mater.Res.* **1998**, *39*, 266-276.
124. Kantlehner M, Finsinger D, Meyer J, Schaffner P, Jonczyk A, Diefenbach B, Nies B, Kessler H. Selective RGD-mediated adhesion of osteoblasts at surfaces of implants, *Angew.Chem.Int.Ed.* **1999**, *38*, 560-562.
125. Mendes PM. Stimuli-responsive surfaces for bio-applications, *Chem.Soc.Rev.* **2008**, *37*, 2512-2529.

References

126. Biltresse S, Attolini M, Marchand-Brynaert J. Cell adhesive PET membranes by surface grafting of RGD peptidomimetics, *Biomaterials* **2005**, *26*, 4576-4587.
127. DeForest CA, Polizzotti BD, Anseth KS. Sequential click reactions for synthesizing and patterning three-dimensional cell microenvironments, *Nat.Mater.* **2009**, *8*, 659-664.
128. Luo Y and Shoichet MS. A photolabile hydrogel for guided three-dimensional cell growth and migration, *Nat.Mater.* **2004**, *3*, 249-253.
129. Lutolf MP and Hubbell JA. Synthetic biomaterials as instructive extracellular microenvironments for morphogenesis in tissue engineering, *Nat.Biotechnol.* **2005**, *23*, 47-55.
130. Shin H, Jo S, Mikos AG. Biomimetic materials for tissue engineering, *Biomaterials* **2003**, *24*, 4353-4364.
131. Cooke MJ, Zahir T, Phillips SR, Shah DSH, Athey D, Lakey JH, Shoichet MS, Przyborski SA. Neural differentiation regulated by biomimetic surfaces presenting motifs of extracellular matrix proteins, *J.Biomed.Mater.Res., Part A* **2010**, *93*, 824-832.
132. Jun HW and West JL. Modification of polyurethaneurea with PEG and YIGSR peptide to enhance endothelialization without platelet adhesion, *J.Biomed.Mater.Res., Part B* **2005**, *72*, 131-139.
133. Yang XB, Roach HI, Clarke NMP, Howdle SM, Quirk R, Shakesheff KM, Oreffo ROC. Human osteoprogenitor growth and differentiation on synthetic biodegradable structures after surface modification, *Bone* **2001**, *29*, 523-531.
134. Patel S, Thakar RG, Wong J, McLeod SD, Li S. Control of cell adhesion on poly(methyl methacrylate), *Biomaterials* **2006**, *27*, 2890-2897.
135. Abrams GA, Goodman SL, Nealey PF, Franco M, Murphy CJ. Nanoscale topography of the basement membrane underlying the corneal epithelium of the rhesus macaque, *Cell Tissue Res.* **2000**, *299*, 39-46.

References

136. Berthiaume F, Moghe PV, Toner M, Yarmush ML. Effect of extracellular matrix topology on cell structure, function, and physiological responsiveness: hepatocytes cultured in a sandwich configuration, *FASEB J.* **1996**, *10*, 1471-1484.
137. Gentile F, Tirinato L, Battista E, Causa F, Liberale C, di Fabrizio EM, Decuzzi P. Cells preferentially grow on rough substrates, *Biomaterials* **2010**, *31*, 7205-7212.
138. Thomson HA, Treharne AJ, Backholer LS, Cuda F, Grossel MC, Lotery AJ. Biodegradable poly(α -hydroxy ester) blended microspheres as suitable carriers for retinal pigment epithelium cell transplantation, *J.Biomed.Mater.Res., Part A* **2010**, *95*, 1233-1243.
139. Moroni L, Licht R, de Boer J, de Wijn JR, van Blitterswijk CA. Fiber diameter and texture of electrospun PEOT/PBT scaffolds influence human mesenchymal stem cell proliferation and morphology, and the release of incorporated compounds, *Biomaterials* **2006**, *27*, 4911-4922.
140. Lampin M, Warocquier-Clérout R, Legris C, Degrange M, Sigot-Luizard MF. Correlation between substratum roughness and wettability, cell adhesion, and cell migration, *J.Biomed.Mater.Res.* **1997**, *36*, 99-108.
141. Britland S, Perridge C, Denyer M, Morgan H, Curtis A, Wilkinson C. Morphogenetic guidance cues can interact synergistically and hierarchically in steering nerve cell growth, *Exp.Biol.Online* **1997**, *1*, 1-15.
142. Guillemette MD, Cui B, Roy E, Gauvin R, Giasson CJ, Esch MB, Carrier P, Deschambeault A, Dumoulin M, Toner M, Germain L, Veres T, Auger F. Surface topography induces 3D self-orientation of cells and extracellular matrix resulting in improved tissue function, *Integr.Biol.* **2009**, *1*, 196-204.
143. Leipzig ND and Shoichet MS. The effect of substrate stiffness on adult neural stem cell behavior, *Biomaterials* **2009**, *30*, 6867-6878.

References

- 144.Saha K, Keung AJ, Irwin EF, Li Y, Little L, Schaffer DV, Healy KE. Substrate modulus directs neural stem cell behavior, *Biophys.J.* **2008**, *95*, 4426-4438.
- 145.Kloxin AM, Benton J, Anseth KS. In situ elasticity modulation with dynamic substrates to direct cell phenotype, *Biomaterials* **2010**, *31*, 1-8.
- 146.Klassen H. Transplantation of cultured progenitor cells to the mammalian retina, *Expert Opin.Biol.Ther.* **2006**, *6*, 443-451.
- 147.Anderson JM and Shive MS. Biodegradation and biocompatibility of PLA and PLGA microspheres, *Adv.Drug Del.Rev.* **1997**, *28*, 5-24.
- 148.Thissen H, Chang KY, Tebb TA, Tsai WB, Glattauer V, Ramshaw JAM, Werkmeister JA. Synthetic biodegradable microparticles for articular cartilage tissue engineering, *J.Biomed.Mater.Res., Part A* **2006**, *77*, 590-598.
- 149.Jain RA. The manufacturing techniques of various drug loaded biodegradable poly(lactide-co-glycolide) (PLGA) devices, *Biomaterials* **2000**, *21*, 2475-2490.
- 150.Chau DYS, Agashi K, Shakesheff KM. Microparticles as tissue engineering scaffolds: Manufacture, modification and manipulation, *Mater.Sci.Technol.* **2008**, *24*, 1031-1044.
- 151.Kim TK, Yoon JJ, Lee DS, Park TG. Gas foamed open porous biodegradable polymeric microspheres, *Biomaterials* **2006**, *27*, 152-159.
- 152.Yang YY, Chung TS, Ping Ng N. Morphology, drug distribution, and in vitro release profiles of biodegradable polymeric microspheres containing protein fabricated by double-emulsion solvent extraction/evaporation method, *Biomaterials* **2001**, *22*, 231-241.
- 153.Gabler F, Frauenschuh S, Ringe J, Brochhausen C, Götz P, Kirkpatrick CJ, Sittinger M, Schubert H, Zehbe R. Emulsion-based synthesis of PLGA-microspheres for the in vitro expansion of porcine chondrocytes, *Biomol.Eng.* **2007**, *24*, 515-520.

References

154. Rafati H, Coombes AGA, Adler J, Holland J, Davis SS. Protein-loaded poly(dl-lactide-co-glycolide) microparticles for oral administration: Formulation, structural and release characteristics, *J.Controlled Release* **1997**, *43*, 89-102.
155. Berklund C, Kim K, Pack DW. Fabrication of PLG microspheres with precisely controlled and monodisperse size distributions, *J.Controlled Release* **2001**, *73*, 59-74.
156. Giunchedi P, Conti B, Maggi L, Conte U. Cellulose acetate butyrate and polycaprolactone for ketoprofen spray-dried microsphere preparation, *J.Microencapsulation* **1994**, *11*, 381-393.
157. Eley JG and Mathew P. Preparation and release characteristics of insulin and insulin-like growth factor-one from polymer nanoparticles, *J.Microencapsulation* **2007**, *24*, 225-234.
158. Senuma Y, Franceschin S, Hilborn JG, Tissières P, Bisson I, Frey P. Bioresorbable microspheres by spinning disk atomization as injectable cell carrier: from preparation to in vitro evaluation, *Biomaterials* **2000**, *21*, 1135-1144.
159. Ju XJ, Liu L, Xie R, Niu CH, Chu LY. Dual thermo-responsive and ion-recognizable monodisperse microspheres, *Polymer* **2009**, *50*, 922-929.
160. Sinha VR, Singla AK, Wadhawan S, Kaushik R, Kumria R, Bansal K, Dhawan S. Chitosan microspheres as a potential carrier for drugs, *Int.J.Pharm.* **2004**, *274*, 1-33.
161. Varde NK and Pack DW. Microspheres for controlled release drug delivery, *Expert Opin.Biol.Ther.* **2004**, *4*, 35-51.
162. von Burkersroda F, Schedl L, Göpferich A. Why degradable polymers undergo surface erosion or bulk erosion, *Biomaterials* **2002**, *23*, 4221-4231.
163. Mundargi RC, Babu VR, Rangaswamy V, Patel P, Aminabhavi TM. Nano/micro technologies for delivering macromolecular therapeutics using poly(d,l-lactide-co-glycolide) and its derivatives, *J.Controlled Release* **2008**, *125*, 193-209.

References

164. Menei P, Montero-Menei C, Venier MC, Benoit JP. Drug delivery into the brain using poly(lactide-co-glycolide) microspheres, *Expert Opin. Drug Deliv.* **2005**, *2*, 363-376.
165. Herrero-Vanrell R and Refojo MF. Biodegradable microspheres for vitreoretinal drug delivery, *Adv. Drug Del. Rev.* **2001**, *52*, 5-16.
166. Janoria KG, Gunda S, Boddu SH, Mitra AK. Novel approaches to retinal drug delivery, *Expert Opin. Drug Deliv.* **2007**, *4*, 371-388.
167. Sinha VR and Trehan A. Biodegradable microspheres for protein delivery, *J. Controlled Release* **2003**, *90*, 261-280.
168. Yeh MK. The stability of insulin in biodegradable microparticles based on blends of lactide polymers and polyethylene glycol, *J. Microencapsulation* **2000**, *17*, 743-756.
169. Fattal E, Pecquet S, Couvreur P, Andremont A. Biodegradable microparticles for the mucosal delivery of antibacterial and dietary antigens, *Int. J. Pharm.* **2002**, *242*, 15-24.
170. Jung T, Koneberg R, Hungerer KD, Kissel T. Tetanus toxoid microspheres consisting of biodegradable poly(lactide-co-glycolide)- and ABA-triblock-copolymers: immune response in mice, *Int. J. Pharm.* **2002**, *234*, 75-90.
171. Johansen P, Moon L, Tamber H, Merkle HP, Gander B, Sesardic D. Immunogenicity of single-dose diphtheria vaccines based on PLA/PLGA microspheres in guinea pigs, *Vaccine* **1999**, *18*, 209-215.
172. Sheridan C. Gene therapy finds its niche, *Nat. Biotechnol.* **2011**, *29*, 121-128.
173. Abbas AO, Donovan MD, Salem AK. Formulating poly(lactide-co-glycolide) particles for plasmid DNA delivery, *J. Pharm. Sci.* **2008**, *97*, 2448-2461.
174. Parsa S, Wang Y, Fuller J, Langer R, Pfeifer B. A comparison between polymeric microsphere and bacterial vectors for macrophage P388D1 gene delivery, *Pharm. Res.* **2008**, *25*, 1202-1208.

References

175. Bible E, Chau DYS, Alexander MR, Price J, Shakesheff KM, Modo M. The support of neural stem cells transplanted into stroke-induced brain cavities by PLGA particles, *Biomaterials* **2009**, *30*, 2985-2994.
176. Borden M, Attawia M, Laurencin CT. The sintered microsphere matrix for bone tissue engineering: In vitro osteoconductivity studies, *J.Biomed.Mater.Res.* **2002**, *61*, 421-429.
177. Newman KD and McBurney MW. Poly(d,l lactic-co-glycolic acid) microspheres as biodegradable microcarriers for pluripotent stem cells, *Biomaterials* **2004**, *25*, 5763-5771.
178. Tatard VM, Venier-Julienne MC, Saulnier P, Prechter E, Benoit JP, Menei P, Montero-Menei CN. Pharmacologically active microcarriers: a tool for cell therapy, *Biomaterials* **2005**, *26*, 3727-3737.
179. Chan BP, Hui TY, Yeung CW, Li J, Mo I, Chan GCF. Self-assembled collagen–human mesenchymal stem cell microspheres for regenerative medicine, *Biomaterials* **2007**, *28*, 4652-4666.
180. D'Amico DJ, Dryja TP, Tyo MA, Craft JL, Albert DM. Mass cultivation of bovine ocular pigment epithelial cells in microcarrier suspension culture, *Invest.Ophthalmol.Vis.Sci.* **1982**, *23*, 332-339.
181. Gabrielian K, Oganessian A, Farrokh-Siar L, Rezai KA, Verp MS, Patel SC, Ernest JT. Growth of human fetal retinal pigment epithelium as microspheres, *Graefe's Arch.Clin.Exp.Ophthalmol.* **1999**, *237*, 241-248.
182. Andrieu-Soler C, Aubert-Pouëssel A, Doat M, Picaud S, Halhal M, Simonutti M, Venier-Julienne MC, Benoit JP, Behar-Cohen F. Intravitreal injection of PLGA microspheres encapsulating GDNF promotes the survival of photoreceptors in the rd1/rd1 mouse, *Mol.Vis.* **2005**, *11*, 1002-1011.
183. Yao J, Tucker B, Zhang X, Checa-Casalengua P, Herrero-Vanrell R, Young MJ. Robust cell integration from co-transplantation of

References

- biodegradable MMP2-PLGA microspheres with retinal progenitor cells, *Biomaterials* **2011**, *32*, 1041-1050.
184. Tucker BA, Redenti SM, Jiang C, Swift JS, Klassen HJ, Smith ME, Wnek GE, Young MJ. The use of progenitor cell/biodegradable MMP2-PLGA polymer constructs to enhance cellular integration and retinal repopulation, *Biomaterials* **2009**, *31*, 9-19.
185. Schmack I, Berglin L, Nie X, Wen J, Kang SJ, Marcus AI, Yang H, Lynn MJ, Kapp J, Grossniklaus HE. Modulation of choroidal neovascularization by subretinal injection of retinal pigment epithelium and polystyrene microbeads, *Mol.Vis.* **2009**, *15*, 146-161.
186. Stover NP, Bakay RAE, Subramanian T, Raiser CD, Cornfeldt ML, Schweikert AW, Allen RC, Watts RL. Intrastratial implantation of human retinal pigment epithelial cells attached to microcarriers in advanced Parkinson disease, *Arch.Neurol.* **2005**, *62*, 1833-1837.
187. Jeong YI, Song JG, Kang SS, Ryu HH, Lee YH, Choi C, Shin BA, Kim KK, Ahn KY, Jung S. Preparation of poly(dl-lactide-co-glycolide) microspheres encapsulating all-trans retinoic acid, *Int.J.Pharm.* **2003**, *259*, 79-91.
188. Armstrong JK, Wenby RB, Meiselman HJ, Fisher TC. The hydrodynamic radii of macromolecules and their effect on red blood cell aggregation, *Biophys.J.* **2004**, *87*, 4259-4270.
189. Gupta P, Elkins C, Long T, Wilkes G. Electrospinning of linear homopolymers of poly(methyl methacrylate): exploring relationships between fiber formation, viscosity, molecular weight and concentration in a good solvent, *Polymer* **2005**, *46*, 4799-4810.
190. Opas M. Substratum Mechanics and Cell Differentiation, *Int.Rev.Cytol.* **1994**, *150*, 119-137.
191. Heath DE and Cooper SL. Interaction of endothelial cells with methacrylic terpolymer biomaterials, *J.Biomed.Mater.Res., Part B* **2010**, *92B*, 289-297.

References

192. Heath DE and Cooper SL. Design and characterization of PEGylated terpolymer biomaterials, *J.Biomed.Mater.Res., Part A* **2010**, *94A*, 1294-1302.
193. Heuberger M, Drobek T, Spencer ND. Interaction forces and morphology of a protein-resistant poly(ethylene glycol) layer, *Biophys.J.* **2005**, *88*, 495-504.
194. Sonoda S, Sreekumar PG, Kase S, Spee C, Ryan SJ, Kannan R, Hinton DR. Attainment of polarity promotes growth factor secretion by retinal pigment epithelial cells: relevance to age-related macular degeneration., *Aging (Albany NY)* **2009**, *27*, 28-42.
195. Sill TJ and von Recum H. Electrospinning: Applications in drug delivery and tissue engineering, *Biomaterials* **2008**, *29*, 1989-2006.
196. Huang Z. A review on polymer nanofibers by electrospinning and their applications in nanocomposites, *Compos.Sci.Technol.* **2003**, *63*, 2223-2253.
197. Han T, Reneker DH, Yarin AL. Buckling of jets in electrospinning, *Polymer* **2007**, *48*, 6064-6076.
198. Yarin AL, Koombhongse S, Reneker DH. Bending instability in electrospinning of nanofibers, *J.Appl.Phys.* **2001**, *89*, 3018-3026.
199. Doshi J and Reneker DH. Electrospinning process and applications of electrospun fibers, *J.Electrostatics* **1995**, *35*, 151-160.
200. Deitzel JM, Kleinmeyer J, Harris D, Beck Tan NC. The effect of processing variables on the morphology of electrospun nanofibers and textiles, *Polymer* **2001**, *42*, 261-272.
201. Jiang H, Fang D, Hsiao BS, Chu B, Chen W. Optimization and characterization of dextran membranes prepared by electrospinning, *Biomacromolecules* **2004**, *5*, 326-333.
202. Megelski S, Stephens JS, Chase DB, Rabolt JF. Micro- and nanostructured surface morphology on electrospun polymer fibers, *Macromolecules* **2002**, *35*, 8456-8466.

References

203. Koombhongse S, Liu W, Reneker DH. Flat polymer ribbons and other shapes by electrospinning, *J. Polym. Sci. B Polym. Phys.* **2001**, *39*, 2598-2606.
204. Liu J and Kumar S. Microscopic polymer cups by electrospinning, *Polymer* **2005**, *46*, 3211-3214.
205. Stoiljkovic A, Ishaque M, Justus U, Hamel L, Klimov E, Heckmann W, Eckhardt B, Wendorff JH, Greiner A. Preparation of water-stable submicron fibers from aqueous latex dispersion of water-insoluble polymers by electrospinning, *Polymer* **2007**, *48*, 3974-3981.
206. Boland ED, Wnek GE, Simpson DG, Pawlowski KJ, Bowlin GL. Tailoring tissue engineering scaffolds using electrostatic processing techniques: A study of poly(glycolic acid) electrospinning, *J. Macromol. Sci., Pure Appl. Chem.* **2001**, *38*, 1231-1243.
207. Theron A, Zussman E, Yarin AL. Electrostatic field-assisted alignment of electrospun nanofibres, *Nanotechnology* **2001**, *12*, 384-390.
208. Li WJ, Laurencin CT, Caterson EJ, Tuan RS, Ko FK. Electrospun nanofibrous structure: a novel scaffold for tissue engineering, *J. Biomed. Mater. Res.* **2002**, *60*, 613-621.
209. Matthews J, Wnek GE, Simpson DG, Bowlin GL. Electrospinning of collagen nanofibers, *Biomacromolecules* **2002**, *3*, 232-238.
210. Venugopal J, Zhang YZ, Ramakrishna S. Fabrication of modified and functionalized polycaprolactone nanofibre scaffolds for vascular tissue engineering, *Nanotechnology* **2005**, *16*, 2138-2142.
211. Sell S, McClure MJ, Garg K, Wolfe PS, Bowlin GL. Electrospinning of collagen/biopolymers for regenerative medicine and cardiovascular tissue engineering, *Adv. Drug Del. Rev.* **2009**, *61*, 1007-1019.

References

- 212.Li M, Mondrinos MJ, Gandhi MR, Ko FK, Weiss AS, Lelkes PI. Electrospun protein fibers as matrices for tissue engineering, *Biomaterials* **2005**, *26*, 5999-6008.
- 213.Li M, Guo Y, Wei Y, MacDiarmid AG, Lelkes PI. Electrospinning polyaniline-contained gelatin nanofibers for tissue engineering applications, *Biomaterials* **2006**, *27*, 2705-2715.
- 214.McManus M, Boland E, Sell S, Bowen W, Koo H, Simpson D, Bowlin G. Electrospun nanofibre fibrinogen for urinary tract tissue reconstruction, *Biomed.Mater.* **2007**, *2*, 257-262.
- 215.Schofer MD, Veltum A, Theisen C, Chen F, Agarwal S, Fuchs-Winkelmann S, Paletta JRJ. Functionalisation of PLLA nanofiber scaffolds using a possible cooperative effect between collagen type I and BMP-2: impact on growth and osteogenic differentiation of human mesenchymal stem cells, *J.Mater.Sci.Mater.Med.* **2011**, *22*, 1753-1762.
- 216.Boland ED, Coleman B, Barnes CP, Simpson DG, Wnek GE, Bowlin GL. Electrospinning polydioxanone for biomedical applications, *Acta Biomater.* **2005**, *1*, 115-123.
- 217.Sell SA, McClure MJ, Barnes CP, Knapp DC, Walpoth BH, Simpson DG, Bowlin GL. Electrospun polydioxanone-elastin blends: potential for bioresorbable vascular grafts, *Biomed.Mater.* **2006**, *1*, 72-80.
- 218.Kidoaki S, Kwon IK, Matsuda T. Mesoscopic spatial designs of nano- and microfiber meshes for tissue-engineering matrix and scaffold based on newly devised multilayering and mixing electrospinning techniques, *Biomaterials* **2005**, *26*, 37-46.
- 219.Li M, Mondrinos MJ, Chen X, Gandhi MR, Ko FK, Lelkes PI. Co-electrospun poly(lactide-co-glycolide), gelatin, and elastin blends for tissue engineering scaffolds, *J.Biomed.Mater.Res., Part A* **2006**, *79*, 963-973.
- 220.Yang F, Murugan R, Ramakrishna S, Wang X, Ma YX, Wang S. Fabrication of nano-structured porous PLLA scaffold intended for nerve tissue engineering, *Biomaterials* **2004**, *25*, 1891-1900.

References

221. Li WJ, Tuli R, Okafor C, Derfoul A, Danielson KG, Hall DJ, Tuan RS. A three-dimensional nanofibrous scaffold for cartilage tissue engineering using human mesenchymal stem cells, *Biomaterials* **2005**, *26*, 599-609.
222. Xie J, Li X, Xia Y. Putting electrospun nanofibers to work for biomedical research, *Macromol.Rapid Commun.* **2008**, *29*, 1775-1792.
223. Han D and Gouma PI. Electrospun bioscaffolds that mimic the topology of extracellular matrix, *Nanomed.Nanotech.Biol.Med.* **2006**, *2*, 37-41.
224. Ghasemi-Mobarakeh L, Prabhakaran MP, Morshed M, Nasr-Esfahani MH, Ramakrishna S. Electrospun poly(ϵ -caprolactone)/gelatin nanofibrous scaffolds for nerve tissue engineering, *Biomaterials* **2008**, *29*, 4532-4539.
225. Bini TB, Gao S, Tan TC, Wang S, Lim A, Hai LB, Ramakrishna S. Electrospun poly(L-lactide-co-glycolide) biodegradable polymer nanofibre tubes for peripheral nerve regeneration, *Nanotechnology* **2004**, *15*, 1459-1464.
226. Yoshimoto H, Shin YM, Terai H, Vacanti JP. A biodegradable nanofiber scaffold by electrospinning and its potential for bone tissue engineering, *Biomaterials* **2003**, *24*, 2077-2082.
227. Kim KH, Jeong L, Park HN, Shin SY, Park WH, Lee SC, Kim TI, Park YJ, Seol YJ, Lee YM, Ku Y, Rhyu IC, Han SB, Chung CP. Biological efficacy of silk fibroin nanofiber membranes for guided bone regeneration, *J.Biotechnol.* **2005**, *120*, 327-339.
228. Sui G, Yang X, Mei F, Hu X, Chen G, Deng X, Ryu S. Poly-L-lactic acid/hydroxyapatite hybrid membrane for bone tissue regeneration, *J.Biomed.Mater.Res., Part A* **2007**, *82*, 445-454.
229. Kim HW, Song JH, Kim HE. Nanofiber generation of gelatin-hydroxyapatite biomimetics for guided tissue regeneration, *Adv.Funct.Mater.* **2005**, *15*, 1988-1994.

References

230. Jang JH, Castano O, Kim HW. Electrospun materials as potential platforms for bone tissue engineering, *Adv. Drug Del. Rev.* **2009**, *61*, 1065-1083.
231. Sell S, Barnes C, Smith M, McClure M, Madurantakam P, Grant J, McManus M, Bowlin G. Extracellular matrix regenerated : tissue engineering via electrospun biomimetic nanofibers, *Polym. Int.* **2007**, *56*, 1349-1360.
232. Blackwood KA, McKean R, Canton I, Freeman CO, Franklin KL, Cole D, Brook I, Farthing P, Rimmer S, Haycock JW, Ryan AJ, MacNeil S. Development of biodegradable electrospun scaffolds for dermal replacement, *Biomaterials* **2008**, *29*, 3091-3104.
233. Gu BK, Ismail Y, Spinks GM, Kim SI, So I, Kim SJ. A linear actuation of polymeric nanofibrous bundle for artificial muscles, *Chem. Mater.* **2009**, *21*, 511-515.
234. Chen H, Fan X, Xia J, Chen P, Zhou X, Huang J, Yu J, Gu P. Electrospun chitosan-graft-poly (ϵ -caprolactone)/poly (ϵ -caprolactone) nanofibrous scaffolds for retinal tissue engineering, *Int. J. Nanomedicine* **2011**, *6*, 453-461.
235. Pritchard CD, Arnér KM, Langer RS, Ghosh FK. Retinal transplantation using surface modified poly(glycerol-co-sebacic acid) membranes, *Biomaterials* **2010**, *31*, 7978-7984.
236. Pritchard CD, Arnér KM, Neal RA, Neeley WL, Bojo P, Bachelder E, Holz J, Watson N, Botchwey EA, Langer RS, Ghosh FK. The use of surface modified poly(glycerol-co-sebacic acid) in retinal transplantation, *Biomaterials* **2010**, *31*, 2153-2162.
237. Nicolson PC and Vogt J. Soft contact lens polymers: an evolution, *Biomaterials* **2001**, *22*, 3273-3283.
238. Koo JS, Smith PGR, Williams RB, Grossel MC, Whitcombe MJ. Synthesis and characterization of methacrylate-based copolymers for integrated optical applications, *Chem. Mater.* **2002**, *14*, 5030-5036.
239. Meechaisue C, Dubin R, Supaphol P, Hoven VP, Kohn J. Electrospun mat of tyrosine-derived polycarbonate fibers for

References

- potential use as tissue scaffolding material, *J.Biomater.Sci.Polym.Ed.* **2006**, *17*, 1039-1056.
- 240.Morpurgo M, Bayer EA, Wilchek M. N-hydroxysuccinimide carbonates and carbamates are useful reactive reagents for coupling ligands to lysines on proteins, *J.Biochem.Bioph.Methods* **1999**, *38*, 17-28.
- 241.Beamish JA, Fu AY, Choi Aj, Haq NA, Kottke-Marchant K, Marchant RE. The influence of RGD-bearing hydrogels on the re-expression of contractile vascular smooth muscle cell phenotype, *Biomaterials* **2009**, *30*, 4127-4135.
- 242.Dillow AK, Ochsenhirt SE, McCarthy JB, Fields GB, Tirrell M. Adhesion of $\alpha 5\beta 1$ receptors to biomimetic substrates constructed from peptide amphiphiles, *Biomaterials* **2001**, *22*, 1493-1505.
- 243.Burridge K and Chrzanowska-Wodnicka M. Focal adhesions, contractility, and signaling, *Annu.Rev.Cell Dev.Biol.* **1996**, *12*, 463-519.
- 244.Miron T and Wilchek M. A simplified method for the preparation of succinimidyl carbonate polyethylene glycol for coupling to proteins, *Bioconjugate Chem.* **1993**, *4*, 568-569.
- 245.da Cruz L, Chen FK, Ahmado A, Greenwood J, Coffey P. RPE transplantation and its role in retinal disease, *Prog.Retin.Eye Res.* **2007**, *26*, 598-635.
- 246.Lin R, Shi Ng L, Wang CH. In vitro study of anticancer drug doxorubicin in PLGA-based microparticles, *Biomaterials* **2005**, *26*, 4476-4485.
- 247.Tan H and Ye J. Surface morphology and in vitro release performance of double-walled PLLA/PLGA microspheres entrapping a highly water-soluble drug, *Appl.Surf.Sci.* **2008**, *255*, 353-356.
- 248.Malda J and Frondoza CG. Microcarriers in the engineering of cartilage and bone, *Trends Biotechnol.* **2006**, *24*, 299-304.

References

249. Greiner A and Wendorff JH. Electrospinning: a fascinating method for the preparation of ultrathin fibers, *Angew.Chem.Int.Ed.Engl.* **2007**, *46*, 5670-5703.
250. Gref R, Lück M, Quellec P, Marchand M, Dellacherie E, Harnisch S, Blunk T, Müller RH. 'Stealth' corona-core nanoparticles surface modified by polyethylene glycol (PEG): influences of the corona (PEG chain length and surface density) and of the core composition on phagocytic uptake and plasma protein adsorption, *Colloids Surf.B.Biointerfaces* **2000**, *18*, 301-313.
251. Pasche S, De Paul SM, Vörös J, Spencer ND, Textor M. Poly(l-lysine)-graft-poly(ethylene glycol) assembled monolayers on niobium oxide surfaces: A quantitative study of the influence of polymer interfacial architecture on resistance to protein adsorption by ToF-SIMS and in situ OWLS, *Langmuir* **2003**, *19*, 9216-9225.